UNIVERSIDAD AUTONOMA DE MADRID

Programa de Doctorado

en Biociencias Moleculares

Caracterización de la función de SRSF4 en la homeostasis del corazón

José Javier Larrasa Alonso

Madrid, 2019

Departamento de Bioquímica

Facultad de Medicina

Caracterización de la función de SRSF4 en la homeostasis del corazón

José Javier Larrasa Alonso

Licenciado en Biología

Dirigida por Dr. Enrique Lara-Pezzi

Fundación Centro Nacional de Investigaciones Cardiovasculares Carlos III (CNIC)

Certificado del Director:

Dr. Enrique Lara Pezzi, Jefe de Grupo en la Fundación Centro Nacional de Investigaciones Cardiovasculares Carlos III.

Certifica:

Que la presente Tesis Doctoral titulada **"Caracterización de la función de SRSF4 en la homeostasis del corazón"** presentada por José Javier Larrasa Alonso, ha sido realizada bajo mi tutela y dirección, autorizándose para presentación ante el tribunal correspondiente.

Y para que así conste a los efectos oportunos, firma la presente en Madrid, a 22 de Octubre de 2019.

Fdo. Enrique Lara Pezzi

AGRADECIMIENTOS

Me gustaría expresar mi más sincero agradecimiento a las personas que me han apoyado durante estos años para que el presente trabajo pudiera salir adelante. En primer lugar, mi director de tesis, el Dr. Enrique Lara Pezzi, que me ofreció la oportunidad de comenzar mi doctorado sin tener conocimiento previo de mi forma de trabajar, gracias por confiar en mí. Agradezco también su supervisión así como su preocupación e interés durante estos años porque mi futuro profesional fuera el más próspero.

Muchas son las personas que han ido y venido del laboratorio durante estos años. La que ha estado desde el principio hasta el final es Marina, esa madre que ya me dijo que sería nada más entrar en el laboratorio y con la que compartí buenos momentos fuera del laboratorio sobre todo al principio de la tesis. También Paula, que acabó ya hace un año y a la cual he echado de menos en esta etapa final. Sin duda ha sido mi compañera de batalla. Empezamos el doctorado casi a la vez y hemos compartido muchos buenos momentos dentro y fuera del laboratorio, también alguno malo por complicaciones en algún experimento que finalmente fuimos capaces de solucionar. Tengo que agradecer también a Eli, por sus conversaciones científicas y sobre aspectos personales especialmente en esta etapa final de la tesis. A las últimas incorporaciones, Laura y Laura "Lala" con las que me hubiera gustado coincidir antes en el laboratorio ya que transmiten mucha energía positiva. A Carlos, que siempre ha estado dispuesto a ayudarme con los datos bioinformáticos. A María, una de las que más me ha ayudado experimentalmente, le tengo que agradecer todo lo que he aprendido sobre imagen y su disposición para explicarme dudas sobre el análisis de ecos y electros.

También me gustaría agradecer a todos los cardiólogos y residentes que han pasado por el grupo, en especial a Fernando y a Esther por ayudarme a resolver dudas desde un punto de vista más clínico. De entre los antiguos compañeros, tengo que agradecer también a Miriam, con la que rápidamente hice una gran amistad y pasé grandes momentos discutiendo sobre ciencia o sobre la vida al salir del laboratorio. A Jesús, que me ayudó a integrarme en el grupo y en el centro, y también

pasamos momentos divertidos fuera del trabajo. A Enrique Gallego, por sus aportaciones sobre vectores virales y también por los buenos momentos fuera del laboratorio. A Laura Padrón, con la que he colaborado en uno de los proyectos más interesantes del laboratorio. También agradezco a Dafne y Lucía su ayuda con algunos experimentos durante sus estancias de verano. A Marta, siempre con una sonrisa y una palabra amable. Y a otros antiguos compañeros como María Donina, Marta Roldán, Enda, Alberto y Girolamo por sus aportaciones.

Tengo que agradecer a muchas otras personas de CNIC que también en lo profesional pero sobre todo en lo personal han hecho que estos años hayan sido únicos. Como no podía ser de otra manera, en primer lugar quiero agradecer a mi amigo Jose, siempre dispuesto a escuchar mis preocupaciones tanto profesionales como personales y a darme consejos para superarlas. A Itziar, por ser una grande. A todo el grupo de "Mis dulSes", Julio, Sergio, Ana, Rebeca, Macarena, Carles, Laura, Jesús, Maruchi, Verdiana, Jesús, Cristina, Briane, Sara y Alberto; por vuestro apoyo en momentos peores, por todas las celebraciones, las yolis, las escapadas y los viajes que hemos compartido juntos durante estos años. A Sergi, por nuestras charlas en los geles, en cultivos, de vuelta a casa, por los viajes… por los buenos momentos. A Estefanía, por nuestros cafés y tus buenos consejos. A Samu, porque también se nos fue el doctorado. A Agus y Ana, por las charlas y los buenos momentos fuera del laboratorio. A todas las personas de otros laboratorios con los que he convivido durante estos años, especialmente en la primera y la segunda sur.

Gracias también al trabajo de las unidades técnicas, sobre todo a vectores virales, genómica, bioinformática y animalario. En especial a Cristina y Dani de vectores y a Frank, Laura, Lorena y Raquel que se han encargado de las colonias de ratones durante estos años. A Lorena, Ana Vanesa y Eva por la adquisición de las imágenes de las ecocardiografías de algunos de mis ratones. Al personal de logística, sobre todo a Mari y Javier Mateos. También a las personas que nos ayudan con los papeleos de los congresos y las becas, en especial a Ana y Cristina, que también les quiero agradecer nuestro agradable encuentro durante mi estancia en Alemania. A mis compañeros de la estancia, y en especial a François McNicoll y a Michaela Müller por sus aportaciones.

Me gustaría también acordarme de mis antiguos jefes y compañeros de laboratorio del IIB y del CNIO, con los cuales me inicié en el mundo de la investigación y con los que cogí mucha experiencia y aprendí técnicas que he podido aplicar durante mi tesis. A mis amigos de Biología y del Colegio, que a pesar del paso de los años siguen estando igual de presentes que el primer día.

A toda mi familia, abuelos, tíos, primos y muy especialmente quiero agradecer el apoyo incondicional de mis padres, Araceli y Pepe. Gracias a ellos he podido llegar a ser la persona que soy hoy. Siempre les agradeceré su apoyo moral y en el ámbito académico durante todas las etapas de mi formación.

Gracias a todos los que me habéis acompañado de un modo u otro durante estos años para que este trabajo haya salido adelante.

Muchas gracias a todos.

Resumen

Las enfermedades cardiovasculares constituyen la mayor causa de muerte a nivel mundial, sin embargo la regulación de los mecanismos post-transcripcionales y el papel de las proteínas de unión a RNA (RBPs) en estas enfermedades continúa siendo un campo por descubrir.

Estudios recientes muestran que la expresión aberrante de RBPs puede afectar a varios puntos del procesamiento del RNA, alterando la función de sus genes diana. La RBP serine-arginine rich factor 4 (SRSF4) está implicada en el desarrollo de patologías neurológicas y en cáncer. Sin embargo, su papel en el corazón es completamente desconocido. Nuestros análisis ecocardiográficos mostraron que los ratones con pérdida cardio-específica de SRSF4 (SRSF4 KO) desarrollan hipertrofia ventricular izquierda por un incremento del área de los cardiomiocitos, y disfunción diastólica en edades más avanzadas. Además, los ratones SRSF4 KO presentaron una actividad electrofisiológica alterada bajo condiciones de estrés cardiaco inducido por isoproterenol, incluyendo una depresión después del QRS y un QT largo, indicando un elevado riesgo de muerte súbita. El análisis por RNA-seq mostró cambios de expresión en un gran número de RNAs largos no codificantes (lncRNAs), entre los que se encontraba el lncRNA-GAS5 (Growth Arrest Specific 5), el cual hemos identificado como diana directa de SRSF4 en cardiomiocitos mediante individual nucleotide-resolution Cross-Linking and ImmunoPrecipitation (iCLIP). GAS5 es un inhibidor del receptor de glucocorticoides (GR), y su expresión se encontraba disminuida en los corazones SRSF4 KO. Consecuentemente, encontramos una elevación de la actividad transcripcional del GR que conducía a un incremento de marcadores de hipertrofia y del área celular. Además la sobreexpresión de GAS5 reducía la hipertrofia de los cardiomiocitos.

Summary

Cardiovascular diseases are the main cause of death worldwide, however the regulation of post-transcriptional mechanisms, like alternative splicing and the role of the RNA Binding Proteins (RBPs) during these diseases continues to be a field to be discovered.

Emerging studies have shown that RBPs play critical roles in human biology and pathogenesis. Aberrant expression of RBP genes affect various steps of RNA processing, altering target gene function. Serine/arginine splicing factor 4 (SRSF4) has been related with neuropathies and cancer. However, its role in the heart is completely unknown. Echocardiographic analysis showed that cardio-specific knockout mice for SRSF4 (SRSF4 KO) develop left ventricular hypertrophy and present an increased cardiomyocyte area compared to controls. These mice also showed increased expression of heart disease markers. Older mice also presented diastolic dysfunction. Moreover, SRSF4 KO mice presented an altered electrophysiological activity under cardiac stress induced by isoproterenol, with a depression after the QRS and long QT interval, indicating an elevated risk of sudden cardiac death. RNA-Seq analysis showed expression changes in several long non-coding RNAs (lncRNAs), among which we found the lncRNA-GAS5 (Growth Arrest Specific 5), which we have identified as a direct target for SRSF4 in cardiomyocytes by individual nucleotide-resolution Cross-Linking and ImmunoPrecipitation (iCLIP). GAS5 is a repressor of the glucocorticoid receptor (GR) and it was downregulated in SRSF4 KO hearts. Consequently, we found an elevated transcriptional activity of GR in cardiomyocytes which leads to an increase in hypertrophy markers and cell size. Furthermore, we also found that the GAS5 overexpression in cardiomyocytes lacking SRSF4 reduces cell hypertrophy.

Índice

Clave de abreviaturas y siglas

- **AAV:** Virus adenoasociado
- **ANF:** Atrial natriuretic factor
- **AS:** Splicing alternativo
- **BNP:** Péptido natriurético B
- **CVDs:** Enfermedades cardiovasculares
- **DCM:** Cardiomiopatía dilatada
- **DEX:** Dexametasona
- **EF:** ejection fraction (del inglés, fracción de eyección)
- **GAS5:** Growth Arrest Specific 5
- **GAPDH:** Deshidrogenasa glyceraldehido-3-fosfato
- **GR:** Receptor de glucocorticoids
- **HCM:** Miocardiopatía hipertrófica
- **iCLIP:** individual nucleotide-resolution Cross-Linking and ImmunoPrecipitation
- **KO:** Knockout
- **LncRNA:** long non coding RNA (del ingles, RNA largo no codificante)
- **Luc:** Luciferasa
- **LVAWd:** pared anterior del ventrículo izquierdo en diástole
- **LVPWd:** pared posterior del ventrículo izquierdo en diástole
- **MI:** Infarto de miocardio
- **MYH7:** cadena pesada de la miosina 7
- **ncRNA:** non coding RNA (del inglés, RNA no codificante)
- **RBP:** Proteína de unión a RNA
- **RNA:** Ácido ribonucleico (del inglés, RiboNucleic Acid)
- **RRM:** motivo de reconocimiento de RNA
- **SEM:** standard error of the mean (del inglés, error estándar de la media)
- **SRSF:** Factor de splicing rico en serina-arginina
- **TAC:** transaortic constriction, del inglés.
- **VI:** Ventrículo izquierdo

INTRODUCCIÓN

Enfermedades Cardiovasculares

Las enfermedades cardiovasculares (ECV) representan la primera causa de muerte en todo el mundo. Se estima que 17.7 millones de personas fallecieron en 2015 a causa de las enfermedades cardiovasculares, lo que representa el 31% de muertes en todo el mundo[1]. Solo en Europa, las ECVs causan 3.9 millones de muertes cada año, constituyendo el 45% de las muertes europeas[2]. A pesar de que la mortalidad asociada a ECVs ha disminuido, la incidencia de las mismas en los últimos 25 años se ha incrementado. Entre las ECVs, la insuficiencia cardiaca (IC) causa el 20% de todas las hospitalizaciones en pacientes de más de 65 años[3]. El infarto agudo de miocardio (IAM) y la hipertrofia son dos de las principales causas de IC.

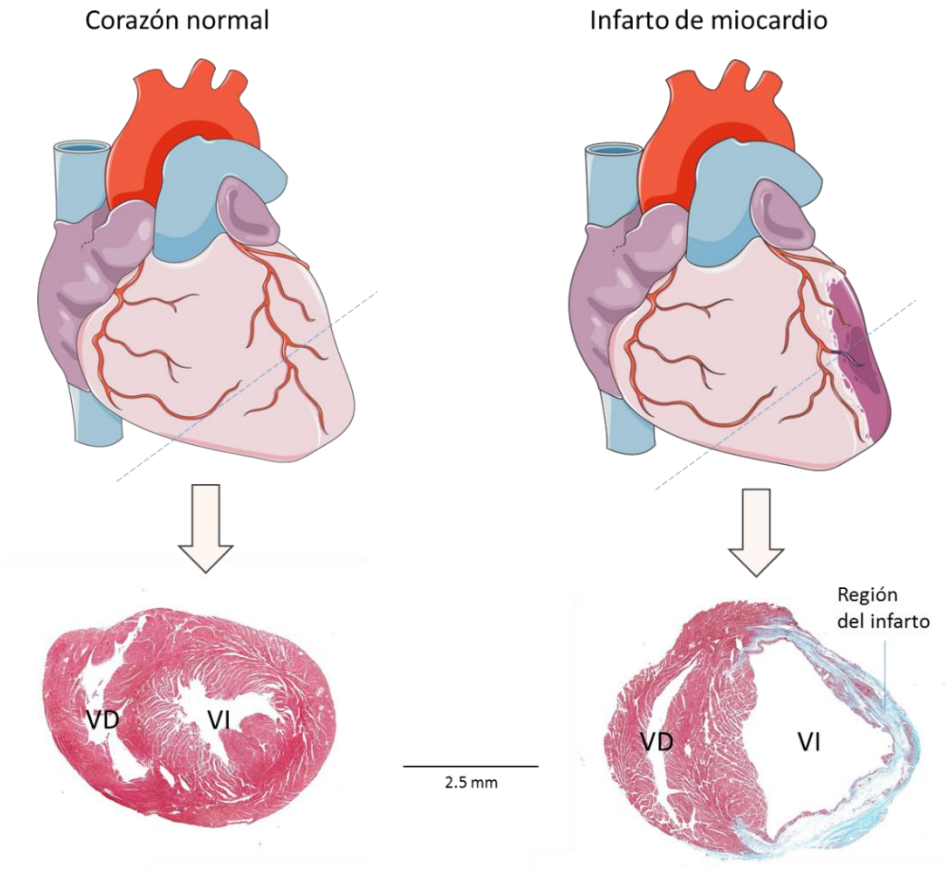

Figura 1. Infarto de miocardio. Tras el infarto, los cardiomiocitos muertos son reemplazados por una cicatriz de matriz extracelular y el ventrículo izquierdo (VI) del corazón se dilata. Tinción de tricrómico de Masson de corazones extraidos de ratones C57BL/6 pre y 28 días post-infarto. VD, ventrículo derecho.

El infarto se produce tras la oclusión de una arteria coronaria epicárdica. Los cardiomiocitos irrigados por dicha arteria mueren progresivamente debido a la falta de oxígeno y nutrientes. Aunque la reperfusión de la arteria ocluida reduce la extensión del infarto (y por consiguiente la mortalidad), la magnitud del daño y el área necrótica son en la mayoría de los casos todavía considerables. Los cardiomiocitos muertos son reemplazados por una cicatriz compuesta mayoritariamente de matriz extracelular (Figura 1). Además de una ausencia de contractilidad del miocardio necrosado, el miocardio remoto (no infartado) sufre un remodelado progresivo consistente en hipertrofia y fibrosis difusa. Todo ello provoca un deterioro progresivo de la función cardiaca post-infarto que desemboca en una situación de insuficiencia cardíaca.

Por otro lado, la hipertrofia ventricular izquierda se caracteriza por el crecimiento en la masa del ventrículo izquierdo causado por un aumento en el tamaño de los cardiomiocitos. Puede representar una adaptación fisiológica al ejercicio físico intenso, como en los atletas, o puede ser causada por una afección patológica, ya sea genética o secundaria a la sobrecarga del ventrículo izquierdo. La hipertrofia fisiológica suele ser benigna y revierte tras la reducción o cese de la actividad física. La hipertrofia patológica es un fenómeno compensatorio, que eventualmente puede descompensarse y evolucionar hacia una disfunción progresiva del ventrículo izquierdo e insuficiencia cardíaca (Figura 2).

A pesar de avances significativos en la práctica clínica, el pronóstico de la insuficiencia cardíaca continúa siendo muy pobre. La identificación de nuevos mecanismos y dianas terapéuticas para su tratamiento y prevención es por lo tanto de gran importancia. Durante los últimos años se ha profundizado en el conocimiento de los patrones de expresión génica durante el desarrollo de las enfermedades cardíacas y de su regulación por rutas de señalización intracelular, factores de transcripción y microRNAs[4,5]. Por desgracia esta información es en gran medida incompleta, ya que la regulación de los mecanismos post-transcripcionales y el papel de las proteínas de unión a RNA (RBPs, por sus siglas en inglés) en las ECVs continúa siendo un campo por explorar.

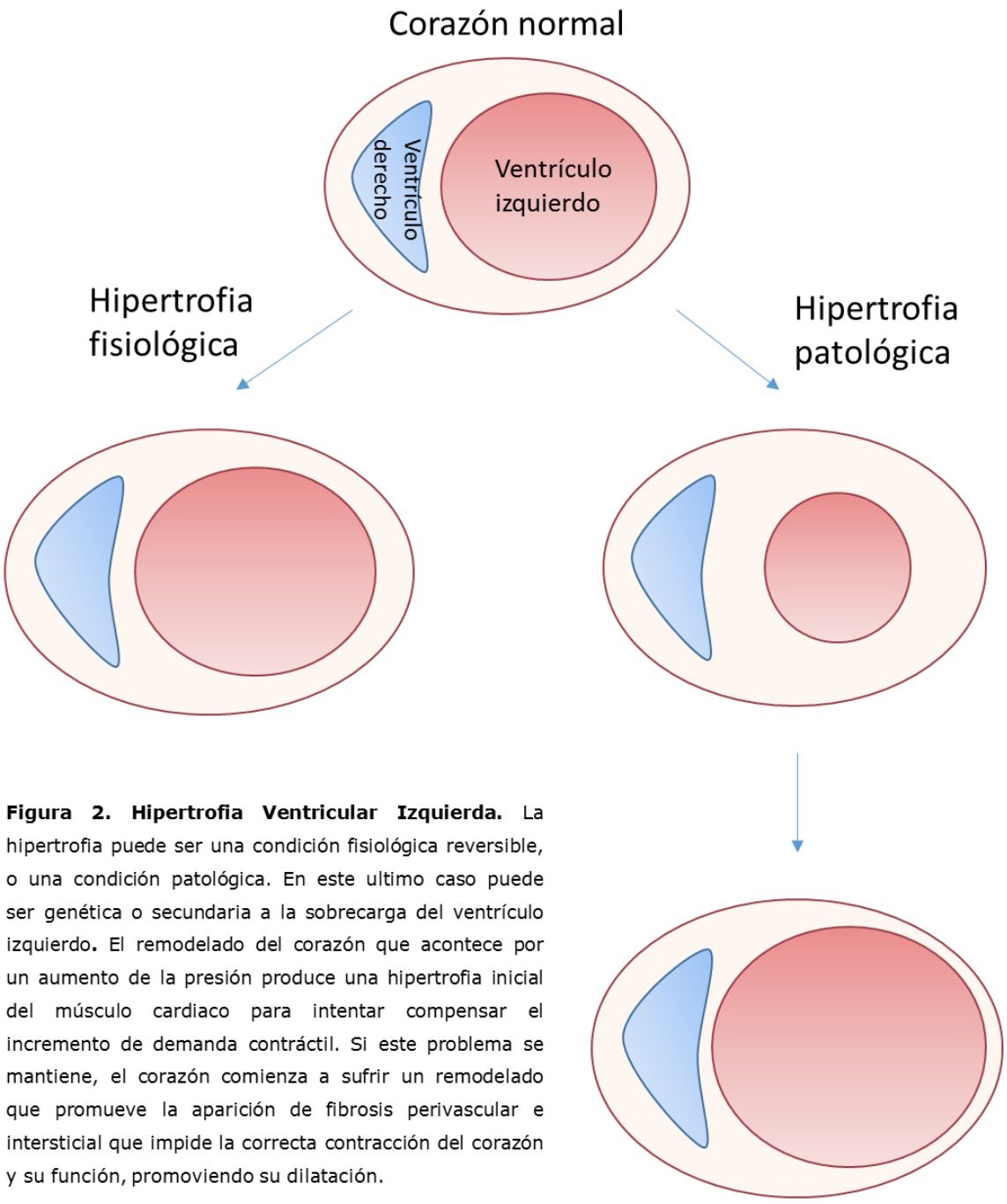

Figura 2. Hipertrofia Ventricular Izquierda. La hipertrofia puede ser una condición fisiológica reversible, o una condición patológica. En este ultimo caso puede ser genética o secundaria a la sobrecarga del ventrículo izquierdo**.** El remodelado del corazón que acontece por un aumento de la presión produce una hipertrofia inicial del músculo cardiaco para intentar compensar el incremento de demanda contráctil. Si este problema se mantiene, el corazón comienza a sufrir un remodelado que promueve la aparición de fibrosis perivascular e intersticial que impide la correcta contracción del corazón y su función, promoviendo su dilatación.

Proteínas de Unión a RNA

La importancia del estudio de proteínas de unión a RNA (RBPs) ha emergido como resultado de su capacidad para regular la expresión génica a través de una gran variedad de mecanismos post-transcripcionales. Son capaces de hacerlo por presentar dominios de unión a RNA. Esta unión se produce gracias al reconocimiento de una secuencia específica de nucleótidos y/o de motivos estructurales presentes en el RNA[6]. De esta forma, las RBPs están implicadas en varios aspectos del metabolismo del RNA, como son el splicing constitutivo y alternativo o el transporte, localización, estabilidad y traducción de RNAs[7].

Se estima que el genoma humano codifica para más de 700 RBPs[8]. Debido a la variedad de procesos que estas proteínas regulan durante la vida de los RNAs, su ausencia o expresión anormal puede tener un fuerte impacto en el mantenimiento de la homeostasis celular. De hecho, se ha relacionado la pérdida de función de un número significativo de RBPs con manifestaciones clínicas en varias enfermedades humanas. La mayoría de ellas son enfermedades neurodegenerativas y neuromusculares, incluidas la enfermedad de Alzheimer, la demencia frontotemporal o la esclerosis lateral amiotrófica (ELA)[9,10]. La alteración de la expresión de RBPs es también una característica común en varios tipos de cáncer[11].

Además, aunque la implicación de las RBPs en el correcto funcionamiento del corazón no ha sido tan explorada como en otros campos, estudios recientes ponen de manifiesto la implicación de estas proteínas en diversas enfermedades cardiovasculares[12]. Un artículo reciente muestra como la pérdida de función de RBM24 lleva a una progresiva cardiomiopatía dilatada (MCD), debido a cambios en el splicing alternativo de genes relacionados con la función cardiaca[13]. También se ha descrito que la alteración en la expresión de RBM20 conduce al desarrollo de MCD como consecuencia de cambios en el splicing de genes como la titina y otros genes relacionados con la contracción cardíaca[14]. No solo en cardiomiopatía dilatada, también hay estudios que muestran que la ausencia o alteración de la expresión de RBPs produce hipertrofia cardíaca, como es el caso de PCBP2. La expresión de esta RBP se encuentra disminuida en ratones con hipertrofia cardíaca. Se describe como un factor anti-hipertrófico que actúa mediante la inhibición de la estabilidad del RNA

mensajero (mRNA) de GPR56[15]. De forma similar, la expresión de RBFox1 también se ve disminuida en corazones enfermos tanto de pacientes como de ratón. Este estudio muestra la relación de RBFox1 con el splicing alternativo de los miembros de la familia de factores de trascripción MEF2, el cual tiene un papel muy relevante en el desarrollo de hipertrofia e insuficiencia cardíaca[16]. De la misma manera, otro estudio asocia la función de RBFox2 como regulador de splicing con insuficiencia cardíaca en un modelo de hipertrofia inducido por constricción aórtica[17]. También, se han descrito alteraciones electrofisiológicas en el corazón asociadas a un mal funcionamiento de los canales de sodio y potasio debido a un cambio en su regulación génica por parte de RBPs[18,19].

La familia SR de proteínas de unión a RNA

Una familia muy conservada de proteínas de unión a RNA es la familia de las proteínas SR (del inglés, serine-arginine rich factors). Esta familia está compuesta por 12 miembros (SRSF1-12). Cada uno de ellos contiene uno o dos motivos de unión a RNA en su región N-terminal, y por un dominio SR rico en serinas y argininas en su extremo C-terminal. El dominio de unión a RNA determina la especificidad de la unión de las proteínas SR a sus respectivos RNAs diana[20], mientras que el dominio SR está principalmente involucrado en las interacciones con otras proteínas (Figura 3). El estado de fosforilación del dominio SR es importante para la función de la proteína. Sin embargo, también hay evidencias que indican que el dominio SR puede interactuar con otros RNAs, y que el dominio de unión a RNA participa en interacciones proteína-proteína[21].

Las proteínas SR fueron definidas originalmente como factores de splicing. El splicing del RNA es el proceso por el cual los intrones son eliminados del pre-mRNA inmaduro y los exones son unidos para crear el mRNA maduro (Figura 4). El proceso de splicing es llevado a cabo por un gran complejo ribonucleoproteico conocido como spliceosoma, compuesto por más de 100 proteínas y cinco RNAs nucleares pequeños, que reconoce tres elementos presentes en todos los intrones: el sitio de splicing 5’ (que incluye los nucleótidos GU), el sitio 3’ (que incluye los nucleótidos AG y la

secuencia de polipirimidina) y la secuencia de ramificación (BPS, por sus siglas en inglés)[22]. El splicing no es un proceso rígido. Muy a menudo ocurren variaciones en la combinación final de exones e intrones en el mRNA maduro. Esta variación es debida al splicing alternativo (SA). Las SR no forman parte de la maquinaria de splicing pero sí tienen un importante papel durante su ensamblaje y activación[21]. Su función es determinar los sitios de corte en el RNA mensajero, influyendo así tanto en el splicing constitutivo como en el alternativo. En este proceso, se ha visto que la unión de las proteínas SR está enriquecida pero no limitada a los exones, ya que también pueden regular el splicing uniéndose a secuencias en los intrones[23,24].

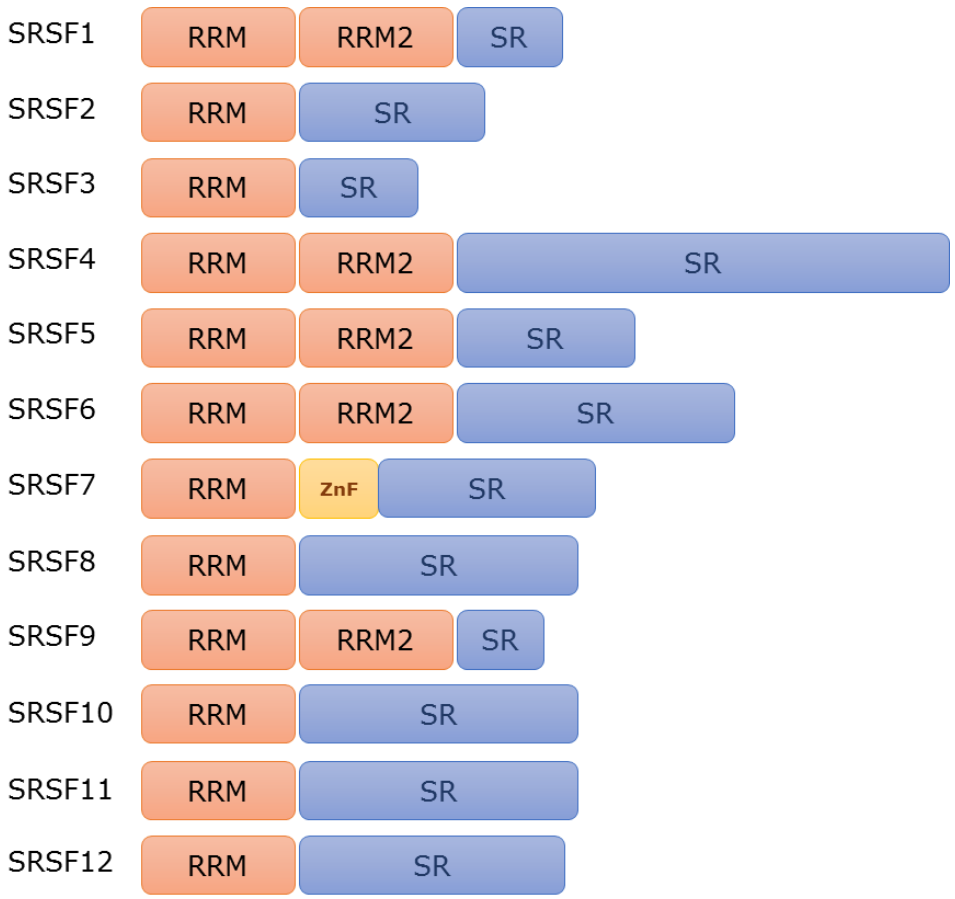

Figura 3. La familia de proteínas SR. La familia está formada por 12 proteínas. Cada uno posee uno o dos dominios de unión a RNA (RRM) y un dominio SR de interacción con otras proteínas. Además, SRSF7 posee un dominio de dedo de zinc (ZnF).

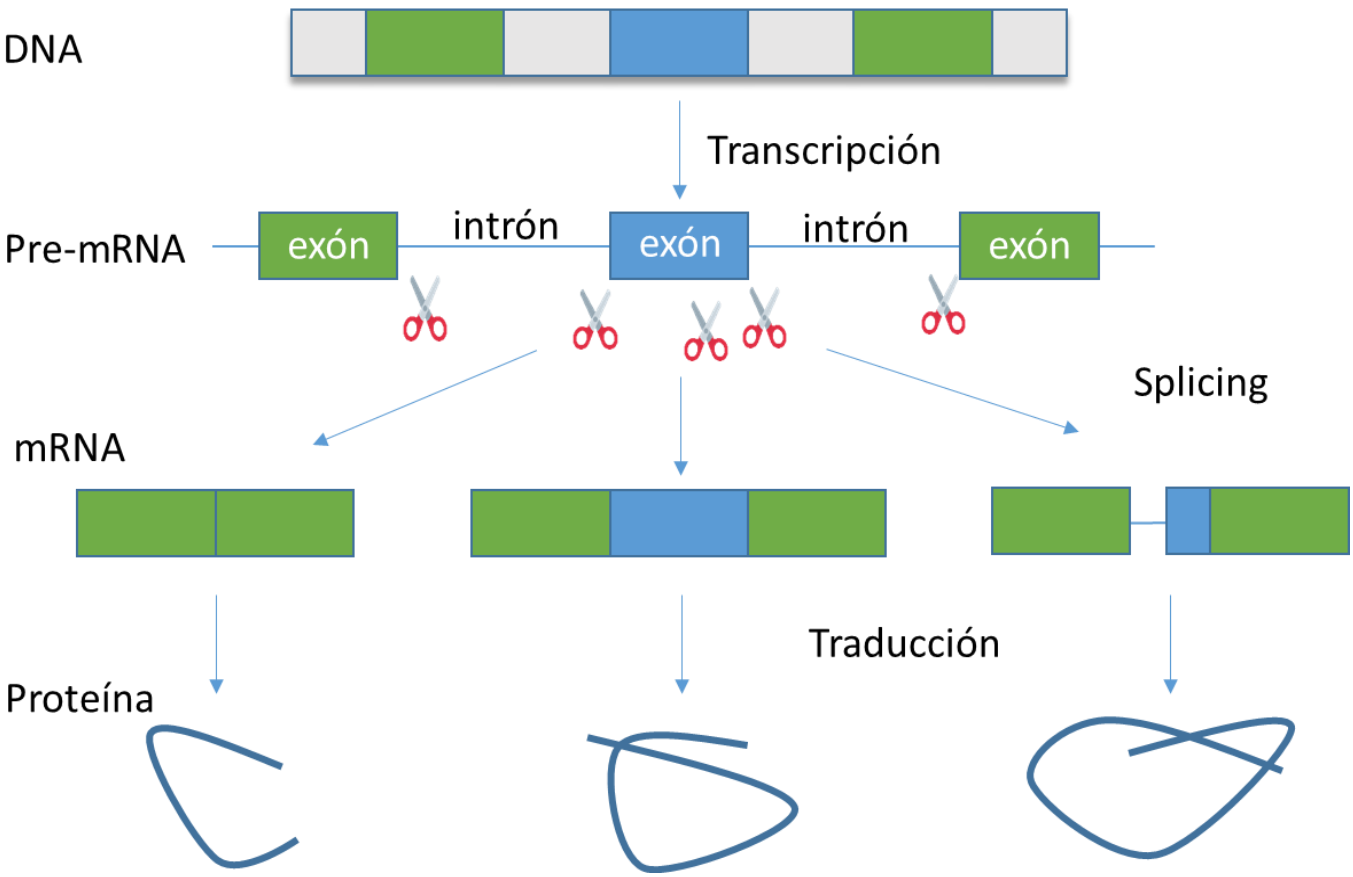

Figura 4. El Splicing Alternativo permite obtener a partir de un transcrito primario de mRNA o pre-mRNA distintas isoformas de mRNA y proteínas, las cuales pueden tener funciones diferentes.

Se ha descrito previamente que la alteración del splicing alternativo contribuye al desarrollo de un gran número de enfermedades humanas[25]. Centrándonos en cardiomiopatías, un estudio muestra que en la hipertrofia cardíaca inducida por constricción aórtica están involucrados un gran número de cambios de isoformas de una misma proteína. Gran parte de estos cambios son comunes al programa de regulación de splicing fetal[26]. Posteriormente, otro estudio predijo los factores que podrían estar regulando los cambios de splicing que se estaban produciendo en un modelo de hipertrofia cardíaca inducido por aumento de presión[27]. Por otro lado recientemente, en un estudio en pacientes con cardiomiopatía dilatada, se han

detectado cambios de splicing en un gran número de genes, 11 de ellos son genes implicados directamente con esta patología, y están relacionados con la maquinaria de contracción de los cardiomiocitos[28]. En otro estudio, Kong y sus colaboradores demostraron por primera vez que el splicing alternativo estaba alterado en humanos con insuficiencia cardíaca. Analizaron los cambios de splicing en muestras del ventrículo izquierdo de pacientes con cardiomiopatía isquémica comparada con muestras control. Los resultados mostraron cambios de splicing en varios genes sarcoméricos[29]. Estos estudios muestran la desregulación del splicing alternativo en distintas patologías cardiacas. No está claro si estos cambios tienen una contribución significativa en el desarrollo de la enfermedad y/o la progresión hacia una insuficiencia cardíaca.

Varios estudios han demostrado que las proteínas SR, además de en el splicing, están implicadas en la regulación de muchos pasos del procesamiento de los RNAs y de la transcripción. Las SR están principalmente localizadas en el núcleo donde llevan a cabo su papel en el splicing, pero también pueden transportarse entre el núcleo y el citoplasma para realizar otras funciones como ayudar al transporte, estabilidad o traducción de RNAs (Figura 5). La función de transporte es imprescindible para poder trasladar los mRNAs desde el núcleo al citoplasma. Un estudio demuestra como las proteínas SR están implicadas en este proceso. La bajada de la expresión de las proteínas SRSF1-7, produce la acumulación de un número significativo de mRNAs en el núcleo. Además se ha descrito la interacción en mayor o menor medida de determinadas proteínas SR con NXF1, que es un factor esencial para el transporte de los mRNAs al citoplasma[30].

Se ha demostrado que las proteínas SR, además de unirse a las regiones exónicas e intrónicas pueden interaccionar con las secuencias 3´UTR (untranslated region, del inglés) de sus RNAs diana para regular su estabilidad[31]. Además las SR pueden mediar la estabilidad de los RNAs mediante la regulación de su degradación. El non-sense mediated decay (NMD) es un proceso de control por el cual los RNAs aberrantes son degradados. Este mecanismo detecta unos codones de stop prematuros (PTC, por sus siglas en inglés), generalmente generados por splicing alternativo. Se determina si un codón de terminación es un PTC en función de la

presencia de un complejo de unión exón-exón (EJC, por sus siglas en inglés) después del codón[32]. Se ha descrito la interacción de las proteínas SR con el EJC, lo que refuerza la participación de las proteínas SR en el proceso de NMD[33].

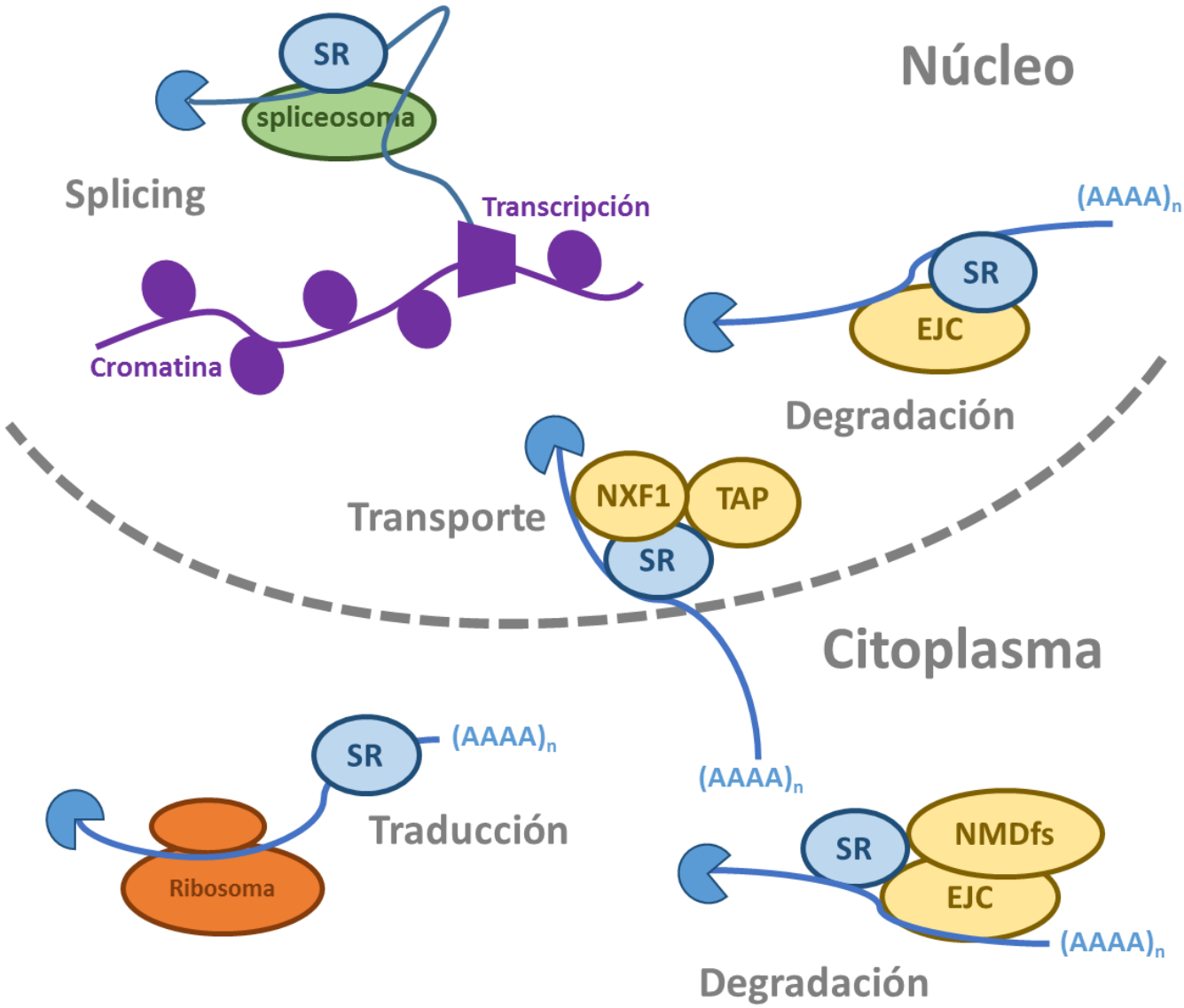

Figura 5. Las proteínas SR desempeñan múltiples funciones. Las proteínas SR intervienen en múltiples pasos del metabolismo de los RNAs, empezando por su transcripción y procesamiento en el núcleo y posterior transporte al citoplasma seguido de su traducción o degradación.

Las proteínas SR también pueden unirse a la región 5´UTR de los RNAs. Se ha descrito que mediante esta interacción, la proteína SRSF3 puede inhibir la traducción de su RNA diana cambiando la localización celular del mismo, lo que produce un descenso en la asociación del mRNA con los ribosomas encargados de la traducción[34]. Además, las proteínas SR pueden regular la traducción de forma opuesta, promoviendo la entrada del mRNA en el ribosoma[35]. Varios estudios describen también el papel de algunas proteínas SR como activadoras de la transcripción[36]. Por tanto, queda claro que las proteínas SR no son solo factores de splicing, sino proteínas multifuncionales que intervienen en diversas vías de regulación génica desde la transcripción hasta la traducción.

Las proteínas SR no solo se unen a distintas regiones de un RNA mensajero sino que también se ha visto que interaccionan con varios tipos de RNAs, incluyendo los RNAs no codificantes largos (lncRNAs) y microRNAs[21,37]. Aunque el papel funcional de las proteínas SR en la biogénesis de los ncRNA es aún bastante desconocido, esta interacción expande la visión de las proteínas SR como reguladores de la expresión génica.

Proteínas SR implicadas en cardiopatías

La expresión en el miocardio de muchas RBPs cambia en insuficiencia cardíaca, en humanos y en modelos de ratón. Esto, unido a la variedad de funciones que las proteínas SR pueden desempeñar en la regulación del metabolismo del RNA, sugiere que la bajada de expresión de estas proteínas en el corazón puede tener un papel importante en el desarrollo de la enfermedad cardíaca. De hecho, la pérdida cardio-específica de SRSF2 en un modelo de ratón, demostrada por primera vez por Ding y sus colaboradores, conduce al desarrollo de cardiomiopatía dilatada (DCM) a las 5 semanas de vida[38].

El mismo grupo demostró un año más tarde que la pérdida cardio-específica de otra proteína de la familia SR en un modelo de ratón, en este caso SRSF1, conducía al desarrollo de cardiomiopatía dilatada 6 semanas después del nacimiento y a una rápida progresión de la enfermedad, que finalmente produce la muerte del ratón a

las 8 semanas debido a una insuficiencia cardíaca. Estos autores identificaron una desregulación del splicing en un conjunto de genes relacionados con la contracción cardíaca en este modelo[39].

Por otro lado, la pérdida generalizada de SRSF10 da lugar a la aparición de severos problemas en la formación del corazón, lo que provoca que la mayoría de embriones mueran alrededor del estadio embrionario E15.5. Esto es debido a un defecto en el splicing de la triadina, el cual está regulado por SRSF10, lo que reduce sus niveles de expresión y finalmente produce un defecto en la liberación del calcio desde el retículo endoplásmico durante la contracción cardíaca[40].

La proteína SRSF4

La proteína más grande de la familia SR es SRSF4. Contiene dos dominios de unión a RNA en su extremo N-terminal encargados de determinar la especificidad de la unión de la proteína al RNA. El dominio SR, en su extremo C-terminal, modula la interacción con otras proteínas. SRSF4 se encuentra principalmente localizado en el núcleo, donde participa en el procesamiento del RNA mensajero, regulando su splicing, pero al igual que otras proteínas SR puede moverse entre el núcleo y el citoplasma para llevar a cabo sus funciones en el transporte, estabilidad y traducción de los mRNAs[41]. Como otras proteínas de la misma familia, SRSF4 fue inicialmente descrita como regulador de splicing. También puede interactuar con diferentes clases de RNA, incluyendo ncRNAs, sugiriendo un papel multifuncional en la regulación del metabolismo del RNA[37].

Durante años se pensó que los intrones no codificantes se eliminaban antes de terminar la transcripción y la polyadenilación de los mRNAs. Sin embargo, hay estudios que han demostrado la existencia de intrones en transcritos polyadenilados[42], estos intrones fueron denominados intrones retenidos (DIs). Estos pueden permanecer en el núcleo con una vida media de aproximadamente 1 hora, sin ser sensibles al punto de control del non-sense medited decay (NMD). En condiciones normales, los transcritos con DIs permanecen en el núcleo. Cuando las células son expuestas a condiciones de estrés, el splicing cambia para protegerlas y

adaptarse a la nueva situación. La traducción de DIs no codificantes puede ser activada o inhibida bajo condiciones de estrés celular. Se ha visto que SRSF4 participa en el splicing de estos intrones retenidos[43].

Se sabe que SRSF4 está asociado con la patología de algunas enfermedades neurodegenerativas llamadas tauopatías, como la enfermedad de Alzheimer o la trisomía 21. SRSF4 regula el splicing del exón 10 del mRNA del gen tau, resultando en un incremento de la isoforma anormal FTDD-17 de este gen[44]. Otro estudio muestra que, SRSF4 puede interactuar con pinin, regulando su splicing, una proteína predominante encargada de la adhesión celular en el epitelio de la córnea[45].Además, se ha descrito el papel de SRSF4 durante la diferenciación neuronal en células P19[46]. También, hay estudios que muestran que SRSF4 participa en la patogénesis de la leucemia mieloide aguda (AML) mediante la regulación del splicing de la caspasa8[47]. De igual forma, mediante la regulación del splicing alternativo de genes relacionados con diferenciación celular, se ha demostrado que SRSF4 está asociado con la proliferación de las células progenitoras hematopoyéticas[48].

Estos estudios muestran la relevancia de SRSF4 para el desarrollo neuronal, y su relación con diferentes patologías neuronales y cáncer. Sin embargo, a diferencia de otras proteínas SR, su función en el corazón aún no ha sido estudiada. Dado el importante papel de las RBPs por su capacidad para regular la expresión génica a través de una gran variedad de mecanismos post-transcripcionales, en esta tesis nos planteamos estudiar el papel de la proteína SRSF4 en el corazón.

OBJETIVOS

Objetivos

1. Estudiar la expresión de SRSF4 en el corazón sano y en enfermedad cardíaca.

2. Caracterizar la función de SRSF4 en el corazón adulto.

3. Describir el mecanismo molecular de acción de SRSF4 en el corazón adulto.

MATERIALES Y MÉTODOS

Materiales y métodos

Aislamiento del RNA y realización de qRT-PCR

Se aisló el RNA de células o tejidos usando el reactivo TRIzol (15596026, Thermo Fisher Scientific). Para la síntesis de cDNA se usaron 100 ng de RNA total por muestra con el kit de Applied Biosystems High Capacity cDNA Reverse Transcription (4368814, Thermo Fisher) que usa cebadores seleccionados aleatoriamente para la reacción (random primers). Para la PCR cuantitativa (qRT-PCR) se utilizó SYBR Green (4367659, Thermo Fisher) y el cDNA se amplificó con los primers indicados en la Tabla 1. Se usó el equipo de Applied Biosystems 7900 Fast real time PCR. Los resultados se analizaron con el programa LinRegPCR[49]. Los valores se normalizaron con GAPDH.

Histología e inmunofluorescencia

Los corazones fueron extraídos y fijados en 4% PFA (Paraformaldehido)/PBS (137 mM NaCl, 10 mM Na_2HPO_4-$2H_2O$, 2.7 mM KCl, 1.8 mM KH_2PO_4) durante 48 horas, lavados en etanol 70%, deshidratados e incluidos en parafina. Se cortaron en secciones de 5 µm. El análisis histológico de los corazones se llevó a cabo mediante tinción de tricrómico de Masson. Para la inmunofluorescencia de corazones, los cortes fueron desparafinados e incubados con aglutinina conjugada (W849, Thermo Fisher Scientific) a una dilución de 1:100. Posteriormente fueron permeabilizados con 0.3% Tritón X-100/PBS y bloqueados con solución de bloqueo que contenía 3% BSA (albúmina de suero bovino), 0.3% Tween20, 2% $MgCl_2$ y 5% de suero de cabra diluido en PBS. Los cortes se incubaron durante la noche a 4ºC con anti-troponina T cardiaca (ab58544, Abcam) a una dilución 1:200. Al día siguiente, tras lavar con PBS, se incubaron durante una hora a temperatura ambiente con el anticuerpo secundario anti-rabbit Alexa 488 (A-11034, Thermo Fisher Scientific). Para la inmunofluorescencia de cardiomiocitos neonatales, las células se sembraron en cubres previamente tratados con fibronectina (F2006, Sigma-Aldrich), y fueron fijados en 4% PFA (Paraformaldehido)/PBS (137 mM NaCl, 10 mM Na_2HPO_4-$2H_2O$,

2.7 mM KCl, 1.8 mM KH_2PO_4) durante 30 minutos. Posteriormente se bloquearon con solución de bloqueo. Los cristales fueron incubados con los mismos anticuerpos que las inmunofluorescencias de los corazones. Tanto en los cortes de tejido como en células asiladas se marcó el núcleo con DAPI (D1306, Thermo Fisher Scientific) y finalmente se añadió medio de montaje Vectashield (H-1000, Vector Laboratories). El área de los cardiomiocitos se midió usando el programa Image J.

Ratones

Los ratones SRSF4 KO fueron originalmente generados en el Mouse Clinical Institute – Institut Clinique de la Souris (France) (EMMA ID: EM: 07637). El cassette de neomicina se eliminó usando el sistema FLP-FRT para obtener una línea de ratón SRSF4 floxeado con sitios LoxP flanqueando el exón 2 de SRSF4. Esta línea se cruzó con animales C57BL/6 para eliminar el cassette FLP y la línea SRSF4 resultante fue cruzada con unos ratones transgénicos que expresan la recombinasa Cre bajo el promotor cardio específico Nkx2.5. La línea resultante fue mantenida en heterocigosis. Los ratones SRSF4 floxeados fueron usados como controles.

Los experimentos se llevaron a cabo en ratones con edades comprendidas entre los 2 y 14 meses. Los ratones se alojaron en una habitación con un ciclo de luz / oscuridad de 12 h y acceso libre a agua y comida. Los animales fueron sacrificados con cámara de dióxido de carbono. Todos los procedimientos fueron aprobados por el comité del CNIC y el gobierno de la Comunidad de Madrid (PROEX 332-15).

Cirugías

El infarto de miocardio se llevó a cabo mediante la ligación permanente de la arteria coronaria descendiente izquierda. Para ello, los ratones fueron anestesiados usando 3-3.5% de sevoflurano administrado con oxígeno al 100%, intubados y mantenidos con ventilación mecánica durante el procedimiento. La cirugía se realizó rasurando el pelo del tórax del animal, desinfectando la piel con etanol y realizando un corte en el tórax que permitiera la visualización de la arteria coronaria. Tras la

ligación de dicha arteria con una sutura no reabsorbible, se procedió a suturar al animal. Todos los animales recibieron una dosis de buprenorfrina (0.1 mg/kg) como analgesia durante los días posteriores al procedimiento.

La inducción de sobrecarga de presión se realizó mediante la ligadura de la aorta. Los ratones fueron anestesiados usando 3-3.5% de sevofluorano administrado con oxígeno al 100%, intubados y mantenidos con ventilación mecánica durante el procedimiento. Para la cirugía se rasuró el pelo de los animales, la piel se desinfectó con etanol y se procedió a la realización de un corte en el tórax que permitiese la visualización de la aorta. Para la constricción de la aorta se usó una sutura no reabsorbible de polifilamento anudado alrededor de la aorta y una aguja roma de 27-gauge. La ligadura se realizó en el cayado aórtico entre la arteria carótida y la arteria innominada. Después de realizar la ligadura, la aguja de 27-gauge se retiró dejando la aorta constreñida al diámetro de la aguja. Posteriormente, se procedió a la sutura de las capas musculares y la piel para cerrar el tórax del animal. Todos los animales recibieron una dosis de buprenorfrina (0.1 mg/kg) como analgesia durante los días posteriores al procedimiento.

Análisis ecocardiográfico

Para el estudio ecográfico se adquirieron imágenes en modo M y en modo bidimensional utilizando un ecógrafo de alta resolución con un transductor de 30 Mhz (Vevo 2100, VisualSonics Inc., Canada). Los ratones fueron anestesiados con isoflurano (Esteve Veterinaria, Proyma Ganadera S.L., Ciudad Real, España) y emplazados en una placa térmica ajustada a 38.3ºC para mantener la temperatura corporal en condiciones de normotermia. El isoflurano se administró con oxígeno al 100%, a través de una mascarilla nasal y utilizando inicialmente una concentración de isoflurano del 2% para la inducción, y del 1.5% para el mantenimiento. La frecuencia cardiaca (FC) se monitorizó constantemente, utilizando 4 electrodos conectados a la placa térmica. La concentración de isoflurano administrado se ajustó con el objetivo de mantener la FC en 450-550 latidos por minuto, para mantener al ratón en un plano superficial durante la adquisición de las imágenes ecográficas. Tras las ecografías los animales fueron mantenidos en una caja aislada iluminada con luz

roja hasta que se despertaron, para asegurar su correcta recuperación y el mantenimiento de su temperatura corporal. El análisis de las imágenes también se hizo de forma ciega, utilizando la estación de trabajo del equipo (Vevo 2100 analysis software, VisualSonic, Toronto, Canadá).

Electrocardiogramas (ECGs)

Los ECG se obtuvieron en ratones SRSF4 KO y control anestesiados con isoflurano, utilizando cables de extremidades bipolares (cables I, II y III) y cables de extremidades unipolares (cables aVR, aVL y aVF), durante 5 minutos en condiciones basales (MP36R, BIOPAC Systems, Inc.). Posteriormente, se inyectó por vía intraperitoneal isoproterenol (I6504, Sigma-Aldrich) (1,5 mg / kg), y se midió la actividad eléctrica durante 15 minutos. Los ECG fueron analizados por un experto ciego utilizando Acqknowledge 4.1.1 para MP36R (BIOPAC Systems, Inc.). Los valores medios se calcularon a partir de 10 intervalos de tiempo y ondas de ECG estándar consecutivos.

RNA-Seq

Para la secuenciación del RNA (RNA-Seq), se extrajo RNA total de corazones SRSF4 KO y control a 2 meses de edad. En el caso de SRSF10 se extrajo RNA total de corazones infartados y sobreexpresantes del virus AAV9-SRSF10 o control, 28 días tras el infarto. La extracción se realizó con el kit de aislamiento de RNA de Qiagen (74104, Qiagen), tratando las muestras con DNAsa. Se aisló RNA de 3 ratones para cada condición. El proceso de secuenciación fue realizado por la Unidad de Genómica del CNIC. Las librerías se prepararon haciendo selección positiva por polyA y la secuenciación se llevó a cabo usando la plataforma Illumina-Hiseq y asegurando 15 millones de lecturas por muestra. El alineamiento de las lecturas fue realizado por la Unidad de Bioinformática del CNIC. Para ello, las lecturas se mapearon en el transcriptoma de ratón GRCm38 y se cuantificaron usando RSEM v1.2.3. El análisis de expresión diferencial se realizó usando el paquete edgeR Bioconductor. Se

consideraron cambios significativos aquellos con un p valor ajustado <0.05. El análisis de ontología genética se realizó usando el recurso libre GOrilla.

Producción de RNA modificado

La producción y purificación de los RNAs modificados (modRNA) se realizó usando el kit de transcripción MegaScript T7 (AM1334, Thermo Fisher Scientific). Para evitar la activación de la vía de señalización del interferón se incluyeron dos nucleótidos modificados: 5-methyl-CTP y pseudo-UTP (N-1014 y N-1019, Trilink). Estos nucleótidos producen un cambio en la estructura de la cadena de RNA que evita su detección por parte del sistema del interferón, a la vez que permite su traducción por el ribosoma[50,51]. Así mismo, se añadió un grupo CAP al inicio del tránscrito durante el proceso de transcripción in vitro. No obstante, se ha descrito que este proceso sólo es eficiente aproximadamente en un 60% de las moléculas, por lo que los tránscritos producidos requerían ser desfosforilados tras su purificación. La desfosforilación de los RNA se realizó a 37ºC durante 30 minutos en un bloque térmico usando fosfatasa alcalina (M0289S, NEB). Tras la desfosforilación los transcritos fueron purificados con el kit MEGAclear Transcription Clear-Up (AM1908, Thermo Fisher Scientific).

iCLIP

Cardiomiocitos neonatales de animales wild type C57BL/6 fueron aislados como se describe previamente[52]. Un total de 8 millones de cardiomiocitos neonatales fueron sembrados en placas de 10 cm^2. Al día siguiente, las células fueron transfectadas con 15 µg de SRSF4-GFP modRNA usando 21 µl de Lipofectamina 2000 (11668027, Thermo Fisher Scientific). Tras 48 horas, las células fueron irradiadas una vez con 100 mJ de luz UV (254 nm), y el protocolo del iCLIP se llevó a cabo como se describió anteriormente[53]. Brevemente, El RNA irradiado con luz UV fue digerido con RNasaI (Ambion) para producir fragmentos de 80-200 nucleótidos, y los complejos RNA-proteína fueron inmunoprecipitados con Protein G Dynabeads anti-GFP® (ThermoFisher Scientific). Los fragmentos de RNA fueron entonces ligados a

un adaptador 3´ de DNA pre-adenilado (IDT) y retrotranscritos usando unos primers-RT barcoded y SuperscriptIV (ThermoFisher Scientific). Tras la selección del tamaño, los fragmentos de cDNA fueron circularizados usando CircLigaseTM (Epicentre) y relinearizados con BamHI (NEB). Las librerías finales de cDNA que contenían adaptadores en 5´ y 3´ fueron amplificadas usando AccuPrime (ThermoFisher Scientific), y fueron secuenciadas en la máquina Illumina HiSeq2000 (single-end 75 nucleotide reads, 20 millones de reads por réplica). La secuenciación fue llevada a cabo en la Universidad de Dresden, Alemania. El alineamiento de las lecturas fue realizado por la Unidad de Bioinformática del CNIC, usando Bowtie (version 0.10.1).

Construcciones de DNA

La construcción de la quimera SRSF4-GFP se realizó mediante la amplificación de SRSF4 y su inserción en pEGFP-N1. El clonaje de los cDNAs para la producción de RNA modificados se realizó según el protocolo descrito por Pankaj K. Mandal y Derrik Rossi[54]. Brevemente, la región codificante de GFP o SRSF4-GFP fue fusionada a una región 5'UTR que contenía un sitio de unión para la T7 polimerasa junto a una secuencia Kozak, y a la región 3'UTR de la alfa globina para favorecer unos altos niveles de expresión. El cDNA de GAS5 se obtuvo de la empresa abm (ORF020064).

Las construcciones de los virus adeno-asociados (AAV) se realizaron clonando SRSF4, tras el promotor de troponina T cardiaca en un vector que contiene las secuencias ITR necesarias para el empaquetamiento del DNA dentro de la cápsida viral. A continuación de SRSF4 se clonó IRES-Luciferasa para que el DNA tuviera el tamaño óptimo para su empaquetamiento. El virus contienen al final de las secuencias codificantes el polyA de SV40.

Todas las amplificaciones por PCR se realizaron usando el kit de alta fidelidad KAPA HiFi HotStart ReadyMixPCR kit (KR0370, Kapa Biosystems) y se clonaron en el vector pGEM-T Easy (A1360, Promega) para proceder a su secuenciación antes de clonarlos en el vector final.

Aislamiento de cardiomiocitos, transfecciones y tratamientos in vitro

Los cardiomiocitos neonatales fueron extraídos de ratones SRSF4 y control el mismo día del parto o un día después según el protocolo previamente descrito[52]. Brevemente, se extrajeron los corazones en el mismo día del nacimiento de la cría de ratón o un día después, se hicieron digestiones parciales con colagenasa Tipo 2 (LS004176, Worthington) y se fueron guardando las células extraídas en suero fetal bovino hasta la completa digestión de los corazones. Se sembraron las células en placas de 10 cm2 pretratadas con gelatina 1% y se mantuvieron en medio DMEM suplementado con 20% medio 199, 15% suero fetal bovino, 15% HEPES (ácido 4-(2-hidroxietil)-1-piperazinaetanosulfónico) y 2 mM L-glutamina. Al día siguiente las células fueron tratadas con 100 μM dexametasona (DEX) (D4902, Sigma-Aldrich) o DMSO (D2650, Sigma-Aldrich), durante 72 horas. Para los experimentos de sobrexpresión de GAS5 las células fueron transfectadas con GAS5modRNA o el modRNA control usando Lipofectamina 2000 (11668027, Thermo Fisher Scientific), un día después del tratamiento con DEX. Para los experimentos de estabilidad de GAS5, las células fueron tratadas con 10 μg/mL actinomicina D (ActD) (A9415, Sigma), comenzando 24 horas tras el aislamiento celular, y las células fueron recogidas 0, 4, 8 y 14 horas tras el tratamiento.

Western Blot

Los cardiomiocitos neonatales fueron aislados de corazones de ratones wild type. Posteriormente fueron lisados con RIPA (150 mM NaCl, 1% IGEPAL, 0.5% deoxicolato sódico, 0.1% SDS y 50 mM Tris pH 8.0) en presencia de inhibidores de proteasas (04693159001, Roche Diagnostics). Los lisados fueron separados en geles SDS-PAGE y transferidos a membranas PVDF (polifluoruro de vinilideno). El bloqueo se realizó con solución de leche en polvo desnatada al 3% en PBS. La incubación con el anticuerpo primario, anti-SRSF4 (NBP2-04144, Novus Biologicals), se realizó durante toda la noche a 4ºC, y al día siguiente se incubó con el anticuerpo secundario marcado con HRP (anti-rabbit P0448, Dako) durante una hora a temperatura ambiente. Las membranas se revelaron utilizando el reactivo ECL (RPN2106, GE

Healthcare Life Sciences). El brillo y contraste de las membranas ha sido ajustado linealmente utilizando PowerPoint.

Producción de virus adeno-asociados

La producción de los virus adeno-asociados se llevó a cabo en la Unidad de Vectores Virales del CNIC en el caso de SRSF4, a quienes se les proporcionaron las construcciones de DNA de los mismos. Previamente se comprobó la correcta secuencia de los ITRs mediante digestiones con BglI y AhdI. La producción vírica se llevó a cabo en células HEK293 y utilizando las proteínas de la cápsida de serotipo 9. El título obtenido fue de $7.41 \cdot 10^{12}$ partículas virales (VP)/ml para AAV-SRSF4.

Inyección de virus adeno-asociados por vena femoral

Para la administración de los virus adeno-asociados se anestesió a los ratones usando 3-3.5% de sevoflurano administrado con oxígeno al 100%. Se mantuvo al ratón bajo anestesia hasta el final de la inyección utilizando una mascarilla nasal. Para la administración del virus se desinfectó la piel del ratón con etanol y se realizó un corte en la piel de la extremidad trasera que permitiese visualizar la vena femoral. A través de dicha vena se inyectó un total de 50 µl por ratón, conteniendo $1 \cdot 10^{11}$ partículas virales (VP). Al finalizar se suturó la piel del animal y se esperó a la completa recuperación de la anestesia antes de devolverlo a su caja. AAV-SRSF4.

Muestras de pacientes

Para averiguar si pacientes con hipertrofia idiopática mostraban mutaciones en SRSF4 se usaron muestras de sangre de 98 pacientes gracias a la colaboración con el Dr. Pablo García Pavía del Hospital Puerta de Hierro de Majadahonda. Se extrajo el DNA genómico, se amplificó cada exón, y se secuenció por el método de Sanger. Para determinar la expresión de SRSF4 en algunos de estos pacientes se extrajo tejido cardíaco y se aisló el RNA del tejido para posteriormente cuantificar la

expresión de RNA mensajero de SRSF4 por qRT-PCR. En cuanto a los resultados de los pacientes con enfermedad de Cushing, con la ayuda de Carlos Martí, se extrajeron los datos crudos publicados previamente en GEO, cuyo número de acceso es GSE66446, y se generó la gráfica a partir de estos resultados.

Análisis estadístico

Para el análisis estadístico de los datos se usaron: T-Test para dos condiciones a un tiempo, ANOVA de 1 vía seguido del post-test de Bonferroni para más de dos condiciones a un tiempo, y ANOVA de 2 vías seguido del post-test de Bonferroni para análisis de múltiples condiciones y dos variables, como se indica en la leyenda de las figuras. El test de Fisher se usó para asociar dos variables cualitativas. Los datos se analizaron con GraphPad Prism 5.0 y los cambios se consideraron significativos a partir de $p<0.05$.

Tabla 1. Secuencia de los primers de SYBR Green utilizados para la qRT-PCR (5'-3').

Gen	Forward	Reverse
SRSF4	GATCCTGGAGGTGGATCTGA	ACAGGTCTTTGCCGTTCAGT
GAPDH	CTGCACCACCAACTGCTTAG	AGATCCACGACGGACACATT
BNP	GCCAGTCTCCAGAGCAATTC	TCTTTTGTGAGGCCTTGGTC
MYH7	CAACTGGAGGAGGAGGTCAA	CCTCTGTATGGCATCCGTCT
GAS5	TCTCACAGCCAGTTCTGTGG	TCTGGTCTTCTATTCTAGCACATTG
ANF	GATGGATTTCAAGAACCTGCT	CCTGCTTCCTCAGTCTGCTC
Fkbp5	CGAAGGAGCAACGGTAAAAG	ATCGGAATGTCGTGGTCTTC
Gilz	AGGCCATGGACCTCGTGA	TCAGGTGCTGGCTCTTCAG

RESULTADOS

Caracterización de la expresión de SRSF4 en el corazón sano y en enfermedad cardíaca

Expresión y localización de SRSF4 en el corazón

Para el estudio de la expresión de SRSF4 en el corazón, se extrajeron corazones de ratones C57BL/6 a distintos tiempos comprendidos entre el estadío embrionario E12.5 hasta los 6 meses de edad y se cuantificaron por qRT-PCR los niveles de expresión del mRNA de SRSF4. Los resultados mostraron que la expresión de SRSF4 es mayor durante el desarrollo embrionario y en general decrece progresivamente hasta la etapa adulta (Figura 6A).

Para el estudio de la localización de SRSF4 en el corazón, se hicieron cortes histológicos de corazones C57BL/6 a distintos estadíos del desarrollo embrionario, que es cuando más se expresa SRSF4. Los anticuerpos usados no fueron capaces de reconocer la proteína de SRSF4 en tejido cardíaco por inmunohistoquímica ni inmunofluorescencia. Por ello se llevó a cabo un aislamiento de cardiomiocitos neonatales para medir la expresión de la proteína de SRSF4 por WB. Los resultados mostraron que al menos la proteína de SRSF4 se expresa en cardiomiocitos (Figura 6B).

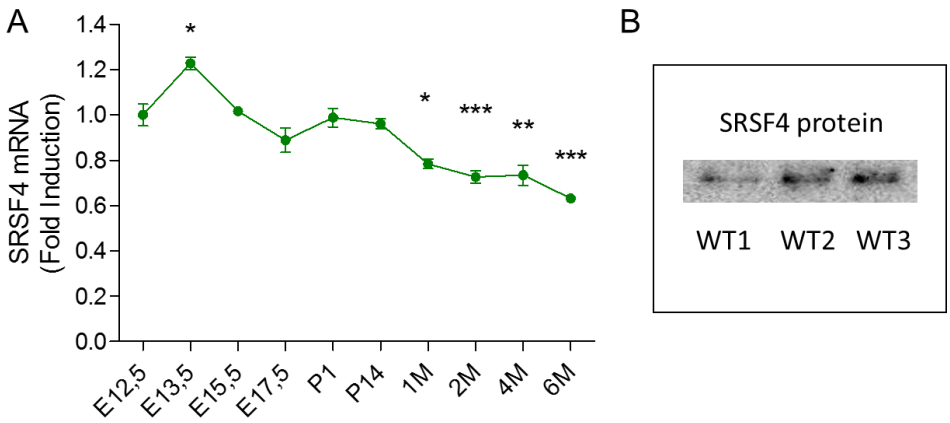

Figura 6. Expresión de SRSF4 en animales wild type. **A**, La expresión de SRSF4 se cuantificó por qRT-PCR en corazones extraídos de ratones C57BL/6 de distintas edades desde estadíos embrionarios (E) hasta días (P) y meses (M) post-parto. Los datos están representados como la media ±SEM. n=3-4 ratones por grupo. *p<0.05, **p<0.01, ***p<0.001 vs E12.5, ANOVA de una vía con test de Bonferroni de comparación múltiple. B, Expresión de la proteína SRSF4 en cardiomiocitos neonatales aislados por Western Blot en tres muestras (WT1, WT2, WT3).

Expresión de SRSF4 en enfermedad cardíaca

Para investigar la posible relación entre SRSF4 y la patología cardíaca, se decidió estudiar su expresión en el infarto de miocardio. Para ello se midió la expresión del mRNA de SRSF4 por qRT-PCR en ratones en los que se les indujo un infarto de miocardio por ligación permanente de la arteria coronaria descendente izquierda. Los resultados mostraron que la expresión de SRSF4 no cambia ni a 7 ni a 28 días después del infarto (Figura 7A).

Además, se estudió la expresión de SRSF4 en el miocardio tras la inducción de hipertrofia cardiaca patológica, la cual se indujo mediante constricción aórtica (TAC). De la misma forma, la expresión de SRSF4 no cambió pasados 21 días tras la cirugía (Figura 7B).

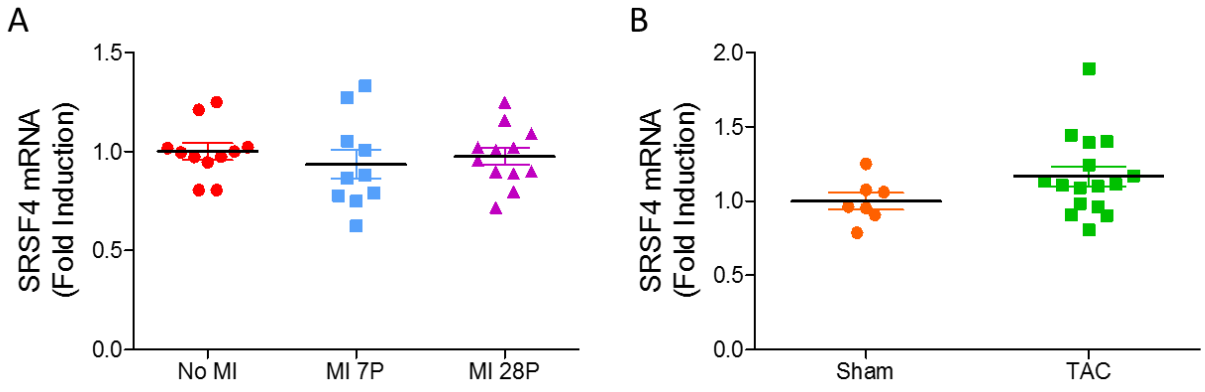

Figura 7. La expresión de SRSF4 no cambia después del infarto de miocardio (MI) ni tampoco en un modelo de hipertrofia inducida por constricción aórtica (TAC). A, Análisis por qRT-PCR de la expresión cardíaca de SRSF4 en animales no infartados (No MI) y en animales a 7 y a 28 días tras el infarto (MI 7P y MI 28P). Los datos están representados como la media ±SEM. Cada símbolo representa un ratón. **B**, Análisis por qRT-PCR de la expresión cardíaca de SRSF4 en animales control (Sham) y animales con constricción aórtica (TAC) 21 días después de la cirugía. Los datos están representados como la media ±SEM. Cada símbolo representa un ratón. No se encontraron cambios estadísticamente significativos ni en A ni en B.

Caracterización de la función de SRSF4 en el corazón

La pérdida cardio-específica de SRSF4 induce una hipertrofia del ventrículo izquierdo

Para estudiar el papel de SRSF4 en el corazón, se cruzaron ratones que contenían sitios loxP flanqueando el exón 2 del gen de SRSF4 con ratones transgénicos que sobreexpresaban la recombinasa Cre bajo el promotor de Nkx2.5. De esta forma se generó un modelo de ratón knockout (KO) cardio-específico para SRSF4 (SRSF4 KO). La pérdida cardio-específica de SRSF4 no afectó a la viabilidad de los ratones. Se comprobó por qRT-PCR la bajada de expresión de SRSF4 en el corazón de los ratones SRSF4 KO comparada con los ratones control (Figura suplementaria 1).

Se hicieron ecocardiografías de los ratones control y los SRSF4 KO a diferentes edades en un rango comprendido entre los 2 meses y los 14 meses. El análisis del resultado mostró que la pared del ventrículo izquierdo de los ratones KO era significativamente más gruesa que la de los controles. Al normalizar con el peso del cuerpo, los ratones SRSF4 KO presentaban un aumento de la masa cardíaca. En consonancia con los resultados ecocardiográficos, los corazones KO se ven más gruesos a la lupa y por histología y mostraron un incremento en la expresión de marcadores de enfermedad cardiaca BNP y MYH7 (Figura 8A-D y tabla suplementaria 1).

Para comprobar si el fenotipo observado se debe a un problema cardiaco o está asociado a otros factores externos, se midió la presión arterial a 2 y 4 meses en los ratones KO y control. Los resultados no mostraron ningún cambio significativo entre los grupos, sugiriendo que el fenotipo observado está asociado a un problema intrínseco en el corazón (Figura 9A-B).

Con el objetivo de averiguar si el incremento en las paredes del corazón que observamos por ecocardiografía estaba asociado con un incremento del tamaño de los cardiomiocitos, se hicieron cortes histológicos de los corazones SRSF4 KO y control para medir el área de los cardiomiocitos. Los resultados mostraron que los ratones KO presentan un incremento del tamaño de los cardiomiocitos. Además

detectamos focos de fibrosis en el ventrículo izquierdo de los ratones SRSF4 KO a los 10 meses de edad (Figura suplementaria 2).

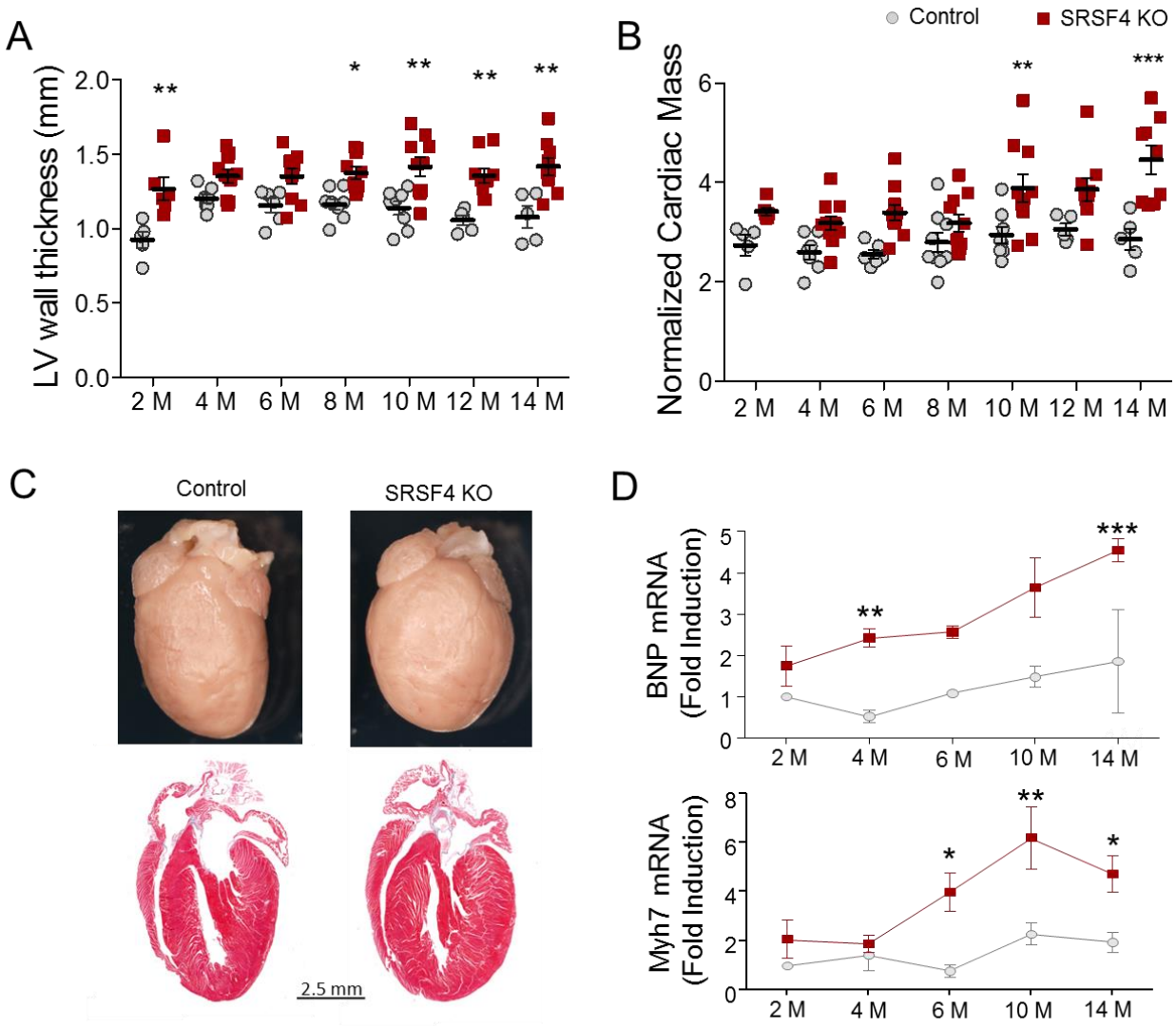

Figura 8. La pérdida cardio-específica de SRSF4 lleva a una hipertrofia del ventrículo izquierdo. A-B, Análisis ecocardiográfico en los animales control y en los SRSF4 KO del grosor de las paredes del ventrículo izquierdo (A), y la masa cardíaca normalizada con el peso del cuerpo del ratón (B). Los datos están representados como la media ±SEM. Cada símbolo representa un animal. *p<0.05, **p<0.01, ***p<0.001 SRSF4 KO vs Control. ANOVA de dos vías con post-test de Bonferroni. **C**, Imagen e histología con tinción tricrómica de Masson representativa de corazones control y SRSF4 KO a 6 meses de edad. **D**, Análisis por qRT-PCR de la expresión cardíaca del RNA mensajero de BNP y Myh7 en animales control y SRSF4 KO. Los datos están representados como la media ±SEM. n=4-5 ratones por grupo. *p<0.05, **p<0.01, ***p<0.001 SRSF4 KO vs Control. ANOVA de dos vías con post-test de Bonferroni. M, meses.

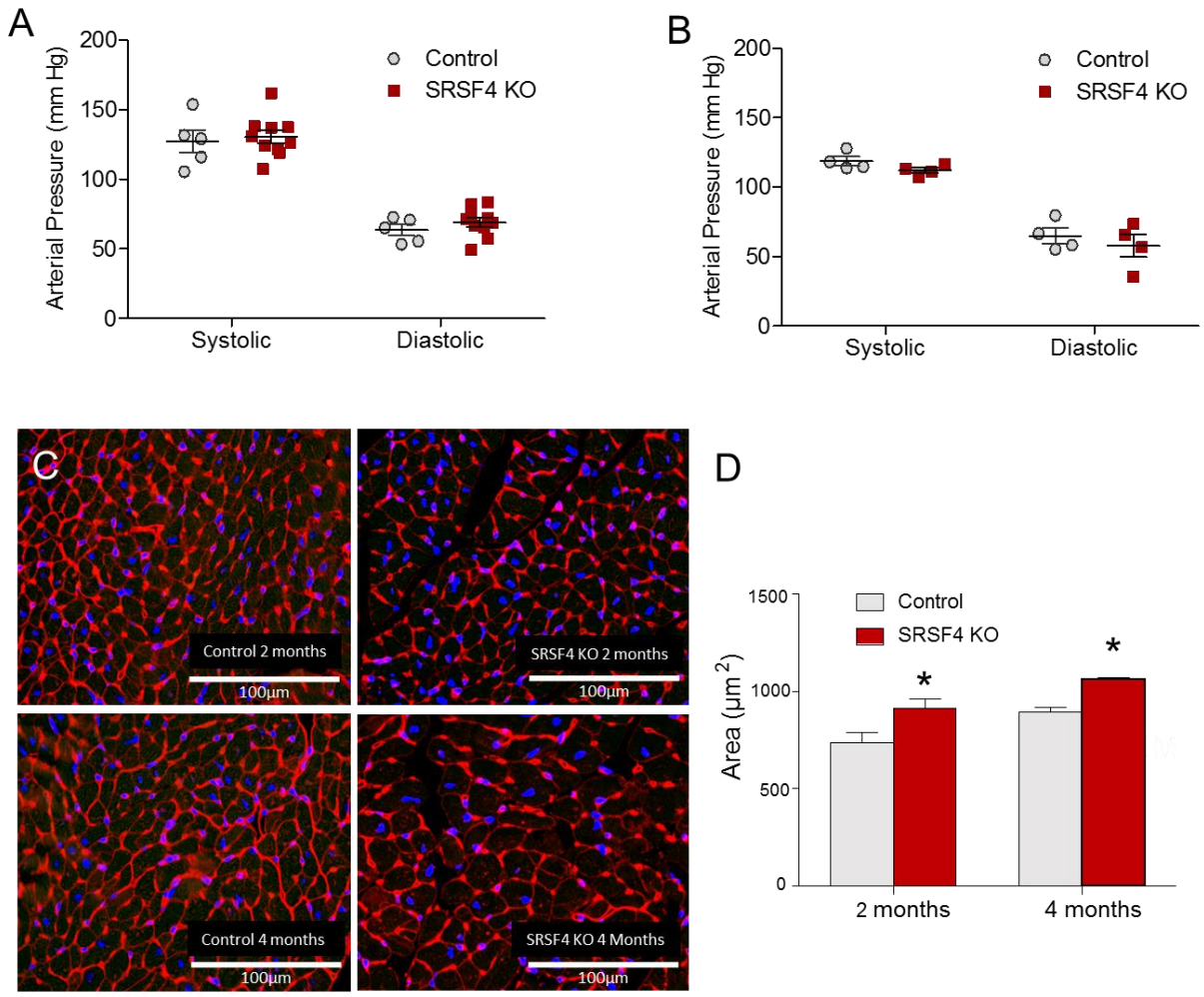

Figura 9. La hipertrofia de los ratones SRSF4 está asociada a un incremento del área del cardiomiocito. A-B, Presión arterial medida en la cola de los animales en un equipo BP2000 (Visitech Systems) a 2 (A) y 4 meses (B) de edad en ratones control y SRSF4 KO conscientes. Los datos se han expresado como media ±SEM, $p>0.05$. No se encontraron diferencias estadísticamente significativas ($p<0,05$) en un ANOVA de dos vías. Cada símbolo representa un ratón. **C**, Inmunofluorescencias representativas de cortes histológicos del corazón de ratones control y SRSF4 KO a 2 y 4 meses. WGA (rojo) y DAPI (azul). **D**, Análisis de la medida del área de los cardiomiocitos de ratones control y KO a 2 y 4 meses. Los datos están representados como la media ±SEM. *$p<0.05$ SRSF4 KO vs Control. ANOVA de dos vías con post-test de Bonferroni.

La sobreexpresión de SRSF4 tras la constricción de la aorta no reduce la hipertrofia patológica

Tras el fenotipo observado, y a pesar de que no observamos una bajada de SRSF4 tras la constricción de la aorta (TAC), se investigó si la sobrexpresión de SRSF4 podría reducir la hipertrofia en un modelo en el cual la hipertrofia se indujo por constricción aórtica. Para ello se generó un virus adenoasociado serotipo 9 (AAV9), que contenía el promotor TnT para sobrexpresar SRSF4 de forma cardio-específica. Primero se comprobó que había sobrexpresión de SRSF4 por qRT-PCR en animales no sometidos a cirugía a distintos tiempos tras la inyección del virus (Figura 10A). Tras comprobar que había sobrexpresión de SRSF4, se realizaron las cirugías por constricción aórtica. La inyección del virus se produjo dos días después de la cirugía. Se llevó a cabo un análisis ecocardiográfico de animales control y animales sometidos a cirugía a los que se les había inyectado el virus control y el virus sobrexpresante de SRSF4. Los resultados mostraron que la sobreexpresión de SRSF4 no reducía la hipertrofia del ventrículo izquierdo (Figura 10B-D).

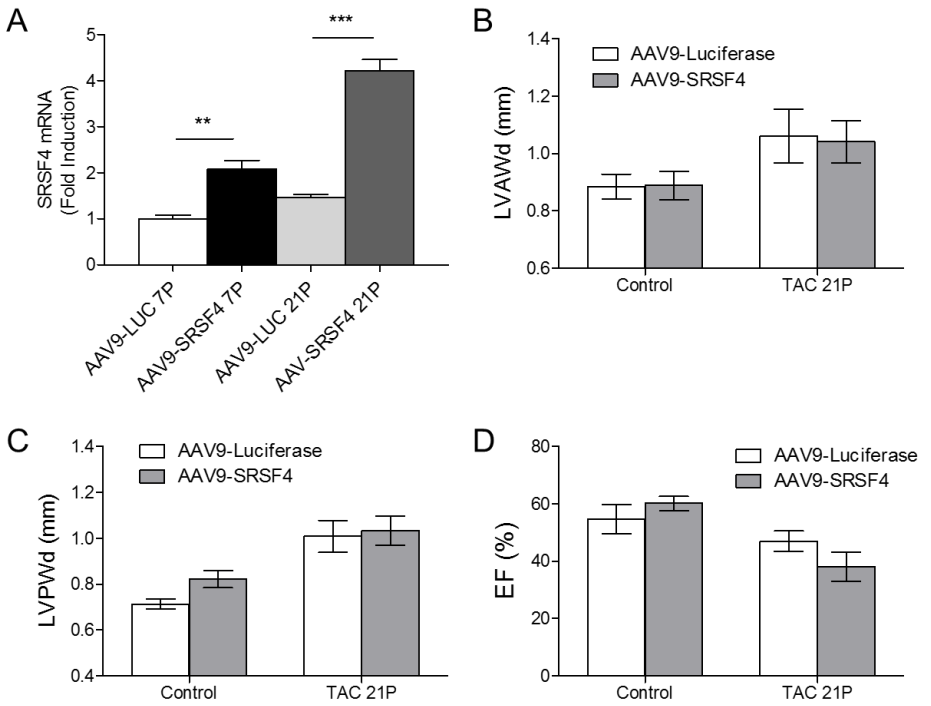

Figura 10. Efecto de la sobrexpresión de SRSF4 tras la constricción de la aorta. A, Análisis por qRT-PCR de la expresión cardiaca de SRSF4 en animales wild type inyectados con el virus control (AAV9-LUC) y el virus sobrexpresante de SRSF4 (AAV9-SRSF4) a 7 y 21 días tras la inyección. N=3-4 ratones. **p<0.01, ***p<0.001 AAV9 SRSF4 vs AAV9 LUC. ANOVA de dos vías con post-test de Bonferroni. **B-**

D, Análisis ecocardiográfico del grosor de las paredes del ventrículo izquierdo (B, C), y la función sistólica (D) en los animales control y con TAC 21 días tras la cirugía, con virus control y virus sobrexpresante de SRSF4. Los datos están representados como la media ±SEM. n=3-5 ratones por grupo. No se encontraron diferencias estadísticamente significativas con una ANOVA de dos vías con post-test de Bonferroni.

Los ratones SRSF4 KO desarrollan disfunción diastólica

Con el fin de estudiar si la hipertrofia observada en los ratones SRSF4 KO podría conducir a una disfunción cardíaca, se analizó la función sistólica y diastólica por ecocardiografía en los ratones control y los SRSF4 KO (Figura 11A-D). La pérdida de SRSF4 no alteró la función sistólica como muestran los datos de fracción de eyección del ventrículo izquierdo (Fig. 11A). Tampoco encontramos cambios significativos del volumen en diástole del ventrículo izquierdo entre ambos grupos. Para analizar la función diastólica se midió la relación entre las ondas E y A del flujo mitral y el tiempo de relajación isovolumétrico (IVRT). De esta forma se vio que el número de ratones con un flujo mitral normal decrecía en los SRSF4 KO comparado con los controles mientras que el IVRT incrementaba. Estos resultados demuestran que aunque los ratones SRSF4 KO no desarrollan disfunción sistólica, la función diastólica se ve alterada con el tiempo.

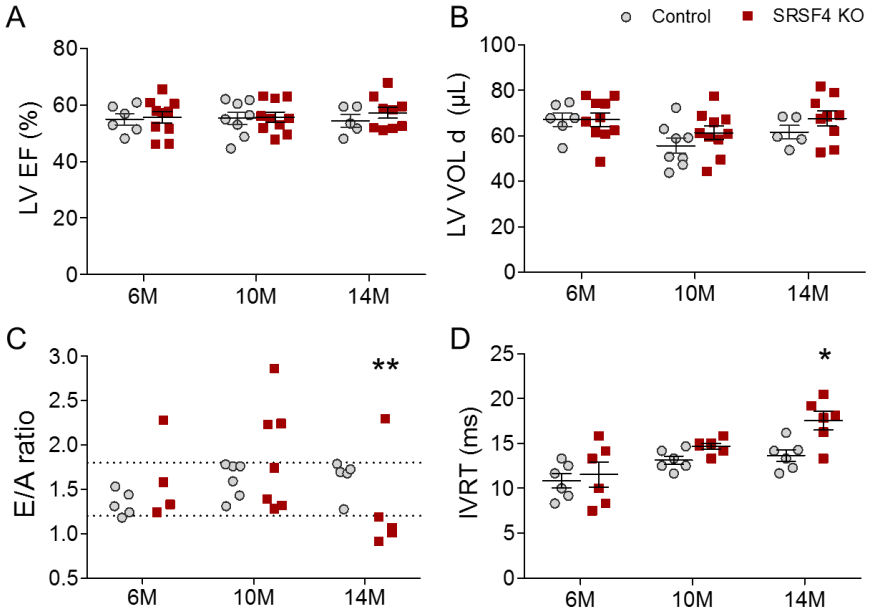

Figura 11. Análisis de la función cardíaca del ventrículo izquierdo. A, Fracción de eyección del ventrículo izquierdo. **B**, Volumen en diástole del ventrículo izquierdo. **C**, E/A ratio del flujo mitral,

considerando flujo normal el comprendido entre 1.2 y 1.8. **p<0.01 normal E/A ratio (1.2-1.8) vs anormal, Fisher's test. **D**, Tiempo de relajación isovolumétrico. En A, B y D los datos están representados como la media ±SEM. *p<0.05 SRSF4 KO vs Control. Cada símbolo representa un ratón. ANOVA de dos vías con post-test de Bonferroni.

Los ratones SRSF4 KO muestran características electrofisiológicas de hipertrofia cardíaca y una repolarización anormal

Para estudiar si la hipertrofia causada por la pérdida de SRSF4 puede llevar a una alteración de la actividad electrofisiológica del corazón, se hizo un estudio electrocardiográfico a los ratones control y SRSF4 KO en condiciones basales y de estrés cardíaco (Figura 12A).

Los ratones KO mostraron un incremento significativo del ritmo cardíaco y un ensanchamiento del complejo QRS, que es una característica de la hipertrofia cardíaca. La condición de estrés cardíaco fue simulada farmacológicamente por inyección intraperitoneal de isoproterenol. Bajo estas condiciones los ratones SRSF4 KO presentaron una repolarización anormal, como se pudo observar por un alargamiento del intervalo QT, así como una depresión ST con una onda J negativa, que está normalmente relacionado con una isquemia subendocárdica (Figura 12B-E). Estos resultados muestran que la pérdida de SRSF4 provoca una actividad electrofisiológica anormal asociada con una hipertrofia cardíaca patológica y una prolongación del intervalo QT con depresión ST en condiciones de estrés, lo cual está asociado con un incremento del riesgo de padecer muerte súbita.

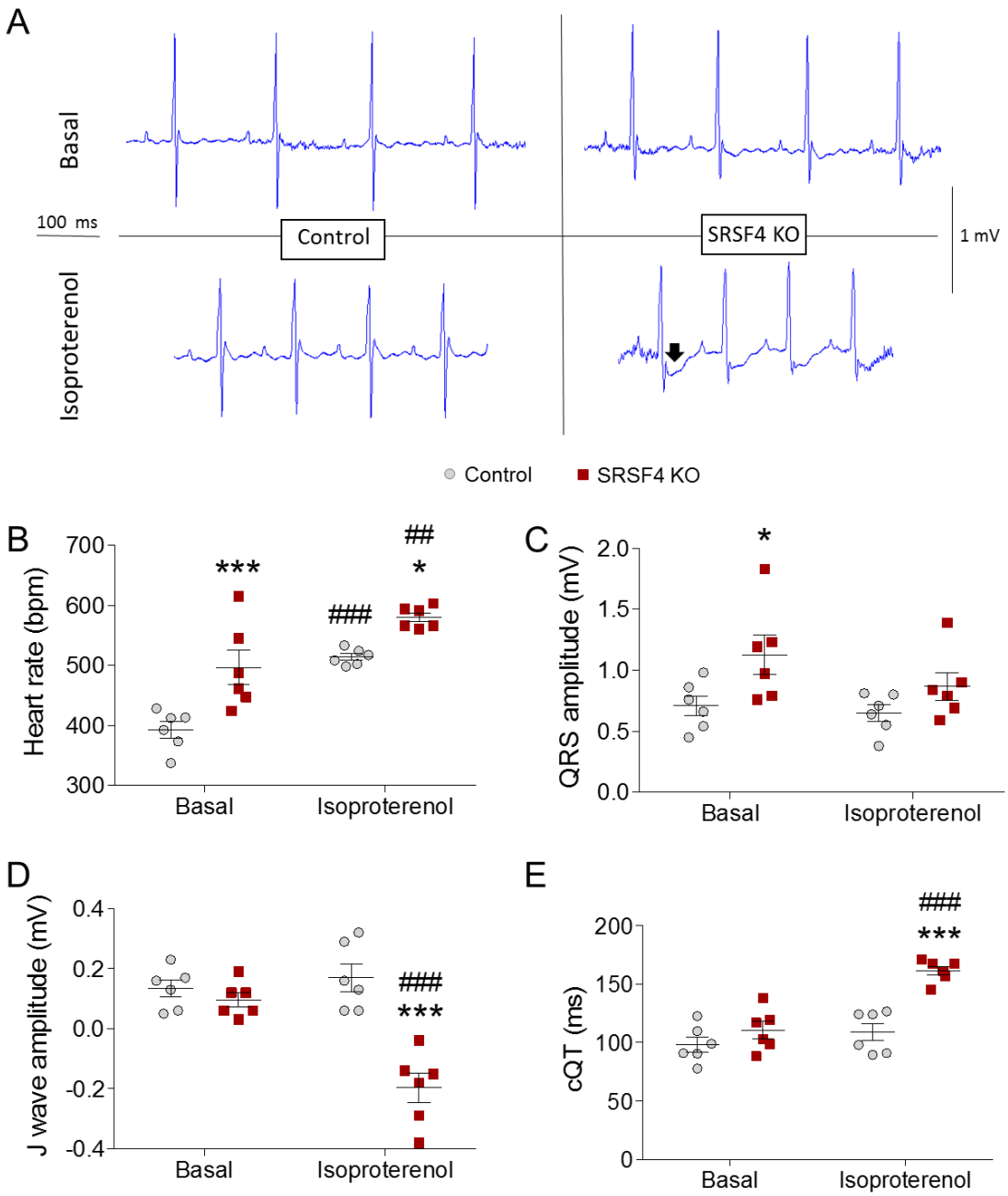

Figura 12. Los ratones SRSF4 KO desarrollan alteraciones electrofisiológicas. A, ECGs representativos de ratones control y KO en condiciones basales y tras inyección de isoproterenol. La flecha marca la depresión tras el complejo QRS. B-E, Análisis de la frecuencia cardíaca (B), Amplitud QRS (C), Amplitud de la onda J (D), y el intervalo QT corregido (E) en condiciones basales y con isoproterenol. Los datos están representados como la media ±SEM. Cada símbolo representa un ratón a los 6 meses de edad. *p<0.05, ***p<0.001, SRSF4 KO vs control; ##p<0.01, ###p<0.001, isoproterenol vs basal; ANOVA de dos vías con post-test de Bonferroni.

Caracterización del mecanismo molecular de acción de SRSF4 en el corazón

El lncRNA GAS5 es una diana directa de SRSF4 en cardiomiocitos y su expresión baja en los ratones KO

Con el objetivo de estudiar el mecanismo molecular de acción de SRSF4 por el cual los ratones SRSF4 KO desarrollaban hipertrofia del ventrículo izquierdo, se llevó a cabo un análisis por RNA-seq para comparar el patrón de expresión génica entre los corazones de los ratones control y los KO a los 2 meses de edad. Se detectaron cambios de expresión en 858 genes (Tabla Suplementaria 2), incluyendo un número significativo de RNAs largos no codificantes (lncRNAs). El análisis de ontología genética (GO) de los genes diferencialmente expresados en los ratones KO, muestra un enriquecimiento en genes asociados con el transporte de sodio, vasoconstricción y regulación del potencial de acción (Figura 13A-C).

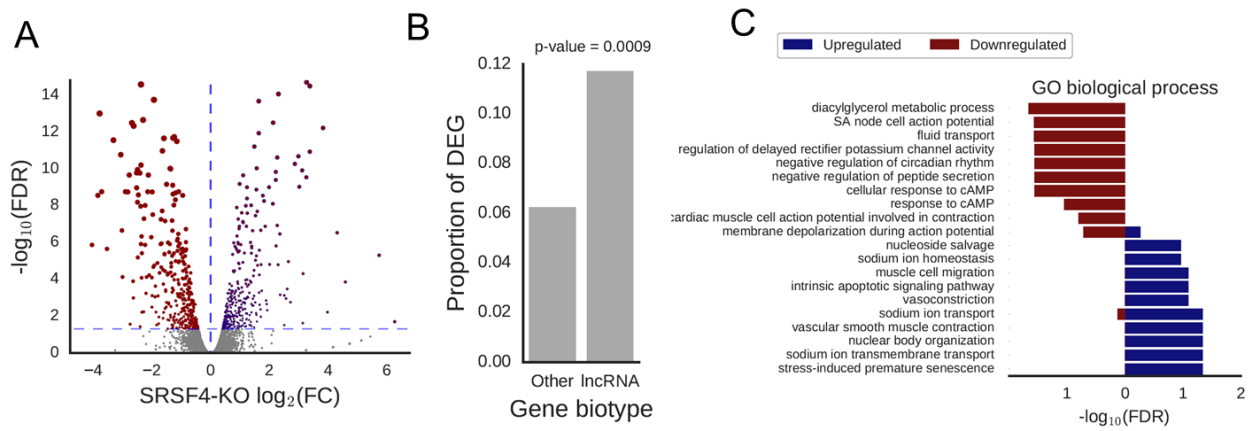

Figura 13. Genes diferencialmente expresados en el ratón KO de SRSF4. A, Volcano plot para los resultados del análisis de expresión diferencial de genes. Los puntos corresponden con los genes que se consideran diferencialmente expresados (DEG) en el SRSF4 KO, en rojo y azul se encuentran los que tienen un p-valor ajustado <0.05. **B**, Proporción de genes anotados como lncRNAs en Ensembl, comparados con anotaciones diferentes, entre aquellos diferencialmente expresados en el ratón KO. Test de Fisher. **C**, Análisis de GO donde se ven representadas las principales categorías enriquecidas en los DEG en el ratón KO de SRSF4.

El ánalisis del splicing alternativo en los corazones de los ratones control y SRSF4 KO, sin embargo, reveló cambios de isoformas significativos en pocos genes, sugiriendo que el splicing no estaba severamente afectado por la pérdida de SRSF4 (Tabla Suplementaria 3, Figura 14).

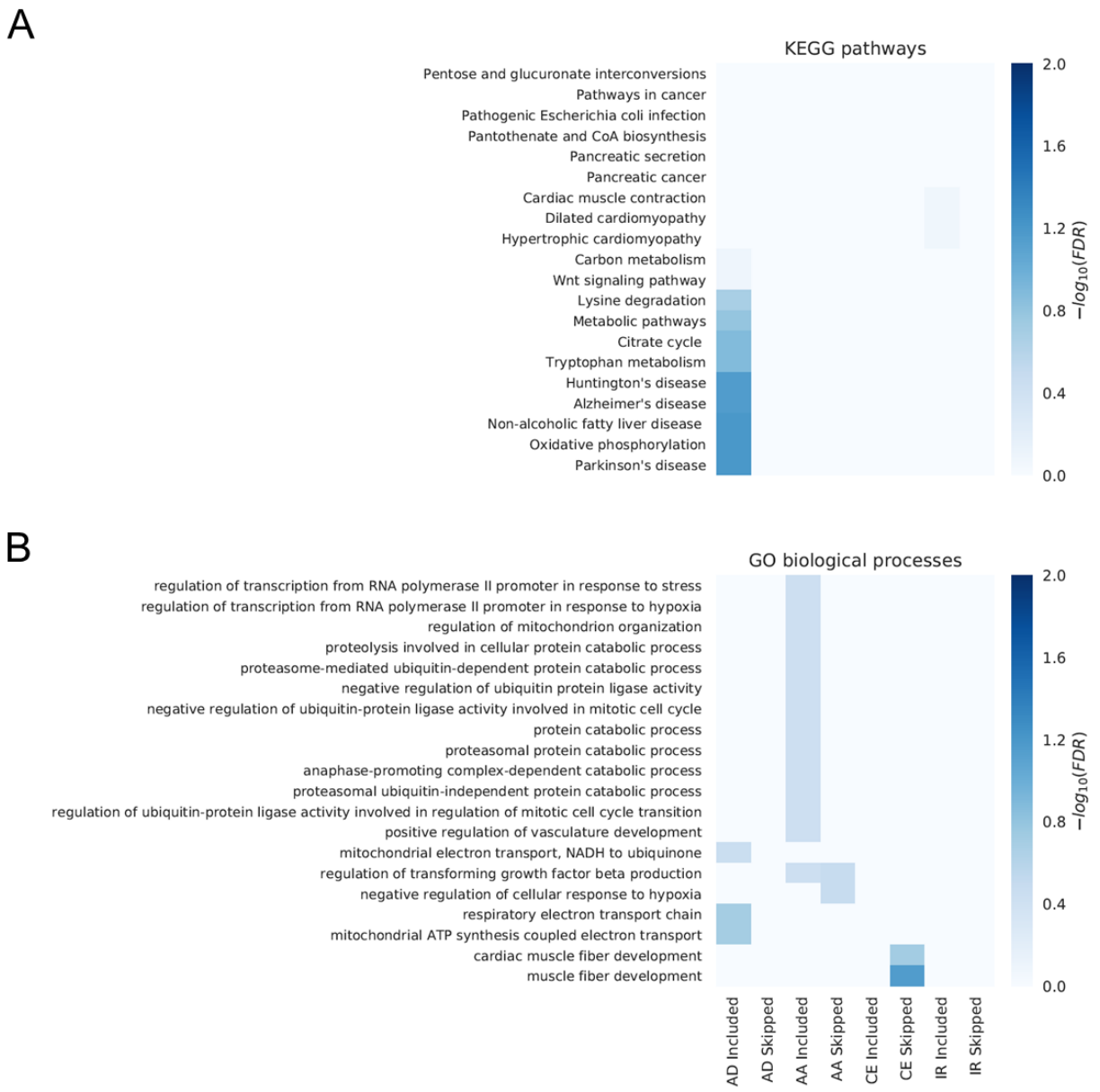

Figura 14. Principales categorías afectadas por los cambios de splicing alternativo en los ratones SRSF4 KO. Análisis de rutas KEGG (A) y ontología genética (B) donde se ven representadas las principales categorías enriquecidas en los genes afectados por splicing alternativo en el ratón KO de SRSF4 en distintos eventos de splicing.

Para conocer las dianas directas de SRSF4 en el corazón, se usó una técnica llamada *Individual-nucleotide resolution Cross-Linking and ImmunoPrecipitation* (iCLIP). Esta herramienta permite la identificación de interacciones directas entre proteínas y RNAs. Los resultados del iCLIP mostraron que SRSF4 se une específicamente a 836 genes en cardiomiocitos.

Para poder determinar cuáles de los RNAs que aparecían diferencialmente expresados en el análisis de RNA-seq son dianas directas de SRSF4 en cardiomiocitos, se comparó el resultado obtenido en el iCLIP con el del RNA-seq. De esta forma se obtuvo una lista de 44 genes (Tabla Suplementaria 4), entre los cuales se encontraba el lncRNA GAS5 (Growth Arrest Specific 5). GAS5 también se encontraba en la lista de genes que sufrían splicing alternativo (Tabla suplementaria 3). Aunque no pudimos validar este cambio de splicing alternativo por qRT-PCR, el análisis del mapeo de las lecturas del RNA-seq sugiere que se podría estar expresando otra isoforma de GAS5 aunque en menor cantidad. En consonancia con el resultado del RNA-seq, se validó por qRT-PCR la bajada de expresión de GAS5 en los corazones SRSF4 KO. Además, se estudió la expresión de GAS5 en el corazón de ratones wild type, la cual sigue un patrón similar a la de SRSF4 (Figura 15A-B).

Posteriormente, para investigar si la bajada de expresión de GAS5 en ausencia de SRSF4 se debía a una mayor tasa de degradación, se inhibió la trascripción en cardiomiocitos neonatales de ratones control y SRSF4 KO usando actinomicina D (ActD), y se midió la expresión de GAS5 a distintos tiempos tras el tratamiento. La expresión de GAS5 decreció a una velocidad significativamente mayor en los cardiomiocitos SRSF4 KO comparados con los de los controles (Figura 15C).

Con el objetivo de determinar si la degradación de GAS5 en ausencia de SRSF4 podría estar mediada por la ruta del non sense mediated decay (NMD), se trataron cardiomiocitos neonatales de ratones control y SRSF4 KO con un inhibidor del NMD. Los resultados mostraron un incremento significativo de GAS5 tras el bloqueo del NMD en las células control y SRSF4 KO. Además, se midió la expresión de GADD45, una diana conocida del NMD, para confirmar la eficacia del inhibidor (Figura 15D-E).

Todos estos resultados sugieren que SRSF4 se une de forma directa a GAS5 protegiéndolo así de la degradación.

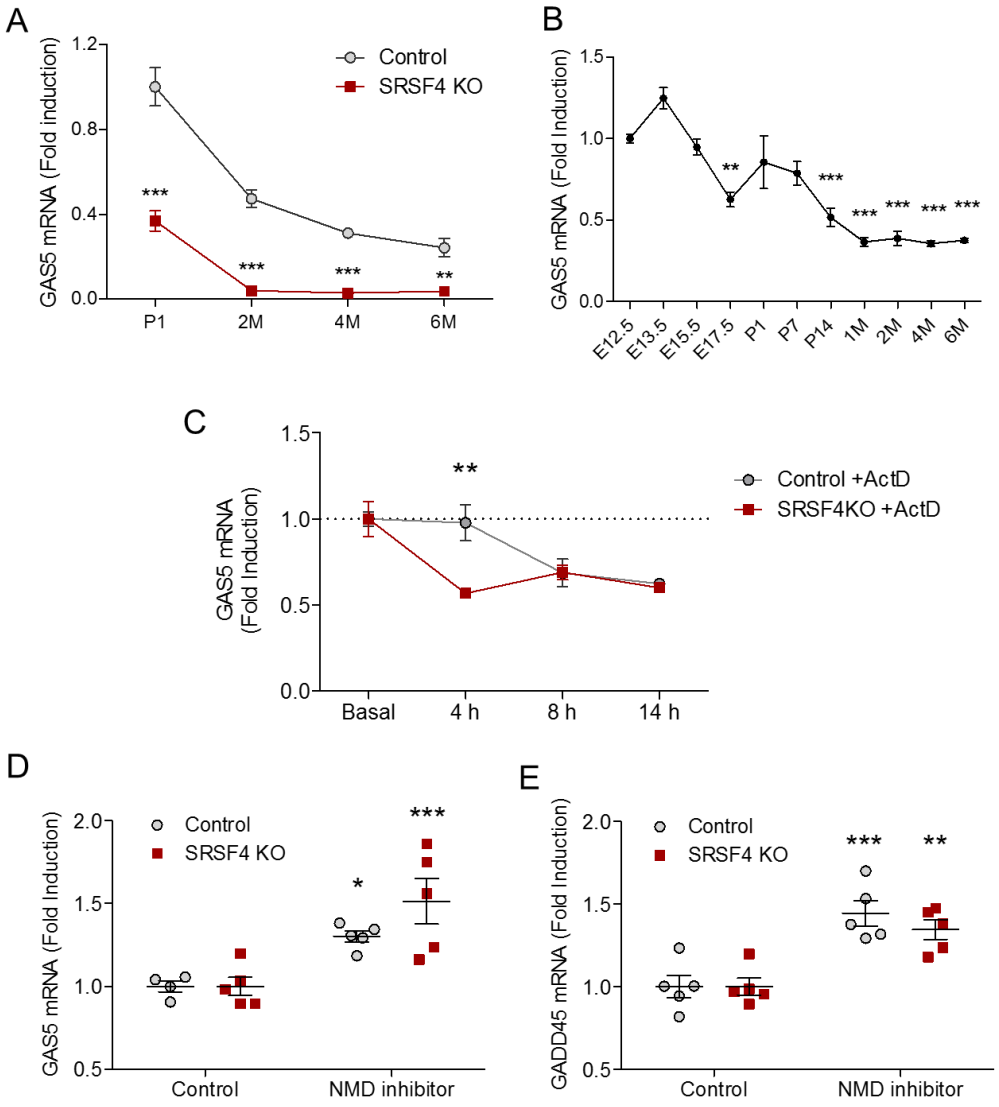

Figura 15. La bajada de GAS5 está mediada por la ruta del NMD. A, Análisis por qRT-PCR de la expresión cardíaca del RNA mensajero de GAS5 en el corazón de ratones control y KO a distintas edades desde la etapa postnatal (P) hasta la adulta (M=meses). Los datos están representados como la media ±SEM. n= 4-5 ratones por grupo. **p<0.01, ***p<0.001 SRSF4 KO vs Control. ANOVA de dos vías con post-test de Bonferroni. **B**, Análisis por qRT-PCR de la expresión cardíaca del RNA mensajero de GAS5 en el corazón de ratones wild type a distintas edades desde estadíos embrionarios (E) hasta días (P) y meses (M) post-parto. Los datos están representados como la media ±SEM. n= 3-4 ratones por grupo. **p<0.01, ***p<0.001 vs E12.5, ANOVA de una vía con test de Bonferroni de comparación múltiple. **C**, Análisis por qRT-PCR de la expresión de GAS5 en cardiomiocitos neonatales controles y KO tratados con ActD. Los valores están normalizados para cada tiempo por el valor medio de cada grupo sin tratar

y con la media de las células control tratadas con DMSO (línea de puntos). Los datos están representados como la media ±SEM. n= 3 ratones por grupo. **p<0.01 SRSF4 KO vs Control; ANOVA de dos vías con post-test de Bonferroni. **D**, **E**, Análisis por QRT-PCR, de la expresión de GAS5 (D) y GADD45 (E) en cardiomiocitos neonatales control y SRSF4 KO tratados con DMSO o inhibidor de NMD durante 7 horas. Los valores fueron normalizados por el valor medio de cada grupo tratado con DMSO. Los datos están representados como la media ±SEM. Cada símbolo representa un animal. *p<0.05, **p<0.01, ***p<0.001 Control vs NMD inhibitor. ANOVA de dos vías con post-test de Bonferroni.

El incremento del tamaño de los cardiomiocitos de los ratones SRSF4 KO se debe a una actividad transcripcional aumentada del receptor de glucocorticoides, causada por la bajada de expresión de GAS5.

Se ha descrito previamente que el lncRNA GAS5 es un represor del receptor de glucocorticoides (GR). Además, también se ha visto que la activación del GR induce cambios hipertróficos en células H9C2 y en cardiomiocitos neonatales de rata.

Con el objetivo de averiguar si los corazones de los ratones SRSF4 KO podrían presentar una menor mayor actividad del GR debida a la bajada de expresión de GAS5, se trataron in vitro con dexametasona (DEX), un glucocorticoide sintético, cardiomiocitos neonatales aislados de los corazones control y KO, con el fin de activar el GR. Tras 72 horas de tratamiento con DEX, se midió por qRT-PCR la expresión génica de diferentes marcadores de hipertrofia y de algunas dianas directas conocidas del GR en los cardiomiocitos control y en los KO. Los resultados mostraron un incremento en la expresión de los genes analizados en las células tratadas con DEX comparando con las no tratadas en ambos grupos. Además, se observó que el aumento de los marcadores de hipertrofia ANF y BNP era significativamente mayor en los cardiomiocitos del KO comparado con los de los controles en las células tratadas con DEX (Figura 16A-B). De la misma forma, la expresión de las dianas directas del GR, Fkbp5 y Gilz, estaba también significativamente incrementada en las células del KO de SRSF4 tratadas con DEX (Figura 16C-D). Además de la expresión génica, se midió el área de los cardiomiocitos y se observó un incremento significativo en los cardiomiocitos del KO tratados con DEX comparados con los controles tratados con DEX y con las células que no recibieron tratamiento (Figura 16E).

Estos resultados demuestran que la hipertrofia de los cardiomiocitos de los ratones SRSF4 KO es debida a un incremento de la actividad transcripcional del GR, la cual podría explicarse por la bajada de GAS5.

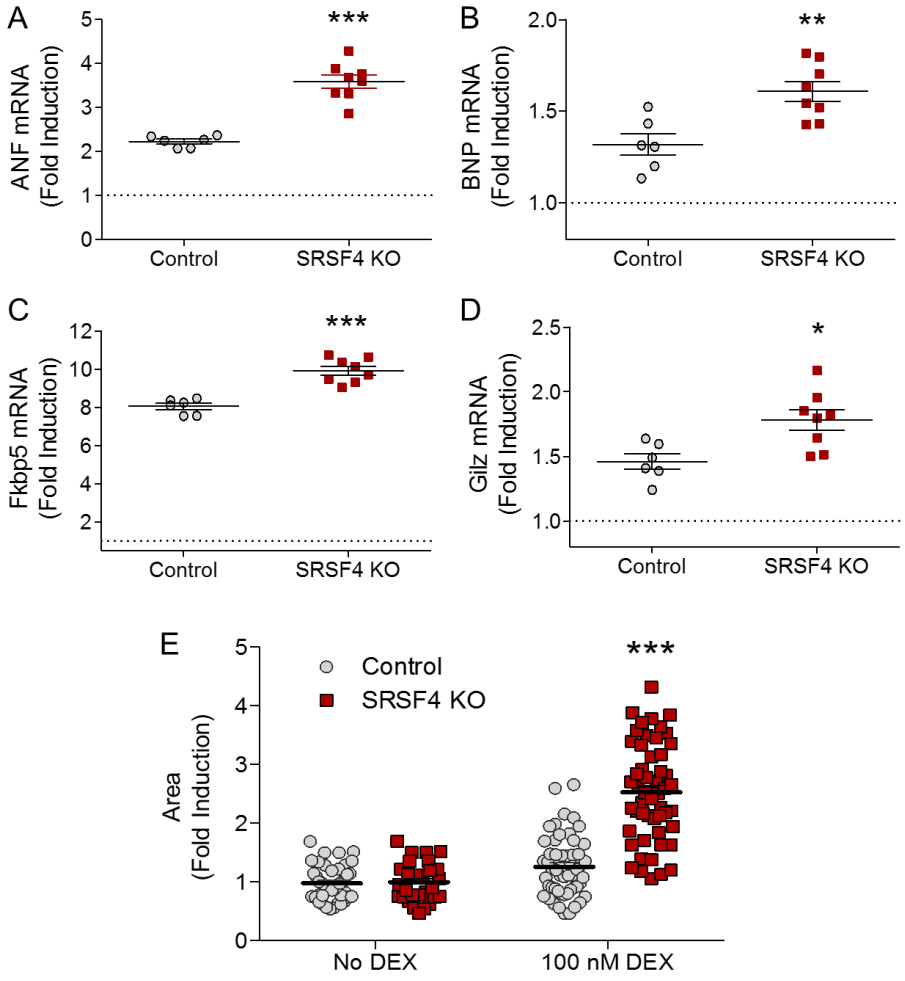

Figura 16. Los cardiomiocitos de los ratones SRSF4 KO presentan más hipertrofia en presencia de DEX que los controles. Análisis por qRT-PCR de la expresión de marcadores de hipertrofia (**A, B**) y de dianas directas del GR (**C, D**) en cardiomiocitos neonatales aislados de ratones control y SRSF4 KO tratados con 100 nM de DEX. Cada grupo está normalizado con la media de las muestras control tratadas con DMSO (tratamiento control) representado por la línea de puntos. Los datos están representados como la media ±SEM. Cada símbolo representa un pocillo. *p<0.05, **p<0.01, ***p<0.001. T-test. **E**, Análisis de la medida del área de lo cardiomiocitos neonatales aislados de ratones control y SRSF4 KO tratados con 100 nM de DEX y DMSO como tratamiento control (No DEX). Los datos están representados como la media ±SEM. Cada símbolo representa un cardiomiocito. ***p<0.001 SRSF4 KO vs Control con 100 nM DEX. ANOVA de dos vía con test de Bonferroni.

La sobrexpresión del lncRNA GAS5 reduce la hipertrofia de los cardiomiocitos de los ratones SRSF4 KO in vitro.

Para determinar si el aumento del tamaño de los cardiomiocitos de los ratones SRSF4 KO en respuesta a DEX está asociado a la bajada de expresión de GAS5, se sobrexpresó el lncRNA GAS5 en cardiomiocitos neonatales aislados del corazón de los ratones control y SRSF4 KO tratados con DEX.

La eficiencia de transfección de DNA en cardiomiocitos neonatales es baja. Por ello, para incrementar esa eficiencia en lugar de transfectar el DNA de GAS5, se procedió a sintetizar el RNA modificado químicamente (RNAmod) de forma exógena para después transfectar el RNA directamente, lo cual es más eficiente. Una vez producido el RNAmod de GAS5 y su respectivo control se procedió con la transfección de los mismos. Después de 72 horas desde la transfección y del tratamiento con DEX, se midió por qRT-PCR la expresión de marcadores de hipertrofia y de dianas conocidas del GR en los cardiomiocitos control y SRSF4 KO (Figura 17A-D). Además, se midió el área celular en ambos grupos (Figura 17E). Se encontró un descenso significativo del marcador de hipertrofia ANF y también una disminución del área celular en los cardiomiocitos aislados de los ratones SRSF4 KO tratados con DEX que sobreexpresaban GAS5 comparado con los no sobrexpresantes.

Estos resultados demuestran que la sobrexpresión de GAS5 reduce la hipertrofia de los cardiomiocitos SRSF4 KO.

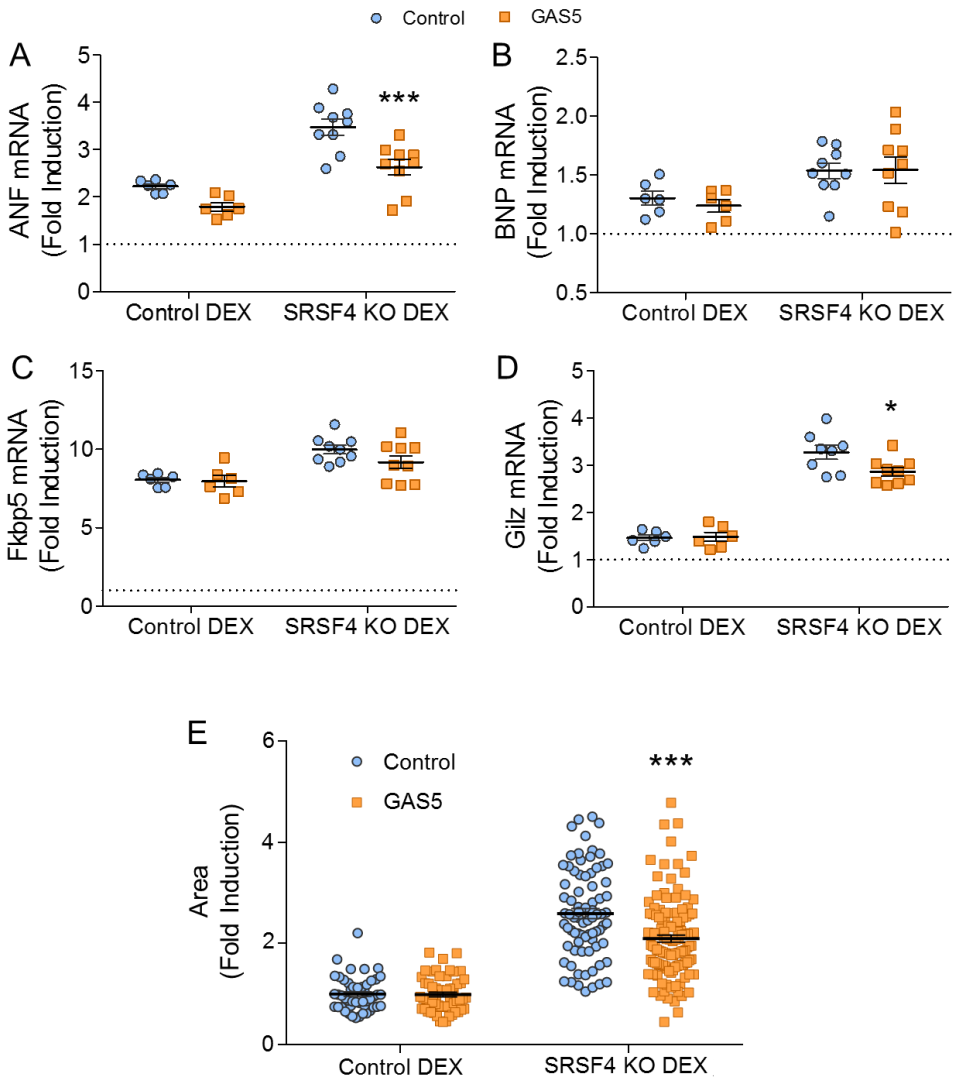

Figura 17. La sobrexpresión de GAS5 reduce la hipertrofia en los cardiomiocitos SRSF4 KO. Análisis por qRT-PCR de la expresión de marcadores de hipertrofia (**A, B**) y de dianas directas del GR (**C, D**) en cardiomiocitos neonatales aislados de ratones control y SRSF4 KO tratados con 100 nM de DEX y transfectados con GAS5 RNAmod o control RNAmod. Cada grupo está normalizado con la media de las muestras control tratadas con DMSO (tratamiento control) representado por la línea de puntos. Los datos están representados como la media ±SEM. Cada símbolo representa un pocillo. *p<0.05, ***p<0.001. ANOVA de dos vía con test de Bonferroni. **E**, Análisis de la medida del área de lo cardiomiocitos neonatales aislados de ratones control y SRSF4 KO tratados con 100 nM de DEX y transfectados con GAS5 RNAmod o control modRNA. Los datos están representados como la media ±SEM. Cada símbolo representa un cardiomiocito. ***p<0.001 SRSF4 KO DEX GAS5 RNAmod vs control RNAmod. ANOVA de dos vía con test de Bonferroni.

Estudio de SRSF4 en pacientes con hipertrofia idiopática y pacientes con enfermedad de Cushing

El fenotipo observado en el modelo de pérdida de función de SRSF4 tiene características en común con la miocardiopatía hipertrófica. Se han descrito mutaciones en varios genes sarcoméricos y no sarcoméricos asociados con esta patología. Tras los resultados obtenidos quisimos averiguar si pacientes con hipertrofia idiopática podrían presentar una mutación en SRSF4 que pudiera explicar el origen de su patología. Para ello se usaron muestras de sangre de 98 pacientes gracias a la colaboración con el Dr. Pablo García Pavía del Hospital Puerta de Hierro de Majadahonda. Se extrajo el DNA genómico de las células sanguíneas de cada paciente. Posteriormente, se puso a punto la PCR para cada uno de los 6 exones del gen de SRSF4. El producto de PCR de cada exón y de cada paciente fue enviado a la empresa Secugen donde fueron secuenciados por el método de Sanger. El análisis de la secuenciación no mostró mutaciones en ninguno de los 6 exones de SRSF4 en ninguno de los 98 pacientes.

También se quiso averiguar si la expresión de SRSF4 podría estar disminuida en algún paciente con hipertrofia idiopática. Para ello se extrajo tejido cardíaco de pacientes, se procedió a la extracción de RNA del tejido y se cuantificó la expresión del RNA mensajero de SRSF4 por qRT-PCR. Los resultados mostraron que no había una bajada de expresión de SRSF4 en los pacientes con hipertrofia idiopática analizados (Figura 18).

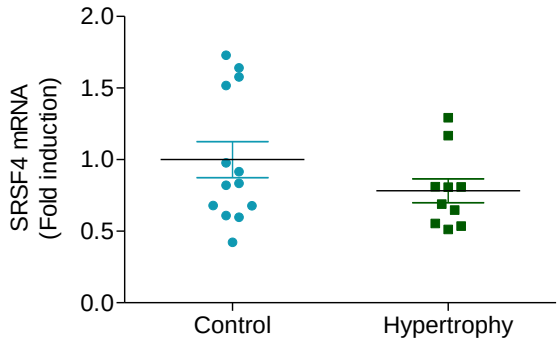

Figura 18. La expresión de SRSF4 no baja en pacientes con hipertrofia idiopática. Análisis por qRT-PCR de la expresión cardíaca del RNA mensajero de SRSF4 en pacientes con hipertrofia idiopática

y en controles. Los datos están representados como la media ±SEM. Cada símbolo representa un paciente. No se encontraron diferencias estadísticamente significativas.

Según los resultados obtenidos, que implican una regulación del GR por parte de SRSF4 y GAS5, nos planteamos averiguar que ocurre con estos genes en pacientes con enfermedad de Cushing, la cual se caracteriza por un aumento del nivel de glucocorticoides en sangre. Encontramos un paper en el cual no miraban específicamente estos genes, pero en el análisis de su RNA-seq hecho en pacientes con Cushing y controles en tejido adiposo, encontramos una bajada de expresión de GAS5 y SRSF4[55] (Figura 19).

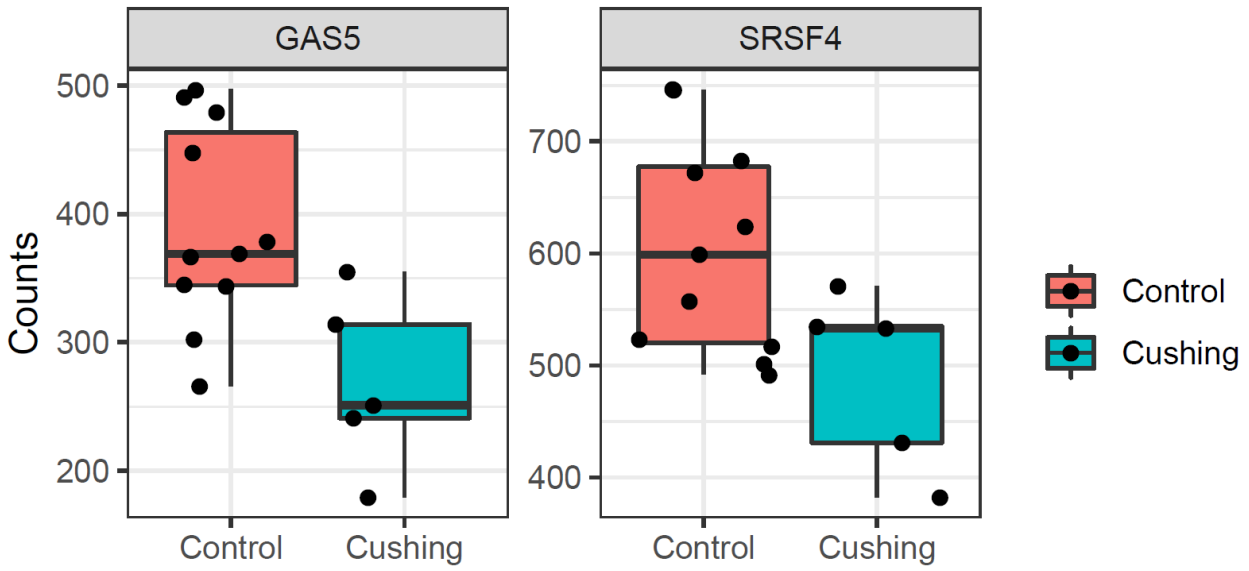

Figura 19. Expresión del mRNA de GAS5 y SRSF4 analizado por RNA-Seq en tejido adiposo procedente de pacientes con enfermedad de Cushing y controles.

DISCUSIÓN

La pérdida cardio-específica de SRSF4 da lugar a un fenotipo patológico

El creciente interés por el estudio de las proteínas de unión a RNA ha surgido como resultado de su potencial como reguladores de la expresión génica dado su papel en la regulación de un gran número de mecanismos post-transcripcionales, mientras que el viejo paradigma se centraba solo en la activación de programas transcripcionales por proteínas de unión a DNA. Defectos en un gran número de RBPs han sido vinculados con el desarrollo de diversas patologías, incluyendo enfermedades cardiovasculares. La RBP SRSF4 ha sido vinculada con el desarrollo de neuropatías y cáncer, sin embargo su papel en el corazón no había sido estudiado previamente.

En esta tesis se describen por primera vez las consecuencias de la pérdida cardio-específica de SRSF4. Nuestros análisis ecocardiográficos demuestran que los ratones deficientes en SRSF4 desarrollan hipertrofia del ventrículo izquierdo, acompañada por un aumento de marcadores de enfermedad cardíaca. Se sabe que la hipertensión puede dar lugar a hipertrofia cardíaca. Sin embargo, los valores de la presión arterial de los ratones SRSF4 sugieren que la hipertrofia es debida a un problema intrínseco en el corazón y no a hipertensión. Por otro lado, la medida del área de los cardiomiocitos en los corazones de los ratones SRSF4 KO muestra que la hipertrofia está asociada a un aumento del tamaño de las células. Además, los análisis histológicos revelan que los ratones SRSF4 KO desarrollan focos de fibrosis a partir de los 10 meses de edad. En cuanto a la función cardíaca, los datos muestran que la función sistólica se mantiene, sin embargo los ratones desarrollan disfunción diastólica de forma progresiva siendo más visible a edades avanzadas. Por tanto, el primer síntoma que observamos tras la pérdida de SRSF4 en el corazón es la hipertrofia, y posteriormente los ratones desarrollan disfunción diastólica con la edad. La disfunción diastólica del ventrículo izquierdo está asociada con una variedad de condiciones médicas. La hipertrofia ventricular izquierda es una de las anomalías más comunes que inducen disfunción diastólica[56]. Además, encontramos cambios electrofisiológicos que apoyaban la presencia de hipertrofia. En condiciones de estrés cardíaco, los ratones muestran una onda J negativa y un QT-largo, por lo que

presentan un mayor riesgo de padecer una muerte súbita. Está descrito que la hipertrofia cardíaca es un factor de riesgo para la prolongación del intervalo QT y la muerte súbita cardíaca[57]. Por tanto, creemos que estas alteraciones electrofisiológicas y de la función cardiaca podrían ser causadas por la hipertrofia de forma secundaria a la pérdida de SRSF4, aunque sería interesante profundizar en ello. Con estos resultados podemos concluir que la pérdida cardio-especifica de SRSF4 produce un fenotipo patológico.

La hipertrofia se debe a una actividad transcripcional aumentada del receptor de glucocorticoides, causada por la bajada de expresión de GAS5

Nuestros datos de RNA-seq revelan que la pérdida de SRSF4 en el corazón produce cambios de expresión en un número significativo de RNAs largos no codificantes (lncRNAs). Estas moléculas de RNA tienen una longitud de alrededor de 200 nucleótidos[58]. Otros ncRNAs como son los microRNAS (miRNAs) han sido muy estudiados y se entiende su papel como reguladores de la expresión génica[59]. Por el contrario, el papel de los lncRNAs es menos conocido. Muchos lncRNAs han sido funcionalmente asociados con el desarrollo de algunas enfermedades humanas, en particular varios tipos de cáncer[60]. También, estudios recientes sugieren un papel fundamental de los lncRNAs en el desarrollo de varias patologías cardiovasculares, incluyendo ateroesclerosis, remodelado cardiaco post-infarto o miocardiopatía hipertrófica[61]. En concreto, en el caso de la hipertrofia cardíaca, se ha visto que Mhrt (del inglés, Myosin heavy chain associated RNA transcript) es el primer ejemplo de lncRNA que actúa inhibiendo la hipertrofia cardíaca patológica, mediante su interacción directa con Brg1, un factor remodelador de cromatina[62]. De igual forma, se ha descrito que la expresión del lncRNA Chast (del inglés, cardiac hypertrophy-associated transcript) se encuentra elevada en cardiomiocitos procedentes de animales sometidos a constricción aórtica, y también en tejido cardíaco hipertrófico procedente de pacientes con estenosis aórtica. El mecanismo por el cual se produce esta hipertrofia tiene que ver con la regulación de Plkhm1, un gen que se encuentra

en la hebra opuesta a Chast, de forma que se inhibe la autofagia en el cardiomiocito y se induce así la hipertrofia[63]. Otros lncRNAs también han sido identificados como reguladores de la hipertrofia cardiaca mediante su papel como secuestradores de miRNAs, como es el caso del lncRNA CHRF[64] (del inglés, cardiac hypertrophy-related factor) o ROR[65] (del inglés, RNA regulator of reprogramming).

En nuestro caso, el análisis del iCLIP de SRSF4 identifica al lncRNA GAS5 como una diana directa de SRSF4 en cardiomiocitos, cuya expresión se encuentra disminuida en los ratones SRSF4 KO, dato que observamos en el RNA-seq y validamos por qRT-PCR. Además observamos que en ratones wild type el patrón de expresión de SRSF4 y GAS5 es similar. Los resultados del experimento con Actinomicina D muestran que GAS5 se degrada más rápidamente en ausencia de SRSF4, sugiriendo que SRSF4 podría estar regulando de alguna forma la estabilidad o degradación del RNA de GAS5. El NMD (del inglés, non sense mediated decay) fue descrito por primera vez como un proceso de control por el cual los RNAs aberrantes son degradados[66]. El NMD reconoce estos RNAs aberrantes gracias a la presencia en los mismos de unos codones de parada de la traducción prematuros (PTC, por sus siglas en inglés). Por tanto se presenta como un mecanismo íntimamente ligado con la traducción[67]. Sin embargo, el NMD no está restringido únicamente a los mRNAs. Varios estudios en diversas especies incluyendo ratón[68] y humano[69], han identificado lncRNAs como dianas directas del NMD teniendo en cuenta que éstos pueden asociarse a la maquinaria de traducción, incluyendo el lncRNA GAS5[70]. Aunque ha sido objeto de debate si la unión de ciertos lncRNAs a los ribosomas hace que se produzca una traducción activa, los estudios más recientes que abordan concretamente esta cuestión muestran la presencia de ribosomas que participan activamente en la traducción de lncRNAs. Los productos han sido nombrados como micropéptidos, o sPEPs (del inglés, small peptides), y su papel en procesos fisiológicos y patológicos demuestran su importancia biológica[71–73]. No hay evidencias de que el lncRNA GAS5 llegue a producir un producto a pesar de su demostrada interacción ribosómica.

Se ha descrito que GAS5 puede ser degradado por NMD; la eliminación de UPF1, uno de los componentes esenciales de la maquinaria del NMD, induce la bajada

de expresión del RNA de GAS5 con la consecuente bajada de expresión de algunos genes cuyos promotores están regulados por el receptor de glucocorticoides, una de las dianas de GAS5[74]. Otro estudio muestra como la bajada de expresión de la maquinaria del NMD es esencial para la diferenciación de los progenitores neuronales y está acompañada por la subida de expresión de varias dianas directas del NMD, incluyendo GAS5[75]. Otro trabajo también muestra que además de los mRNAs, los miRNAs y lncRNAs como GAS5 son dianas directas del NMD[76]. Aunque desconocemos el mecanismo preciso por el cual SRSF4 regula a GAS5, es probable que implique la degradación del RNA a través de NMD. Nuestros resultados demuestran que al inhibir el NMD los niveles de expresión del RNA de GAS5 suben. A pesar de que la pérdida cardio-específico de SRSF4 en general no parezca tener una gran repercusión en el splicing alternativo en el corazón, según nuestros datos SRSF4 podría estar regulando la expresión de otra isoforma de GAS5. No hemos podido validar este cambio ya que hemos observado que aunque se estuviera produciendo otra isoforma, ésta podría estar degradándose rápidamente. Esto podría explicarse debido a que ante la ausencia de SRSF4, se produce una isoforma de GAS5 capaz de interaccionar con la maquinaria de traducción y por tanto ser degrada por NMD. De esta forma, SRSF4 estaría regulando si se produce la forma codificante, la cual no sería funcional ya que se degradaría por NMD, o la no codificante de GAS5.

El lncRNA GAS5 se expresa en tejido adulto y durante el desarrollo embrionario, y su expresión baja en varios tipos de cáncer, incluyendo el cáncer de mama[77]. GAS5 se localiza tanto en el núcleo como en el citoplasma[78] y tiene una vida media de ~6 horas[79]. En los linfocitos, GAS5 regula la apoptosis y el ciclo celular[80]. Además, GAS5 disminuye en pacientes con diabetes mellitus tipo 2; se une al promotor del receptor de insulina para regular su expresión, y su eliminación inhibe la absorción de glucosa y la señalización de insulina[81]. También se ha descrito que GAS5 interacciona con el dominio a unión de DNA del receptor de glucocorticoides (GR), inhibiendo así la unión de éste a los GRE (del inglés, glucocorticoid response elements) de sus genes diana, modulando de esta forma la actividad transcripcional del GR[78]. Nuestros resultados sugieren que la interacción SRSF4-GAS5 regula la actividad transcripcional del GR en el corazón, en línea con los estudios *in vivo* e *in vitro* que implican la relación que existe entre los glucocorticoides y el desarrollo de

hipertrofia cardiaca[82–84], y la inducción de cambios hipertróficos mediante la activación del GR en células H9C2 y cardiomiocitos neonatales de rata[85]. Nuestros resultados demuestran que la actividad transcripcional del GR se encuentra incrementada en los cardiomiocitos neonatales de los ratones SRSF4 KO, en los cuales la expresión de GAS5 se encuentra disminuida. Además, mostramos que los cardiomiocitos neonatales de los ratones SRSF4 KO responden a una activación del GR mediada por dexametasona con un incremento más pronunciado en la expresión de marcadores de hipertrofia y un área celular superior a lo observado en los cardiomiocitos control. Estos resultados son consistentes con la acción pro-hipertrófica que tienen los glucocorticoides sugerida por los estudios previos. Además, también encontramos que la sobreexpresión de GAS5 reduce la hipertrofia en los cardiomiocitos KO SRSF4, lo que sugiere un papel causal de la pérdida de expresión de GAS5 en la respuesta hipertrófica observada en ausencia de SRSF4.

Por tanto, nuestros resultados muestran que la pérdida de SRSF4 en cardiomiocitos produce una degradación mayor de GAS5 que conlleva a una bajada en la expresión del mismo, lo que conduce a un incremento de la actividad transcripcional del GR, ya que se pierde la inhibición por parte de GAS5, lo cual a su vez causa la hipertrofia del cardiomiocito (Figura 20).

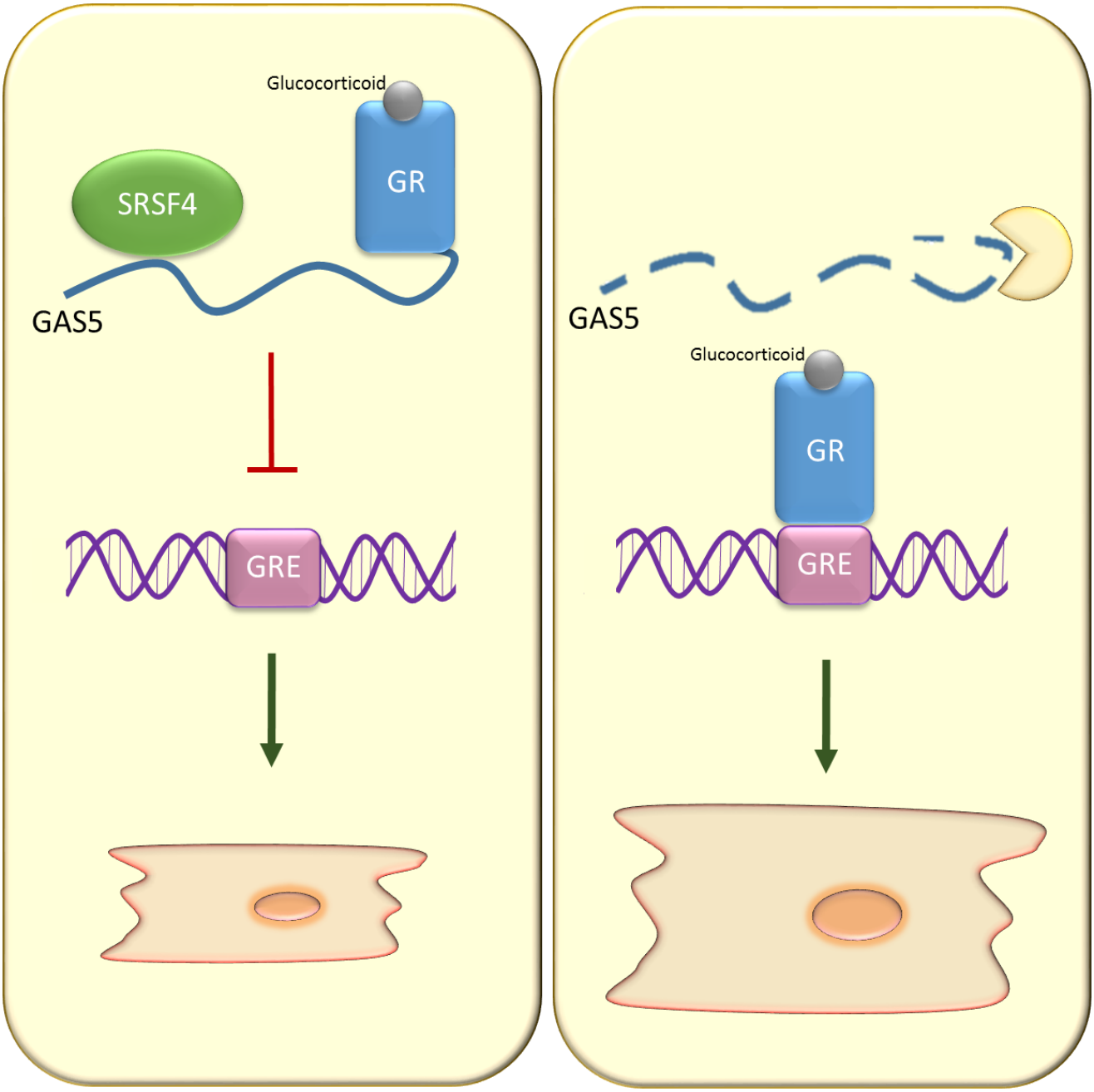

Figura 20. Mecanismo molecular por el cual se produce hipertrofia cardiaca en ausencia de SRSF4. GAS5 es una diana directa de SRSF4 en cardiomiocitos. Cuando SRSF4 está presente, GAS5 se une al GR e inhibe su unión a la región GRE de sus genes diana. En ausencia de SRSF4, la expresión de GAS5 disminuye y el GR induce la expresión de genes diana implicados en la hipertrofia de los cardiomiocitos.

Comparación de SRSF4 con otras proteínas SR

Haciendo un repaso del resto de proteínas SR cuyo papel en el corazón ha sido también estudiado, podemos decir que la depleción constitutiva y ubicua de SRSF1, SRSF2, SRSF3 y SRSF10 resultan letales en estadíos embrionarios[39,40,86,87]. En el caso de la depleción de SRSF10, los ratones desarrollan un fenotipo cardíaco patológico y la mayoría de los ratones mueren durante el desarrollo debido a múltiples defectos en la formación del corazón[40]. Sin embargo, la eliminación cardio-específica de SRSF1 y SRSF2 no parece tener el mismo efecto, ya que en ambos casos las camadas de ratones cumplen con la proporción mendeliana esperada [38,39], al igual que ocurre con SRSF4. En el caso de SRSF3, la pérdida en el corazón desde el desarrollo también resulta letal para los embriones[88].

En el corazón adulto, la pérdida cardíaca de SRSF1 resulta letal para los animales, que empiezan a morir entre las 6-8 semanas tras el parto[39], mientras que la eliminación cardíaca de SRSF2 no tiene efecto sobre la vida media de los animales[38], como ocurre también en SRSF4. Sin embargo, la pérdida de SRSF3 en el corazón adulto causa un fenotipo muy severo, los animales apenas son capaces de sobrevivir una semana[88]. Los fenotipos causados por la pérdida de estas tres proteínas también difieren mucho. En el KO de SRSF3 observamos una falta de contracción, pero a diferencia del KO de SRSF2, el corazón no se dilata y no se llega a producir cardiomiopatía dilatada [38]. Los ratones KO de SRSF1 muestran un fenotipo opuesto, donde los cardiomiocitos desarrollan hipercontracción[39]. En el caso de SRSF4, como ya se ha descrito antes vemos una hipertrofia del ventrículo izquierdo.

De acuerdo a la variedad en los fenotipos cardiacos de las distintas proteínas SR, sus dianas y mecanismos de acción también son distintos. Los fenotipos causados por la pérdida de SRSF1, SRSF2 o SRSF10 parecen estar causados por un determinado RNA, mientras que las dianas cardíacas de SRSF3 son más variadas. SRSF1 afecta al splicing de CaMKIIδ, la pérdida de SRSF2 reduce los niveles de expresión de RyR2 y SRSF10 afecta al splicing de triadina reduciendo sus niveles de expresión y los de calsequestrina (CASQ2) [38–40]. En SRSF3, multitud de genes implicados en la contracción cardiaca disminuyen su expresión[88].

En resumen, los estudios previamente mencionados demuestran que las funciones de las proteínas SR en el corazón no son redundantes, ya que su eliminación causa fenotipos patológicos distintos. Dicho esto, en el caso de SRSF4 nuestros datos de RNA-seq muestran un aumento en los niveles de expresión de otro miembro de esta familia, SRSF6. Hay estudios que sugieren que SRSF4 y SRSF6 compiten por la unión a mRNA similares, y que la depleción de ambas proteínas es letal[30]. Esto sugiere que podría existir un mecanismo compensatorio entre ambas y podría por tanto explicar el fenotipo menos agresivo de SRSF4 comparado con el de otras proteínas SR.

Sería interesante observar qué ocurre con la expresión de SRSF4 en otros pacientes con hipertrofia idiopática y enfermedad de Cushing

Como se ha mencionado, SRSF4 se ha relacionado con el desarrollo de diversas patologías neurológicas y cáncer. Sin embargo, su papel en el corazón no había sido estudiado hasta ahora. A pesar de que hemos demostrado que la pérdida cardio-específica de SRSF4 produce hipertrofia cardíaca, los niveles de SRSF4 no varían en un modelo de ratón de hipertrofia inducida por constricción de la aorta, ni la inducción de SRSF4 consigue minimizar la hipertrofia en este mismo modelo. Tampoco hemos visto un cambio de expresión de SRSF4 en otras patologías cardíacas como el infarto de miocardio inducido por la constricción permanente de la arteria coronaria descendente izquierda en ratón.

Por ello, y dado que los cambios estructurales y funcionales observados en el corazón de los ratones SRSF4 KO son parecidos a los que se encuentran en una miocardiopatía hipertrófica en humanos, quisimos averiguar si pacientes con hipertrofia idiopática podrían presentar una mutación en SRSF4 que pudiera explicar el origen de su patología. La mayoría de las causas genéticas están relacionadas con mutaciones en genes sarcoméricos, pero se observan también mutaciones genéticas no sarcoméricas en una proporción importante de pacientes[89]. Nuestros resultados muestran que la cohorte de pacientes analizada no presenta mutaciones en SRSF4

en ninguno de los exones. Todos los pacientes proceden de la misma o de localizaciones cercanas por lo que sería interesante observar más cohortes de pacientes con hipertrofia idiopática en otras zonas geográficas.

Por otro lado, según el mecanismo molecular que hemos descrito, que implica que como consecuencia de una bajada de SRSF4 y por tanto de GAS5, hay una mayor activación del receptor de glucocorticoides, sería interesante observar qué ocurre con SRSF4 y GAS5 en pacientes con síndrome y/o enfermedad de Cushing. Esta enfermedad se caracteriza por la presencia de niveles elevados de glucocorticoides en sangre, lo cual puede ser consecuencia del uso de medicamentos con corticoesteroides orales, pero también puede producirse cuando el cuerpo genera demasiado cortisol por sí solo debido a defectos en el funcionamiento de la hipófisis o las glándulas suprarrenales. Como consecuencia de estos niveles elevados de glucocorticoides en sangre, la hipertensión y la hipertrofia del ventrículo izquierdo son características entre otras, en la enfermedad de Cushing[90]. Aunque también, un elevado número de pacientes desarrollan hipertrofia sin presencia de hipertensión. Estudios recientes indican que es más probable que el exceso de glucocorticoides induzca cambios cardiovasculares estructurales y funcionales que no pueden explicarse únicamente por el desarrollo de hipertensión[91,92]. Por tanto, sería interesante observar si la hipertrofia del ventrículo izquierdo en estos pacientes estaría favorecida por la presencia de algún defecto en la expresión de SRSF4 y GAS5, que hiciera que la actividad del receptor de glucocorticoides estuviera aumentada en los cardiomiocitos. De hecho, los datos del RNA-seq de un estudio que analiza los cambios de expresión génica en tejido adiposo de pacientes con Cushing, muestran que hay una bajada de expresión de SRSF4 y GAS5 en este tejido[55]. Sería interesante observar si esto ocurre también en los cardiomiocitos.

CONCLUSIONES

Conclusiones

1. La expresión de SRSF4 es mayor durante el desarrollo embrionario y decrece progresivamente hasta la etapa adulta.

2. La expresión de SRSF4 en ratón no cambia significativamente tras la inducción de un infarto de miocardio, ni tampoco en un modelo de hipertrofia inducida por constricción aórtica.

3. La pérdida cardio-específica de SRSF4 induce hipertrofia del ventrículo izquierdo asociado con un incremento del tamaño de los cardiomiocitos, disfunción diastólica y alteraciones electrofisiológicas.

4. La sobreexpresión de SRSF4 tras la constricción aórtica no reduce la hipertrofia patológica.

5. En la cohorte de pacientes con hipertrofia idiopática analizados, no se han encontrado mutaciones ni bajada de expresión de SRSF4.

6. SRSF4 se une a GAS5 y regula su degradación.

7. La hipertrofia de los cardiomiocitos producida por la ausencia de SRSF4 se debe, al menos en parte, al aumento de la actividad del receptor de glucocorticoides, causada por la bajada de expresión de GAS5.

8. La sobrexpresión de GAS5 reduce la hipertrofia de los cardiomiocitos de los ratones SRSF4 KO *in vitro*.

Conclusions

1. SRSF4 expression is higher during embryonic development and decreases progressively until adulthood.

2. In mice, SRSF4 expression does not change significantly neither after myocardial infarction nor in a hypertrophic model induced by trans-aortic constriction.

3. Cardio-specific loss of SRSF4 results in left ventricular hypertrophy associated to an increase in the cardiomyocyte size, diastolic dysfunction and electrophysiological alterations.

4. SRSF4 overexpression after trans-aortic constriction does not reduce pathological hypertrophy significantly.

5. In the cohort of patients with idiopathic hypertrophy that was analysed in this study, neither mutations nor downregulation of SRSF4 expression were found.

6. SRSF4 binds to GAS5 and regulates its degradation.

7. Cardiac hypertrophy induced by the lack of SRSF4 is associated with an increase in the transcriptional activity of the glucocorticoid receptor, which is caused by GAS5 downregulation.

8. GAS5 overexpression reduces hypertrophy in cardiomyocyte isolated from SRSF4 KO mice *in vitro*.

Bibliografía

1. WHO. Cardiovascular Diseases (CVDs). 2017;[Online].
2. Wilkins E., Wilson L., Wickramasinghe K., Bhatnagar P., Leal J., Luengo-Fernandez R.Townsend N. European Cardiovascular Disease Statistics 2017 edition. *Eur Hear Network, Brussels*. 2017;p. 192.
3. Jessup S. Heart Failure. *N Engl J Med*. 2003;348:2007–2018.
4. Heineke J, Molkentin JD. Regulation of cardiac hypertrophy by intracellular signalling pathways. *Nat Rev Mol Cell Biol*. 2006;7:589.
5. Thum T, Galuppo P, Wolf C, Fiedler J, Kneitz S, Laake LW Van, Doevendans PA, Mummery CL, Borlak J, Haverich A, Gross C, Engelhardt S, Ertl G, Bauersachs J. MicroRNAs in the Human Heart A Clue to Fetal Gene Reprogramming in Heart Failure. 2007;258–267.
6. Hentze MW, Castello A, Schwarzl T, Preiss T. A brave new world of RNA-binding proteins. *Nat Rev Mol Cell Biol*. 2018;19:327.
7. Corbett AH. Post-transcriptional regulation of gene expression and human disease. *Curr Opin Cell Biol*. 2018;52:96–104.
8. Beckmann BM, Horos R, Fischer B, Castello A, Eichelbaum K, Alleaume AM, Schwarzl T, Curk T, Foehr S, Huber W, Krijgsveld J, Hentze MW. The RNA-binding proteomes from yeast to man harbour conserved enigmRBPs. *Nat Commun*. 2015;6.
9. Conlon EG, Manley JL. RNA-binding proteins in neurodegeneration: mechanisms in aggregate. *Genes Dev*. 2017;31:1509–1528.
10. Maziuk B, Ballance HI, Wolozin B. Dysregulation of RNA Binding Protein Aggregation in Neurodegenerative Disorders. *Front Mol Neurosci*. 2017;10:1–9.

11. Wang ZL, Li B, Luo YX, Lin Q, Liu SR, Zhang XQ, Zhou H, Yang JH, Qu LH. Comprehensive Genomic Characterization of RNA-Binding Proteins across Human Cancers. *Cell Rep*. 2018;22:286–298.

12. De Bruin RG, Rabelink TJ, Van Zonneveld AJ, Van Der Veer EP. Emerging roles for RNA-binding proteins as effectors and regulators of cardiovascular disease. *Eur Heart J*. 2017;38:1380–1388.

13. Liu J, Kong X, Zhang M, Yang X, Xu X. RNA binding protein 24 deletion disrupts global alternative splicing and causes dilated cardiomyopathy. *Protein Cell*. 2019;10(6):405-416

14. Guo W, Schafer S, Greaser ML, Radke MH, Liss M, Govindarajan T, Maatz H, Schulz H, Li S, Parrish AM, Dauksaite V, Vakeel P, Klaassen S, Gerull B, Thierfelder L, Regitz-Zagrosek V, Hacker TA, Saupe KW, Dec GW, Ellinor PT, MacRae CA, Spallek B, Fischer R, Perrot A, ̈zcelik C, Saar K, Hubner N, Gotthardt M. RBM20, a gene for hereditary cardiomyopathy, regulates titin splicing. *Nat Med*. 2012;18:766–773.

15. Zhang Y, Si Y, Ma N, Mei J. The RNA-binding protein PCBP2 inhibits Ang II-induced hypertrophy of cardiomyocytes though promoting GPR56 mRNA degeneration. *Biochem Biophys Res Commun*. 2015;464:679–684.

16. Gao C, Ren S, Lee J, Qiu J, Chapski DJ, Rau CD, Zhou Y, Abdellatif M, Nakano A, Vondriska TM, Xiao X, Fu X, Chen J, Wang Y. RBFox1-mediated RNA splicing regulates cardiac hypertrophy and heart failure. *J Clin Invest*. 2016;126:195–206.

17. Wei C, Qiu J, Zhou Y, Xue Y, Hu J, Ouyang K, Banerjee I, Zhang C, Chen B, Li H, Chen J, Song LS, Fu XD. Repression of the central splicing regulator RBFox2 is functionally linked to pressure overload-induced heart failure. *Cell Rep*. 2015;10:1521–1533.

18. Freyermuth F, Rau F, Kokunai Y, Linke T, Sellier C, Nakamori M, Kino Y, Arandel L, Jollet A, Thibault C, Philipps M, Vicaire S, Jost B, Udd B, Day JW, Duboc D, Wahbi K, Matsumura T, Fujimura H, Mochizuki H, Deryckere F, Kimura T, Nukina N, Ishiura S, Lacroix V, Campan-Fournier A, Navratil V, Chautard E, Auboeuf D, Horie M, Imoto K, Lee KY, Swanson MS, De Munain AL, Inada S, Itoh H, Nakazawa K, Ashihara T, Wang E, Zimmer T, Furling D, Takahashi MP, Charlet-Berguerand N. Splicing misregulation of SCN5A contributes to cardiac-conduction delay and heart arrhythmia in myotonic dystrophy. *Nat Commun*. 2016;7.

19. Li J, Xie D, Huang J, Lv F, Shi D, Liu Y, Lin L, Geng L, Wu Y, Liang D, Chen YH. Cold-inducible RNA-binding protein regulates cardiac repolarization by targeting transient outward potassium channels. *Circ Res*. 2015;116:1655–1659.

20. Bourgeois CF, Lejeune F, Ste J. Broad Specificity of SR (Serine / Arginine) Proteins in the Regulation of Alternative Splicing of Pre-Messenger RNA I . Introduction More than 25 years after the discovery of introns in higher eukaryotes , the. *Nucleic Acid Res Mol Biol*. 2004;78:37–88.

21. Änkö ML. Regulation of gene expression programmes by serine-arginine rich splicing factors. *Semin Cell Dev Biol*. 2014;32:11–21.

22. Wang Z, Burge CB. Splicing regulation : From a parts list of regulatory elements to an integrated splicing code. *RNA*. 2008;802–813.

23. Blencowe BJ. Exonic splicing enhancers : mechanism of action , diversity and role in human genetic diseases. 2000;0004:106–110.

24. Lou H, Neugebauer KM, Gagel RF, Berget SM. Regulation of Alternative Polyadenylation by U1 snRNPs and SRp20. *Mol Cell Biol*. 1998;18:4977 LP-4985.

25. Scotti MM, Swanson MS. RNA mis-splicing in disease. *Nat Rev Genet*. 2015;17:19.

26. Park JY, Li W, Zheng D, Zhai P, Zhao Y, Matsuda T, Vatner SF, Sadoshima J, Tian B. Comparative Analysis of mRNA Isoform Expression in Cardiac Hypertrophy and Development Reveals Multiple Post-Transcriptional Regulatory Modules. *PLoS One*. 2011;6.

27. Kim T, Kim JO, Oh JG, Hong S, Kim DH. Pressure-Overload Cardiac Hypertrophy Is Associated with Distinct Alternative Splicing Due to Altered Expression of Splicing Factors. *Mol Cells*. 2014;37:81–87.

28. Heinig M, Adriaens ME, Schafer S, Deutekom HWM Van, Lodder EM, Ware JS, Schneider V, Felkin LE, Creemers EE. Natural genetic variation of the cardiac transcriptome in non-diseased donors and patients with dilated cardiomyopathy. *Genome Biol*. 2017;18:1–21.

29. Kong SW, Hu YW, Ho JWK, Ikeda S, Polster S, John R, Hall JL, Bisping E, Pieske B, Remedios CG, Pu WT. Heart Failure – Associated Changes in RNA Splicing of Sarcomere Genes. *Circ Cardiovasc Genet*. 2010;138–146.

30. Müller-McNicoll M, Botti V, de Jesus Domingues AM, Brandl H, Schwich OD, Steiner MC, Curk T, Poser I, Zarnack K, Neugebauer KM. SR proteins are NXF1 adaptors that link alternative RNA processing to mRNA export. *Genes Dev*. 2016;30:553–566.

31. Lemaire R, Prasad J, Kashima T, Gustafson J, Manley JL, Lafyatis R. Stability of a PKCI-1 -related mRNA is controlled by the splicing factor ASF / SF2 : a novel function for SR proteins. *Genes Dev*. 2002;16:594–607.

32. Lejeune F, Maquat LE. Mechanistic links between nonsense-mediated mRNA decay and pre-mRNA splicing in mammalian cells. *Curr Opin Cell Biol*. 2005;17:309–315.

33. Singh G, Kucukural A, Cenik C, Leszyk JD, Shaffer SA, Weng Z, Moore MJ. The Cellular EJC Interactome Reveals Higher-Order mRNP Structure and an EJC-SR Protein Nexus. *Cell*. 2012;151:750–764.

34. Kim J, Park RY, Chen JK, Kim J, Jeong S, Ohn T. Splicing factor SRSF3 represses the translation of programmed cell death 4 mRNA by associating with the 5′-UTR region. *Cell Death Differ*. 2014;21:481–490.

35. Sanford JR, Gray NK, Beckmann K, Cáceres JF. A novel role for shuttling SR proteins in mRNA translation. *Genes Dev*. 2004;18:755–768.

36. Mo S, Ji X, Fu X. Unique role of SRSF2 in transcription activation and diverse functions of the SR and hnRNP proteins in gene expression regulation. *Transcription*. 2013;1264.

37. Änkö ML, Müller-McNicoll M, Brandl H, Curk T, Gorup C, Henry I, Ule J, Neugebauer KM. The RNA-binding landscapes of two SR proteins reveal unique functions and binding to diverse RNA classes. *Genome Biol*. 2012;13:R17.

38. Ding JH, Xu X, Yang D, Chu PH, Dalton ND, Ye Z, Yeakley JM, Cheng H, Xiao RP, Ross J, Chen J, Fu XD. Dilated cardiomyopathy caused by tissue-specific ablation of SC35 in the heart. *EMBO J*. 2004;23:885–896.

39. Xu X, Yang D, Ding JH, Wang W, Chu PH, Dalton ND, Wang HY, Bermingham JR, Ye Z, Liu F, Rosenfeld MG, Manley JL, Ross J, Chen J, Xiao RP, Cheng H, Fu XD. ASF/SF2-regulated CaMKIIδ alternative splicing temporally reprograms excitation-contraction coupling in cardiac muscle. *Cell*. 2005;120:59–72.

40. Feng Y, Valley MT, Lazar J, Yang AL, Bronson RT, Firestein S, Coetzee WA, Manley JL. SRp38 Regulates Alternative Splicing and Is Required for Ca2+ Handling in the Embryonic Heart. *Dev Cell*. 2009;16:528–538.

41. Grishina I, Lorenz M, Pabis M, Poser I, Rollins J, Sapra AK. SR Protein Family Members Display Diverse Activities in the Formation of Nascent and Mature mRNPs In Vivo. *Mol Cell*. 2009;179–190.

42. Perales R, Bentley D. ‘“ Cotranscriptionality ”’: The Transcription Elongation Complex as a Nexus for Nuclear Transactions. *Mol Cell*. 2009;36:178–191.

43. Boutz PL, Bhutkar A, Sharp PA. Detained introns are a novel, widespread class of post-transcriptionally spliced introns. *Genes Dev*. 2015;29:63–80.

44. Wang Y, Wang J, Gao L, Stamm S, Andreadis A. An SRp75 / hnRNPG complex interacting with hnRNPE2 regulates the 5 ’ splice site of tau exon 10 , whose misregulation causes frontotemporal dementia. *Gene*. 2011;485:130–138.

45. Zimowska G, Shi J, Munguba G, Jackson MR, Alpatov R, Simmons MN, Shi Y, Sugrue SP. Pinin/DRS/memA Interacts with SRp75, SRm300 and SRrp130 in Corneal Epithelial Cells. *Invest Ophthalmol Vis Sci*. 2003;44.

46. Änkö ML, Morales L, Henry I, Beyer A, Neugebauer KM. Global analysis reveals SRp20-and SRp75-specific mRNPs in cycling and neural cells. *Nat Struct Mol Biol*. 2010;17:962–970.

47. Liu J, Huang B, Xiao Y, Xiong HM, Li J, Feng DQ, Chen XM, Zhang H Bin, Wang XZ. Aberrant expression of splicing factors in newly diagnosed acute myeloid leukemia. *Onkologie*. 2012;35:335–340.

48. Lucena-Araujo AR, Santana-Lemos BA, Thome CH, Ferreira GA, Ruggero D, Faça VM, Rego EM. Early Hematopoietic Progenitors of Dkc1 Hypomorphic Mutant Mice Display Decreased Proliferation Rate and an Impaired Control of Serine/Arginine-Rich Splicing Factor 4 (Srsf4) Translation. *Blood*. 2014;124:2937.

49. Ruijter JM, Ramakers C, Hoogaars WMH, Karlen Y, Bakker O, Hoff MJB Van Den, Moorman AFM. Amplification efficiency : linking baseline and bias in the analysis of quantitative PCR data. *Nucleic Acids Res*. 2009;37.

50. Karikó K, Buckstein M, Ni H, Weissman D. Suppression of RNA recognition by Toll-like receptors: The impact of nucleoside modification and the evolutionary origin of RNA. *Immunity*. 2005;23:165–175.

51. Warren L, Manos PD, Ahfeldt T, Loh YH, Li H, Lau F, Ebina W, Mandal PK, Smith ZD, Meissner A, Daley GQ, Brack AS, Collins JJ, Cowan C, Schlaeger TM, Rossi DJ. Highly efficient reprogramming to pluripotency and directed differentiation of human cells with synthetic modified mRNA. *Cell Stem Cell*. 2010;7:618–630.

52. Brand NJ, Lara-pezzi E, Rosenthal N, Barton PJR. Analysis of Cardiac Myocyte Biology in Transgenic Mice: A Protocol for Preparation of Neonatal Mouse Cardiac Myocyte Cultures. *Methods Mol Biol*. 2010;633:113–124.

53. Konig J, Zarnack K, Rot G, Curk T, Kayikci M, Zupan B, Turner DJ, Luscombe NM, Ule J. iCLIP - Transcriptome-wide Mapping of Protein-RNA Interactions with Individual Nucleotide Resolution. *J Vis Exp*. 2011;2–8.

54. Mandal PK, Rossi DJ. Reprogramming human fibroblasts to pluripotency using modified mRNA. *Nat Protoc*. 2013;8:568–582.

55. Hochberg I, Harvey I, Tran QT, Stephenson EJ. Gene expression changes in subcutaneous adipose tissue due to Cushing ' s disease. *J Mol Endocrinol*. 2015;55:81–94.

56. Kattel S, Memon S, Saito K, Narula J, Saito Y. An effect of left ventricular hypertrophy on mild-to-moderate left ventricular diastolic dysfunction. *Hell J Cardiol*. 2016;57:92–98.

57. Kang Y. Cardiac hypertrophy: A risk factor for QT-prolongation and cardiac sudden death. *Toxicol Pathol*. 2006;34:58–66.

58. Esteller M. Non-coding RNAs in human disease. *Nat Rev Genet*. 2011;12:861–874.

59. He L, Hannon GJ. MicroRNAs: small RNAs with a big role in gene regulation. *Nat Rev Genet*. 2004;5:522–531.

60. Gutschner T, Diederichs S. The hallmarks of cancer. *RNA Biol*. 2012;9:703–719.

61. Physiology C. Long Non-Coding RNAs in Cardiac Remodeling. *Cell Physiol Biochem*. 2017;200444:1830–1837.

62. Han P, Li W, Lin C-H, Yang J, Shang C, Nurnberg ST, Jin KK, Xu W, Lin C-Y, Lin C-J, Xiong Y, Chien H-C, Zhou B, Ashley E, Bernstein D, Chen P-S, Chen H-SV, Quertermous T, Chang C-P. A long noncoding RNA protects the heart from pathological hypertrophy. *Nature*. 2014;514:102.

63. Viereck J, Kumarswamy R, Foinquinos A, Xiao K, Avramopoulos P, Kunz M, Dittrich M, Maetzig T, Zimmer K, Remke J, Just A, Fendrich J, Scherf K, Bolesani E, Schambach A, Weidemann F, Zweigerdt R, Windt LJ De, Engelhardt S, Dandekar T, Batkai S, Thum T. Long noncoding RNA Chast promotes cardiac remodeling. *Sci Transl Med*. 2016;8:1–13.

64. Wang K, Liu F, Zhou L, Long B, Yuan S, Wang Y, Liu C. The Long Noncoding RNA CHRF Regulates Cardiac Hypertrophy by Targeting miR-489. *Circ Res*. 2014;114:1377–1388.

65. Jiang F, Zhou X, Huang J. Long Non-Coding RNA-ROR Mediates the Reprogramming in Cardiac Hypertrophy. *PLoS One*. 2016;4:1–10.

66. Maquat LE. When cells stop making sense : Effects of nonsense codons on RNA metabolism in vertebrate cells. *RNA*. 1995;1:453–465.

67. Kervestin S, Jacobson A. NMD: a multifaceted response to premature translational termination. *Nat Rev Mol Cell Biol*. 2012;13:700–712.

68. Hurt JA, Robertson AD, Burge CB. Global analyses of UPF1 binding and function reveal expanded scope of nonsense-mediated mRNA decay. *Genome Res*. 2013;23:1636–1650.

69. Bazzini AA, Johnstone TG, Christiano R, Mackowiak SD, Obermayer B, Fleming ES, Vejnar CE, Lee MT, Rajewsky N, Walther TC, Giraldez AJ. Identification of small ORFs in vertebrates using ribosome footprinting and evolutionary conservation. *EMBO J*. 2014;33:981–993.

70. Smith JE, Ã KEB. Nonsense-mediated RNA decay – aswitch and dial for regulating geneexpression. *Bioessays*. 2015;37:612–623.

71. Physiology M. A peptide encoded by a transcript annotated as long noncoding RNA enhances SERCA activity in muscle. *Science (80-)*. 2016;351.

72. Matsumoto A, Pasut A, Matsumoto M, Yamashita R, Fung J, Monteleone E, Saghatelian A, Nakayama KI, Clohessy JG, Pandolfi PP. mTORC1 and muscle regeneration are regulated by the LINC00961-encoded SPAR polypeptide. *Nature*. 2016;541:228.

73. Rion N, Rüegg MA. LncRNA-encoded peptides: More than translational noise? *Cell Res*. 2017;27:604–605.

74. Tani H, Torimura M, Akimitsu N. The RNA Degradation Pathway Regulates the Function of GAS5 a Non-Coding RNA in Mammalian Cells. *PLoS One*. 2013;8:1–9.

75. Karousis ED, Mühlemann O. Nonsense-mediated mRNA decay : novel mechanistic insights and biological impact. *WIREs RNA*. 2016;7:661–682.

76. Colombo M, Karousis ED, Bourquin J, Bruggmann R, Mühlemann O. Transcriptome-wide identification of NMD-targeted human mRNAs reveals extensive redundancy between SMG6- and SMG7-mediated degradation pathways. *RNA*. 2017;189–201.

77. Yu XIN, Li Z. Long non - coding RNA growth arrest-specific transcript 5 in tumor biology. *Oncol Lett*. 2015;10:1953–1958.

78. Kino T, Hurt DE, Ichijo T, Nader N, Chrousos GP. Noncoding RNA Gas5 is a growth arrest- and starvation-associated repressor of the glucocorticoid receptor. *Sci Signal*. 2010;3:1–16.

79. Tani H, Mizutani R, Salam KA, Tano K, Ijiri K, Wakamatsu A, Isogai T, Suzuki Y, Akimitsu N. Genome-wide determination of RNA stability reveals hundreds of short-lived noncoding transcripts in mammals. *Genome Res*. 2012;947–956.

80. Mourtada-Maarabouni M, Pickard MR, Hedge VL, Farzaneh F, Williams GT. GAS5, a non-protein-coding RNA, controls apoptosis and is downregulated in breast cancer. *Oncogene*. 2008;28:195.

81. Shi Y, Parag S, Patel R, Lui A, Murr M, Cai J, Shi Y, Parag S, Patel R, Lui A, Murr M, Cai J, Patel NA. Stabilization of lncRNA GAS5 by a Small Molecule and Its Implications in Diabetic Adipocytes Article Stabilization of lncRNA GAS5 by a Small Molecule and Its Implications in Diabetic Adipocytes. *Cell Chem Biol*. 2019;26:319–330.e6.

82. dDe Vries WB, van der Leij FR, Bakker JM, Kamphuis PJGH, van Oosterhout MFM, Schipper MEI, Smid GB, Bartelds B, van Bel F. Alterations in Adult Rat Heart after Neonatal Dexamethasone Therapy. *Pediatr Res*. 2002;52:900.

83. Lister K, Autelitano DJ, Jenkins A, Hannan RD, Sheppard KE. Cross talk between corticosteroids and alpha-adrenergic signalling augments cardiomyocyte hypertrophy : A possible role for SGK1. *Cardiovasc Res*. 2006;70:555–565.

84. Muiesan ML, Lupia M, Salvetti M, Grigoletto C, Sonino N, Boscaro M, Rosei EA, Mantero F. Left Ventricular Structural and Functional Characteristics in Cushing ' s Syndrome. *J Am Coll Cardiol*. 2003;41:2275–2279.

85. Ren R, Oakley RH, Cruz-topete D, Cidlowski JA. Dual Role for Glucocorticoids in Cardiomyocyte Hypertrophy and Apoptosis. *Endocrinology*. 2012;153:1–15.

86. Wang H-Y, Xu X, Ding J-H, Bermingham JR, Fu X-D. SC35 Plays a Role in T Cell Development and Alternative Splicing of CD45. *Mol Cell*. 2001;7:331–342.

87. Jumaa H, Wei G, Nielsen PJ. Blastocyst formation is blocked in mouse embryos lacking the splicing factor SRp20. *Curr Biol*. 1999;9:899–902.

88. Ortiz-sánchez P, Villalba-orero M, López-olañeta MM, Larrasa-alonso J, Sánchez-cabo F, Martí-gómez C, Camafeita E, Gómez-salinero JM, Ramos-hernández L, Nielsen PJ, Vázquez J, Müller-mcnicoll M, García-pavía P, Lara-pezzi E. Loss of SRSF3 in Cardiomyocytes Leads to Decapping of Contraction-Related mRNAs and Severe Systolic Dysfunction. *Circ Res*. 2019;125:170–183.

89. Veselka J, Anavekar NS, Charron P. Hypertrophic obstructive cardiomyopathy. *Lancet*. 2017;389:1253–1267.

90. Iwasaki H. Reversible alterations in cardiac morphology and functions in a patient with Cushing ' s syndrome. *Endocrinol Diabetes Metab*. 2014;

91. Avenatti E, Rebellato A, Iannaccone A, Battocchio M. Left ventricular geometry and 24-h blood pressure profile in Cushing ' s syndrome. *Endocrine*. 2017;55:547–554.

92. Tsagarakis DAVS. Cardiac hypertrophy in Cushing ' s syndrome : if not hypertension then what ? *Endocrine*. 2017;453–455.

Material Suplementario: Figuras

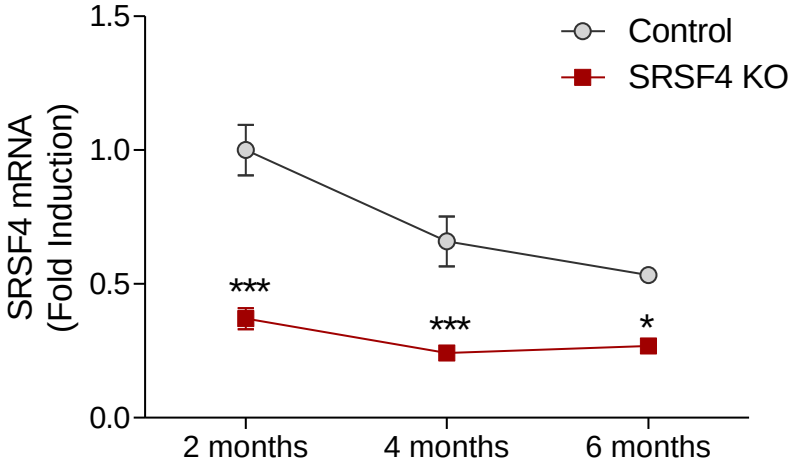

Figura suplementaria 1. Expresión de SRSF4 en corazones control y SRSF4 KO. Análisis por qRT-PCR de la expresión del mRNA de SRSF4 en corazones control y SRSF4 KO a diferentes edades. Los datos están representados como la media ±SEM, n=4-5 ratones por grupo. *p<0.05, **p<0.01, ***p<0.001 SRSF4 KO vs Control, ANOVA de dos vía con test de Bonferroni.

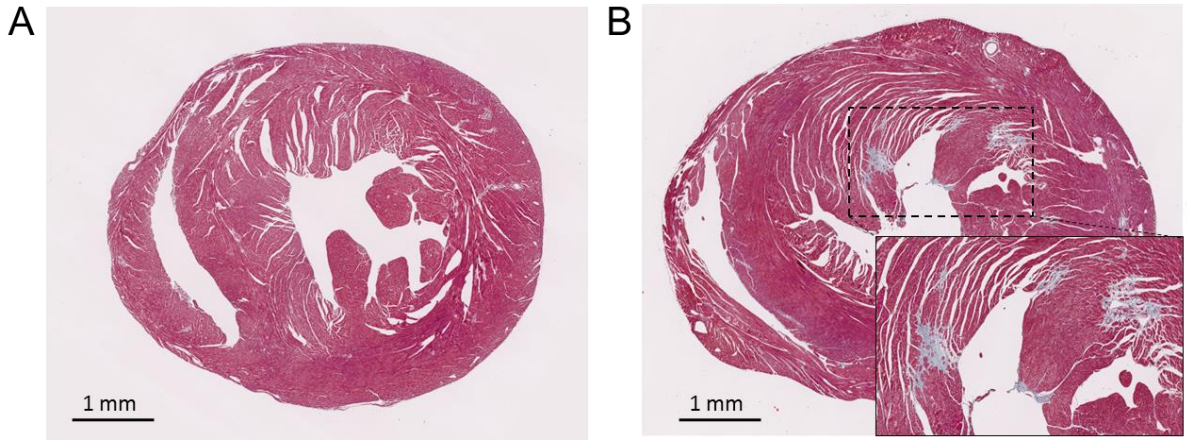

Figura suplementaria 2. Focos de fibrosis en los ratones SRSF4 KO. Imagen representativa de cortes histológicos de corazón de ratones control (A) y SRSF4 KO (B) a los 10 meses de edad con tinción tricrómico de Masson.

Material Suplementario: Tablas

Tabla suplementaria 1. Datos ecocardiográficos de ratones control y SRSF4 KO a distintas edades. Los datos están representados como la media ±SEM. LVWT, left ventricular wall thickness, del inglés; LVEF, left ventricular ejection fraction, del inglés; LVVOLd, left ventricular end diastolic volume; IVRT, isovolumetric relaxation time. *p<0.05, **p<0.01, ***p<0.001 for SRSF4 KO vs Control; 2-way ANOVA followed by the Bonferroni post-test.

	6 months		10 months		14 months	
	Control	**SRSF4 KO**	**Control**	**SRSF4 KO**	**Control**	**SRSF4 KO**
LVWT (mm)	1.15±0.04	1.35±0.05	1.13±0.05	1.41±0.06**	1.07±0.07	1.38±0.05**
Normalized Cardiac Mass	2.55±0.09	3.39±0.20	2.94±0.16	3.88±0.28**	2.85±0.22	4.46±0.28***
LVEF (%)	54.97±2.01	53.44±2.83	55.26±2.22	50.86±5.12	54.46±2.23	57.21±1.94
LVVOLd (µl)	67.20±2.97	67.14±2.91	55.72±3.32	61.36±3.01	61.73±2.87	67.64±3.37
n	6	10	8	10	5	9
IVRT (ms)	10.83±0.80	11.52±1.38	13.13±0.46	14.67±0.34	13.65±0.65	17.53±1.01*
n	6	6	6	6	6	6

Tabla Suplementaria 2. Análisis de diferencia de expresión génica en corazones de ratones SRSF4 KO. Se encuentra incluida en el CD adjuntado con esta Tesis Doctoral.

Tabla suplementaria 3. Eventos de Splicing Alternativo en los corazones de los ratones control y SRSF4 KO. Se encuentra incluida en el CD adjuntado con esta Tesis Doctoral.

Tabla suplementaria 4. Genes que están diferencialmente expresados en los corazones SRSF4 KO y que son dianas directas de SRSF4 en cardiomiocitos.

ID Ensembl	Gene
ENSMUSG00000001870	Ltbp1
ENSMUSG00000003228	Grk5
ENSMUSG00000011256	Adam19
ENSMUSG00000016921	Srsf6
ENSMUSG00000017692	Rhbdl3
ENSMUSG00000019848	Popdc3
ENSMUSG00000020646	Mboat2
ENSMUSG00000021219	Rgs6
ENSMUSG00000022111	Uchl3
ENSMUSG00000022587	Ly6e
ENSMUSG00000023067	Cdkn1a
ENSMUSG00000024072	Yipf4
ENSMUSG00000024780	Cdc37l1
ENSMUSG00000025579	Gaa
ENSMUSG00000026131	Dst
ENSMUSG00000026483	Fam129a
ENSMUSG00000026520	Pycr2
ENSMUSG00000026610	Esrrg
ENSMUSG00000026944	Abca2
ENSMUSG00000027381	Bcl2l11
ENSMUSG00000028911	Srsf4
ENSMUSG00000031636	Pdlim3
ENSMUSG00000037270	4932438A13Rik
ENSMUSG00000037940	Inpp4b
ENSMUSG00000038335	Tsr1
ENSMUSG00000039958	Mettl20
ENSMUSG00000042719	Naa25
ENSMUSG00000043445	Pgp
ENSMUSG00000050565	Tor1aip2
ENSMUSG00000051451	Crebzf
ENSMUSG00000053332	**GAS5**
ENSMUSG00000053886	Sh2d4a
ENSMUSG00000054752	Fsd1l
ENSMUSG00000059895	Ptp4a3
ENSMUSG00000060913	Trim55
ENSMUSG00000061589	Dot1l
ENSMUSG00000062210	Tnfaip8

ENSMUSG00000064302	Clasp1
ENSMUSG00000066232	Ipo7
ENSMUSG00000070509	Rgma
ENSMUSG00000073409	H2-Q6
ENSMUSG00000074221	Zfp568

Material Suplementario: Publicaciones

Actualmente se encuentra en fase de revisión en *Circulation Research* el siguiente manuscrito:

- **Javier Larrasa-Alonso**, María Villalba-Orero, Carlos Martí-Gómez, Paula Ortiz-Sánchez, Marina M López-Olañeta, Fátima Sánchez-Cabo, François McNicoll, Michaela Müller-McNicoll, Pablo García-Pavía and Enrique Lara-Pezzi. "SRSF4–GAS5-lncRNA interaction regulates left ventricular hypertrophy by inhibiting the glucocorticoid receptor"

Durante esta Tesis Doctoral se ha contribuido a las siguientes publicaciones:

- Laura Padrón-Barthe, María Villalba-Orero, Jesús M. Gómez-Salinero, Fernando Domínguez, Marta Román, **Javier Larrasa-Alonso**, Paula Ortiz-Sánchez, Fernando Martínez, Marina López-Olañeta, Elena Bonzón-Kulichenko, Jesús Vázquez, Carlos Martí-Gómez, Demetrio J. Santiago, Belén Prados, Giovanna Giovinazzo, María Victoria Gómez-Gaviro, Silvia Priori, Pablo Garcia-Pavia, and Enrique Lara-Pezzi. "Severe cardiac dysfunction and death caused by ARVC type 5 is improved by inhibition of GSK3b". *Circulation,* 2019;140(14):1188-1204.

- Paula Ortiz-Sánchez, María Villalba-Orero, Marina M López-Olañeta, **Javier Larrasa-Alonso**, Fátima Sánchez-Cabo, Carlos Martí-Gómez, Emilio Camafeita, Jesús M Gómez-Salinero, Laura Ramos-Hernández, Peter J Nielsen, Jesús Vázquez, Michaela Müller-McNicoll, Pablo García-Pavía and Enrique Lara-Pezzi. "Loss of SRSF3 in cardiomyocytes leads to decapping of contraction related mRNAs and severe systolic dysfunction". *Circ Res*. 2019, 5;125(2):170-183.

- Jesús M Gómez-Salinero, Marina M López-Olañeta, Paula Ortiz-Sánchez, **Javier Larrasa-Alonso**, Alberto Gatto, Leanne E Felkin, Paul JR Barton, Inmaculada Navarro-Lérida, Miguel Ángel del Pozo, Pablo García-Pavía, Balaji Sundararaman, Giovanna Giovinaz, Gene W. Yeo and Enrique Lara-Pezzi. "The Calcineurin Variant CnAbeta1 Controls Mouse Embryonic Stem Cell Differentiation by Directing mTORC2 Membrane Localization and Activation". *Cell Chem Biol*. 2016, 23(11):1372-82.

Circulation

ORIGINAL RESEARCH ARTICLE

Severe Cardiac Dysfunction and Death Caused by Arrhythmogenic Right Ventricular Cardiomyopathy Type 5 Are Improved by Inhibition of Glycogen Synthase Kinase-3β

BACKGROUND: Arrhythmogenic cardiomyopathy/arrhythmogenic right ventricular cardiomyopathy (ARVC) is an inherited cardiac disease characterized by fibrofatty replacement of the myocardium, resulting in heart failure and sudden cardiac death. The most aggressive arrhythmogenic cardiomyopathy/ARVC subtype is ARVC type 5 (ARVC5), caused by a p.S358L mutation in TMEM43 (transmembrane protein 43). The function and localization of TMEM43 are unknown, as is the mechanism by which the p.S358L mutation causes the disease. Here, we report the characterization of the first transgenic mouse model of ARVC5.

METHODS: We generated transgenic mice overexpressing TMEM43 in either its wild-type or p.S358L mutant (TMEM43-S358L) form in postnatal cardiomyocytes under the control of the α-myosin heavy chain promoter.

RESULTS: We found that mice expressing TMEM43-S358L recapitulate the human disease and die at a young age. Mutant TMEM43 causes cardiomyocyte death and severe fibrofatty replacement. We also demonstrate that TMEM43 localizes at the nuclear membrane and interacts with emerin and β-actin. TMEM43-S358L shows partial delocalization to the cytoplasm, reduced interaction with emerin and β-actin, and activation of glycogen synthase kinase-3β (GSK3β). Furthermore, we show that targeting cardiac fibrosis has no beneficial effect, whereas overexpression of the calcineurin splice variant calcineurin Aβ1 results in GSK3β inhibition and improved cardiac function and survival. Similarly, treatment of TMEM43 mutant mice with a GSK3β inhibitor improves cardiac function. Finally, human induced pluripotent stem cells bearing the p.S358L mutation also showed contractile dysfunction that was partially restored after GSK3β inhibition.

CONCLUSIONS: Our data provide evidence that TMEM43-S358L leads to sustained cardiomyocyte death and fibrofatty replacement. Overexpression of calcineurin Aβ1 in TMEM43 mutant mice or chemical GSK3β inhibition improves cardiac function and increases mice life span. Our results pave the way toward new therapeutic approaches for ARVC5.

Laura Padrón-Barthe, PhD
María Villalba-Orero, PhD
Jesús M. Gómez-Salinero, PhD
Fernando Domínguez, MD, PhD
Marta Román, MLT
Javier Larrasa-Alonso, MSc
Paula Ortiz-Sánchez, PhD
Fernando Martínez, PhD
Marina López-Olañeta, MLT
Elena Bonzón-Kulichenko, PhD
Jesús Vázquez, PhD
Carlos Martí-Gómez, MSc
Demetrio J. Santiago, PhD
Belén Prados, PhD
Giovanna Giovinazzo, PhD
María Victoria Gómez-Gaviro, PhD
Silvia Priori, MD, PhD
Pablo Garcia-Pavia, MD, PhD*
Enrique Lara-Pezzi, PhD*

*Drs Garcia-Pavia and Lara-Pezzi contributed equally as senior authors.

Key Words: arrhythmogenic right ventricular dysplasia ■ calcineurin ■ GSK3β ■ therapy ■ TMEM43

Sources of Funding, see page 1203

https://www.ahajournals.org/journal/circ

Clinical Perspective

What Is New?

- This is the first animal model to reproduce human arrhythmogenic right ventricular cardiomyopathy (ARVC) type 5, the most aggressive subtype of arrhythmogenic cardiomyopathy.
- Transgenic mice expressing TMEM43 (transmembrane protein 43)–S358L show fibrofatty replacement of the myocardium and die at a young age.
- This model confirms that TMEM43 is localized mostly at the nuclear membrane and provides new information on the pathophysiological mechanism of ARVC5.
- As in other forms of ARVC, the glycogen synthase kinase-3β signaling pathway plays an important role in this disease.

What Are the Clinical Implications?

- Using this animal model, our work tests 2 new therapeutic approaches for ARVC5, for which there are currently no effective therapies to prevent disease progression in humans.
- Although the antifibrotic drug GM-CT-01 did not show a beneficial effect on transgenic mice expressing TMEM43-S358L, inhibition of glycogen synthase kinase-3β improved cardiac function and survival, opening the way to a new therapeutic approach focused on glycogen synthase kinase-3β inhibition that could be used in humans with ARVC5 in the future.

Arrhythmogenic cardiomyopathy (ACM)/arrhythmogenic right ventricular cardiomyopathy (ARVC) is an incurable genetically inherited disease that causes heart failure and sudden cardiac death.[1,2] ACM/ARVC is an autosomal dominant disease with rare recessive forms. To date, 15 independent loci and 13 dominant ACM/ARVC–causing genes have been linked to the condition. Up to 60% of ACM/ARVC cases have been attributed to mutations in genes encoding proteins of the desmosomal complex, with a significant minority caused by mutations in nondesmosomal genes.[3–5] The most aggressive ACM/ARVC subtype is ACM/ARVC type 5 (ARVC5), which is caused by a point substitution (p.S358L) in a highly conserved TMEM43/LUMA (transmembrane region of transmembrane protein 43). The causal gene for ARVC5 was first described in families from Newfoundland (Canada) in 2008 as the cause of a fully penetrant aggressive disease with a high incidence of malignant ventricular arrhythmias.[6] Since then, several other patients have been diagnosed around the globe. Prognosis is very poor, with more than half of affected men dying by the age of 50 years.[7] The pathogenic mechanism of ARVC5 and the role of TMEM43 in the genesis of the disease are poorly understood, precluding the development of effective therapies.

Here, we report the characterization of the first transgenic mouse model of ARVC5. We analyzed disease development and progression in depth and determined the localization, function, and mechanism of action of TMEM43. Finally, we show that glycogen synthase kinase-3β (GSK3β) inhibition with a chemical inhibitor or by calcineurin Aβ1 (CnAβ1) overexpression improves cardiac function and survival of mice with ARVC5.

METHODS

Data Availability

The data that support the findings of this study are available from the corresponding authors on reasonable request. RNA sequencing data are available at the GEO repository (GSE101301). Proteomic data are available at the PeptideAtlas repository (http://www.peptideatlas.org/PASS/PASS01063). Full Methods can be found in the online-only Data Supplement.

Mice

TMEM43 wild-type (TMEM43WT) and TMEM43 mutant (TMEM43mut) mice, in the C57BL/6JCrl (Charles River Laboratories) background, express human WT TMEM43 and human TMEM43-S358L, respectively, specifically in cardiomyocytes under the control of the myosin heavy chain (MHC) promoter. WT C57BL/6JCrl mice were used as controls. TMEM43mut male mice were crossed with α-myosin heavy chain–CnAβ1 mice[8] to generate the double-transgenic mouse line TMEM43mut-CnAβ1. Male and female mice were used throughout the study. Mice were housed in an air-conditioned room with a 12-hour light/dark cycle with free access to water and chow. For the inhibition of galectin 3, TMEM43mut mice were randomized to the saline-treated control group (n=8) or the GM-CT-01–treated group (n=8). Mice were treated twice a week with intravenous injections of GM-CT-01 (120 mg/kg) or placebo (normal saline) in the tail vein from 5 weeks to 4 months of age. For GSK3β inhibition, mice were injected intraperitoneally daily with SB216763 (2.5 mg/kg per day). All procedures were approved by the Centro Nacional de Investigaciones Cardiovasculares Carlos III Ethics Committee and the Regional Government of Madrid (PA-27/13, PROEX-177/17). All animal experiments conformed to EU Directive 2010/63EU and Recommendation 2007/526/EC, enforced in Spanish law under Real Decreto 53/2013.

Echocardiography

Cardiac function, chamber dilatation, and wall thickness were analyzed in neonatal mice and in mice 3 and 5 weeks and 2 and 4 months of age by transthoracic 2D and M-mode echocardiography. Measurements were carried out by a blinded operator using a high-frequency ultrasound system with a 50-MHz linear probe for neonates and a 30-MHz probe for older mice (Vevo 2100, Visualsonics Inc). For ultrasound scans, mice were

placed on a heating pad; neonates were not anesthetized, whereas older mice were kept under light anesthesia with isoflurane adjusted to obtain a target heart rate of 500±50 bpm. Left ventricular (LV) ejection fraction (EF) and LV end-diastolic volume were obtained from the long-axis view, and LV posterior wall in diastole was obtained from the short-axis view. Right ventricular systolic function was assessed indirectly from the tricuspid annular plane systolic excursion, estimated from maximum lateral tricuspid annulus movement obtained from a 2D 4-chamber apical view. Images were analyzed offline by an expert using the Vevo 2100 Workstation software. Animals were euthanized by gradually filling the chamber with carbon dioxide. Mice, hearts, and lungs were weighed after death.

Electrocardiograms

ECGs were obtained in unanesthetized neonates and in 3- and 5-week-old and 2- and 4-month-old anesthetized mice with bipolar limb leads (leads I, II, and III) and unipolar limb leads (leads aVR, aVL, and aVF) for 60 to 90 seconds. Measurements were taken by a blinded operator with mice (except for neonates) placed under light anesthesia with isoflurane (MP36R, BIOPAC Systems, Inc). ECGs were analyzed by an expert using Acqknowledge 4.1.1. for MP36R (BIOPAC Systems, Inc). Mean values were calculated from 10 consecutive standard ECG time intervals and waves.

Cell Culture, Transfection, and Immunofluorescence

P19 cells were transfected with the following HA-tagged expression vectors for TMEM43: TMEM43WT-Ct-HA, Nt-HA-TMEM43WT, TMEM43-S358L-Ct-HA, and Nt-HA-TMEM43-S358L, where Nt and Ct indicate attachment of the HA tag to the N-terminus or the C-terminus. Cells were fixed in 4% paraformaldehyde in PBS for 10 minutes at 4°C, permeabilized for 10 minutes with 0.1% Triton X-100/PBS, and incubated in 10% goat serum/PBS for 30 minutes at room temperature. Cells were incubated overnight in 1% goat serum/PBS with anti-HA (11583816001, Roche). After primary antibody incubation, cells were washed with PBS, incubated for 1 hour at room temperature with Alexa Fluor 488 goat anti-mouse immunoglobulin G (A-11029; Thermo Fisher Scientific) and DAPI in 1% goat serum/PBS, and mounted in Vectashield mounting medium. Images were acquired with a Nikon A1R multiline inverted confocal microscope, a Plan Apo VC 60×/1,4 Oil DIC N2 Oil objective, and Nikon NIS reprocessing software. Brightness and contrast were linearly adjusted with Adobe Photoshop CS5.1.

Immunoprecipitation

TMEM43 immunoprecipitation experiments were performed in the P19 cell line. Briefly, cells were transfected as described above. Cells were lysed with TBS buffer (150 mmol/L NaCl, 20 mmol/L Tris-HCl, pH 7.4) supplemented with 1% Nonidet P-40, 5 mmol/L EDTA, 5 mmol/L $MgCl_2$, and 1× complete protease, phosphatase, and acetylase inhibitors. Protein extracts were incubated with anti-HA–conjugated Dynabeads (Life Technologies) for 1 hour at 4°C. Beads were washed 3 times with lysis buffer containing 0.05% Nonidet P-40 and 5 times with lysis buffer without added detergent. Bound proteins were released from beads by boiling in 4× Laemmli sample buffer. Immunoprecipitates and input samples were resolved by SDS-PAGE or subjected to protein digestion followed by nanoliquid chromatography coupled to mass spectrometry for protein identification and quantification by peptide counting.[9] The proteomics data set (raw and msf files and protein database) is available in the PeptideAtlas repository (http://www.peptideatlas.org/PASS/PASS01063, which can be downloaded via ftp.peptideatlas.org: username, PASS01063; password, FZ6532b).

Statistical Analysis

All data are presented as mean±SEM. All data sets were analyzed for statistical significance by regular or repeated-measures 1-way ANOVA followed by Bonferroni or Dunnett posttest for multiple comparisons or 2-way ANOVA followed by Bonferroni posttest (GraphPad Prism), as indicated in the figure legends. Survival curves were compared by the log-rank (Mantel-Cox) test. Differences were considered statistically significant at $P<0.05$.

RESULTS

Cardiac-Restricted Expression of Human TMEM43-S358L Induces Biventricular Dysfunction and Reduces Survival

We generated transgenic mice expressing human TMEM43-S358L under the control of the α-myosin heavy chain promoter (TMEM43mut mice) to provide cardiac-specific expression of the mutant protein. As controls, we used mice overexpressing human WT TMEM43 (TMEM43WT mice) and WT littermates (Figure IA–IC in the online-only Data Supplement). TMEM43mut mice were dead by 6 months of age, with a median life span of 23 weeks, whereas TMEM43WT and WT mice showed no notable mortality at this age (Figure 1A).

Echocardiography showed a decline in LVEF that was already evident in the TMEM43mut group at 2 months of age, indicating a loss of LV contractility (Figure 1B and Table I and Video I in the online-only Data Supplement). Accordingly, TMEM43mut mice also developed progressive LV dilatation with a high LV end-diastolic volume (Figure 1C). Right ventricular contractility was also reduced in TMEM43mut mice at 4 months of age (Figure 1D). Although death was slightly delayed in females, no significant differences in survival and cardiac function were observed between males and females (Figure ID–IF in the online-only Data Supplement).

Gross morphology at 4 months revealed a clear enlargement of TMEM43mut hearts compared with TMEM43WT and WT hearts (Figure 1E). TMEM43mut mice also had an elevated ratio of heart weight to body weight at 4 months (Figure 1F). However, no changes were observed in ventricular wall thickness (Figure 1G). Decreased cardiac function in TMEM43mut mice was accompanied by pulmonary congestion at 4 months (Figure 1H).

Electrocardiographic analysis showed progressive P-wave prolongation and defective depolarization of the

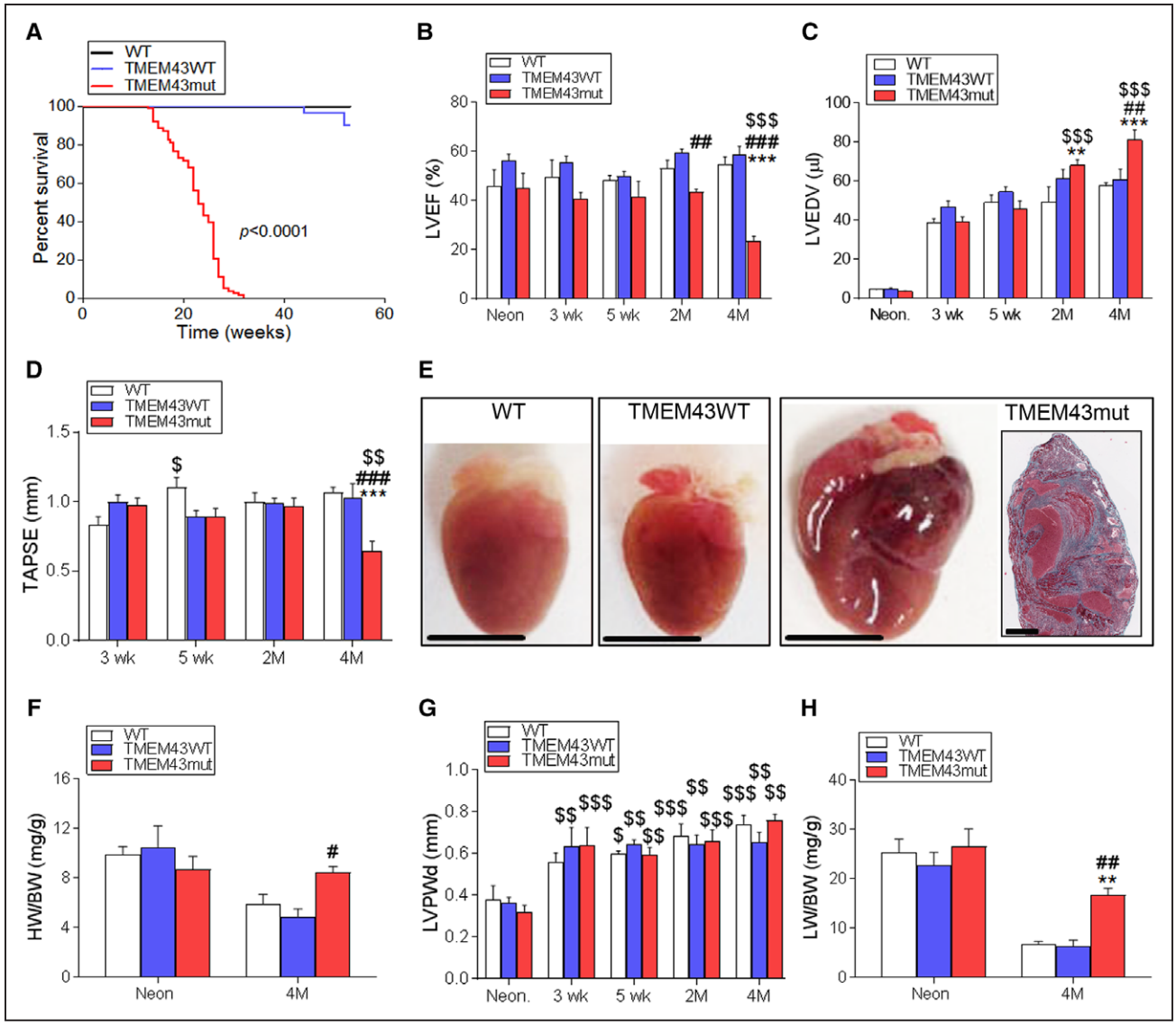

Figure 1. TMEM43 (transmembrane protein 43)–S358L expression in cardiomyocytes causes severe cardiac dysfunction.
A, Wild-type mice (WT; n=27) and mice overexpressing either WT TMEM43 (TMEM43WT; n=29) or TMEM43-S358L (TMEM43mut; n=84) under the control of the α-myosin heavy chain (αMHC) promoter were monitored for 60 weeks, and their survival rate was determined from a Kaplan-Meier curve. The indicated *P* value was obtained with a log-rank test. **B** through **D**, Left ventricular ejection fraction (LVEF), end-diastolic volume (LVEDV), and tricuspid annular plane systolic excursion (TAPSE) measured by echocardiography at birth (Neon) and at 3 and 5 weeks and 2 and 4 months of age. **E**, Gross morphology of representative hearts from 4-month-old WT, TMEM43WT, and TMEM43mut mice; bar, 500 µm. Inset, A thrombus in the left atrium of a TMEM43mut mouse; bar, 50 µm. **F**, Ratio of heart weight to body weight (HW/BW) determined at birth and at 4 months. **G**, LV posterior wall thickness in diastole (LVPWd) analyzed by echocardiography. **H**, Ratio of lung weight to body weight (LW/BW) determined at birth and at 4 months. Graphs show mean±SEM. ***P*<0.01, ****P*<0.001, TMEM43mut vs WT. #*P*<0.05, ##*P*<0.01, ###*P*<0.001, TMEM43mut vs TMEM43WT. $*P*<0.05, $$*P*<0.01, $$$*P*<0.001 for different time points vs neonates (**B**, **C**, and **G**) or 3 weeks (**D**) for each mouse line; 2-way regular (**B**, **C**, **F**, and **H**) or repeated-measures (**D** and **G**) ANOVA was used, followed by Bonferroni post-test; n=5 to 6 per group.

atria in TMEM43mut mice, some of which developed atrial fibrillation and atrial paralysis (Figure 2A and 2D and Table II in the online-only Data Supplement). Similarly, TMEM43mut mice had ventricular disease, as evidenced by a progressive widening of the QRS complex (Figure 2B and 2E) and a progressive decrease in QRS amplitude (Figure 2C and 2F). No differences were observed between males and females (Figure II in the online-only Data Supplement). Together, the results of the ECG suggest that TMEM43mut mice develop electric defects already noticeable at 5 weeks of age.

TMEM43-S358L Expression in the Heart Induces Cardiomyocyte Death and Fibrofatty Replacement

An important hallmark of human ACM/ARVC is the progressive fibrofatty replacement of the ventricular myocardium[10]; however, whether fibrofatty replacement is preceded by cardiomyocyte death has not been clearly demonstrated. We found a significant increase in circulating cardiac troponin I levels in TMEM43mut mice as early as 5 weeks of age (Figure 3A), indicating

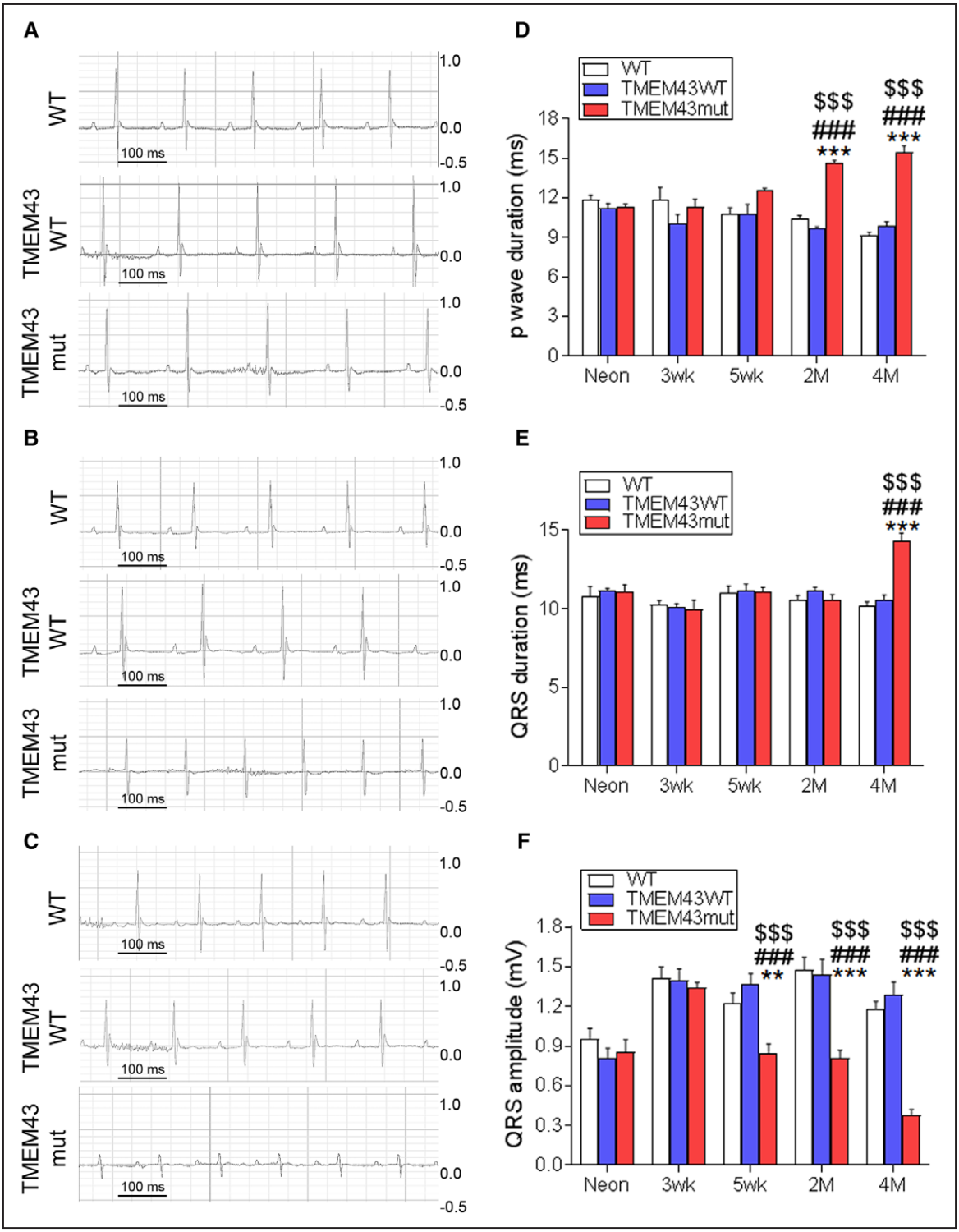

Figure 2. TMEM43 (transmembrane protein 43) mutant (mut) mice show cardiac conduction defects.
A through **C**, Surface electrocardiographic analysis of cardiac conduction in wild-type (WT), TMEM43WT, and TMEM43mut mice 1 day (**A**), 5 weeks (**B**), and 4 months (**C**) of age. Shown are 0.6-second traces from the V_3 lead. **D** through **F**, The p-wave duration (**D**) and QRS duration and amplitude (**E** and **F**) assessed at birth (Neon) and at 3 and 5 weeks and 2 and 4 months of age. Graphs show mean±SEM. ***P*<0.01, ****P*<0.001, TMEM43mut vs WT. ###*P*<0.001, TMEM43mut vs TMEM43WT. $$$*P*<0.001 for different time points vs neonates for each mouse line; 2-way repeated-measures ANOVA followed by Bonferroni post-test; n=6.

cardiomyocyte necrosis. We also investigated the activation of apoptosis by assessing the presence of procaspase 3 and cleaved caspase 3 in the hearts of these mice. At 2 months of age, TMEM43mut mice showed increased levels of cleaved caspase 3, which were maintained at 4 months, although the differences did not reach statistical significance (Figure 3B and Figure IIIA in the online-only Data Supplement). In addition, a similar

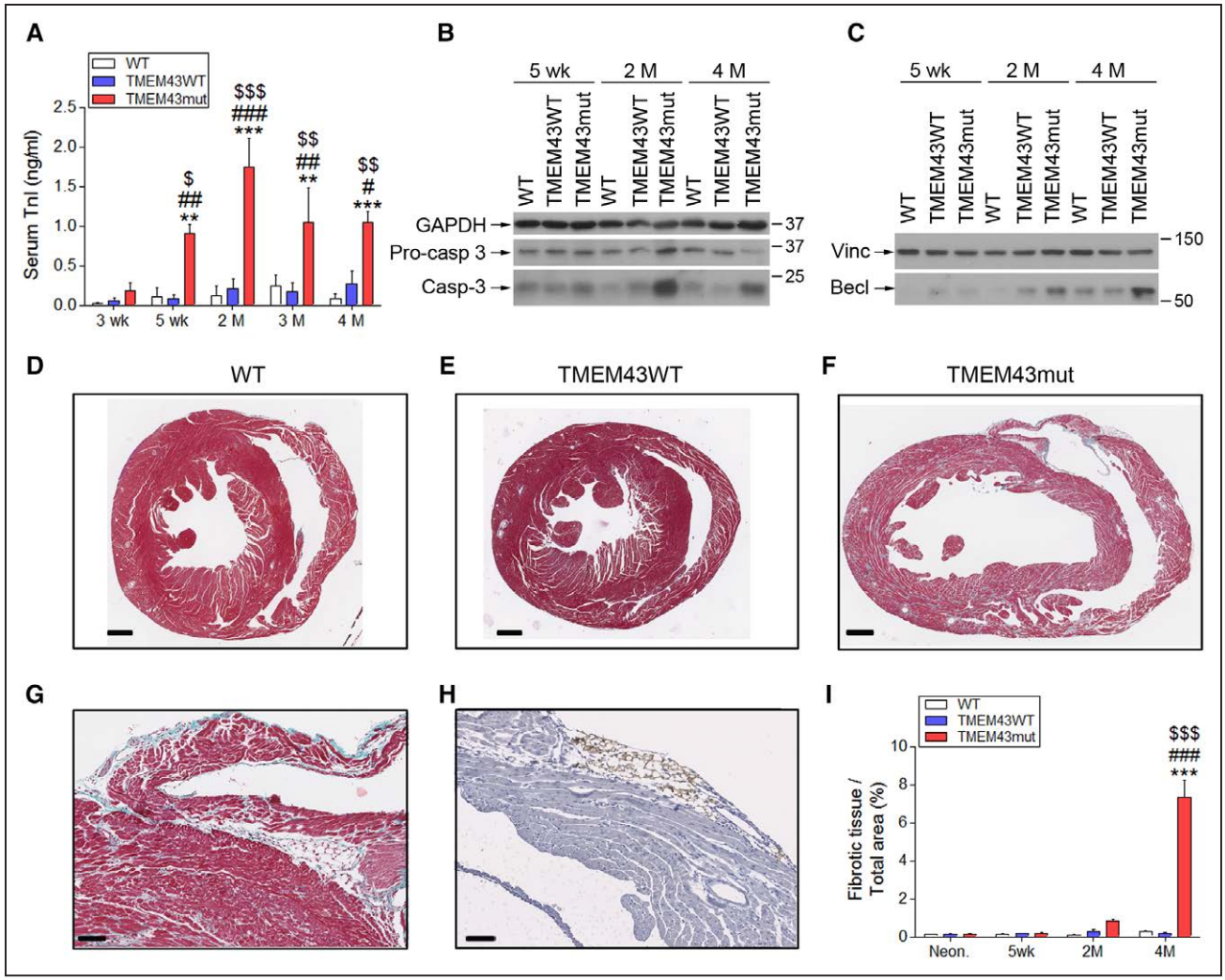

Figure 3. TMEM43 (transmembrane protein 43)–S358L causes cardiomyocyte death and replacement by fibrofatty tissue.
A, Serum troponin I (TnI) determined by ELISA in mice 3 and 5 weeks and 2, 3, and 4 months of age. **B** and **C**, Western blot analysis of the presence in myocardium of activated and total caspase 3 (casp-3; **B**) and beclin1 (Becl; **C**) at the indicated time points. **D** through **I**, Masson trichrome staining in myocardial sections from wild-type (WT; **D**), TMEM43WT (**E**), and TMEM43 mutant (mut) mice (**F** and **G**). Subepicardial adipocytes were stained with perilipin (**H**), and the percentage of fibrotic tissue was quantified (**I**). Bar, 500 µm (**D**–**F**), 50 µm (**G**), and 100 µm (**H**). Graphs show data points for individual mice and mean±SEM. Vinc indicates vinculin. **A** and **I**, ***P*<0.01, ****P*<0.001, TMEM43mut vs WT; #*P*<0.05, ##*P*<0.01, ###*P*<0.001, TMEM43mut vs TMEM43WT; $*P*<0.05, $$*P*<0.01, $$$*P*<0.001 for different time points vs 3 weeks (**A**) or neonates (**I**) for each mouse line; 2-way regular ANOVA followed by Bonferroni post-test; n=6 to 18.

trend was found for Beclin1, a key protein involved in autophagy[11] (Figure 3C and Figure IIIB in the online-only Data Supplement). These results provide the first clear evidence implicating cell-death pathways in the early and sustained cardiomyocyte loss in ARVC5.

To determine whether dead cardiomyocytes were substituted by fibrotic tissue, we analyzed heart sections by Masson trichrome staining. TMEM43mut mice showed massive fibrosis in both ventricles at 4 months of age (Figure 3D–3G). Mutant mice also showed accumulation of adipose tissue in the subepicardial layer and the myocardium, as revealed by perilipin staining (Figure 3H). Quantification of the fibrotic area confirmed the strong fibrotic response as disease progressed (Figure 3I). In line with these results, TMEM43mut mice showed an increase in collagen 1α1 mRNA at 2 and 4 months, together with strong induction of lysyl oxidase, which crosslinks collagen and elastin (Figure IIIC and IIID in the online-only Data Supplement). These changes were accompanied by increased expression of the myocardial remodeling markers skeletal muscle actin α1 and brain natriuretic peptide (Figure IIIE and IIIF in the online-only Data Supplement). Together, these results demonstrate that TMEM43-S358L induces cardiomyocyte death followed by fibrotic replacement.

Epicardium-Derived Cells Contribute to the Fibrotic Replacement of Cardiomyocytes

Using the *Cre-LoxP* technology and cell type–specific promoters, we generated 4 sets of lineage-tracing mice to determine the contribution made to the fibrotic replacement by endothelial cells (Tie2-Cre), mac-

rophages (LysM-Cre), cardiomyocytes (cTnT-Cre), and epicardium-derived cells (Wt1-Cre). In addition to the TMEM43mut transgene, each line carried a floxed reporter allele (*EYFP*, *RFP*, or *GFP*) preceded by a STOP codon that was removed on recombination by the Cre recombinase. In these mice, Cre-expressing cells and their progeny were permanently labeled by expression of the reporter (Figure IVA–IVQ in the online-only Data Supplement). To locate collagen fibers in myocardial tissue, we used second-harmonic-generation microscopy (Figure IVA in the online-only Data Supplement), which highlights organized mature collagen fibers, and confocal reflection microscopy (Figure IVB in the online-only Data Supplement), which reveals general tissue fibrosis. Labeled macrophages were found in the tissue but did not colocalize with the collagen fibers (Figure IVC–IVE in the online-only Data Supplement), and neither did the cardiomyocytes or endothelial cells (Figure IVF–IVH and IVO–IVQ in the online-only Data Supplement). In contrast, both second-harmonic-generation and reflection microscopy revealed colocalization of epicardium-derived cells and collagen fibers in TMEM43mut hearts (Figure IVI–IVN in the online-only Data Supplement). These results indicate that epicardium-derived cells (which are likely resident fibroblasts derived from the epicardium during development) are the main cell type contributing to the massive interstitial fibrosis observed in ARVC5.

TMEM43 Is Located in the Nuclear Membrane and Interacts With Cytoskeleton-Binding Proteins

There is currently controversy about whether TMEM43 is located within the nuclear rim,[12] the endoplasmic reticulum,[13] or the intercalated disk.[14] To investigate the cellular localization of WT and S358L human TMEM43 and their interacting partners, we first modeled TMEM43-S358L and WT TMEM43 proteins in silico. The p.S358L mutation in transmembrane domain 3 (red in Figure 4A and 4B) predicted disruption of 3D protein structure and lower structural stability for TMEM43-S358L compared with WT TMEM43. TMEM43-S358L also showed higher hydrophobicity than the WT form, reducing the availability of the transmembrane domain 4 (dark blue in Figure 4A and 4B), which is predicted to interact with a partner protein. The p.S358L mutation also affected the structure of the transmembrane domain 1 (orange in Figure 4A and 4B), which is necessary for TMEM43 dimerization. Because a previous report suggested that TMEM43 function requires dimerization through transmembrane domain 1,[15] we also modeled homodimers and heterodimers of TMEM43WT and TMEM43mut. In silico modeling of the heterodimer WT TMEM43-TMEM43-S358L revealed a distorted structure compared with the WT TMEM43 homodimer (Figure 4C and 4D).

TMEM43 protein sequence is highly conserved along evolution.[8] Nevertheless, the in silico model of mouse TMEM43 shows a different tertiary structure compared with the human protein, with a nonstructured loop arranging transmembrane domains 3 and 4 differently (Figure VA in the online-only Data Supplement). Most important, the p.S358L mutation has virtually no effect on the mouse TMEM43 structure, and mouse TMEM43-S358L shows only minimal differences with the WT protein (Figure VB and VC in the online-only Data Supplement). These results probably explain why TMEM43-S358L knock-in mice have no disease phenotype,[16] whereas transgenic mice expressing the human protein develop ARVC5.

TMEM43 has been suggested to interact with emerin (Emery-Dreifuss muscular dystrophy [EMD]) and SUN2 (SUN domain-containing protein).[15] We therefore modeled the interaction of these proteins with human TMEM43 dimers. The WT-mutant TMEM43 heterodimer showed an interaction with EMD (purple in Figure 4E); however, this interaction was predicted to abnormally embed EMD in the nuclear membrane (Figure 4F). This would have the effect of blocking EMD function because it would prevent its interaction with lamin A (the pocket in EMD that interacts with lamin A is indicated by an arrow in Figure 4E and 4F). This in silico prediction was validated by immunoprecipitation in P19 cells transfected with expression plasmids for HA-tagged WT TMEM43 and TMEM43-S358L, which revealed weaker interaction of EMD with TMEM43-S358L than with the WT form (Figure 4G). These results suggest that the p.S358L point mutation in human TMEM43 results in a dominant-negative form of TMEM43, disrupting the activity of the WT form.

Histological analysis of hearts from 4-month-old mice using 3 different anti-TMEM43 antibodies showed perinuclear localization of TMEM43 in TMEM43WT mice, whereas the TMEM43-S358L protein was partially delocalized in the cytoplasm in TMEM43mut mice (Figure 4H–4M). As in desmoplakin ACM/ARVC and other ARVC models,[17,18] TMEM43mut mouse hearts showed mislocalization of connexin 43 (Figure VI in the online-only Data Supplement).

To validate those results, we analyzed TMEM43 localization in P19 cells transfected with plasmids expressing HA-tagged TMEM43 proteins. We found partial cytoplasmic localization of TMEM43-S358L, regardless of whether the HA tag was placed at the N- or the C-terminus, whereas the WT protein showed a mainly perinuclear staining (Figure VII in the online-only Data Supplement). The perinuclear localization of WT TMEM43 in the nuclear membrane is in agreement with several previous reports.[13,15,16,19–21] It should be acknowledged, however, that TMEM43 has also been reported in desmosomes.[14] Although we could not detect TMEM43 in these structures by immunofluorescence, we did see an

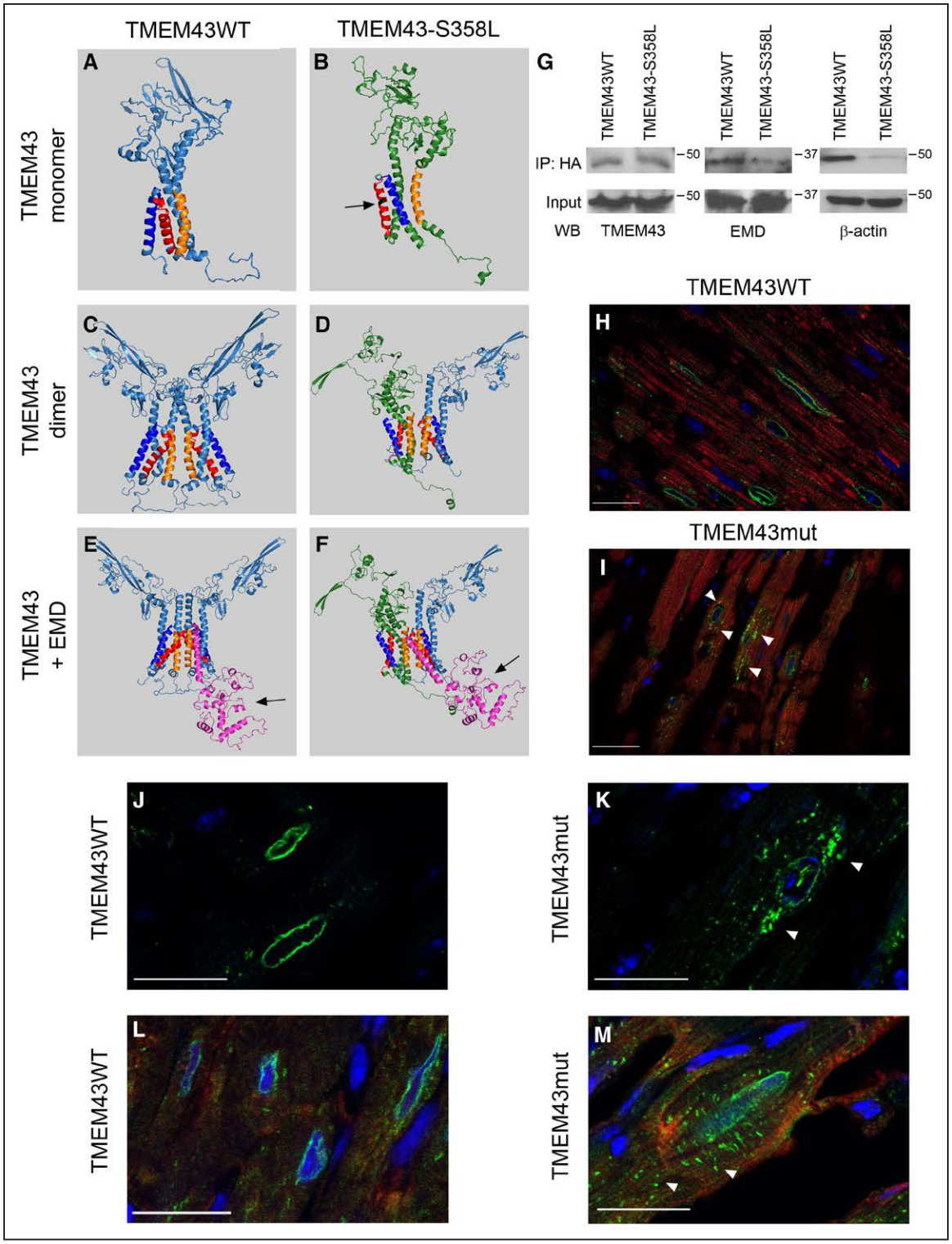

Figure 4. The S358L mutation alters TMEM43 (transmembrane protein 43) conformation and protein interactions.
A through **F**, In silico modeling of the tertiary structure of wild-type (WT; **A**, **C**, and **E**, light blue) and mutant (mut) TMEM43 (**B**, **D**, and **F**, green) as monomers (**A** and **B**), dimers (**C** and **D**), or in complexes with emerin (EMD; purple molecule; **E** and **F**). Orange indicates transmembrane domain 1; red, transmembrane domain 3; dark blue, transmembrane domain 4; and black residue, S358L mutation. **G**, HA-tagged TMEM43WT and TMEM43mut were expressed in P19 cells and immunoprecipitated (IP) with anti-HA. The presence of TMEM43, EMD, and β-actin in the input and immunoprecipitate was analyzed by Western blot. **H** through **M**, Immunofluorescence analysis of TMEM43 localization in myocardial sections from 4-month-old TMEM43WT (**H**, **J**, and **L**) and TMEM43mut mice (**I**, **K**, and **M**) with 3 different anti-TMEM43 antibodies (**H** and **I**, Abcam; **J** and **K**, Santa Cruz; **L** and **M**, antibodies generated by Franke et al[14]). Green indicates TMEM43; red, troponin I (only for **H** and **I**); and blue, DAPI. White arrowheads indicate partial TMEM43 localization in the cytoplasm. Bar, 20 μm.

interaction with desmosomal proteins in immunoprecipitation experiments (Table III in the online-only Data Supplement), suggesting that a fraction of TMEM43 may be localized in desmosomes.

To gain insight into the molecular partners of TMEM43, we immunoprecipitated the WT and the mutant protein from transfected P19 cells using an anti-HA antibody. Quantitative proteomics of the co-precipitating proteins identified several cytoskeleton and cytoskeleton-interacting proteins among the binding partners for WT TMEM43, including actin, actinin, spectrin, shroom 3, myosin, and formin-like 2 (Table III in the online-only Data Supplement). Many of these interactions were reduced in cells expressing TMEM43-S358L. Immunoprecipitation and Western blot analysis confirmed the reduced interaction of TMEM43-S358L with α-actin compared with the WT TMEM43 form (Figure 4G). Interestingly, the mutant TMEM43 protein showed increased interaction with the AKT modulator Pa2g4 (Table III in the online-only Data Supplement), which might affect this signaling pathway.

Antifibrotic Treatment Does Not Improve Cardiac Function in ARVC5 Mice

Increased interstitial fibrosis is a hallmark of human ARVC5 and was evident in TMEM43mut mice. Interstitial fibrosis increases passive stiffness, causes electric remodeling, and enhances arrhythmogenicity, further contributing to cardiac remodeling and dysfunction.[1,22] To investigate whether reducing interstitial fibrosis could improve heart function in ARVC5, we treated mice with the β-galactoside–binding lectin Gal-3 (galectin-3) inhibitor GM-CT-01, a known antifibrotic drug[23].

Gal-3 is highly expressed in fibrotic tissues[23] and mediates extracellular matrix remodeling in heart failure.[24] Gal-3–null mice are resistant to fibrotic disease of several organs, including liver, kidney, and lung.[25] RNA sequencing revealed increased expression of the Gal-3-encoding gene (*Lgals3*) in the hearts of 2-month-old TMEM43mut mice, together with other genes involved in the immune response and fibrosis (Table IV and Figure VIII in the online-only Data Supplement). No major changes in transcript isoforms were detected (Table V in the online-only Data Supplement). Validation by quantitative reverse-transcribed polymerase chain reaction showed a strong induction of Lgals3 in TMEM43mut mice at 2 and 4 months of age (Figure 5A), which was confirmed by Western blot (Figure 5B and 5C). To investigate whether inhibition of Gal-3–regulated profibrotic pathways could improve heart function in ARVC5, we conducted blinded controlled in vivo experiments in TMEM43mut mice. The mice were treated with either saline or GM-CT-01, a galactomannan with antifibrotic properties[26] that inhibits Gal-3 by binding to its carbohydrate-binding domain, which is necessary for the formation of Gal-3 pentamers.[23] We then analyzed heart sections for collagen content by Masson trichrome staining and type by staining with Picrosirius red. Picrosirius red binds specifically to collagen fibrils of varying diameters and distinguishes between collagen type I, which confers stiffness to the tissue, and collagen type III, which is more elastic. Treatment with GM-CT-01 triggered a significant switch in the collagen type in TMEM43mut hearts from collagen type I to collagen type III (Figure 5D). Although the sum of the collagen fibers seemed to decrease with GM-CT-01, the total fibrotic area was not reduced (Figure 5E). LVEF was comparable in GM-CT-01–treated and saline-treated TMEM43mut mice (Figure 5F). These results suggest that although collagen in the heart changes to a more elastic type, this is not sufficient to restore cardiac function.

TMEM43-S358L Causes Cell Death by Activating GSK3β

GSK3β is mislocalized and activated in other ARVCs, both in patients and in mouse models.[18,27] In addition, GSK3β inactivation is beneficial in several pathological settings, including myocardial infarction[28,29] and pressure overload.[30] To determine whether this signaling pathway was disturbed in ARVC5, we first investigated whether GSK3β activation was altered by TMEM43-S358L. We observed that GSK3β phosphorylation is decreased in TMEM43mut mice compared with their WT littermates (Figure 6A and 6B), indicating increased GSK3β activation. This was accompanied by reduced phosphorylation (indicating decreased activation) of its upstream regulatory kinase AKT (Figure 6A and 6C). To determine whether TMEM43-S358L had any effect on β-catenin transcriptional activity, which is inhibited by GSK3β we transfected neonatal cardiomyocytes with an expression vector for the different TMEM43 constructs together with a reporter plasmid in which luciferase is controlled by several β-catenin–activated TCF binding sites. We found that human TMEM43-S358L decreased β-catenin activation, whereas mouse TMEM43-S358L did not (Figure 6D). This decrease was prevented by the GSK3β inhibitor CHIR99021 (Figure 6E).

Because the AKT pathway is strongly involved in cell survival, we investigated the effect of TMEM43-S358L on cell viability. Expression of TMEM43-S358L in P19 cells resulted in increased cell death in the absence of growth factors. This effect was precluded by the GSK3β inhibitor (Figure 6F). Together, these results indicate that TMEM43-S358L expression interferes with the AKT signaling pathway, resulting in GSK3β activation and increased cell death.

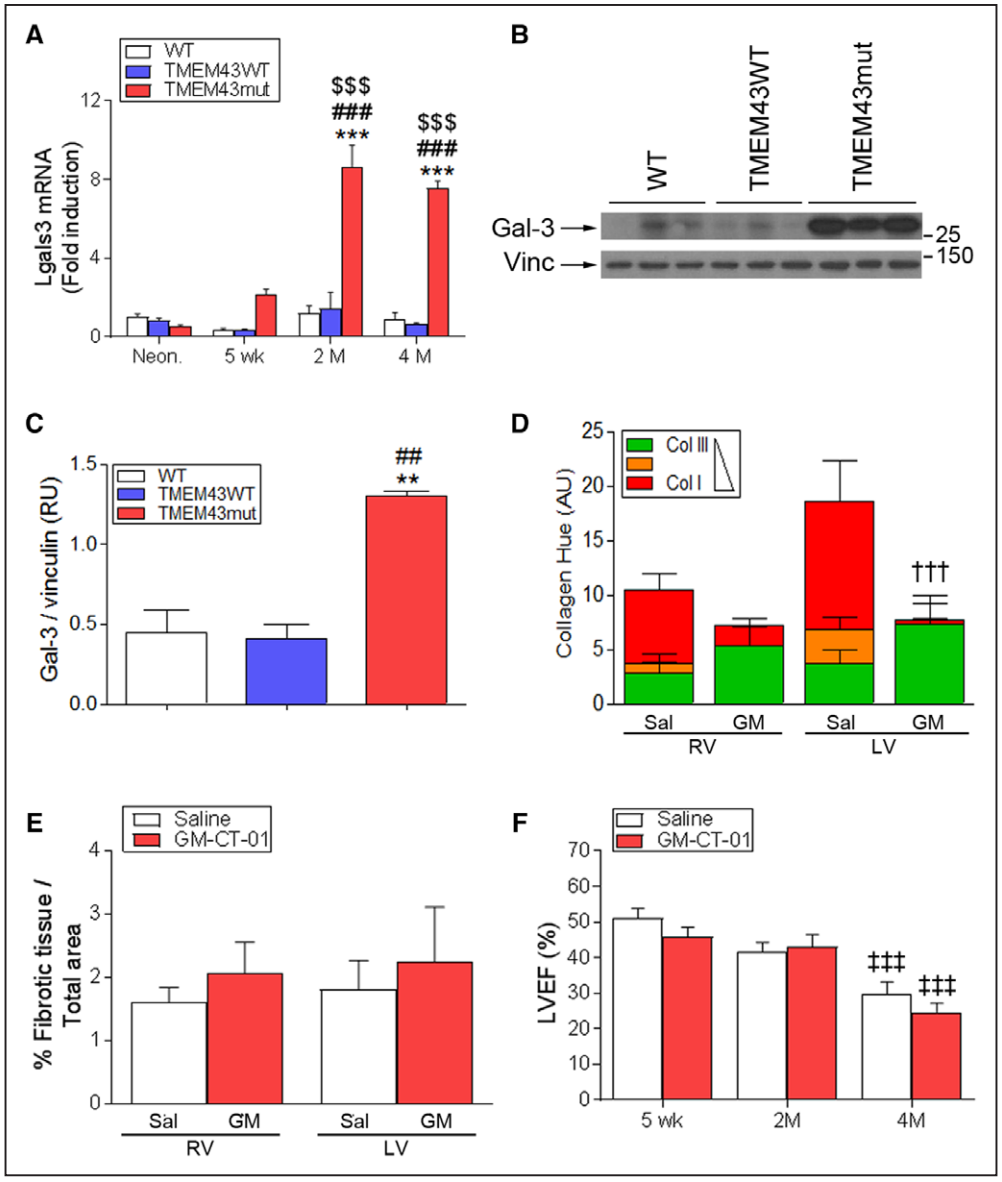

Figure 5. Inhibition of fibrosis does not improve cardiac function in TMEM43 (transmembrane protein 43) mutant (mut) mice. **A**, Quantitative reverse-transcribed polymerase chain reaction analysis of myocardial galectin-3 (Lgals3) expression in the mouse lines at the indicated ages. **B** and **C**, Western blot analysis (**B**) and quantification (**C**) of Gal-3 (galectin-3) protein levels at different time points in the 3 mouse lines at 4 months of age. **D**, TMEM43mut mice were treated with GM-CT-01 (GM; 120 mg/kg) or saline (Sal), and myocardial sections were stained with Picrosirius red to determine the maturity of the collagen fibers in each ventricle. **E**, The percentage of fibrotic tissue in the hearts of 4-month-old mice was quantified by Masson trichrome staining. **F**, Echocardiography-determined left ventricular (LV) ejection fraction (LVEF) in 5-week-, 2-month-, and 4-month-old TMEM43mut mice treated with GM-CT-01 or saline. Graphs show data points for individual mice and mean±SEM. AU indicates arbitrary units; and RV, right ventricle. **A**, ***P<0.001, TMEM43mut vs WT; ###P<0.001, TMEM43mut vs TMEM43WT; $$$$P$<0.001 for different ages vs neonates for each mouse line; n=3 to 8; 2-way regular ANOVA followed by Bonferroni post-test. **C**, **P<0.01, TMEM43mut vs WT; ##P<0.01, TMEM43mut vs TMEM43WT; 1-way ANOVA with Bonferroni correction. **D**, †††P<0.001, GM-CT-01 vs saline. **E** and **F**, ‡‡‡P<0.001 vs 5 weeks; 2-way regular ANOVA followed by Bonferroni post-test; n=7 to 8.

Treatment of TMEM43mut Mice With CnAβ1 Prolongs Survival and Improves Cardiac Function

CnAβ1, a naturally occurring splice variant of calcineurin Aβ, has a beneficial effect on the heart after injury.[8,31] The distinct properties of CnAβ1 are conferred by a unique C-terminal domain, not present in any other known protein.[32] More important, CnAβ1 is required for the activation of the AKT/GSK3β/β-catenin signaling pathway, which results in inhibition of GSK3β and activation of β-catenin.[33]

To determine whether CnAβ1 overexpression could revert the activation of GSK3β induced by TMEM43-S358L, we crossed TMEM43mut mice with mice overexpressing CnAβ1 in a cardiomyocyte-specific manner.[8] We found that AKT activity was preserved in the hearts of double-transgenic mice and that, accordingly, GSK3β

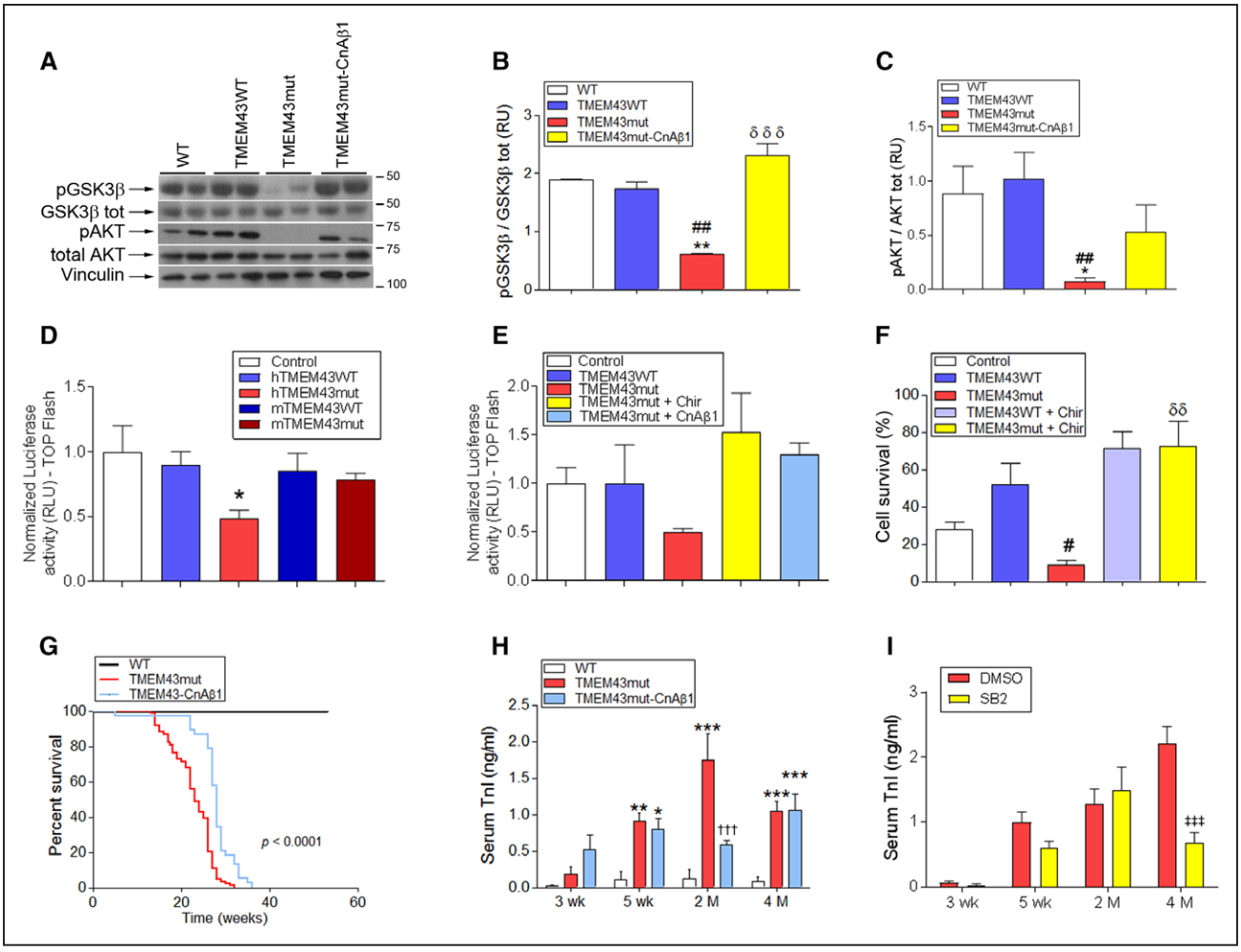

Figure 6. TMEM43 (transmembrane protein 43) p.S358L promotes cell death by activating glycogen synthase kinase-3β (GSK3β).
A through **C**, TMEM43 mutant (mut) mice were crossed with α-myosin heavy chain–calcineurin Aβ1(CnAβ1) mice overexpressing CnAβ1 in cardiomyocytes (TMEM43mut-CnAβ1 mice). The presence of total and phosphorylated (Ser9) GSK3β, as well as total and phosphorylated (Ser473) AKT, was assessed by Western blot in myocardial samples from wild-type (WT), TMEM43WT, TMEM43mut, and TMEM43mut-CnAβ1 mice (**A**) and quantified (**B** and **C**). Increased phosphorylation of GSK3β indicates inactivation; n=3 to 11. **D** and **E**, Neonatal mouse cardiomyocytes were transfected with a reporter plasmid in which luciferase expression is controlled by a β-catenin–dependent TCF multimer, together with expression plasmids for human (h; **D** and **E**) or mouse (m; only in **D**) WT TMEM43, TMEM43-S358L, and CnAβ1. Empty pcDNA3.1 was used as a negative control. When indicated, the GSK3β inhibitor CHIR99021 (Chir; 3 μmol/L) was added. **F**, Percentage of viable P19 cells transfected with expression plasmids for human WT TMEM43 and TMEM43-S358L grown in the absence of serum for 32 hours. The GSK3β inhibitor CHIR99021 (3 μmol/L) was added when indicated. As a positive control of cell death, P19 cells were incubated with 10% ethanol for 5 hours. **G**, Sixty-week Kaplan-Meier survival curves for WT (n=27), TMEM43mut (n=84), and TMEM43mut-CnAβ1 mice (n=38). The indicated *P* value was obtained with a log-rank test. **H** and **I**, Serum troponin I (TnI) determined by ELISA in the indicated mice 3 and 5 weeks and 2 and 4 months of age. In **I**, TMEM43mut mice were treated with the GSK3β inhibitor SB-216763 (SB) or dimethyl sulfoxide (DMSO) as a vehicle control; n=4 to 5. Graphs show mean±SEM. **B** through **D** and **F**, **P*<0.05, ***P*<0.01, ****P*<0.001 vs WT animals or control vector; ##*P*<0.01, ###*P*<0.001 vs TMEM43WT. **B**, δδδ*P*<0.001 vs TMEM43mut; δδ*P*<0.01 CHIR99021-treated cells vs untreated. **H**, ***P*<0.01, ****P*<0.001 vs WT; †††*P*<0.001, TMEM43mut vs TMEM43mut-CnAβ1. **I**, ‡‡‡*P*<0.001, SB vs DMSO. **B** through **F**, One-way ANOVA followed by Dunnett posttest; n=3 to 11. **H** and **I**, Two-way ANOVA followed by Bonferroni posttest; n=10. Note that WT and TMEM43mut mice data for **G** and **H** are those shown in Figures 1A and 3A, respectively, and are repeated here for comparative purposes.

was not activated (Figure 6A–6C). In addition, CnAβ1 restored β-catenin activity (Figure 6E).

Given that CnAβ1 activates AKT and inhibits GSK3β, we next investigated whether CnAβ1 overexpression improves cardiac function in the double-transgenic animals. Most notably, CnAβ1 significantly expanded the life span of the mutant mice to a median of 28 weeks (Figure 6G). Circulating cardiac troponin I levels were significantly reduced at 2 months of age in TMEM43mut-CnAβ1 mice (Figure 6H), suggesting a partial reduction of cardiomyocyte necrosis in the double-transgenic mice. Similarly, chemical inhibition of GSK3β with SB-216763 in TMEM43mut mice resulted in reduced serum cardiac troponin I, reinforcing the idea that GSK3β activation has a causal role in cardiomyocyte death induced by TMEM43-S358L.

Echocardiography assessment showed significantly superior LV function in TMEM43mut-CnAβ1 mice compared with TMEM43mut mice at 4 months of age (Figure 7A and Table VI and Video II in the online-only Data Supplement). LV dilatation was also reduced in double-transgenic animals, although the differences

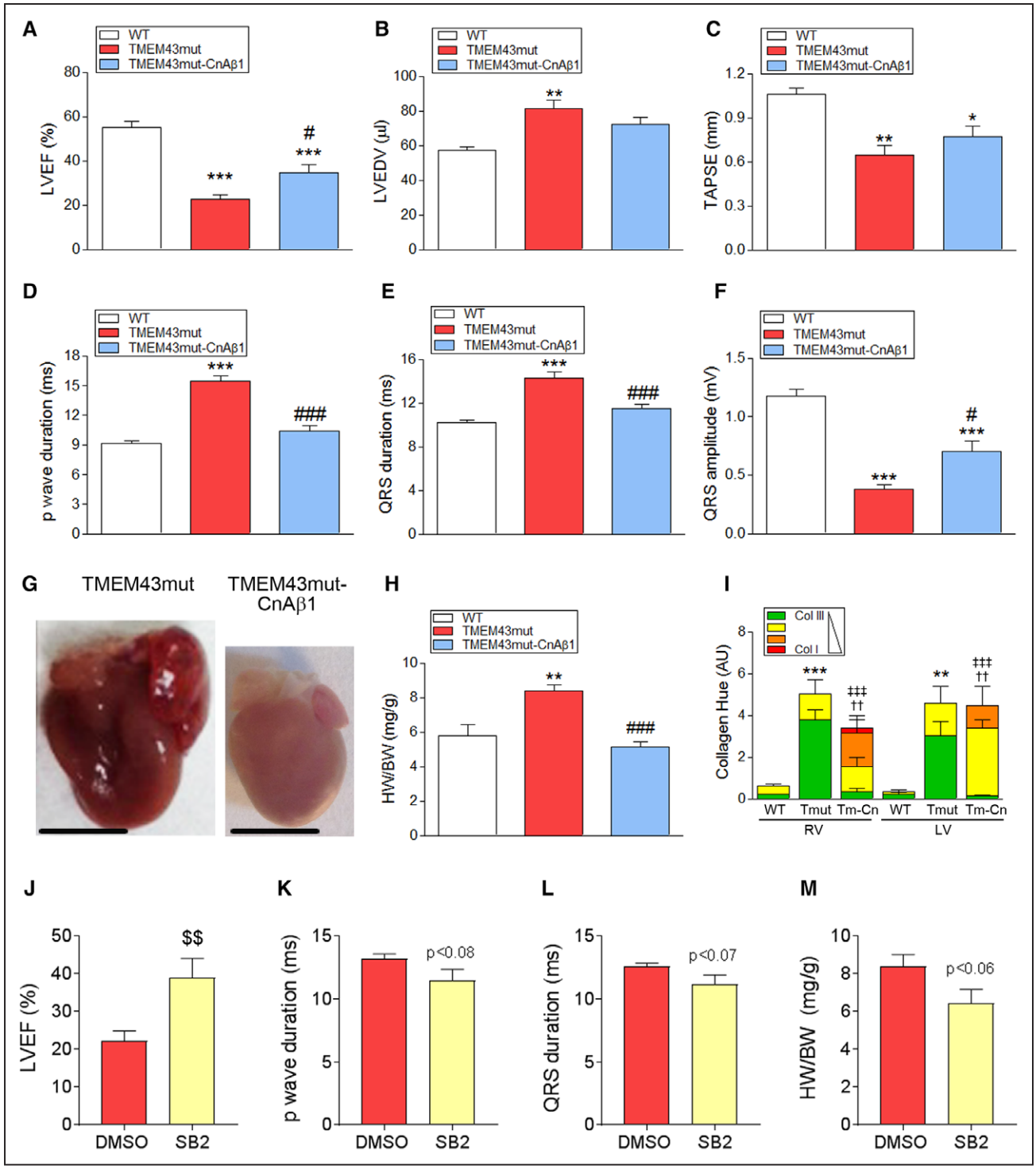

Figure 7. Calcineurin Aβ1 (CnAβ1) overexpression and chemical inhibition of glycogen synthase kinase-3β (GSK3β) improve cardiac function in TMEM43 (transmembrane protein 43) mutant (mut) mice.

A through **C**, Left ventricular (LV) ejection fraction (EF; **A**), LV end-diastolic volume (LVEDV; **B**), and tricuspid annular plane systolic excursion (TAPSE; **C**) were determined by echocardiography in 4-month-old mice. **D** through **F**, Surface electrocardiographic determination of p-wave duration (**D**) and QRS duration and amplitude (**E** and **F**). **G** and **H**, Gross heart morphology (**G**) and ratio of heart weight to body weight (HW/BW; **H**) in 4-month-old mice; bar, 500 μm. **I**, Picrosirius red staining analysis of collagen fibers in myocardial sections. **J,** LVEF was determined by echocardiography in 4-month-old TMEM43mut mice treated with the GSK3β inhibitor SB-216763 (SB) or dimethyl sulfoxide (DMSO) as a control. **K** and **L**, The p-wave (**K**) and QRS (**L**) durations were analyzed by ECG in TMEM43mut (Tmut) mice treated as in **J**. **M**, Ratio of heart weight to body weight (HW/BW; **H**) in 4-month-old TMEM43mut mice treated as in J. Graphs in A to F, H and J-M show data with mean±SEM. **A** through **F** and **H**, **P*<0.05, ***P*<0.01, ****P*<0.001, TMEM43mut or TMEM43-CnAβ1 vs WT; #*P*<0.05, ###*P*<0.001, TMEM43mut-CnAβ1 (Tm-Cn) vs TMEM43mut; 1-way ANOVA followed by Bonferroni posttest; n=6 to 8. **I**, ***P*<0.01, ****P*<0.001, collagen (Col) type III TMEM43mut vs WT; ††*P*<0.01 Col I TMEM43mut-CnAβ1 vs TMEM43mut; ‡‡‡*P*<0.001, Col III TMEM43-CnAβ1 vs TMEM43mut; 2-way ANOVA followed by Bonferroni posttest; n=3 to 6. Note that WT and TMEM43mut mice data for **A** through **F** and **H** are those shown in Figures 1B through 1D, 2D through 2F, and 1F and are repeated here for comparative purposes. **J** through **M**, $$*P*<0.01, SB2 vs DMSO, 2-sample *t* test; n=7 to 9.

with TMEM43mut mice did not reach significance (Figure 7B). TMEM43mut-CnAβ1 mice also showed a small improvement in right ventricular function (tricuspid annular plane systolic excursion; Figure 7C) and improved electrocardiographic parameters compared with TMEM43mut mice (Figure 7D–7F and Table VII in the online-only Data Supplement).

Evaluation of gross heart morphology at 4 months showed that TMEM43-CnAβ1 hearts were considerably smaller than those of the TMEM43mut mice (Figure 7G). In addition, TMEM43-CnAβ1 mice had a significantly lower ratio of heart weight to body weight than TMEM43mut mice (Figure 7H) and showed no evidence of pulmonary congestion (Figure IXA in the online-only Data Supplement).

Examination of fibrotic tissue by Masson trichrome staining revealed no differences in total collagen content between TMEM43-CnAβ1 and TMEM43mut hearts (Figure IXB and IXC in the online-only Data Supplement). However, analysis of fibers by Picrosirius red staining indicated that TMEM43-CnAβ1 mice accumulated stiffer fibers (richer in collagen I) than TMEM43mut mice (Figure 8I).

In agreement with the beneficial effect of CnAβ1 on cardiac function, treatment of TMEM43mut mice with the GSK3β inhibitor SB-216763 resulted in improved EF and a partial normalization of electric abnormalities (Figure 7J–7M). Together, these results demonstrate that GSK3β inhibition, either chemically or by CnAβ1 overexpression, improves cardiac function in mice with ARVC5.

Human Induced Pluripotent Stem Cell–Derived Cardiomyocytes Bearing the p.S358L Mutation Show Contraction Abnormalities That Are Normalized by GSK3β Inhibition

To determine whether the p.S358L mutation induces a disease-associated phenotype also in human cells, we developed mutant human induced pluripotent stem cell (hiPSC)–derived cardiomyocytes (hiPSC-CMs) and compared their contraction behavior with that of WT cells. No significant differences in Ca^{2+} transient parameters were found between phenotypes at baseline (Figure 8A–8C). However, in the presence of 1 μmol/L isoproterenol, both the rising and decay phases of the Ca^{2+} transient were slower in the mutant phenotype. These results were confirmed by measuring hiPSC-CM contraction with a recently reported algorithm.[34] We found significantly increased contraction duration, time to peak, and relaxation time in mutant hiPSC-CMs, accompanied by decreased contraction amplitude (Figure 8D–8G). GSK3β inhibition partially reduced contraction time and improved contraction overall (Figure 8H–8K), reinforcing the idea that GSK3β plays a relevant role in ARVC5.

DISCUSSION

ARVC5 is a devastating disease that causes sudden cardiac death and heart failure.[6] It is caused by a point mutation in TMEM43, a transmembrane protein that, as shown here, is located in the nuclear membrane in its WT form. Despite efforts, this disease remains incurable and has no specific therapy. To develop therapies to delay the onset or to slow the progression of ARVC5, it is necessary to define the initial molecular events and pathophysiological mechanisms. We therefore performed a step-by-step characterization of the first ARVC5 transgenic mouse line (TMEM43mut) from the early stages of the disease to the latest manifestations of the ACM/ARVC phenotype. TMEM43mut mice show biventricular systolic dysfunction as the disease progresses and considerable accumulation of fibrofatty tissue, thus reproducing the human condition, which also shows biventricular affectation in 43% of the cases.[7] Unlike other ACM/ARVC mouse models,[17,27,35–37] TMEM43mut hearts accumulate fat in the right ventricle, although to a lower extent than observed in human patients, likely as a result of the absence of subepicardial fat in the mouse heart.

The first disease manifestations in TMEM43mut mice are electric abnormalities, observed as early as 5 weeks of age in ECG. Interestingly, no sudden cardiac death or appropriate implantable cardioverter-defibrillator discharge has been reported so far in ARVC5 patients <19 years of age.[38] This corresponds to the onset of the disease at 5 weeks of age observed in our ARVC5 mouse model. Electric features preceded anatomic defects, as also described in other ARVC mouse models.[39] Although the molecular mechanisms that underlie cellular uncoupling and consequent conduction abnormalities are poorly understood,[40] mislocalization of connexin 43 that results in gap-junction remodeling would contribute to defects in impulse propagation and might explain the early phenotype.[17]

We show that mutant TMEM43 causes progressive cardiomyocyte loss through activation of cell-death pathways. Necrosis started early in life, as shown by cardiac troponin I levels, whereas apoptosis and autophagy appeared only in the later stages of the disease, suggesting that necrosis is the main pathway leading to early cardiomyocyte death. Sustained cardiomyocyte loss in TMEM43mut hearts progressively led to the replacement of dead cells by fibrofatty tissue, eventually leading to massive interstitial fibrosis in all 4 chambers. We show that epicardium-derived cells contribute strongly to cardiac fibrosis in this model, as has also been shown for other heart diseases, including myo-

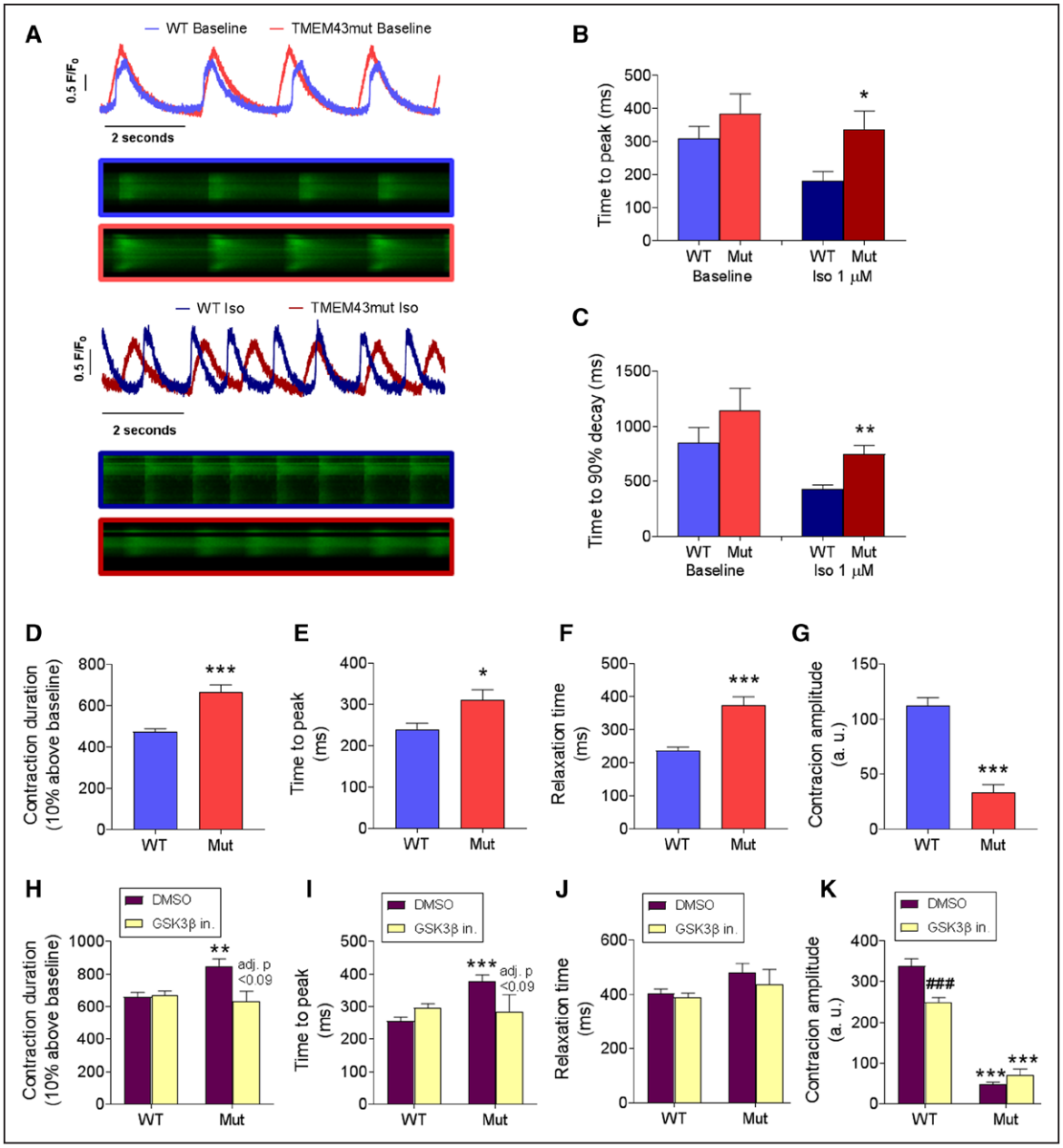

Figure 8. Human induced pluripotent stem cell–derived cardiomyocytes (hiPSC-CMs) bearing the p.TMEM43 (transmembrane protein 43)–S358L mutation develop contractile dysfunction.

A through **C**, hiPSC-CMs bearing the wild-type (WT) alleles or a heterozygous p.TMEM43-S358L mutation (Mut) were loaded with 5 µmol/L Fluo 4-AM, and Ca^{2+} transients were imaged in individual cells under a confocal microscope in the presence or absence of 1 µmol/L isoproterenol (Iso). **D** through **G**, WT and mutant hiPSC-CM beating was video recorded, and contraction duration (**D**), time to peak (**E**), relaxation time (**F**), and contraction amplitude (**G**) were measured. **H** through **K**, WT and mutant hiPSC-CMs were treated with the glycogen synthase kinase-3β (GSK3β) inhibitor CHIR99021 (GSK3β in.) or dimethyl sulfoxide (DMSO) as a control and different contraction parameters were measured. **P*<0.05, ***P*<0.01, ****P*<0.001, mutant vs WT cells. ###*P*<0.001 and adjusted *P* values in **H** and **I** refer to GSK3β inhibitor vs DMSO. **D** through **G**, Two-sample *t* test; **H** through **K**, regular 2-way ANOVA with Bonferroni posttest; n=10 to 20; (**B** and **C**) 46 to 49; and (**D**–**G**); n=12-69.

cardial infarction.[41] Given that many resident fibroblasts in the adult heart are derived from Wt1+ epicardial cells during embryonic development, it is likely that the epicardium-derived cells contributing to cardiac fibrosis in TMEM43mut mice are resident cardiac fibroblasts. We found no contribution from macrophages, endothelial cells, or cardiomyocytes, although we cannot rule out contributions from other cell types not tested here.

The role of fibrosis in ACM/ARVC is unclear; it could represent either a pathological mechanism or a compensatory response. Treating our mouse lines with a Gal-3 inhibitor that has antifibrotic properties altered the collagen type III/I ratio to a more elastic fiber conformation. This, however, had no beneficial effect on cardiac function. These results suggest that the fibrotic response developed in ARVC5 tries to compensate for

the loss of cardiomyocytes but would not be an appropriate therapeutic target.

The Wnt/GSK3β/β-catenin signaling pathway seems to play a central role in the pathogenesis of other forms of ARVC and is a key regulator of myogenesis[7].GSK3β modulates this signaling pathway by phosphorylating β-catenin, promoting its rapid turnover by the proteasome. We show here that TMEM43-S358L inhibits AKT, which results in GSK3β activation and inhibition of β-catenin–dependent transcription. We also show that expression of mutant TMEM43 in cell culture causes significant cell death in a GSK3-dependent manner, demonstrating the functional involvement of GSK3β in the deleterious effects of TMEM43-S358L. Although it is unclear how it inhibits AKT, we found that TMEM43-S358L interacts with the AKT modulator Pa2g4 (EBP1 [Erbb3 interacting protein]). Interaction of Pa2g4 with AKT inhibits apoptosis and promotes cell survival.[42,43] Therefore, it is tempting to speculate that by binding Pa2g4, TMEM43-S358L interferes with the Pa2g4-AKT interaction and thereby reduces the antiapoptotic effect of AKT. Overexpression of the calcineurin variant CnAβ1, which activates the AKT pathway and inhibits GSK3β, significantly expands the life span and improves cardiac function in TMEM43mut mice. TMEM43mut-CnAβ1 mice showed a partial reduction in cardiomyocyte death and less severe electric abnormalities, suggesting that CnAβ1 overexpression preserves cardiomyocyte function in the TMEM43mut myocardium. Similarly, chemical inhibition of GSK3β reduced cardiomyocyte death and electric abnormalities and improved cardiac contraction in TMEM43mut mice. The role of GSK3β in the pathogenesis of ARVC5 was further confirmed in hiPSC-CMs bearing the p.S358L mutation, which showed improved contraction after GSK3β inhibition.

Our computer models show that the p.S358L point mutation in TMEM43 increases the hydrophobicity of the molecule and would lead to a distorted protein, impairing its function. The dimer formed between TMEM43-S358L and the WT form adopts a deformed structure that reduces its interaction with other nuclear membrane proteins such as EMD, as well as with cytoskeleton-interacting proteins. This defective interaction is illustrated by the partial delocalization of TMEM43-S358L to the cytoplasm. The functional implications of these protein-protein interactions need to be fully clarified; however, it is plausible that a reduced interaction between the nucleus and the cytoskeleton contributes to cardiomyocyte death under biomechanical stress.

Interestingly, our computer models also showed that the third transmembrane domain in mouse TMEM43 has a different conformation and orientation from that of the human protein. More important, the p.S358L mutation has no effect on the structure of mouse TMEM43. The lack of a structural change in the mutant mouse protein is likely the reason why it does not inhibit β-catenin signaling and why knock-in mice bearing the p.S358L mutation have no pathological phenotype.[14] In addition, by using a cardiomyocyte-specific promoter to express TMEM43-S358L, we can conclude that ARVC5 is originated in cardiomyocytes and not in other cell types.

We show that human TMEM43-S358L causes cardiomyocyte death and fibrofatty replacement. Although it appears that fibrosis is not an effective therapeutic target, GSK3β inhibition by CnAβ1 overexpression or a chemical inhibitor has a beneficial effect on the mutant hearts. It will be interesting to explore GSK3β inhibitors as potential therapeutic agents for ARVC5 to improve the life of patients with this incurable disease.

Limitations

Although our transgenic mouse is the only model that reproduces human ARVC5, certain characteristics of the human disease were not presented by this model. No significant differences were found between males and females, in contrast to human patients. In addition, mice show fat infiltration in the myocardium but not to the extent found in ARVC5 human hearts.

ARTICLE INFORMATION

Received February 19, 2019; accepted July 3, 2019.

The online-only Data Supplement is available with this article at https://www.ahajournals.org/doi/suppl/10.1161/circulationaha.119.040366.

Correspondence

Enrique Lara-Pezzi, PhD, Myocardial Pathophysiology Area, Centro Nacional de Investigaciones Cardiovasculares Carlos III, Melchor Fernandez Almagro, 3, 28029 Madrid, Spain; or Pablo Garcia-Pavia, MD, PhD, Inherited Cardiac Diseases Unit, Department of Cardiology, Hospital Universitario Puerta de Hierro, Manuel de Falla, 2. Majadahonda, Madrid, 28222, Spain. Email elara@cnic.es or pablogpavia@yahoo.es

Affiliations

Centro Nacional de Investigaciones Cardiovasculares Carlos III (CNIC), Madrid, Spain (L.P.-B., M.V.-O., J.M.G.-S., F.D., J.L.-A., P.O.-S., F.M., M.L.-O., E.B.-K., J.V., C.M.-G., D.J.S., B.P., G.G., S.P., E.L.-P.). Heart Failure and Inherited Cardiac Diseases Unit, Department of Cardiology, Hospital Universitario Puerta de Hierro Majadahonda, Madrid, Spain (L.P.-B., F.D., M.R., P.G.-P.). CIBER Cardiovascular Diseases (CIBERCV), Madrid, Spain (L.P.-B., F.D., E.B.-K., J.V., C.M.-G., P.G.-P., E.L.-P.). ERN GUARD-HEART (European Reference Network for Rare and Complex Diseases of the Heart) (F.D., S.P., P.G.-P.). Departamento de Medicina y Cirugía Experimental, Instituto de Investigación Sanitaria Gregorio Marañón, Madrid, Spain (M.V.G.-G.). Centro de Investigación Biomédica en Red de Salud Mental (CIBERSAM), Madrid, Spain (M.V.G.-G.). Molecular Cardiology, IRCCS Istituti Clinici Scientifici Maugeri, Pavia, Italy (S.P.). Facultad de Ciencias de la Salud, Universidad Francisco de Vitoria, Pozuelo de Alarcón, Madrid, Spain (P.G.-P.). Faculty of Medicine, Universidad Autónoma de Madrid (UAM), Madrid, Spain (P.G.-P.). Faculty of Medicine, National Heart & Lung Institute, Imperial College London, UK (E.L.-P.).

Acknowledgments

The authors thank F. Montoya for mouse work, E. Arza and V. Labrador from the Centro Nacional de Investigaciones Cardiovasculares Carlos III Microscopy Unit for help with microscopy, R. Doohan for immunostaining advice, J.A. Bernal for the hiPSC line, M.A. Sanguino for assistance with hiPSCs, J. Jalife for

the Gal3 inhibitor treatment, and S. Bartlett for English editing. RNA sequencing experiments were performed in the Centro Nacional de Investigaciones Cardiovasculares Carlos III Genomics Unit and analyzed by the Bioinformatics Unit. Anti-TMEM43 was a kind gift of Dr Franke Werner (DKFZ, Heidelberg, Germany). Conceptualization: E.L.-P., P.G.-P., and L.P.-B.; methodology: L.P.-B., M.V.-O., J.G.-S., P.O.-S., C.M.-G., F.M., D.J.S., B.P., G.G., E.B.-K., J.V., and M.V.G.-G.; investigation: L.P.-B., M.V.-O., J.G.-S., M.R., J.L.-A., P.O.-S., C.M.-G., F.M., M.L.-O., E.B.-K., J.V., D.J.S, B.P., G.G., S.P., F.D., and M.V.G.-G.; formal analysis: L.P.-B., M.V.-O., E.B.-K., J.V., F.M., M.V.G.-G., C.M.-G., S.P., D.J.S., P.G.-P., and E.L.-P.; writing, original draft: L.P.-B., E.L.-P., and P.G-P.; writing, review and editing: L.P.-B., E.L.-P., and P.G-P.; funding acquisition: E.L.-P. and P.G.-P.; supervision, E.L.-P. and P.G.-P.; and project administration, E.L.-P. and P.G.-P.

Sources of Funding

This work was supported by grants from the European Union (CardioNeT-ITN-289600 and CardioNext-608027 to Dr Lara-Pezzi), the Spanish Ministry of Economy and Competitiveness (RTI2018-096961-B-I00, SAF2015-65722-R, and SAF2012-31451 to Dr Lara-Pezzi; SAF2015-71863-REDT to Dr Garcia-Pavia), the Spanish Carlos III Institute of Health (PI14/0967 to Dr Garcia-Pavia, CPII14/00027 to Dr Lara-Pezzi; RD012/0042/0066 to Drs Garcia-Pavia and Lara-Pezzi), the Regional Government of Madrid (2010-BMD-2321 "Fibroteam" to Dr Lara-Pezzi), the Isabel Gemio Foundation (Todos somos Raros grant to Dr Garcia-Pavia), and the Spanish Society of Cardiology (2014 Basic Research Grant to Dr Garcia-Pavia). This work was also supported by the Plan Estatal de I+D+I 2013-2016–European Regional Development Fund (FEDER) "A way of making Europe," Spain. The Centro Nacional de Investigaciones Cardiovasculares Carlos III is supported by the Ministerio de Ciencia, Innovación y Universidades (MCNU), and Pro Centro Nacional de Investigaciones Cardiovasculares Carlos III Foundation and is a Severo Ochoa Center of Excellence (SEV-2015-0505).

Disclosures

None.

REFERENCES

1. Corrado D, Link MS, Calkins H. Arrhythmogenic right ventricular cardiomyopathy. *N Engl J Med*. 2017;376:61–72. doi: 10.1056/NEJMra1509267
2. Stadiotti I, Catto V, Casella M, Tondo C, Pompilio G, Sommariva E. Arrhythmogenic cardiomyopathy: the guilty party in adipogenesis. *J Cardiovasc Transl Res*. 2017;10:446–454. doi: 10.1007/s12265-017-9767-8
3. James CA, Bhonsale A, Tichnell C, Murray B, Russell SD, Tandri H, Tedford RJ, Judge DP, Calkins H. Exercise increases age-related penetrance and arrhythmic risk in arrhythmogenic right ventricular dysplasia/cardiomyopathy-associated desmosomal mutation carriers. *J Am Coll Cardiol*. 2013;62:1290–1297. doi: 10.1016/j.jacc.2013.06.033
4. Padrón-Barthe L, Domnguez F, Garcia-Pavia P, Lara-Pezzi E. Animal models of arrhythmogenic right ventricular cardiomyopathy: what have we learned and where do we go? Insight for therapeutics. *Basic Res. Cardiol*. 2017;112:50-56.
5. Ye L, Ni X, Zhao ZA, Lei W, Hu S. The application of induced pluripotent stem cells in cardiac disease modeling and drug testing. *J Cardiovasc Transl Res*. 2018;11:366–374. doi: 10.1007/s12265-018-9811-3
6. Merner ND, Hodgkinson KA, Haywood AF, Connors S, French VM, Drenckhahn JD, Kupprion C, Ramadanova K, Thierfelder L, McKenna W, et al. Arrhythmogenic right ventricular cardiomyopathy type 5 is a fully penetrant, lethal arrhythmic disorder caused by a missense mutation in the TMEM43 gene. *Am J Hum Genet*. 2008;82:809–821. doi: 10.1016/j.ajhg.2008.01.010
7. Hodgkinson KA, Connors SP, Merner N, Haywood A, Young TL, McKenna WJ, Gallagher B, Curtis F, Bassett AS, Parfrey PS. The natural history of a genetic subtype of arrhythmogenic right ventricular cardiomyopathy caused by a p.S358L mutation in TMEM43. *Clin Genet*. 2013;83:321–331. doi: 10.1111/j.1399-0004.2012.01919.x
8. Felkin LE, Narita T, Germack R, Shintani Y, Takahashi K, Sarathchandra P, López-Olañeta MM, Gómez-Salinero JM, Suzuki K, Barton PJ, et al. Calcineurin splicing variant calcineurin Aβ1 improves cardiac function after myocardial infarction without inducing hypertrophy. *Circulation*. 2011;123:2838–2847. doi: 10.1161/CIRCULATIONAHA.110.012211
9. Villarroya-Beltri C, Gutiérrez-Vázquez C, Sánchez-Cabo F, Pérez-Hernández D, Vázquez J, Martin-Cofreces N, Martinez-Herrera DJ, Pascual-Montano A, Mittelbrunn M, Sánchez-Madrid F. Sumoylated hnRNPA2B1 controls the sorting of miRNAs into exosomes through binding to specific motifs. *Nat Commun*. 2013;4:2980. doi: 10.1038/ncomms3980
10. Marcus FI, McKenna WJ, Sherrill D, Basso C, Bauce B, Bluemke DA, Calkins H, Corrado D, Cox MG, Daubert JP, et al. Diagnosis of arrhythmogenic right ventricular cardiomyopathy/dysplasia: proposed modification of the task force criteria. *Circulation*. 2010;121:1533–1541. doi: 10.1161/CIRCULATIONAHA.108.840827
11. Lavandero S, Chiong M, Rothermel BA, Hill JA. Autophagy in cardiovascular biology. *J Clin Invest*. 2015;125:55–64. doi: 10.1172/JCI73943
12. Dreger M, Bengtsson L, Schöneberg T, Otto H, Hucho F. Nuclear envelope proteomics: novel integral membrane proteins of the inner nuclear membrane. *Proc Natl Acad Sci USA*. 2001;98:11943–11948. doi: 10.1073/pnas.211201898
13. Bengtsson L, Otto H. LUMA interacts with emerin and influences its distribution at the inner nuclear membrane. *J Cell Sci*. 2008;121(pt 4):536–548. doi: 10.1242/jcs.019281
14. Franke WW, Dörflinger Y, Kuhn C, Zimbelmann R, Winter-Simanowski S, Frey N, Heid H. Protein LUMA is a cytoplasmic plaque constituent of various epithelial adherens junctions and composite junctions of myocardial intercalated disks: a unifying finding for cell biology and cardiology. *Cell Tissue Res*. 2014;357:159–172. doi: 10.1007/s00441-014-1865-1
15. Liang WC, Mitsuhashi H, Keduka E, Nonaka I, Noguchi S, Nishino I, Hayashi YK. TMEM43 mutations in Emery-Dreifuss muscular dystrophy-related myopathy. *Ann Neurol*. 2011;69:1005–1013. doi: 10.1002/ana.22338
16. Stroud MJ, Fang X, Zhang J, Guimarães-Camboa N, Veevers J, Dalton ND, Gu Y, Bradford WH, Peterson KL, Evans SM, et al. Luma is not essential for murine cardiac development and function. *Cardiovasc Res*. 2018;114:378–388. doi: 10.1093/cvr/cvx205
17. Lyon RC, Mezzano V, Wright AT, Pfeiffer E, Chuang J, Banares K, Castaneda A, Ouyang K, Cui L, Contu R, et al. Connexin defects underlie arrhythmogenic right ventricular cardiomyopathy in a novel mouse model. *Hum Mol Genet*. 2014;23:1134–1150. doi: 10.1093/hmg/ddt508
18. Chelko SP, Asimaki A, Andersen P, Bedja D, Amat-Alarcon N, DeMazumder D, Jasti R, MacRae CA, Leber R, Kleber AG, et al. Central role for GSK3β in the pathogenesis of arrhythmogenic cardiomyopathy. *JCI Insight*. 2016;1:e85923.
19. Schirmer EC, Florens L, Guan T, Yates JR 3rd, Gerace L. Nuclear membrane proteins with potential disease links found by subtractive proteomics. *Science*. 2003;301:1380–1382. doi: 10.1126/science.1088176
20. Dreger M, Bengtsson L, Schöneberg T, Otto H, Hucho F. Nuclear envelope proteomics: novel integral membrane proteins of the inner nuclear membrane. *Proc Natl Acad Sci USA*. 2001;98:11943–11948. doi: 10.1073/pnas.211201898
21. Rajkumar R, Sembrat JC, McDonough B, Seidman CE, Ahmad F. Functional effects of the TMEM43 Ser358Leu mutation in the pathogenesis of arrhythmogenic right ventricular cardiomyopathy. *BMC Med Genet*. 2012;13:21. doi: 10.1186/1471-2350-13-21
22. van Spreeuwel ACC, Bax NAM, van Nierop BJ, Aartsma-Rus A, Goumans MTH, Bouten CVC. Mimicking cardiac fibrosis in a dish: fibroblast density rather than collagen density weakens cardiomyocyte function. *J Cardiovasc Transl Res*. 2017;10:116–127. doi: 10.1007/s12265-017-9737-1
23. Traber PG, Zomer E. Therapy of experimental NASH and fibrosis with galectin inhibitors. *PLoS One*. 2013;8:e83481. doi: 10.1371/journal.pone.0083481
24. Yu L, Ruifrok WP, Meissner M, Bos EM, van Goor H, Sanjabi B, van der Harst P, Pitt B, Goldstein IJ, Koerts JA, et al. Genetic and pharmacological inhibition of galectin-3 prevents cardiac remodeling by interfering with myocardial fibrogenesis. *Circ Heart Fail*. 2013;6:107–117. doi: 10.1161/CIRCHEARTFAILURE.112.971168
25. Takemoto Y, Ramirez RJ, Yokokawa M, Kaur K, Ponce-Balbuena D, Sinno MC, Willis BC, Ghanbari H, Ennis SR, Guerrero-Serna G, et al. Galectin-3 regulates atrial fibrillation remodeling and predicts catheter ablation outcomes. *JACC Basic Transl. Sci*. 2016;1:143–154.
26. Ahmad N, Gabius HJ, André S, Kaltner H, Sabesan S, Roy R, Liu B, Macaluso F, Brewer CF. Galectin-3 precipitates as a pentamer with synthetic multivalent carbohydrates and forms heterogeneous cross-linked complexes. *J Biol Chem*. 2004;279:10841–10847. doi: 10.1074/jbc.M312834200
27. Martherus R, Jain R, Takagi K, Mendsaikhan U, Turdi S, Osinska H, James JF, Kramer K, Purevjav E, Towbin JA. Accelerated cardiac remodeling in desmoplakin transgenic mice in response to endurance exercise is associated with perturbed Wnt/β-catenin signaling. *Am J Physiol Heart Circ Physiol*. 2016;310:H174–H187. doi: 10.1152/ajpheart.00295.2015
28. Woulfe KC, Gao E, Lal H, Harris D, Fan Q, Vagnozzi R, DeCaul M, Shang X, Patel S, Woodgett JR, et al. Glycogen synthase kinase-3beta

regulates post-myocardial infarction remodeling and stress-induced cardiomyocyte proliferation in vivo. *Circ Res.* 2010;106:1635–1645. doi: 10.1161/CIRCRESAHA.109.211482
29. Miura T, Tanno M. Mitochondria and GSK-3beta in cardioprotection against ischemia/reperfusion injury. *Cardiovasc Drugs Ther.* 2010;24:255–263. doi: 10.1007/s10557-010-6234-z
30. Matsuda T, Zhai P, Maejima Y, Hong C, Gao S, Tian B, Goto K, Takagi H, Tamamori-Adachi M, Kitajima S, et al. Distinct roles of GSK-3alpha and GSK-3beta phosphorylation in the heart under pressure overload. *Proc Natl Acad Sci U S A.* 2008;105:20900–20905. doi: 10.1073/pnas.0808315106
31. López-Olañeta MM, Villalba M, Gómez-Salinero JM, Jiménez-Borreguero LJ, Breckenridge R, Ortiz-Sánchez P, García-Pavía P, Ibáñez B, Lara-Pezzi E. Induction of the calcineurin variant CnAβ1 after myocardial infarction reduces post-infarction ventricular remodelling by promoting infarct vascularization. *Cardiovasc Res.* 2014;102:396–406. doi: 10.1093/cvr/cvu068
32. Lara-Pezzi E, Winn N, Paul A, McCullagh K, Slominsky E, Santini MP, Mourkioti F, Sarathchandra P, Fukushima S, Suzuki K, et al. A naturally occurring calcineurin variant inhibits FoxO activity and enhances skeletal muscle regeneration. *J Cell Biol.* 2007;179:1205–1218. doi: 10.1083/jcb.200704179
33. Gómez-Salinero JM, López-Olañeta MM, Ortiz-Sánchez P, Larrasa-Alonso J, Gatto A, Felkin LE, Barton PJR, Navarro-Lérida I, Ángel Del Pozo M, García-Pavía P, et al. The calcineurin variant CnAβ1 controls mouse embryonic stem cell differentiation by directing mTORC2 membrane localization and activation. *Cell Chem Biol.* 2016;23:1372–1382. doi: 10.1016/j.chembiol.2016.09.010
34. Sala L, van Meer BJ, Tertoolen LGJ, Bakkers J, Bellin M, Davis RP, Denning C, Dieben MAE, Eschenhagen T, Giacomelli E, et al. MUSCLEMOTION: a versatile open software tool to quantify cardiomyocyte and cardiac muscle contraction in vitro and in vivo. *Circ Res.* 2018;122:e5–e16. doi: 10.1161/CIRCRESAHA.117.312067
35. Pilichou K, Remme CA, Basso C, Campian ME, Rizzo S, Barnett P, Scicluna BP, Bauce B, van den Hoff MJ, de Bakker JM, et al. Myocyte necrosis underlies progressive myocardial dystrophy in mouse dsg2-related arrhythmogenic right ventricular cardiomyopathy. *J Exp Med.* 2009;206:1787–1802. doi: 10.1084/jem.20090641
36. Kant S, Krull P, Eisner S, Leube RE, Krusche CA. Histological and ultrastructural abnormalities in murine desmoglein 2-mutant hearts. *Cell Tissue Res.* 2012;348:249–259. doi: 10.1007/s00441-011-1322-3
37. Garcia-Gras E, Lombardi R, Giocondo MJ, Willerson JT, Schneider MD, Khoury DS, Marian AJ. Suppression of canonical Wnt/beta-catenin signaling by nuclear plakoglobin recapitulates phenotype of arrhythmogenic right ventricular cardiomyopathy. *J Clin Invest.* 2006;116:2012–2021. doi: 10.1172/JCI27751
38. Hodgkinson KA, Howes AJ, Boland P, Shen XS, Stuckless S, Young T-L, Curtis F, Collier A, Parfrey PS, Connors SP. Long-term clinical outcome of arrhythmogenic right ventricular cardiomyopathy in individuals with a p.S358L mutation in TMEM43 following implantable cardioverter defibrillator therapy. *Circ Arrhythm Electrophysiol.* 2016;9:e003589. doi: 10.1161/CIRCEP.115.003589
39. Gomes J, Finlay M, Ahmed AK, Ciaccio EJ, Asimaki A, Saffitz JE, Quarta G, Nobles M, Syrris P, Chaubey S, et al. Electrophysiological abnormalities precede overt structural changes in arrhythmogenic right ventricular cardiomyopathy due to mutations in desmoplakin-A combined murine and human study. *Eur Heart J.* 2012;33:1942–1953. doi: 10.1093/eurheartj/ehr472
40. Li J, Patel VV, Kostetskii I, Xiong Y, Chu AF, Jacobson JT, Yu C, Morley GE, Molkentin JD, Radice GL. Cardiac-specific loss of n-cadherin leads to alteration in connexins with conduction slowing and arrhythmogenesis. *Circ Res.* 2005;97:474–481.
41. Smart N, Bollini S, Dubé KN, Vieira JM, Zhou B, Davidson S, Yellon D, Riegler J, Price AN, Lythgoe MF, et al. De novo cardiomyocytes from within the activated adult heart after injury. *Nature.* 2011;474:640–644. doi: 10.1038/nature10188
42. Liu Z, Ahn JY, Liu X, Ye K. Ebp1 isoforms distinctively regulate cell survival and differentiation. *Proc Natl Acad Sci USA.* 2006;103:10917–10922. doi: 10.1073/pnas.0602923103
43. Ahn JY, Liu X, Liu Z, Pereira L, Cheng D, Peng J, Wade PA, Hamburger AW, Ye K. Nuclear Akt associates with PKC-phosphorylated Ebp1, preventing DNA fragmentation by inhibition of caspase-activated DNase. *EMBO J.* 2006;25:2083–2095. doi: 10.1038/sj.emboj.7601111

OPEN

Loss of SRSF3 in Cardiomyocytes Leads to Decapping of Contraction-Related mRNAs and Severe Systolic Dysfunction

Paula Ortiz-Sánchez, María Villalba-Orero, Marina M. López-Olañeta, Javier Larrasa-Alonso, Fátima Sánchez-Cabo, Carlos Martí-Gómez, Emilio Camafeita, Jesús M. Gómez-Salinero, Laura Ramos-Hernández, Peter J. Nielsen, Jesús Vázquez, Michaela Müller-McNicoll, Pablo García-Pavía, Enrique Lara-Pezzi

Rationale: **RBPs (RNA binding proteins) play critical roles in the cell by regulating mRNA transport, splicing, editing, and stability. The RBP SRSF3 (serine/arginine-rich splicing factor 3) is essential for blastocyst formation and for proper liver development and function. However, its role in the heart has not been explored.**

Objective: **To investigate the role of SRSF3 in cardiac function.**

Methods and Results: **Cardiac SRSF3 expression was high at mid gestation and decreased during late embryonic development. Mice lacking SRSF3 in the embryonic heart showed impaired cardiomyocyte proliferation and died in utero. In the adult heart, SRSF3 expression was reduced after myocardial infarction, suggesting a possible role in cardiac homeostasis. To determine the role of this RBP in the adult heart, we used an inducible, cardiomyocyte-specific SRSF3 knockout mouse model. After SRSF3 depletion in cardiomyocytes, mice developed severe systolic dysfunction that resulted in death within 8 days. RNA-Seq analysis revealed downregulation of mRNAs encoding sarcomeric and calcium handling proteins. Cardiomyocyte-specific SRSF3 knockout mice also showed evidence of alternative splicing of mTOR (mammalian target of rapamycin) mRNA, generating a shorter protein isoform lacking catalytic activity. This was associated with decreased phosphorylation of 4E-BP1 (eIF4E-binding protein 1), a protein that binds to eIF4E (eukaryotic translation initiation factor 4E) and prevents mRNA decapping. Consequently, we found increased decapping of mRNAs encoding proteins involved in cardiac contraction. Decapping was partially reversed by mTOR activation.**

Conclusions: **We show that cardiomyocyte-specific loss of SRSF3 expression results in decapping of critical mRNAs involved in cardiac contraction. The molecular mechanism underlying this effect likely involves the generation of a short mTOR isoform by alternative splicing, resulting in reduced 4E-BP1 phosphorylation. The identification of mRNA decapping as a mechanism of systolic heart failure may open the way to the development of urgently needed therapeutic tools. (*Circ Res*. 2019;125:170-183. DOI: 10.1161/CIRCRESAHA.118.314515.)**

Key Words: alternative splicing ■ mRNA decapping ■ myocardial contraction ■ myocardial infarction ■ phosphorylation

Cardiovascular disease is the main cause of mortality worldwide, causing. 17.7 million deaths in 2015, corresponding to 31% of all deaths worldwide. Of these, 6.7 million were caused by myocardial infarction (MI), which is thus one of the main causes of cardiovascular disease deaths.[1] Knowledge about the molecular mechanisms that regulate the progression from MI to heart failure is incomplete, precluding the development of new therapeutic approaches. In recent years, the development of massive mRNA sequencing technologies has identified gene expression patterns associated with the development of heart failure.[2] However, understanding remains limited about post-transcriptional regulation and, more specifically, the role of RBPs (RNA binding proteins) in MI progression and in the development of heart failure.

In This Issue, see p 147
Meet the First Author, see p 148

RBPs contain RNA-binding domains that enable them to bind RNA molecules and regulate different processes associated with RNA metabolism, including constitutive and alternative

Received December 11, 2018; revision received April 29, 2019; accepted May 29, 2019.

From the Centro Nacional de Investigaciones Cardiovasculares (CNIC), Madrid, Spain (P.O.-S., M.V.-O., M.M.L.-O., J.L.-A., F.S.-C., C.M.-G., E.C., J.M.G.-S., L.R.-H., J.V., E.L.-P.); Heart Failure and Inherited Cardiac Diseases Unit, Department of Cardiology, Hospital Universitario Puerta de Hierro, Madrid, Spain (P.O.-S., P.G.-P.); Max Planck Institute of Immunobiology and Epigenetics, Freiburg, Germany (P.J.N.); Centro de Investigacion Biomedica en Red Cardiovascular (CIBERCV), Madrid, Spain (J.V., P.G.-P., E.L.-P); Goethe-University Frankfurt, Institute of Cell Biology and Neuroscience, Frankfurt/Main, Germany (M.M.-M.); Facultad de Ciencias de la Salud, Universidad Francisco de Vitoria (UFV), Pozuelo de Alarcón, Madrid, Spain (P.G.-P.); and National Heart and Lung Institute, Imperial College London, United Kingdom (E.L.-P.).

The online-only Data Supplement is available with this article at https://www.ahajournals.org/doi/suppl/10.1161/CIRCRESAHA.118.314515.

Correspondence to Enrique Lara-Pezzi, PhD, Myocardial Pathophysiology Area, Centro Nacional de Investigaciones Cardiovasculares Carlos III, Melchor Fernandez Almagro, 3, 28029 Madrid, Spain. Email elara@cnic.es

Novelty and Significance

What Is Known?

- RNA binding proteins regulate mRNA localization, stability, splicing, and activity.
- SRSF3 (serine/arginine splicing factor 3) plays a role in blastocyst formation and in liver function.

What New Information Does This Article Contribute?

- The expression of SRF3 in the adult heart is essential for proper cardiac contraction and animal survival.
- Loss of SRSF3 results in expression of a smaller mTOR (mammalian target of rapamycin) isoform, which has no enzymatic capacity.
- SRSF3 prevents mRNA decapping and loss of SRSF3 results in increased mRNA decapping and degradation of mRNAs encoding sarcomeric proteins, which leads to systolic dysfunction.

RNA binding proteins play diverse roles in the cell, including mRNA transport, regulation of mRNA stability, and post-transcriptional mRNA modifications, among others. SRSF3 is an RNA binding protein that plays a role in embryonic development and in the liver. Its role in the heart was unknown. Using mice that lack SRSF3 specifically in cardiomyocytes, we found that SRSF3 is necessary for embryonic cardiomyocyte proliferation and heart development. In the adult heart, loss of SRSF3 causes severe cardiac contraction defects that lead to heart failure. We show that the loss of SRSF3 leads to decapping and degradation of mRNAs, specifically those encoding sarcomeric proteins. This is the main mechanism underlying cardiac dysfunction in our mice. We also show that the absence of SRSF3 causes aberrant splicing of mTOR, producing a shorter isoform with reduced enzymatic activity, which is known to be necessary to prevent decapping. Based on these findings, it is tempting to speculate that mRNA decapping may have an important role in heart disease and that therapies aiming at modulating decapping may have a positive impact on cardiac contraction.

Nonstandard Abbreviations and Acronyms

iCLIP	individual-nucleotide resolution cross-linking and immunoprecipitation
LV	left ventricular
MI	myocardial infarction
mTOR	mammalian target of rapamycin
NMD	nonsense-mediated decay
RBP	RNA Binding Protein
SRSF3	serine/arginine splicing factor 3
UTR	untranslated region

splicing, nucleo-cytoplasmic transport, intracellular localization, translation, and degradation.[3] Loss of function of specific RBPs is associated with clinical manifestations, including neuropathies, muscular atrophies, and cancer.[3] In addition, recent studies show that some RBPs are crucial for proper cardiac function; loss of RBM20 (RNA-binding motif protein 20), TRBP (TAR RNA-binding protein), or RBFox2 (RNA-binding Fox-1 homolog 2) triggers the development and progression of dilated cardiomyopathy,[4–7] whereas RBFox1 (RNA-binding Fox-1 homolog 1) deficiency leads to hypertrophic cardiomyopathy.[8]

SRSF (serine/arginine-rich splicing factors, also known as SR proteins) are a family of highly conserved RBPs containing one or 2 RNA recognition motifs in their N-terminal region, followed by an SR domain formed of at least 50 amino acids with a serine and arginine content above 40%.[9] SR proteins were originally identified as splicing factors, but several studies have demonstrated that they are multifunctional proteins that take part in many mRNA regulation pathways.[10] SR proteins are localized both in the nucleus and the cytoplasm and regulate both the transport and stability of mRNA.[11] Deficiency of particular SR proteins has been linked to several disease states, including heart disease. SRSF1, SRSF2, and SRSF10 are essential for heart development and function. Loss of SRSF1 in the heart alters CaMKIIδ (calcium/calmodulin kinase IIdelta) splicing, which results in reduced phosphorylation of its target phospholamban, leading to calcium handling defects, hypercontraction, and death of the mice between 6 and 8 weeks of life.[12] Cardiac-specific depletion of SRSF2 leads to excitation-contraction defects and nonlethal dilated cardiomyopathy, associated with a decrease in RyR2 (ryanodine receptor 2) expression.[13] Ubiquitous deletion of SRSF10 induces cardiac developmental defects that result in embryonic death at E15.5.[14] These defects are caused by alternative splicing of triadin, which results in reduced expression of both triadin and calsequestrin 2 and lead to calcium handling defects in cardiomyocytes.[14]

Like other members of the SR family, SRSF3 regulates splicing of several mRNAs,[15–17] mRNA cytoplasmic transport,[11] and mRNA localization.[18] SRSF3 is essential for proper embryonic development. SRSF3-deficient embryos are unable to form blastocysts and die at the morula stage.[19] Specific depletion of SRSF3 in the liver is not lethal, but mice present both embryonic and postnatal growth defects.[20] As these mice get older, they develop hepatic carcinomas, mirroring the human disease, in which SRSF3 is also downregulated, in contrast to other cancer types.[21] SRSF3 has also been reported to act as an oncogene in the liver by promoting cell proliferation.[22] These studies establish the importance of SRSF3 for proper organ development and function. However, unlike other RBPs, the function of SRSF3 in the heart has not been reported previously.

In this study, we show that SRSF3 is essential for heart development in mice and that SRSF3 expression in the adult heart is decreased in the remote myocardium after MI. Induced loss of SRSF3 in adult cardiomyocytes results in widespread changes in alternative splicing and decapping of mRNAs encoding contraction proteins and its subsequent degradation, leading to severe systolic dysfunction and death. We also show that SRSF3 regulates mTOR (mammalian target of rapamycin) splicing, reducing the phosphorylation of 4E-BP1 (eIF4E-binding protein 1) required to prevent mRNA decapping.

Methods

The data that support the findings of this study are available from the corresponding author on reasonable request.

RNA-Seq data are available from GEO (GSE123002; https://www.ncbi.nlm.nih.gov/geo/query/acc.cgi?acc=GSE123002). The entire iCOUNT script for the (individual-nucleotide resolution cross-linking and immunoprecipitation) iCLIP analysis is available on github: https://github.com/tomazc/iCount. Materials used in this work will be made available on request to the corresponding author.

Mice

The SRSF3 knockout mice were originally generated by Dr Peter J. Nielsen.[19] The neomycin cassette was removed by breeding SRSF3-floxed mice with transgenic mice expressing CreERT2 under the polymerase II promoter (PolII-mER-Cre-mER). Treating these mice with low doses of tamoxifen generated an SRSF3-floxed mouse line that contained LoxP sites flanking SRSF3 exons 2 and 3. We performed 3 backcrosses with C57BL/6 to remove the Cre cassette and then crossed the resulting SRSF3-floxed mice with the cardiac-specific Cre lines, Nkx2.5-Cre and αMHC-Cre. Both crosses resulted in embryonic lethality, and lines were, therefore, maintained in heterozygosity for the SRSF3-floxed allele. In addition, we generated the cardiomyocyte-specific and inducible SRSF3 knockout mice by crossing SRSF3-floxed mice with αMHC-mER-Cre-mER mice. The resulting line was maintained in homozygosity. We used αMHC-mER-Cre-mER mice as negative controls. Genotyping was performed using the primers indicated in Online Table I.

Due to the effects of estrogens on the heart, only adult (2–3-month old) male mice were used for all experiments, to avoid potential effects of sex differences. Mice were euthanized by carbon dioxide asphyxiation. All procedures were approved by the ethics committees of the CNIC (Centro Nacional de Investigaciones Cardiovasculares) and the Regional Government of Madrid (PROEX 332-15). Animals were randomly assigned to groups. Researchers were blinded to the allocations.

Tamoxifen and Amino Acid Treatments

To activate the Cre recombinase in inducible knockout mice, SRSF3 knockout and control mice were treated with 3 doses of 1 mg 4-hydroxytamoxifen on alternate days (1 dose/d). To prepare tamoxifen doses, 50 mg of 4-hydroxytamoxifen (H6278, Sigma) was diluted in 500 µL 100% ethanol and stirred at 55°C for 1 hour, until completely dissolved. Preheated corn oil (4.5 mL) was then added, and the incubation continued with stirring at 55°C for a further hour. Once the tamoxifen and corn oil were fully dissolved, the solution was maintained at 4°C until use. Just before injection, the solution was warmed and maintained at 37°C for 10 minutes. A total of 100 µL were injected intraperitoneal per mouse per day. To activate mTOR, mice were injected intraperitoneal daily, for 7 days, starting on the day of the second tamoxifen injection, with 100 µL/g of a solution containing 6.0 g/L isoleucine, 12.0 g/L leucine, 7.2 g/L valine, and 6.04 g/L arginine in PBS (pH 7.4).[23]

Echocardiography

Transthoracic echocardiography was performed by blinded observers using a 40 MHz lineal transducer (Vevo 2100, VisualSonics). Mice were placed on a heating pad at 38.3ºC and lightly anesthetized with isoflurane in 100% oxygen. The Isoflurane concentration was adjusted to maintain heart rate at 450 to 550 bpm.

Left ventricular (LV) systolic function was evaluated using the area/length method, with images acquired and recorded from 2-dimensional parasternal long axis views.[24] Image analysis was performed by blinded observers using Vevo 2100 analysis software (VisualSonics).

Embryo Extraction, In Situ Hybridization, and Histology

Embryos were extracted from C57BL/6, αMHC-Cre, or SRSF3-floxed/αMHC-Cre mice at the stages indicated in the figures. In situ hybridization was performed on whole mount embryos (E9.5–E11.5) or 10 µm sections (E12.5–E14.5).[25] The SRSF3 probe was designed to match the total length of the mRNA. Hematoxylin and eosin staining were performed on 5 µm sections according to standard protocols by the CNIC Histology Unit.

Gene Expression, Alternative Splicing, and Gene Ontology Analyses

Total RNA was extracted from left ventricles after 5 days of tamoxifen treatment using the RNeasy extraction kit (74104, Qiagen), including treatment with DNase. RNA sequencing was performed by the CNIC Genomics Unit. Libraries were prepared using polyA+ selection, and sequencing was performed using an Illumina-HiSeq 2500 platform, ensuring an average of 95 million paired-end reads per sample, with a minimum of 74 mol/L per sample. RNA-Seq analysis was performed by the CNIC Bioinformatics Unit. Fastq files containing the reads for each library were extracted and demultiplexed using the Casava v1.8.2 pipeline. Reads were preprocessed with a pipeline that used cutadapt v1.6 to remove Illumina adaptors, and FastQC to perform quality controls after each step. Gene expression was quantified using Kallisto v0.43.0,[26] and the reference transcriptome was downloaded from Ensembl (Mus_musculus.GRCm38.cdna.all.fa). One hundred bootstraps were performed to account for quantification uncertainty. Sleuth[27] with default parameters was then used to normalize the data and perform differential expression analysis at the gene level. Genes with an adjusted P value <0.05 and an absolute $\beta > 1$ were considered to be differentially expressed for downstream enrichment analysis. Alternative splicing was analyzed using vast-tools to map reads against the mouse reference database and to perform differential splicing analysis.[28,29] Gene ontology categories and KEGG (Kyoto Encyclopedia of Genes and Genomes) pathways were downloaded from the Enrichr website,[28] and enrichment analysis of genes undergoing both differential expression or splicing was performed with one-sided Fisher tests and Benjamini-Hochberg False Discovery Rate correction using custom python scripts. RNA-Seq data were deposited in Gene Expression Omnibus (GSE123002).

Decapping Analysis

Decapped mRNA was quantified as previously described.[30] Briefly, 4 µg of total RNA was treated with DNase and ligated with the rP5_RND primer (Online Table II), which binds specifically to 5′ ends lacking the cap structure and presenting a phosphate group. Afterwards, 100 ng were used for cDNA synthesis, and polymerase chain reaction (qRT-PCR) was performed using the primers indicated in Online Table II. Values were normalized to total mRNA expression.

Statistical Analysis

Data were analyzed for statistical significance using the unpaired Student t test for experiments with 2 conditions and 1 variable, 1-way ANOVA followed by the Bonferroni post-test for more than 2 conditions and 1 variable, and 2-way ANOVA followed by the Bonferroni post-test for analysis of multiple conditions and 2 variables, for normally distributed data, as indicated in each figure legend. The Mann-Whitney test was used for non-normally distributed data. Data were analyzed using GraphPad Prism 5.0, and changes were considered significant at $P<0.05$. Correction for multiple comparisons was used for all analyses with more than one variable.

Results

SRSF3 Expression in the Heart Decreases With Age

In situ hybridization in embryos from E9.5 to E14.5 revealed strong SRSF3 staining in the heart from E12.5 (Figure 1A). For a more detailed analysis of changes in SRSF3 expression during heart development and in adulthood, we isolated hearts from mice ranging from E12.5 to 6 months of age and quantified SRSF3 mRNA levels by qRT-PCR. SRSF3 expression was highest at E12.5 and decreased progressively during later embryonic stages and the postnatal period (Figure 1B). To identify the cardiac cell types expressing SRSF3 in the postnatal heart, we performed an immunofluorescence analysis of heart sections from P1, P7, and 1-month-old mice. Clear staining for SRSF3 was detected in cardiomyocyte nuclei, as well as in other cell types (Figure 1C).

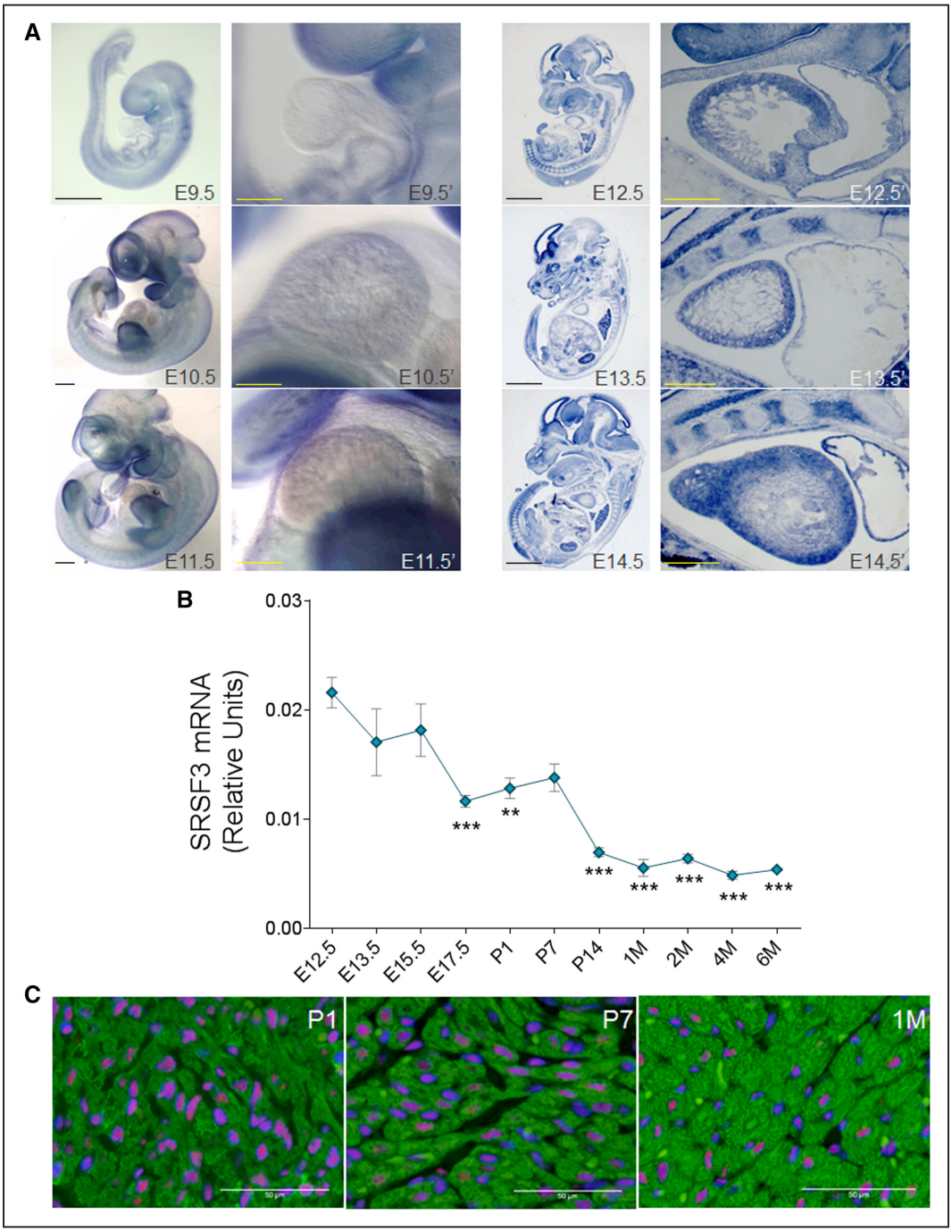

Figure 1. SRSF3 (serine/arginine splicing factor 3) expression in the heart decreases with age. A, In situ hybridization for SRSF3 performed at different embryonic stages, either in whole mount (**Left** set: E9.5, E10.5, and E11.5) or 10 μm sections (**Right** set: E12.5, E13.5, and E14.5). The region including the developing heart is shown at high magnification to the right of each whole-embryo view. **B**, qRT-PCR (polymerase chain reaction) analysis of SRSF3 mRNA expression (exons 3–5) normalized to Gapdh expression in hearts extracted from C57BL/6 mice at different time points. Data are shown as mean±SEM; n=3–4 mice per group. ***P*<0.01, ****P*<0.001 vs E12.5, 1-way ANOVA followed by the Bonferroni multiple comparison test. **C**, Immunofluorescence analysis of hearts isolated from C57BL/6 mice at different ages using anti-SRSF3 (red), anti-TroponinT (green), and DAPI (blue). M, month; Bars, **A**, 1 mm (whole mount, full embryo); 0.5 mm (whole mount, heart); 2 mm (embryo section), 0.5 mm (heart section); **C**, 50 μm.

SRSF3 Downregulation Following MI Is Associated With Inclusion of Exon 4

To determine whether SRSF3 could be altered in heart disease, we measured its expression after MI in the region remote from the infarct (Figure 2A–2E). Both mRNA and protein SRSF3 expression was downregulated after MI (Figure 2B and 2C), suggesting a possible role in cardiac homeostasis. Published evidence shows that SRSF3 is regulated by the alternative splicing of exon 4, inclusion of which leads to degradation of the mRNA through nonsense-mediated decay (NMD; Figure 2A).[31] qRT-PCR analysis revealed increased SRSF3 exon 4 inclusion in infarcted hearts, suggesting a role of this mechanism in the regulation of SRSF3 after MI (Figure 2D).

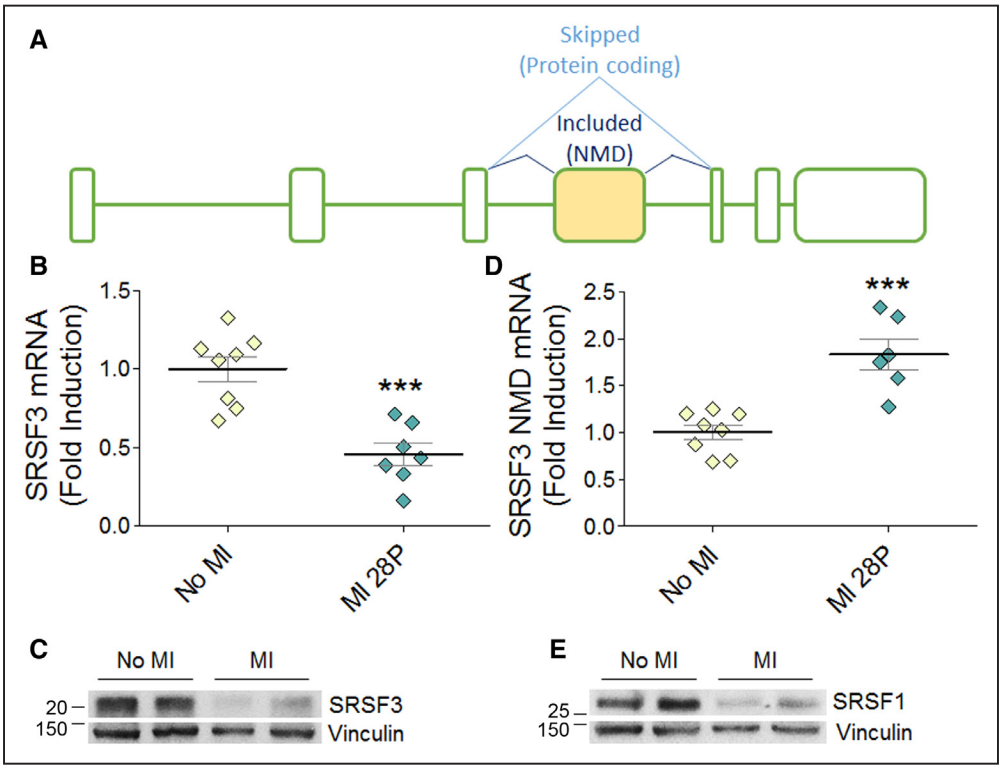

Figure 2. SRSF3 (serine/arginine splicing factor 3) is downregulated after myocardial infarction (MI) by alternative splicing. **A**, Schematic of the SRSF3 mRNA isoforms. The yellow box represents alternative exon 4. **B** and **C**, Analysis by qRT-PCR (polymerase chain reaction; **B**) and Western blot (**C**) of SRSF3 mRNA (exons 3–5 normalized to Gapdh) and protein expression in the remote myocardium of mouse hearts 28 days after induction of MI by left coronary artery ligation. MW markers are indicated. **D**, qRT-PCR analysis of the SRSF3 NMD (nonsense-mediated decay) isoform in the remote myocardium, normalized to total SRSF3 mRNA expression. **E**, Western blot analysis of SRSF1 protein expression in the remote myocardium. Data in **B** and **D** are mean±SEM, and symbols represent individual animals (n=7–8); **P*<0.05 and ****P*<0.001, Student *t* test.

SRSF1 has been shown to regulate SRSF3 expression by promoting exon 4 skipping.[31] The post-MI increase in exon 4 inclusion thus prompted us to investigate whether SRSF1 expression was also affected. Western blot analysis showed decreased SRSF1 expression after MI (Figure 2E). These results suggest that the decrease in SRSF1 expression may favor the inclusion of SRSF3 exon 4, leading to SRSF3 downregulation after MI.

SRSF3 Cardiac Depletion During Embryonic Development Is Lethal

To investigate the role of SRSF3 in the heart, we developed several cardiac-specific knockout mouse models. We first crossed SRSF3-floxed mice with transgenic mice expressing Cre recombinase under the control of the Nkx2.5 promoter. No transgenic animals bearing both the Nkx2.5 promoter and the floxed SRSF3 allele were born (Table), suggesting that early SRSF3 depletion during heart development is embryonically lethal. To limit the recombination to cardiomyocytes and later developmental stages, we crossed SRSF3-floxed mice with mice expressing Cre recombinase under the αMHC promoter, which also was embryonically lethal (Table). Hematoxylin and eosin staining showed a reduction in myocardium thickness in embryonic hearts lacking SRSF3 expression (Figure 3A and 3B). Previous reports that show that SRSF3 promotes proliferation[22] prompted us to investigate if cardiomyocyte proliferation was affected in these animals; we were unable to detect any cardiomyocytes with positive staining for the mitosis marker phospho-histone H3 in myocardium lacking SRSF3 expression (Figure 3C and 3D). These results suggest that SRSF3 expression in cardiomyocytes is essential for cell proliferation, proper heart development, and subsequent embryo survival.

Cardiac-Specific SRSF3 Knockout Mice Develop Severe and Fatal Contraction Defects

To investigate the role of SRSF3 in the adult heart, we developed a cardiac-specific tamoxifen-inducible knockout mouse line by crossing SRSF3-floxed and αMHC-mER-Cre-mER mice (SRSF3 knockout). SRSF3 depletion occurred rapidly, with a strong decline already observed on the first day after tamoxifen administration (Online Figure IA and IB). Immunofluorescence analysis confirmed that SRSF3 was depleted only in cardiomyocytes, although recombination was incomplete, and some cardiomyocytes were still positive for SRSF3 expression (Online Figure IC).

Unlike SRSF2 and SRSF1 cardiac-specific knockout mice, which either have a normal lifespan (SRSF2) or survive for several weeks after birth (SRSF1),[12,13] no SRSF3 knockout mice survived beyond 8 days after SRSF3 depletion (Figure 4A). Echocardiography analysis of SRSF3 knockout mice 5 days after tamoxifen administration revealed a pronounced reduction in left ventricular ejection fraction and a strong increase in LV systolic volume (Figure 4B and 4C and Online Movie I), suggesting that these mice develop severe contraction defects that lead to death. No significant changes were observed in LV diastolic volume, likely due to the short

Table. Genotype of the Srsf3 Allele in the Offspring of Nkx2.5-Cre/Srsf3$^{wt/fl}$ and αMHC-Cre/Srsf3$^{wt/fl}$ Mice

SRSF3 Genotype	Nkx2.5-Cre	αMHC-Cre
wt/wt	33 (30.84%)	29 (29.29%)
floxed/wt	74 (69.16%)	70 (70.71%)
floxed/floxed	0 (0%)	0 (0%)
Total mice	107	99

Number and percentage of mice born in the first 20 litters obtained from Nkx2.5-Cre/Srsf3$^{wt/fl}$ and αMHC-Cre/Srsf3$^{wt/fl}$ mice.

lifespan after SRSF3 knockout (Figure 4D and Online Table III). Systolic dysfunction was accompanied by an increase in Nppb (natriuretic peptide B) and Acta1 gene expression in SRSF3 knockout hearts (Figure 4E and 4F). Together, these results demonstrate that the loss of SRSF3 in cardiomyocytes leads to severe cardiac dysfunction and premature death.

SRSF3 Depletion Results in Downregulation of Contraction-Related Genes

To investigate the mechanism underlying the contraction defects in SRSF3 knockout mice, we performed RNA-Seq in control and knockout hearts 5 days after tamoxifen administration. We found significant expression changes in several genes, both upregulated and downregulated (Online Table IV and Online Figure IIA). Gene ontology analysis showed a decrease in contraction-related genes and an increase in genes related to protein maturation and transport in the ER and to the immune response (Online Figure IIB and IIC). qRT-PCR analysis to confirm these results revealed that the decreased expression of sarcomeric genes was already evident 2 days after SRSF3 depletion (Figure 5A–5F). Protein levels of SERCA2A (sarcoplasmic/endoplasmic reticulum calcium ATPase 2a) and MYH (myosin heavy chain) were unchanged until day 5 after tamoxifen administration (Figure 5G), suggesting that cardiac function is preserved until the expression of contraction proteins decreases. To determine whether the downregulation of sarcomeric gene expression was due to general RNA degradation associated with apoptosis, we first measured the number of apoptotic cardiomyocytes in control and SRSF3 knockout mice 5 days after the last tamoxifen injection. We found a very low number of TUNEL$^+$ (terminal deoxynucleotidyl transferase dUTP nick-end labeling) cardiomyocytes overall and no differences between both mouse lines (Online Figure IIIA). We observed a very mild decline in total RNA integrity 5 days after the last tamoxifen injection in knockout mice, which, in any case, takes place much later than the decrease of sarcomeric mRNA, which is already evident at day 2 (Online Figure IIIB, Figure 5A–5F). We found no differences in the apoptosis markers Raptor and Fas, and only a mild decrease in Bcl2 mRNA expression at late time points in SRSF3 knockout mice that was not accompanied by a decrease in Bclxl (Online Figure IIIC–IIIF). Therefore, the decrease in sarcomeric gene expression precedes early signs of apoptosis, which would start a few days later. Early stages of cell death would be in agreement with the induction of genes associated with the immune response observed in knockout mice 5 days after tamoxifen treatment (Online Figure IIB).

SERCA2A Overexpression Partially Rescues Cardiac Contraction in SRSF3 Knockout Mice

Reduced expression of SERCA2A in cardiomyocytes is strongly associated with heart failure,[32] and SERCA2A overexpression has been shown to improve cardiac function in several animal models.[33,34] To determine whether the decreased expression of cardiac contraction proteins, specifically SERCA2A, is responsible for the severe systolic dysfunction in SRSF3 knockout mice, we overexpressed SERCA2A in control and knockout animals using serotype 9 adeno-associated viruses (AAV9-SERCA2A). AAV9-LUC, carrying the luciferase reporter gene, was used as a negative control. Viruses were injected into control and SRSF3 knockout mice 1 week before tamoxifen induction to ensure transgene overexpression in advance of the loss of SERCA2A expression. SERCA2A overexpression was confirmed by western blot 5 days after tamoxifen induction (Figure 6A).

We found that AAV9-SERCA2A significantly improved survival of SRSF3 knockout mice (Figure 6B). Echocardiography analysis of cardiac function showed a mild but significant improvement in left ventricular ejection fraction in mice overexpressing SERCA2A, and increased stroke volume (Figure 6C and 6D and Online Table V). Although this improvement was far from a full recovery, we conclude that the downregulation of SERCA2A is responsible, at least in part, for the contraction defects observed in SRSF3 knockout mice. Full recovery would likely require overexpression of additional genes involved in cardiac contraction whose expression was reduced in the knockout mice.

SRSF3 Binds to the Untranslated Region of Contraction-Related mRNAs

To gain further insight into the mechanisms underlying the contraction defects in SRSF3 knockout mice, we looked for direct SRSF3 target mRNAs in cardiac tissue. For this, we performed iCLIP on mouse neonatal cardiomyocytes transfected with modified RNA encoding an SRSF3-GFP (green fluorescent protein) chimera, and analyzed the distribution of iCLIP binding sites along different regions of the genes detected to be expressed in the previous RNA-Seq analysis (Online Table VI). SRSF3 showed a tendency to bind exons, particularly in coding regions (Online Figure IVA). Genes with SRSF3-enriched exons were associated with post-transcriptional processing and insulin signaling, whereas SRSF3-bound untranslated regions (UTRs) were present in genes associated with muscle contraction (Online Figure IVB and IVC). These analyses identified SRSF3 binding to several contraction-related mRNAs, including MYBPC3 (myosin-binding protein C), TNNT2 (troponin T2), and TNNC1 (troponin C1; Online Table VI). The SRSF3 consensus motif derived from iCLIP peaks (significant X-links) was identical to the bona fide SRSF3 motif (CNYC) and was independent of the bound transcript region (whole transcript versus UTR; Online Figure VID and VIE).

Based on these results, we decided to study whether SRSF3 could increase the stability of an mRNA by binding to its 3′-UTR. To test this hypothesis, we used a stability assay based on a protein-RNA binding system present in the MS2 virus (Online Figure VA).[35] P19 cells were transfected with MS2-CP or MS2-CP-SRSF3 and Rluc8 (containing 8 repeats of the

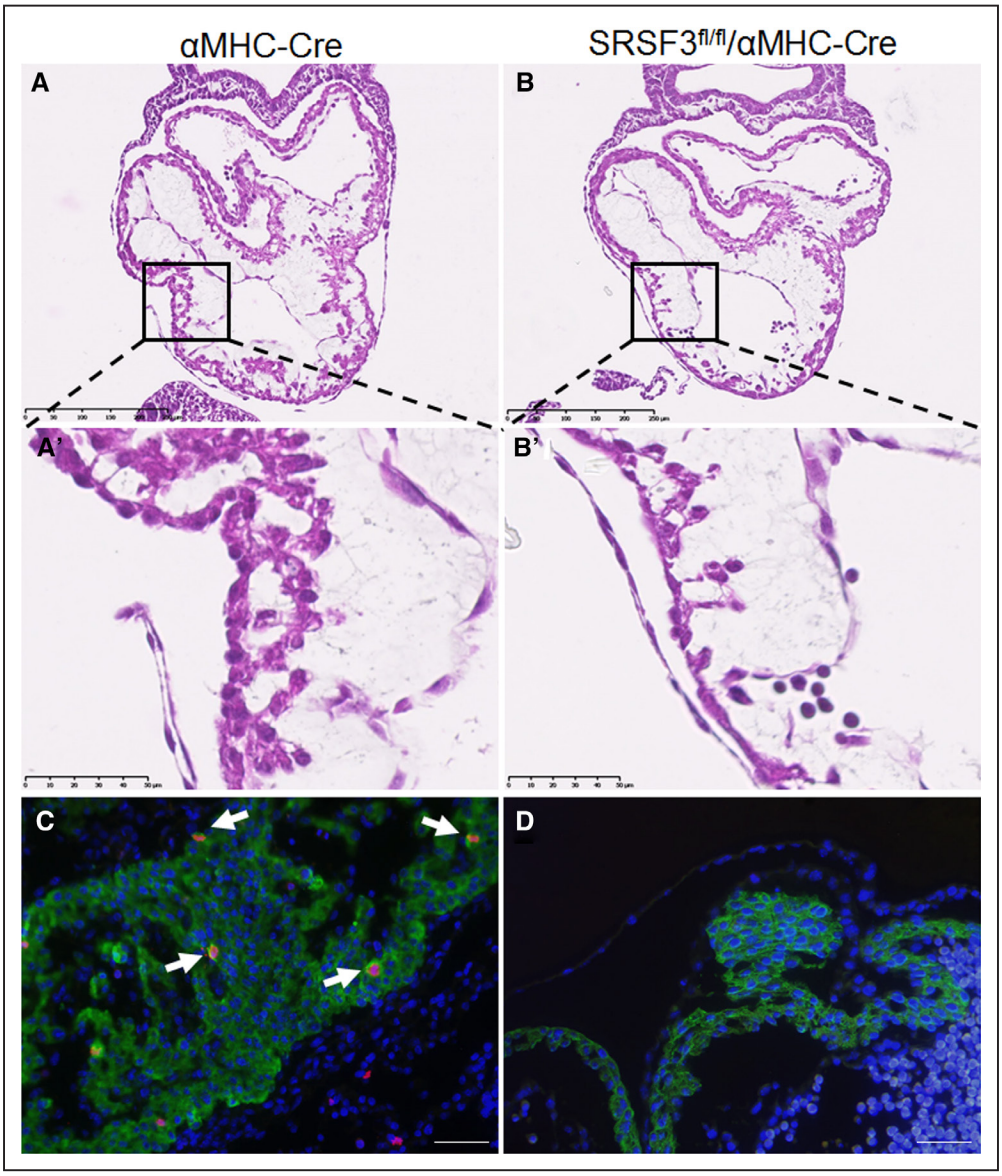

Figure 3. Loss of SRSF3 (serine/arginine splicing factor 3) in the developing heart results in embryonically lethal heart defects. A and **B**, Hematoxylin and eosin (H&E) staining in sections of αMHC-Cre embryos (**A**) and SRSF3-floxed/αMHC-Cre embryos (**B**) at E9.5. The boxed areas in **A** and **B** are shown at high magnification in **A′** and **B′**, illustrating the cell deficit in the developing ventricular wall of SRSF3-floxed/αMHC-Cre embryos. Bar, 250 μm (**A** and **B**), 50 μm (**A′** and **B′**). **C** and **D**, Immunofluorescence analysis in sections of αMHC-Cre embryos (**C**) and SRSF3-floxed/αMHC-Cre embryos (**D**) at E10.5, using anti-phospho-Histone H3 (red), anti-TroponinT (green), and Dapi (blue). Arrows indicate cardiomyocytes positive for phospho-histone H3; the developing SRSF3-floxed/αMHC-Cre heart is devoid of these cells. Bar, 20 μm.

MS2-CP binding loop in the 3′UTR region of R-Luc) or Rluc0 (containing no loops). Cells were treated with Actinomycin D, and R-Luc expression and enzymatic activity were measured at different time points after treatment. Expression of the MS2-CP-SRSF3 chimera had no effect either on luciferase mRNA stability (Online Figure VB and VC) or on protein activity (Online Figure VD and VE). These results suggest that the downregulation of contraction-related genes after SRSF3 depletion is independent of the binding of this RBP to the 3′-UTR in the target mRNAs.

SRSF3 Depletion Leads to a Late Induction of NMD

SRSF3 has been shown to promote the inclusion of alternative exons that lead to the appearance of premature stop codons, triggering mRNA degradation by NMD.[36] Therefore, we explored whether NMD was responsible for the degradation of cardiac contraction-related mRNAs in SRSF3 knockout hearts. qRT-PCR analysis of SRSF3 knockout mouse hearts showed induced expression of the NMD genes SMG1, SMG8, SMG9, SMG6, and RBM8A (Online Figure VIA–VIE). In agreement with these results, we also observed an increased proportion of the NMD isoform of SERCA2A (Online Figure VIF). However, most of these changes took place 4 or 5 days after tamoxifen treatment. Thus, although SRSF3 depletion in the heart induces NMD, it is unlikely that this mechanism mediates the early downregulation of contraction-related mRNAs already observed at day 2.

SRSF3 Regulates mTOR Alternative Splicing

Given that SRSF3 regulates alternative splicing,[15–17] we looked for alternative splicing changes in our RNA-Seq data.

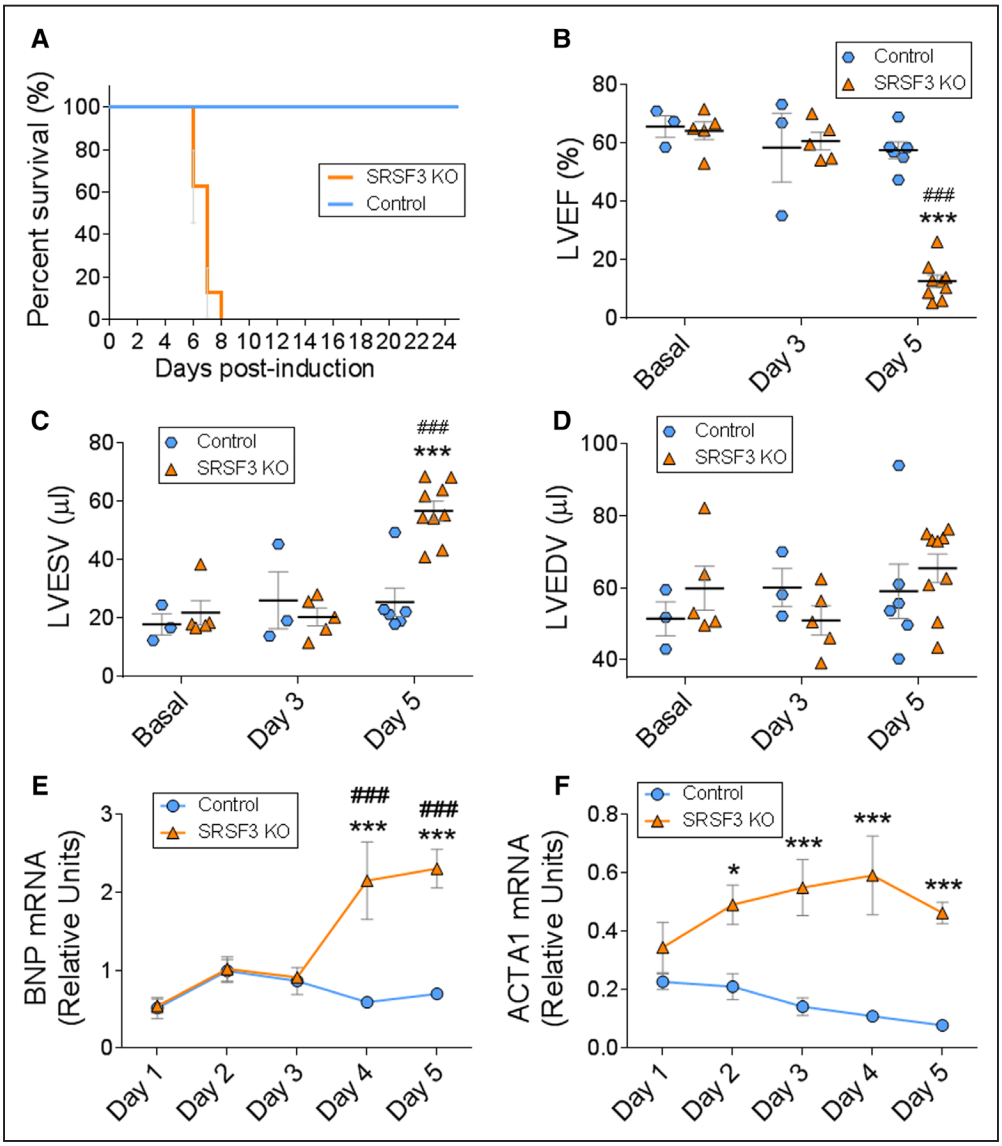

Figure 4. Cardiac-specific SRSF3 (serine/arginine splicing factor 3) knockout (KO) mice develop severe and fatal contraction defects. Deletion of SRSF3 in cardiomyocytes was induced in inducible SRSF3 KO mice by 3 hydroxytamoxifen injections on alternate days (post-induction days 0, 2, and 4). **A**, Survival curves for hydroxytamoxifen-injected control and SRSF3 KO mice. **B–D**, Echocardiography analysis of left ventricular ejection fraction (**B**), left ventricular end-systolic volume (**C**), and left ventricular end-diastolic volume (**D**); ***P<0.001 SRSF3 KO vs Control, ###P<0.001 vs Basal; 2-way ANOVA followed by the Bonferroni post-test. **E** and **F**, qRT-PCR (polymerase chain reaction) analysis of the cardiac expression of BNP (**E**) and Acta1 (**F**) mRNA over 5 days post-induction. Data are shown as mean±SEM. n=5–13 mice per group. Two-way ANOVA followed by Bonferroni post-test. *P<0.05, ***P<0.001 SRSF3 KO vs Control. ###P<0.001 vs day 1. ACTA1 indicates actin alpha 1; BNP, brain natriuretic peptide; LVEDV, left ventricular end diastolic volume; LVEF, left ventricular ejection fraction; and LVESV, left ventricular end systolic volume.

We identified changes in different types of alternative splicing events, ranging from alternative usage of splice donor and acceptors to intron retention (Online Figure VIIA and Online Table VII). Cassette exons were the event type showing the highest proportion (about 7%) of significant changes. There were more than twice as many exons with decreased inclusion rates than exons with increased inclusion, suggesting that the loss of SRSF3 mainly results in exon skipping. Skipped exons were associated with cytoskeletal organization and transcription, whereas retained introns affected genes associated with the regulation of transcription and translation, which could eventually contribute to the decreased expression of contraction-related genes (Online Figure VIIB and VIIC).

To determine whether the observed splicing changes were directly mediated by SRSF3, we identified SRSF3 iCLIP binding sites (significant X-links) on regulated exons and flanking regions that were potentially involved in splicing regulation (Online Figure VIIIA–VIIID and Online Tables VIII and IX). We found that SRSF3 bound preferentially to skipped exons, suggesting that the lack of direct SRSF3 binding results in exclusion of these exons. In contrast, for included exons, we observed increased SRSF3 binding in the flanking introns and exons, suggesting that SRSF3 acts here as an inhibitor of exon inclusion, for example, by promoting skipping (Online Figure VIIIA and VIIIB). For skipped introns, SRSF3 binding sites were over-represented in the intronic region and its flanking

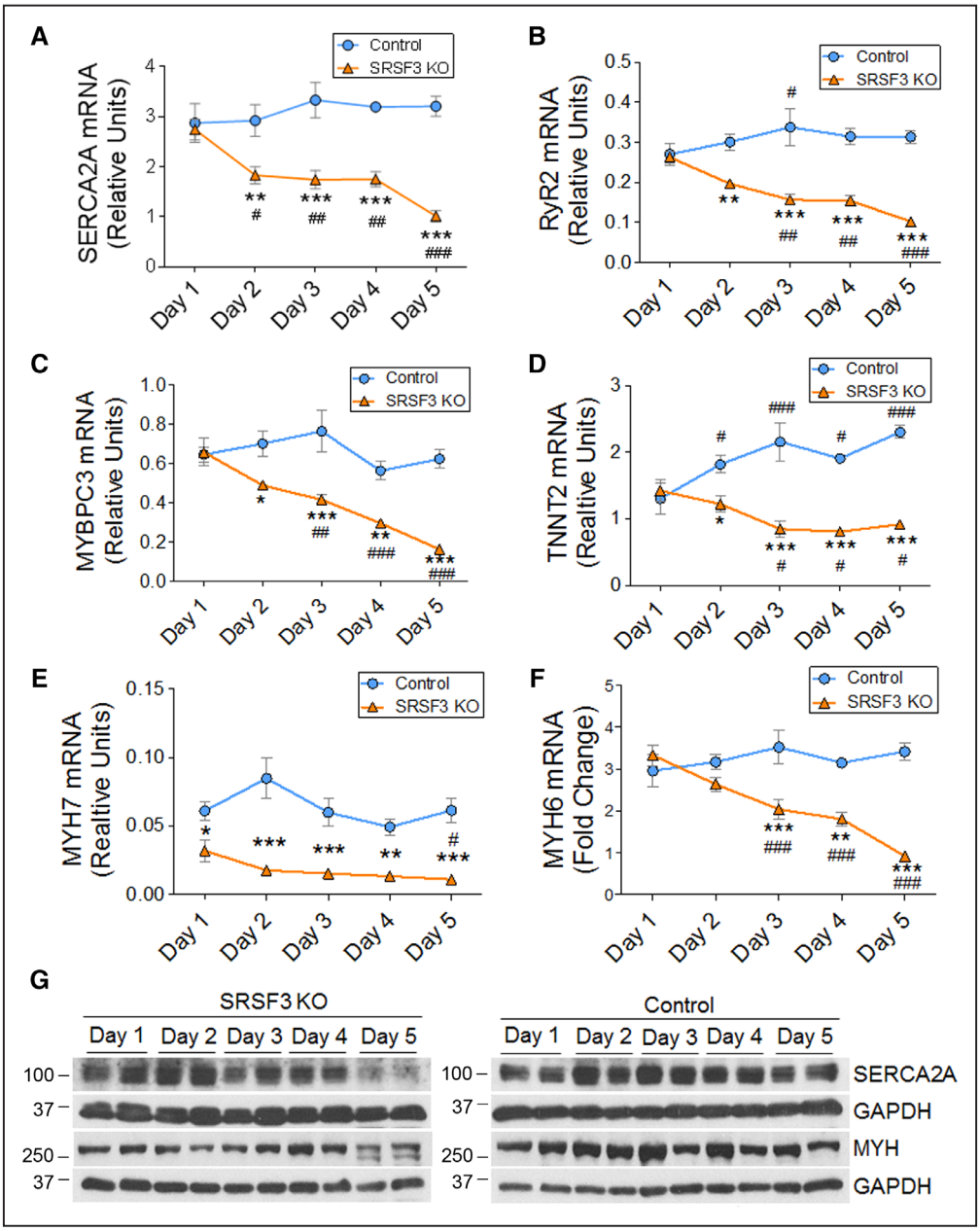

Figure 5. SRSF3 (serine/arginine splicing factor 3) depletion results in downregulation of contraction-related genes. **A**–**F**, qRT-PCR (polymerase chain reaction) analysis of the cardiac expression of SERCA2A (**A**), RyR2 (**B**), MYBPC3 (**C**), TNNT2 (**D**), MYH7 (**E**), and MYH6 (**F**) mRNA in control and SRSF3 KO mice over 5 days post tamoxifen induction. Data are shown as mean±SEM;. n=5–13 mice per group. **P*<0.05, ***P*<0.01, and ****P*<0.001 for SRSF3 knockout (KO) vs control; #*P*<0.05, ##*P*<0.01, ###*P*<0.001 vs day 1; 2-way ANOVA followed by the Bonferroni post-test. **G**, Western blot analysis of MYH and SERCA2A protein expression in the heart over 5 days post tamoxifen induction. MYBPC3 indicates myosin-binding protein C3; MYH6, myosin heavy chain 6; MYH7, myosin heavy chain 7; RYR2, ryanodine receptor 2; SERCA2A, sarcoplasmic/endoplasmic reticulum calcium ATPase 2a; and TNNT2, troponin T2.

exons, indicating that SRSF3 promotes the retention of these introns. On the contrary, introns showing increased retention (inclusion) in knockout mice did not show a significant association with SRSF3 binding sites, suggesting that they may be an indirect consequence of SRSF3 deletion (Online Figure VIIIC and VIIID).

Among other changes, we found a significant change in alternative splicing of mTOR mRNA, which was bound to SRSF3 (Online Tables VI–IX). More specifically, we found that retention of mTOR intron 5 in SRSF3 knockout mice led to a decrease in the full-length mTOR isoform and in turn favored the expression of a much shorter isoform containing only the first 5 exons of the gene. This short isoform lacks the mTOR kinase domain (Figure 7A). We next checked whether this alternative splicing change was already present from day 2 after tamoxifen administration, when mRNAs related to contraction begin to decrease. Western blot analysis of SRSF3 knockout hearts confirmed loss of the long isoform and gain of the short isoform at day 2 after the induction of recombination (Figure 7B). This was associated with decreased phosphorylation of the mTOR targets AKT and 4E-BP1 (Figure 7B).[37,38]

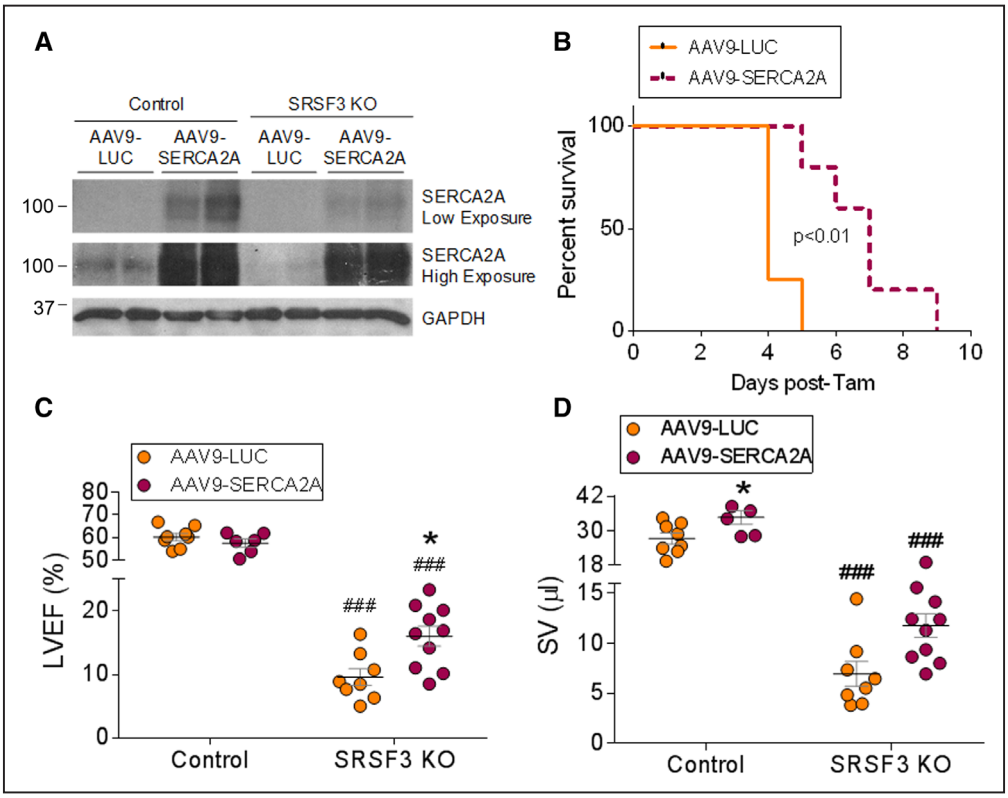

Figure 6. SERCA2A overexpression partially rescues systolic dysfunction in SRSF3 (serine/arginine splicing factor 3) knockout (KO) mice. A, Western blot analysis of SERCA2A protein expression in hearts of tamoxifen-induced control and SRSF3 KO mice administered AAV9 encoding luciferase (LUC) or SERCA2A (see Methods for details). **B**, Survival curve for SRSF3 KO mice treated either with AAV9-SERCA2A (dashed line; n=7) or AAV9-LUC as a control (continuous line; n=4). The *x* axis indicates time (days) after the last tamoxifen injection. **C** and **D**, Echocardiography analysis of left ventricular ejection fraction (**C**) and stroke volume (**D**) in mice treated as in **A**. **P*<0.05 for AAV9-SERCA2A vs AAV9-LUC; ###*P*<0.001 for SRSF3 KO vs control; 2-way ANOVA followed by the Bonferroni post-test. AAV9 indicates adeno-associated virus 9; LVEF, left ventricular ejection fraction; SERCA2A, sarcoplasmic/endoplasmic reticulum calcium ATPase 2a; and SV, stroke volume.

SRSF3 Depletion Induces Decapping of Contraction-Related mRNAs

The phosphorylation state of 4E-BP1 determines its interaction with eIF4E (eukaryotic translation initiation factor 4E); hypo-phosphorylation leads to a stronger interaction, inhibiting eIF4E and preventing its binding to mRNA cap structures.[38] Thus, a potential consequence of reduced 4E-BP1 phosphorylation is increased mRNA decapping due to increased accessibility of the mRNA cap. Decapping of an mRNA induces its degradation,[39] and analysis of the decapping status of contraction-related mRNAs in SRSF3 knockout hearts revealed an increase in the proportion of decapped SERCA2A, RyR2, MYBPC3, and MYH7 mRNAs. Although the largest increase was observed at day 5 post tamoxifen administration, increased decapping could be detected as early as day 2 (Figure 7C–7F). These results indicate that the downregulation of contraction-related genes observed after cardiac SRSF3 depletion might be due to an increase in mRNA decapping activity.

To determine whether loss of mTOR activity was responsible for the increased decapping of these genes, we overactivated mTOR in SRSF3 knockout mice by treating them with amino acid injections starting on the second day of tamoxifen administration and for a total of 7 days. As shown in Online Figure IX, mTOR activation reduced decapping of some sarcomeric genes but did not rescue systolic function overall. Together, these results suggest that the loss of mTOR activity is partially responsible for the decapping of at least some sarcomeric genes. However, it is likely that additional mechanisms controlled by SRSF3 are dysregulated in the knockout mice and contribute to their pathological phenotype.

Discussion

In this study, we describe for the first time the role of SRSF3 in the embryonic and adult heart. The expression pattern of SRSF3 in the heart correlates with cell proliferation, with the highest expression levels found in the developing heart. This finding is in line with the suggestion that it functions as a proto-oncogene by promoting cell cycle progression and tumorigenesis.[22] These results are also consistent with the role that SRSF3 plays during early embryo formation and with the embryonic lethality we observed in constitutive cardiac-specific SRSF3 knockout mice, which died in utero, likely due to deficient cardiomyocyte proliferation.

A key finding of our study is that loss of SRSF3 in adult cardiomyocytes leads to decapping and degradation of mRNAs encoding proteins involved in cardiac contractility, resulting in severe systolic dysfunction and death. mRNA decapping has mostly been viewed as a process for RNA recycling once it is no longer useful.[39,40] However, recent studies have begun to link mRNA decapping to disease progression. Specifically, the expression of the decapping protein DCP1A (decapping

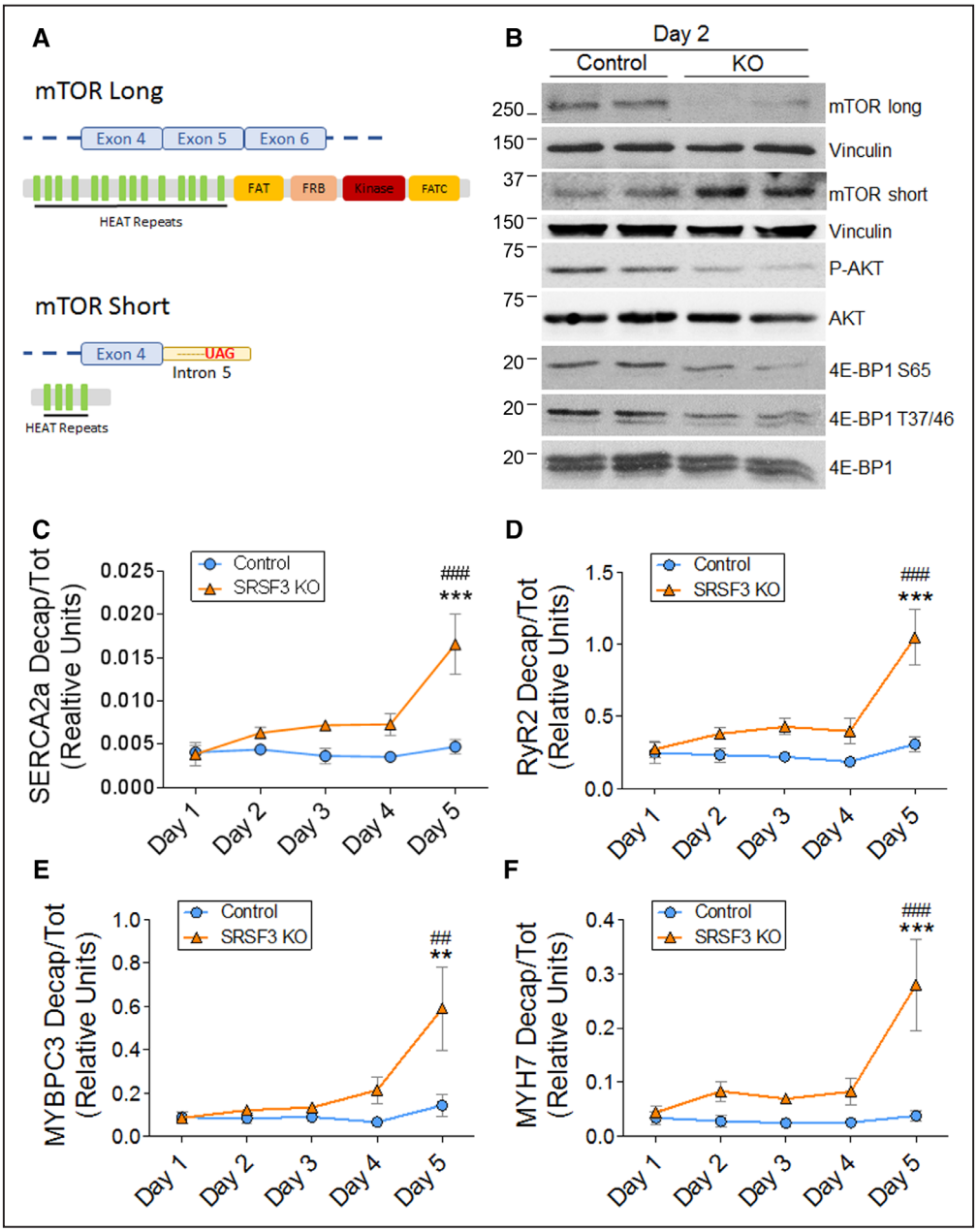

Figure 7. SRSF3 (serine/arginine splicing factor 3) regulates mTOR (mammalian target of rapamycin) splicing, and its depletion induces decapping of contraction-related mRNAs. **A**, mTOR long and short isoforms. **B**, Western blot analysis of mTOR splicing isoforms and the phosphorylation states of AKT and 4E-BP1 in hearts of control and SRSF3 knockout (KO) mice on day 2 post tamoxifen induction. **C–F**, qRT-PCR (polymerase chain reaction) analysis of SERCA2A (**C**), RyR2 (**D**), MYBPC3 (**E**), and MYH7 (**F**) decapped mRNAs in hearts of tamoxifen-induced control and SRSF3 KO mice. Data are normalized to total mRNA expression and are shown as mean±SEM; n=5–9 mice per group. ***P*<0.01 and ****P*<0.001 for SRSF3 KO vs Control; ##*P*<0.01 and ###*P*<0.001 vs day 1; 2-way ANOVA followed by the Bonferroni post-test. 4E-BP1 indicates eIF4E-binding protein 1; eIF4E, eukaryotic translation initiation factor 4E; MYBPC3, myosin-binding protein C3; MYH7, myosin heavy chain 7; RYR2, ryanodine receptor 2; and SERCA2A, sarcoplasmic/endoplasmic reticulum calcium ATPase 2a.

mRNA 1A) has been associated with melanoma progression,[41] and the tumor suppressor PNRC1 (proline-rich nuclear receptor coactivator 1) has been shown to act by recruiting the decapping complex, thus hampering ribosomal RNA maturation.[42] Given that SRSF3 expression is associated with tumor progression,[22,43] it would be interesting to assess if mRNA decapping is affected in cancer types in which SRSF3 is essential for progression; this would provide new insights into tumor progression mechanisms and possible therapeutic targets.

The role of mRNA decapping in heart homeostasis and disease is virtually unknown. Our study provides the first evidence of the importance of decapping deregulation in the adult heart. Overactivation of this process can have fatal consequences for cardiac function, as we observed on SRSF3 depletion. Post-transcriptional regulation plays an important role in heart disease, and several tools have been developed in recent years to modulate this process, most of them based on noncoding RNAs.[44] A recent report showed that an inhibitor of

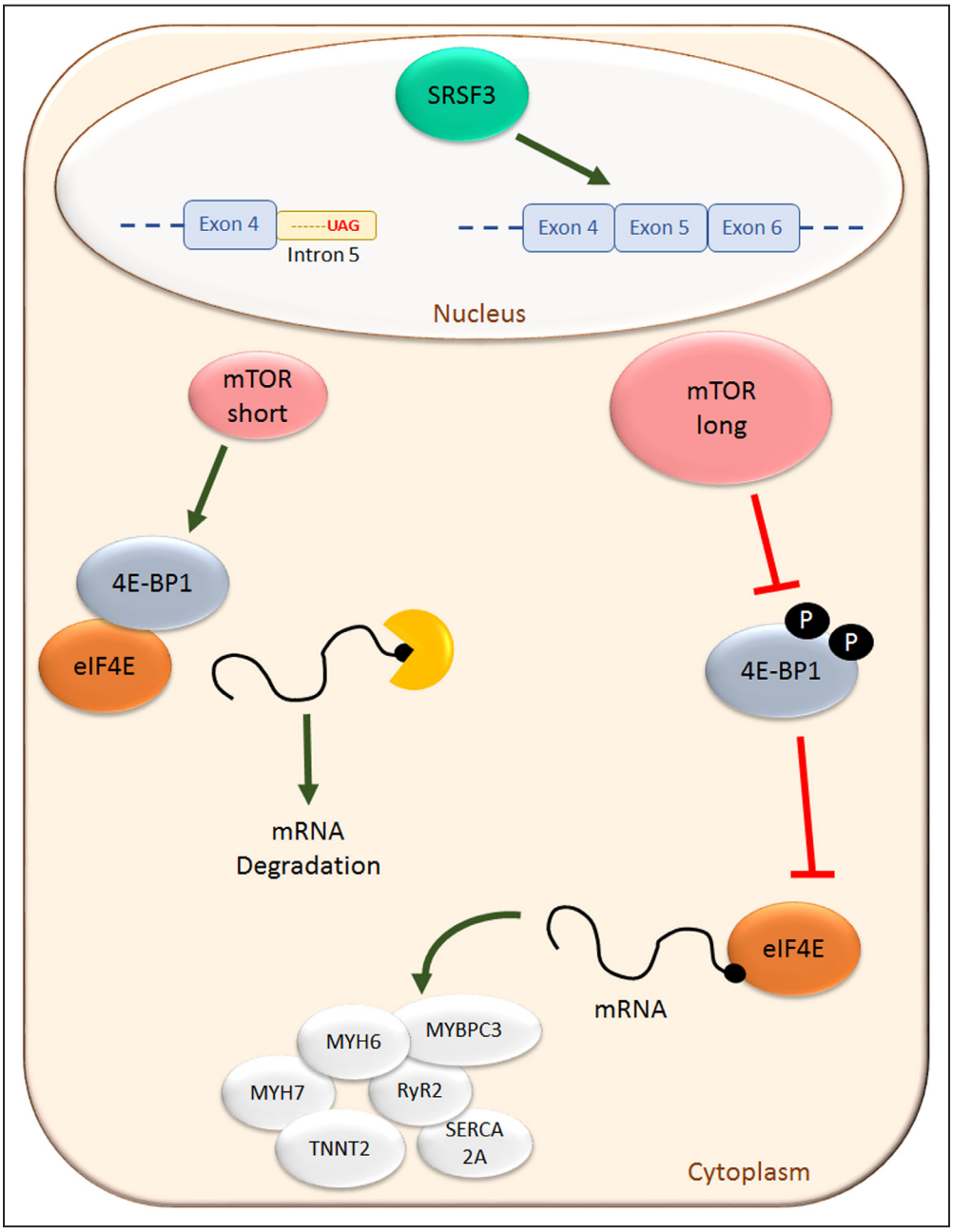

Figure 8. Summary of SRSF3 (serine/arginine splicing factor 3) signaling in cardiomyocytes. SRSF3 regulates mTOR (mammalian target of rapamycin) splicing, promoting synthesis of the long isoform. This isoform phosphorylates 4E-BP1, preventing it from inhibiting interaction of eIF4E with the mRNA caps and the subsequent mRNA translation. In the absence of SRSF3, the short mTOR (mammalian target of rapamycin) isoform prevails, 4E-BP1 phosphorylation is reduced, and mRNA decapping increases, leading to its mRNA degradation. 4E-BP1 indicates eIF4E-binding protein 1; eIF4E, eukaryotic translation initiation factor 4E; MYBPC3, myosin-binding protein C3; MYH6, myosin heavy chain 6; MYH7, myosin heavy chain 7; RYR2, ryanodine receptor 2; and SERCA2A, sarcoplasmic/endoplasmic reticulum calcium ATPase 2a.

the mRNA decapping scavenger enzyme can improve spinal muscular atrophy,[45] suggesting that this mRNA degradation mechanism could become an effective therapeutic target.

The finding that direct binding of SRSF3 to 3′-UTRs has no effect on mRNA stability suggested that SRSF3 likely regulates mRNA degradation indirectly. The function of SRSF3 as a splicing regulator is widely known, and our results confirm this role in the heart. Binding to mTOR mRNA and regulation of its alternative splicing was previously described for the RBP Sam68 during adipogenesis; however, that study did not detect the endogenous short mTOR protein isoform.[46,47] Our results thus provide the first evidence for the protein expression of the endogenous mTOR short isoform, and ours is also the first study to describe this alternative splicing change in heart tissue. Interestingly, a previous iCLIP study also identified mTOR as a direct SRSF3 target in P19 cells.[36] Although this finding was not explored further, taken together with our report, it suggests that SRSF3 may regulate mTOR splicing in several tissues. Moreover, SRSF3 binds a further 210 genes in both P19 cells and cardiomyocytes. These genes are involved

in post-transcriptional mRNA processing and are enriched in nucleic acid binding proteins, suggesting that SRSF3 may regulate these processes in several cell types. In line with our results, loss of mTOR activity has been related to a decrease in 5′-capped mRNA,[48] and mTOR activity in the heart has been reported to be essential for proper cardiac function and survival.[49] However, the phenotype of mTOR knockout mice differs from that of SRSF3 knockout mice. On cardiac mTOR depletion, mice develop dilated cardiomyopathy and survive for several weeks after tamoxifen treatment,[49] whereas in our analysis cardiac SRSF3 depletion led to acute systolic dysfunction and animal death in <8 days after treatment. It is thus likely that SRSF3 knockout animals do not develop dilated cardiomyopathy because there is insufficient time before they die. The phenotype of SRSF3 knockout mice is more aggressive than that of mTOR knockout mice, and hearts lacking SRSF3 expression also undergo many other changes. It is thus possible that the observed phenotype involves contributions from additional molecular processes in which SRSF3 participates, not necessarily through alternative splicing. Alternatively, the mTOR short isoform could act as a dominant negative protein, precluding mTOR proper function and promoting decapping. We also cannot exclude the possibility that the increased decapping and mRNA degradation effects of mTOR deficiency may involve contributions from targets other than 4E-BP1. Furthermore, SRSF3 is involved in other biological processes that could potentially contribute to the severe phenotype observed in knockout mice. SRSF3 controls mRNA nuclear export and translation through a number of different mechanisms, which has an impact on different biological processes, ranging from microglia activation to tumor cell apoptosis.[11,18,50] Although apoptosis and inflammation appear in SRSF3 knockout mice are unlikely to contribute to systolic dysfunction; they may aggravate the animals' condition at late time points.

In conclusion, we have identified SRSF3 as an essential factor for proper heart contraction and animal survival. Loss of SRSF3 in the heart leads to a critical downregulation of contraction-related genes, most probably caused by induction of the decapping process. We have also shown that SRSF3 regulates mTOR alternative splicing and presented the first report of the endogenous mTOR short isoform protein. This alternative splicing change leads to a dephosphorylation of 4E-BP1 that would explain the induction of mRNA decapping (Figure 8). Given that SRSF3 expression is downregulated after MI, we propose both SRSF3 and mRNA decapping as key regulators of cardiac function, paving the way to new therapeutic approaches to treat heart disease.

Acknowledgments

We are grateful to Igor de los Mozos and François McNicoll for assistance with the individual-nucleotide resolution cross-linking and immunoprecipitation experiments and analyses. We thank the CNIC (Centro Nacional de Investigaciones Cardiovasculares) animal facility staff members for mouse work, the Histology Unit for hematoxylin and eosin staining, and the Genomics and Bioinformatics Units for RNA-Seq and analysis.

Sources of Funding

This study was supported by grants from the European Union (CardioNeT-ITN-289600 and CardioNext-ITN-608027 to E. Lara-Pezzi), from the Spanish Ministerio de Economía y Competitividad (RTI2018-096961-B-I00, SAF2015-65722-R, and SAF2012-31451 to E. Lara-Pezzi; BIO2015-67580-P and PGC2018-097019-B-I00 to J. Vázquez), the Spanish Carlos III Institute of Health (CPII14/00027 to E. Lara-Pezzi, RD12/0042/066 to P. García-Pavía and E. Lara-Pezzi, and RD12/0042/0056, PRB2-IPT13/0001-ISCIII-SGEFI/FEDER, ProteoRed to J. Vázquez), the Madrid Regional Government (2010-BMD-2321 Fibroteam to E. Lara-Pezzi). This study was also supported by the Plan Estatal de I+D+I 2013–2016—European Regional Development Fund (ERDF) A way of making Europe, Spain. The CNIC is supported by the Ministerio de Ciencia, Innovación y Universidades (MCNU) and the Pro CNIC Foundation, and is a Severo Ochoa Center of Excellence (SEV-2015-0505).

Disclosures

None.

References

1. WHO. Cardiovascular Diseases (CVDs). 2017.
2. Barth AS, Kumordzie A, Frangakis C, Margulies KB, Cappola TP, Tomaselli GF. Reciprocal transcriptional regulation of metabolic and signaling pathways correlates with disease severity in heart failure. *Circ Cardiovasc Genet*. 2011;4:475–483. doi: 10.1161/CIRCGENETICS.110.957571
3. Corbett AH. Post-transcriptional regulation of gene expression and human disease. *Curr Opin Cell Biol*. 2018;52:96–104. doi: 10.1016/j.ceb.2018.02.011
4. Guo W, Schafer S, Greaser ML, et al. RBM20, a gene for hereditary cardiomyopathy, regulates titin splicing. *Nat Med*. 2012;18:766–773. doi: 10.1038/nm.2693
5. de Bruin RG, Rabelink TJ, van Zonneveld AJ, van der Veer EP. Emerging roles for RNA-binding proteins as effectors and regulators of cardiovascular disease. *Eur Heart J*. 2017;38:1380–1388. doi: 10.1093/eurheartj/ehw567
6. Ding J, Chen J, Wang Y, Kataoka M, Ma L, Zhou P, Hu X, Lin Z, Nie M, Deng ZL, Pu WT, Wang DZ. Trbp regulates heart function through microRNA-mediated Sox6 repression. *Nat Genet*. 2015;47:776–783. doi: 10.1038/ng.3324
7. Wei C, Qiu J, Zhou Y, Xue Y, Hu J, Ouyang K, Banerjee I, Zhang C, Chen B, Li H, Chen J, Song LS, Fu XD. Repression of the central splicing regulator RBFox2 is functionally linked to pressure overload-induced heart failure. *Cell Rep*. 2015;10:1521–1533. doi: 10.1016/j.celrep.2015.02.013
8. Gao C, Ren S, Lee JH, Qiu J, Chapski DJ, Rau CD, Zhou Y, Abdellatif M, Nakano A, Vondriska TM, Xiao X, Fu XD, Chen JN, Wang Y. RBFox1-mediated RNA splicing regulates cardiac hypertrophy and heart failure. *J Clin Invest*. 2016;126:195–206. doi: 10.1172/JCI84015
9. Manley JL, Krainer AR. A rational nomenclature for serine/arginine-rich protein splicing factors (SR proteins). *Genes Dev*. 2010;24:1073–1074. doi: 10.1101/gad.1934910
10. Änkö ML. Regulation of gene expression programmes by serine-arginine rich splicing factors. *Semin Cell Dev Biol*. 2014;32:11–21. doi: 10.1016/j.semcdb.2014.03.011
11. Müller-McNicoll M, Botti V, de Jesus Domingues AM, Brandl H, Schwich OD, Steiner MC, Curk T, Poser I, Zarnack K, Neugebauer KM. SR proteins are NXF1 adaptors that link alternative RNA processing to mRNA export. *Genes Dev*. 2016;30:553–566. doi: 10.1101/gad.276477.115
12. Xu X, Yang D, Ding JH, et al. ASF/SF2-regulated CaMKIIdelta alternative splicing temporally reprograms excitation-contraction coupling in cardiac muscle. *Cell*. 2005;120:59–72. doi: 10.1016/j.cell.2004.11.036
13. Ding JH, Xu X, Yang D, Chu PH, Dalton ND, Ye Z, Yeakley JM, Cheng H, Xiao RP, Ross J, Chen J, Fu XD. Dilated cardiomyopathy caused by tissue-specific ablation of SC35 in the heart. *EMBO J*. 2004;23:885–896. doi: 10.1038/sj.emboj.7600054
14. Feng Y, Valley MT, Lazar J, Yang AL, Bronson RT, Firestein S, Coetzee WA, Manley JL. SRp38 regulates alternative splicing and is required for Ca(2+) handling in the embryonic heart. *Dev Cell*. 2009;16:528–538. doi: 10.1016/j.devcel.2009.02.009
15. Wong J, Garner B, Halliday GM, Kwok JB. Srp20 regulates TrkB pre-mRNA splicing to generate TrkB-Shc transcripts with implications for Alzheimer's disease. *J Neurochem*. 2012;123:159–171. doi: 10.1111/j.1471-4159.2012.07873.x

16. Sen S, Talukdar I, Webster NJ. SRp20 and CUG-BP1 modulate insulin receptor exon 11 alternative splicing. *Mol Cell Biol*. 2009;29:871–880. doi: 10.1128/MCB.01709-08
17. Gonçalves V, Matos P, Jordan P. Antagonistic SR proteins regulate alternative splicing of tumor-related Rac1b downstream of the PI3-kinase and Wnt pathways. *Hum Mol Genet*. 2009;18:3696–3707. doi: 10.1093/hmg/ddp317
18. Kim J, Park RY, Chen JK, Kim J, Jeong S, Ohn T. Splicing factor SRSF3 represses the translation of programmed cell death 4 mRNA by associating with the 5'-UTR region. *Cell Death Differ*. 2014;21:481–490. doi: 10.1038/cdd.2013.171
19. Jumaa H, Wei G, Nielsen PJ. Blastocyst formation is blocked in mouse embryos lacking the splicing factor SRp20. *Curr Biol*. 1999;9:899–902.
20. Sen S, Jumaa H, Webster NJ. Splicing factor SRSF3 is crucial for hepatocyte differentiation and metabolic function. *Nat Commun*. 2013;4:1336. doi: 10.1038/ncomms2342
21. Sen S, Langiewicz M, Jumaa H, Webster NJG. Deletion of splicing factor SRSF3 in hepatocytes predisposes to hepatocellular carcinoma in mice. *Hepatology*. 2015;61:171–183.
22. Jia R, Li C, McCoy JP, Deng CX, Zheng ZM. SRp20 is a proto-oncogene critical for cell proliferation and tumor induction and maintenance. *Int J Biol Sci*. 2010;6:806–826.
23. González-Terán B, López JA, Rodríguez E, Leiva L, Martínez-Martínez S, Bernal JA, Jiménez-Borreguero LJ, Redondo JM, Vázquez J, Sabio G. p38g and d promote heart hypertrophy by targeting the mTOR-inhibitory protein DEPTOR for degradation. *Nat Commun*. 2016;7:10477. doi: 10.1038/ncomms10477
24. Padrón-Barthe L, Villalba-Orero M, Gómez-Salinero JM, Acín-Pérez R, Cogliati S, López-Olañeta M, Ortiz-Sánchez P, Bonzón-Kulichenko E, Vázquez J, García-Pavía P, Rosenthal N, Enríquez JA, Lara-Pezzi E. Activation of serine one-carbon metabolism by calcineurin Aβ1 reduces myocardial hypertrophy and improves ventricular function. *J Am Coll Cardiol*. 2018;71:654–667. doi: 10.1016/j.jacc.2017.11.067
25. Nus M, Martínez-Poveda B, MacGrogan D, Chevre R, D'Amato G, Sbroggio M, Rodríguez C, Martínez-González J, Andrés V, Hidalgo A, de la Pompa JL. Endothelial Jag1-RBPJ signalling promotes inflammatory leucocyte recruitment and atherosclerosis. *Cardiovasc Res*. 2016;112:568–580. doi: 10.1093/cvr/cvw193
26. Bray NL, Pimentel H, Melsted P, Pachter L. Erratum: near-optimal probabilistic RNA-seq quantification. *Nat Biotechnol*. 2016;34:888. doi: 10.1038/nbt0816-888d
27. Pimentel H, Bray NL, Puente S, Melsted P, Pachter L. Differential analysis of RNA-seq incorporating quantification uncertainty. *Nat Methods*. 2017;14:687–690. doi: 10.1038/nmeth.4324
28. Irimia M, Weatheritt RJ, Ellis JD, et al. A highly conserved program of neuronal microexons is misregulated in autistic brains. *Cell*. 2014;159:1511–1523. doi: 10.1016/j.cell.2014.11.035
29. Tapial J, Ha KCH, Sterne-Weiler T, et al. An atlas of alternative splicing profiles and functional associations reveals new regulatory programs and genes that simultaneously express multiple major isoforms. *Genome Res*. 2017;27:1759–1768. doi: 10.1101/gr.220962.117
30. Pelechano V, Wei W, Steinmetz LM. Genome-wide quantification of 5'-phosphorylated mRNA degradation intermediates for analysis of ribosome dynamics. *Nat Protoc*. 2016;11:359–376. doi: 10.1038/nprot.2016.026
31. Jumaa H, Nielsen PJ. The splicing factor SRp20 modifies splicing of its own mRNA and ASF/SF2 antagonizes this regulation. *EMBO J*. 1997;16:5077–5085. doi: 10.1093/emboj/16.16.5077
32. Kawase Y, Hajjar RJ. The cardiac sarcoplasmic/endoplasmic reticulum calcium ATPase: a potent target for cardiovascular diseases. *Nat Clin Pract Cardiovasc Med*. 2008;5:554–565. doi: 10.1038/ncpcardio1301
33. Byrne MJ, Power JM, Preovolos A, Mariani JA, Hajjar RJ, Kaye DM. Recirculating cardiac delivery of AAV2/1SERCA2a improves myocardial function in an experimental model of heart failure in large animals. *Gene Ther*. 2008;15:1550–1557. doi: 10.1038/gt.2008.120
34. del Monte F, Williams E, Lebeche D, Schmidt U, Rosenzweig A, Gwathmey JK, Lewandowski ED, Hajjar RJ. Improvement in survival and cardiac metabolism after gene transfer of sarcoplasmic reticulum Ca(2+)-ATPase in a rat model of heart failure. *Circulation*. 2001;104:1424–1429.
35. Rambout X, Detiffe C, Bruyr J, et al. The transcription factor ERG recruits CCR4-NOT to control mRNA decay and mitotic progression. *Nat Struct Mol Biol*. 2016;23:663–672. doi: 10.1038/nsmb.3243
36. Änkö ML, Müller-McNicoll M, Brandl H, Curk T, Gorup C, Henry I, Ule J, Neugebauer KM. The RNA-binding landscapes of two SR proteins reveal unique functions and binding to diverse RNA classes. *Genome Biol*. 2012;13:R17. doi: 10.1186/gb-2012-13-3-r17
37. Sarbassov DD, Guertin DA, Ali SM, Sabatini DM. Phosphorylation and regulation of Akt/PKB by the rictor-mTOR complex. *Science*. 2005;307:1098–1101. doi: 10.1126/science.1106148
38. Gingras AC, Gygi SP, Raught B, Polakiewicz RD, Abraham RT, Hoekstra MF, Aebersold R, Sonenberg N. Regulation of 4E-BP1 phosphorylation: a novel two-step mechanism. *Genes Dev*. 1999;13:1422–1437. doi: 10.1101/gad.13.11.1422
39. Houseley J, Tollervey D. The many pathways of RNA degradation. *Cell*. 2009;136:763–776. doi: 10.1016/j.cell.2009.01.019
40. Li Y, Kiledjian M. Regulation of mRNA decapping. *Wiley Interdiscip Rev RNA*. 2010;1:253–265. doi: 10.1002/wrna.15
41. Tang Y, Xie C, Zhang Y, Qin Y, Zhang W. Overexpression of mRNA-decapping enzyme 1a predicts disease-specific survival in malignant melanoma. *Melanoma Res*. 2018;28:30–36. doi: 10.1097/CMR.0000000000000406
42. Gaviraghi M, Vivori C, Pareja Sanchez Y, Invernizzi F, Cattaneo A, Santoliquido BM, Frenquelli M, Segalla S, Bachi A, Doglioni C, Pelechano V, Cittaro D, Tonon G. Tumor suppressor PNRC1 blocks rRNA maturation by recruiting the decapping complex to the nucleolus. *EMBO J*. 2018;37:e99179. doi: 10.15252/embj.201899179
43. Chang YL, Hsu YJ, Chen Y, Wang YW, Huang SM. Theophylline exhibits anti-cancer activity via suppressing SRSF3 in cervical and breast cancer cell lines. *Oncotarget*. 2017;8:101461–101474. doi: 10.18632/oncotarget.21464
44. Laina A, Gatsiou A, Georgiopoulos G, Stamatelopoulos K, Stellos K. RNA therapeutics in cardiovascular precision medicine. *Front Physiol*. 2018;9:953. doi: 10.3389/fphys.2018.00953
45. Gopalsamy A, Narayanan A, Liu S, et al. Design of potent mRNA Decapping Scavenger Enzyme (DcpS) inhibitors with improved physicochemical properties to investigate the mechanism of therapeutic benefit in Spinal Muscular Atrophy (SMA). *J Med Chem*. 2017;60:3094–3108. doi: 10.1021/acs.jmedchem.7b00124
46. Huot MÉ, Vogel G, Zabarauskas A, Ngo CT, Coulombe-Huntington J, Majewski J, Richard S. The Sam68 STAR RNA-binding protein regulates mTOR alternative splicing during adipogenesis. *Mol Cell*. 2012;46:187–199. doi: 10.1016/j.molcel.2012.02.007
47. Wang H, Chen Y, Lu XA, Liu G, Fu Y, Luo Y. Endostatin prevents dietary-induced obesity by inhibiting adipogenesis and angiogenesis. *Diabetes*. 2015;64:2442–2456. doi: 10.2337/db14-0528
48. Rahman H, Qasim M, Oellerich M, Asif AR. Crosstalk between Edc4 and mammalian target of rapamycin complex 1 (mTORC1) signaling in mRNA decapping. *Int J Mol Sci*. 2014;15:23179–23195. doi: 10.3390/ijms151223179
49. Zhang D, Contu R, Latronico MV, et al. MTORC1 regulates cardiac function and myocyte survival through 4E-BP1 inhibition in mice. *J Clin Invest*. 2010;120:2805–2816. doi: 10.1172/JCI43008
50. Boutej H, Rahimian R, Thammisetty SS, Béland LC, Lalancette-Hébert M, Kriz J. Diverging mRNA and protein networks in activated microglia reveal SRSF3 suppresses translation of highly upregulated innate immune transcripts. *Cell Rep*. 2017;21:3220–3233. doi: 10.1016/j.celrep.2017.11.058

Article

Cell Chemical Biology

The Calcineurin Variant CnAβ1 Controls Mouse Embryonic Stem Cell Differentiation by Directing mTORC2 Membrane Localization and Activation

Graphical Abstract

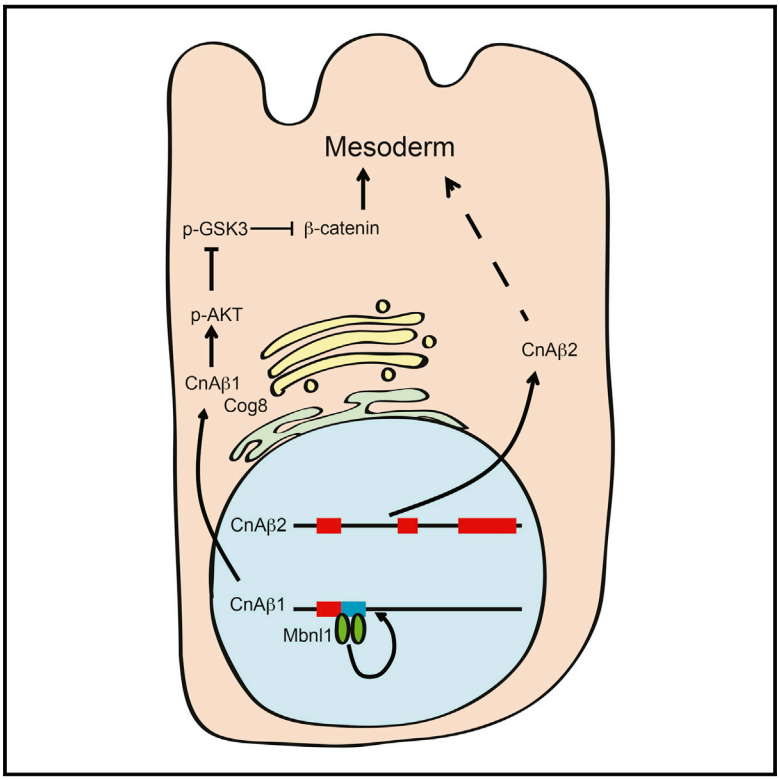

Highlights

- CnAβ1 is mainly localized at the Golgi apparatus through its C-terminal domain
- CnAβ1 is needed for mTORC2 localization and activation at the cellular membranes
- CnAβ1 is necessary for activation of the AKT/GSK3β/β-catenin signaling pathway
- CnAβ1 regulates differentiation of mouse embryonic stem cells to mesoderm

Authors

Jesús M. Gómez-Salinero, Marina M. López-Olañeta, Paula Ortiz-Sánchez, ..., Giovanna Giovinazo, Gene W. Yeo, Enrique Lara-Pezzi

Correspondence

elara@cnic.es

In Brief

Gómez-Salinero et al. show that the calcineurin splicing variant CnAβ1 is enriched in mouse embryonic stem cells and regulates their differentiation to mesoderm. CnAβ1's unique C-terminal domain drives its localization to the Golgi apparatus and is necessary for its interaction with mTOR and activation of the AKT/GSK3β/β-catenin pathway.

Accession Numbers

GSE72103

Gómez-Salinero et al., 2016, Cell Chemical Biology *23*, 1372–1382
November 17, 2016
http://dx.doi.org/10.1016/j.chembiol.2016.09.010

Please cite this article as: Gómez-Salinero et al., The Calcineurin Variant CnAβ1 Controls Mouse Embryonic Stem Cell Differentiation by Directing mTORC2 Membrane Localization and Activation, Cell Chemical Biology (2016), http://dx.doi.org/10.1016/j.chembiol.2016.09.010

The Calcineurin Variant CnAβ1 Controls Mouse Embryonic Stem Cell Differentiation by Directing mTORC2 Membrane Localization and Activation

Jesús M. Gómez-Salinero,[1] Marina M. López-Olañeta,[1] Paula Ortiz-Sánchez,[1] Javier Larrasa-Alonso,[1] Alberto Gatto,[1] Leanne E. Felkin,[2] Paul J.R. Barton,[2,3] Inmaculada Navarro-Lérida,[4] Miguel Ángel del Pozo,[4] Pablo García-Pavía,[5] Balaji Sundararaman,[6] Giovanna Giovinazo,[7] Gene W. Yeo,[6] and Enrique Lara-Pezzi[1,2,8,*]

[1]Myocardial Pathophysiology Program, Fundación Centro Nacional de Investigaciones Cardiovasculares Carlos III (CNIC), 28029 Madrid, Spain
[2]National Heart and Lung Institute, Imperial College London, London SW7 2AZ, UK
[3]NIHR Cardiovascular Biomedical Research Unit, Royal Brompton and Harefield NHS Foundation Trust, London SW7 2AZ, UK
[4]Vascular Pathophysiology Program, Fundación Centro Nacional de Investigaciones Cardiovasculares Carlos III (CNIC), 28029 Madrid, Spain
[5]Heart Failure and Inherited Cardiac Diseases Unit, Department of Cardiology, Hospital Universitario Puerta de Hierro Majadahonda, 28222 Madrid, Spain
[6]Sanford Consortium for Regenerative Medicine, University of California San Diego (UCSD), La Jolla, CA 92037, USA
[7]Pluripotent Cell Technology Unit, Fundación Centro Nacional de Investigaciones Cardiovasculares Carlos III (CNIC), 28029 Madrid, Spain
[8]Lead Contact
*Correspondence: elara@cnic.es
http://dx.doi.org/10.1016/j.chembiol.2016.09.010

SUMMARY

Embryonic stem cells (ESC) have the potential to generate all the cell lineages that form the body. However, the molecular mechanisms underlying ESC differentiation and especially the role of alternative splicing in this process remain poorly understood. Here, we show that the alternative splicing regulator MBNL1 promotes generation of the atypical calcineurin Aβ variant CnAβ1 in mouse ESCs (mESC). CnAβ1 has a unique C-terminal domain that drives its localization mainly to the Golgi apparatus by interacting with Cog8. CnAβ1 regulates the intracellular localization and activation of the mTORC2 complex. CnAβ1 knockdown results in delocalization of mTORC2 from the membrane to the cytoplasm, inactivation of the AKT/GSK3β/β-catenin signaling pathway, and defective mesoderm specification. In summary, here we unveil the structural basis for the mechanism of action of CnAβ1 and its role in the differentiation of mESCs to the mesodermal lineage.

INTRODUCTION

Embryonic stem cells (ESCs) have the ability to proliferate indefinitely in culture and to differentiate into all embryonic lineages. Although the transcriptional program that coordinates pluripotency has been progressively unveiled during the past few years (Hackett and Surani, 2014; Kumar et al., 2014), the signaling pathways that regulate early differentiation events are not completely understood.

Calcineurin (Cn) is a calcium/calmodulin-dependent serine/threonine phosphatase composed of two subunits: a catalytic A subunit (CnA) and a regulatory B subunit (CnB) (Li et al., 2011a). Activation of CnA catalytic activity is mediated by CnB and calmodulin in response to an increase in intracellular calcium. Three *CnA* genes have been described in higher vertebrates: CnAalpha (CnAα) and CnAbeta (CnAβ), which are ubiquitously expressed, and CnAgamma (CnAγ), which is confined to brain and testis. All CnA isoforms share the same functional domains, including a catalytic domain, a CnB-interacting domain, a calmodulin-binding region, and an autoinhibitory domain that maintains the enzyme in an inactive conformation in the absence of calcium. Interestingly, an alternative splicing variant of CnAβ has been described that lacks the autoinhibitory domain present in all other naturally occurring Cn isoforms (Guerini and Klee, 1989; Lara-Pezzi et al., 2007). This alternatively spliced CnAβ isoform was termed CnAβ1, as opposed to the predominant CnAβ2 isoform, and is the result of the retention of intron 12–13, which gives rise to a unique C-terminal domain not present in any other known protein (Figure 1A). Unlike other Cn isoforms, CnAβ1 has no impact on NFAT-regulated genes and instead activates the AKT signaling pathway through its interaction with the mTORC2 complex, which phosphorylates AKT in S473 (Felkin et al., 2011; López-Olañeta et al., 2014). In myoblasts, CnAβ1 prevents differentiation by activating AKT (Lara-Pezzi et al., 2007), whose activation has also been reported to regulate both ESC pluripotency and differentiation (Naito et al., 2005; Watanabe et al., 2006). CnAβ1 is strongly expressed in regenerating tissues and progenitor cells (Lara-Pezzi et al., 2007), however its role in ESCs and its mechanism of action are unknown.

RESULTS

CnAβ1 Is Necessary for Mesoderm Differentiation

We observed that the expression of CnAβ1 is significantly increased in mouse embryonic stem cells (mESCs) compared

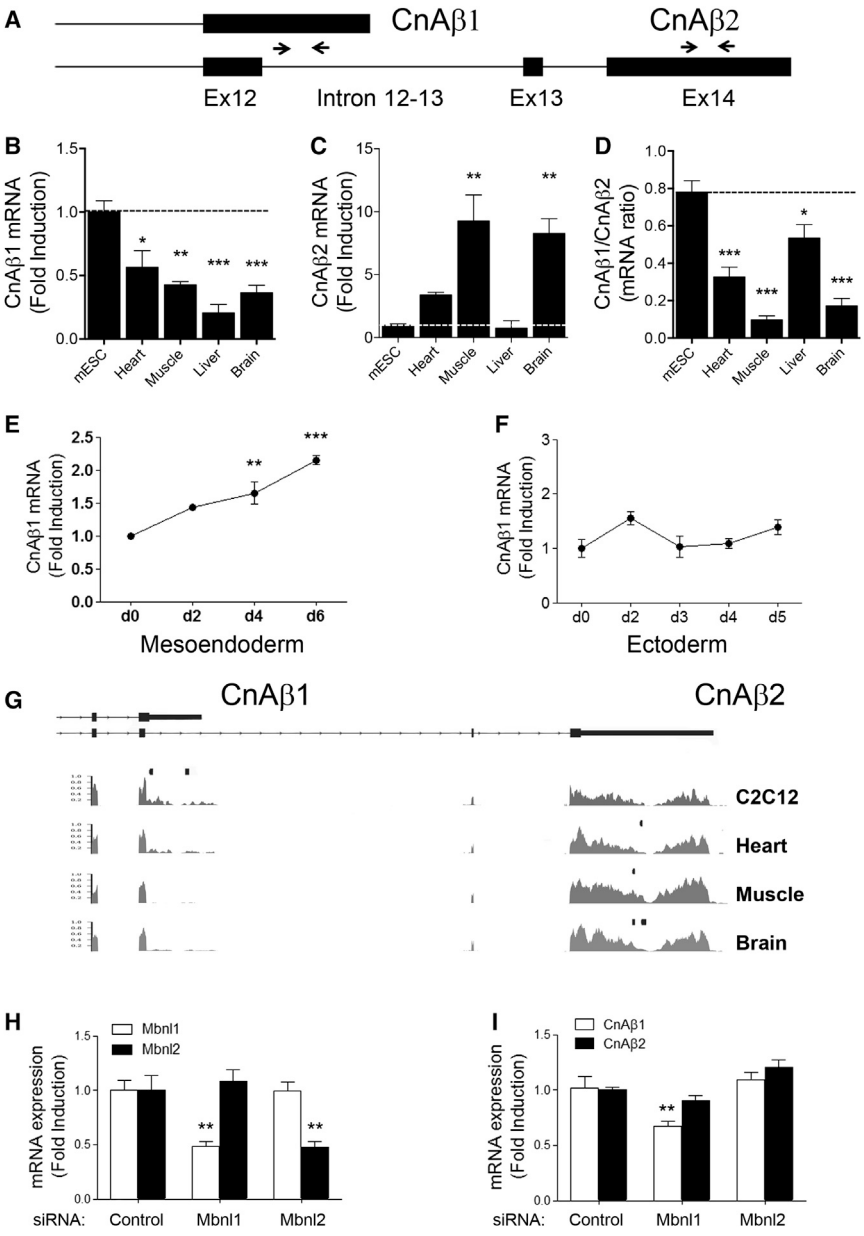

Figure 1. CnAβ1 Expression Is High in mESCs and Is Regulated by the Splicing Factor MBNL1

(A) Schematic representation of the C-terminal region of CnAβ1 and CnAβ2. Arrows indicate the position of the primers used to analyze expression of each isoform.

(B–D) CnAβ1 and CnAβ2 mRNA expression was quantified in mESCs and mouse adult tissues by qRT-PCR and normalized to the expression levels of CnAβ exons 2–3. Data are presented as fold induction over the relative expression of each isoform in mESCs (B and C) or as the ratio of CnAβ1 over CnAβ2 (D).

(E and F) CnAβ1 expression was analyzed by qRT-PCR in mESCs differentiated to mesoendoderm or ectoderm using an EB formation assay.

(G) Fold CnAβ1 and CnAβ2 mRNA expression and MBNL1 binding sites in their 3′ UTRs (small black boxes) were determined by RNA-seq and CLIP-seq, respectively, in C2C12 myoblasts, adult mouse heart, muscle, and brain (GEO: GSE39911).

(H) MBNL1 and MBNL2 expression was analyzed 48 hr after transfection with siRNAs for each isoform in mESCs differentiated to mesoderm.

(I) mESCs were transfected with MBNL siRNAs as in (H), and CnAβ1 and CnAβ2 expression was determined 48 hr after transfection by qRT-PCR. Results are presented as fold induction ± SEM over the values obtained with the control siRNA.

*$p < 0.05$, **$p < 0.01$, ***$p < 0.001$, one-way ANOVA with Dunnett's post-test (A–F) or two-way ANOVA with Bonferroni post-test (H and I), n = 3 for all experiments.

with adult differentiated tissues, whereas CnAβ2 shows an opposite expression pattern (Figures 1B–1D). To investigate the role of CnAβ1 in mESCs, we downregulated CnAβ1 expression with two specific small interfering RNAs (siRNAs) that have no effect on the expression of other CnA isoforms (Figures S1A–S1F). Microarray analysis showed no effect of CnAβ1 knockdown on mESCs in pluripotent conditions, with no gene function significantly affected 48 hr after siRNA transfection (Table S1). These results were validated by RT-PCR analysis, which showed no change in the expression of the pluripotency-related genes Oct3/4, Klf4, Sox2, Gbx2, and Stela (Figures S1G–S1K), suggesting that CnAβ1 is not necessary for the maintenance of pluripotent conditions in mESCs.

We next analyzed the expression of the different CnA isoforms during mESC differentiation. Interestingly, we found that CnAβ1 expression was significantly upregulated during early differentiation to mesoendoderm but not to ectoderm (Figures 1E and 1F), whereas expression of CnAβ2 was increased during differentiation to both lineages (Figures S2A and S2B). It has been recently described that muscle-blind-like (MBNL) proteins are major splicing regulators in ESCs that repress pluripotency and promote differentiation (Han et al., 2013). To investigate the potential regulation of CnAβ splicing by MBNL1, we first explored available cross-linking immunoprecipitation sequencing (CLIP-seq) datasets for this trans-regulatory factor obtained from myoblasts and differentiated tissues (Wang et al., 2012). These datasets have been previously used to identify MBNL1 targets shared between C2C12 and mESCs (Han et al., 2013). We identified two MBNL1 binding sites in CnAβ's intron 12–13 in C2C12 myoblasts that were absent in adult differentiated tissues (Figure 1G). The presence of MBNL1 binding marks in C2C12 cells correlates with CnAβ1 expression, which is higher in myoblasts than in fully differentiated tissues (Lara-Pezzi et al., 2007). To determine the role of MBNL proteins in the regulation of CnAβ1 in mESCs, we downregulated both MBNL1 and MBNL2 using previously reported siRNAs (Han et al., 2013) (Figure 1G). MBNL1 knockdown resulted in a significant downregulation of CnAβ1 expression

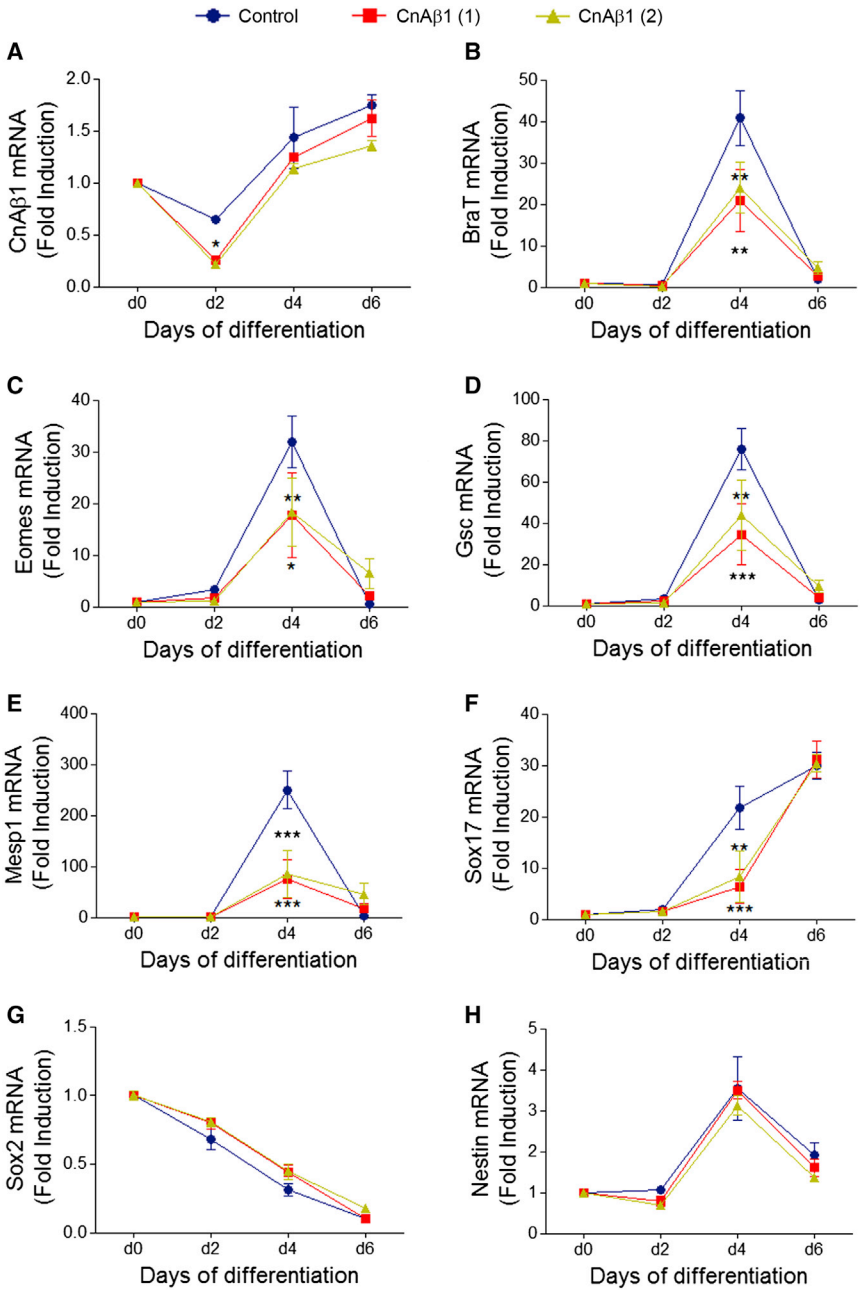

Figure 2. CnAβ1 Knockdown Inhibits Meso-endoderm Differentiation

mESCs were transiently transfected with two different siRNAs for CnAβ1 or a control siRNA and differentiated for 6 days toward mesoderm by using EBs.

(A–H) RNA was extracted at different days of differentiation, and CnAβ1, BraT, Eomes, Gsc, Mesp1, Sox17, Sox2, and Nestin expression was analyzed by qRT-PCR. Results are expressed as fold induction ± SEM over the values for undifferentiated stem cells. *p < 0.05, **p < 0.01, ***p < 0.001, two-way ANOVA with Bonferroni post-test, n = 3.

without altering CnAβ2 levels, whereas MBNL2 knockdown had no effect on either calcineurin isoform (Figures 1H and 1I), suggesting that MBNL1 regulates CnAβ1 expression.

To study the role of CnAβ1 in early mESC differentiation, we transfected mESCs with CnAβ1 siRNAs and induced them to differentiate to mesoderm by using embryoid bodies (EBs). Microarray analysis 48 hr after transfection showed selective downregulation of several genes involved in mesoderm specification (Figure S3A; Tables S2 and S3), which was confirmed by qRT-PCR (Figure S3B). To further investigate the role of CnAβ1 in this process, we allowed the cells to differentiate for 2, 4, and 6 days after CnAβ1 siRNA transfection. We observed that CnAβ1 was significantly downregulated at day 2 post transfection and recovered normal levels by day 4 following siRNA clearance (Figure 2A). In agreement with our microarray results, we found significant downregulation of the mesoendoderm specification markers BraT, Gsc, Eomes, Mesp1, and Sox17 at day 4 of differentiation in the CnAβ1 siRNA group (Figures 2B–2F) that was already evident at day 2. We found no differences in the expression of the pluripotent gene Sox2 and the neuroectoderm differentiation marker Nestin (Figures 2G and 2H).

To determine whether the defective mESC differentiation observed in the presence of CnAβ1 siRNAs could be a consequence of reduced proliferation, we grew the cells in the presence of BrdU for 4 hr, starting 44 hr after siRNA transfection. As shown in Figure S3C, we found no significant differences in BrdU incorporation between control and CnAβ1 knockdown, suggesting that the defect in differentiation was not due to lack of proliferation.

CnAβ1 Regulates Mesoderm Specification through AKT, GSK3, and β-Catenin

We have previously shown that CnAβ1 regulates AKT phosphorylation (Felkin et al., 2011; López-Olañeta et al., 2014). To investigate whether CnAβ1 is controlling this pathway during mESC differentiation, we knocked down CnAβ1 and induced the mESCs to differentiate to mesoderm. Western blot analysis showed decreased phosphorylation of AKT in the samples treated with CnAβ1 siRNAs (Figures 3A and 3B), indicating reduced AKT activation. AKT has been reported to regulate mesoderm differentiation by phosphorylating and inhibiting GSK3β, which is involved in the sequestration and degradation of β-catenin (Naito et al., 2005). We found that GSK3β phosphorylation was reduced after CnAβ1 knockdown, indicating increased GSK3β activation and leading to decreased β-catenin levels. This reduction in β-catenin expression was accompanied by a decrease

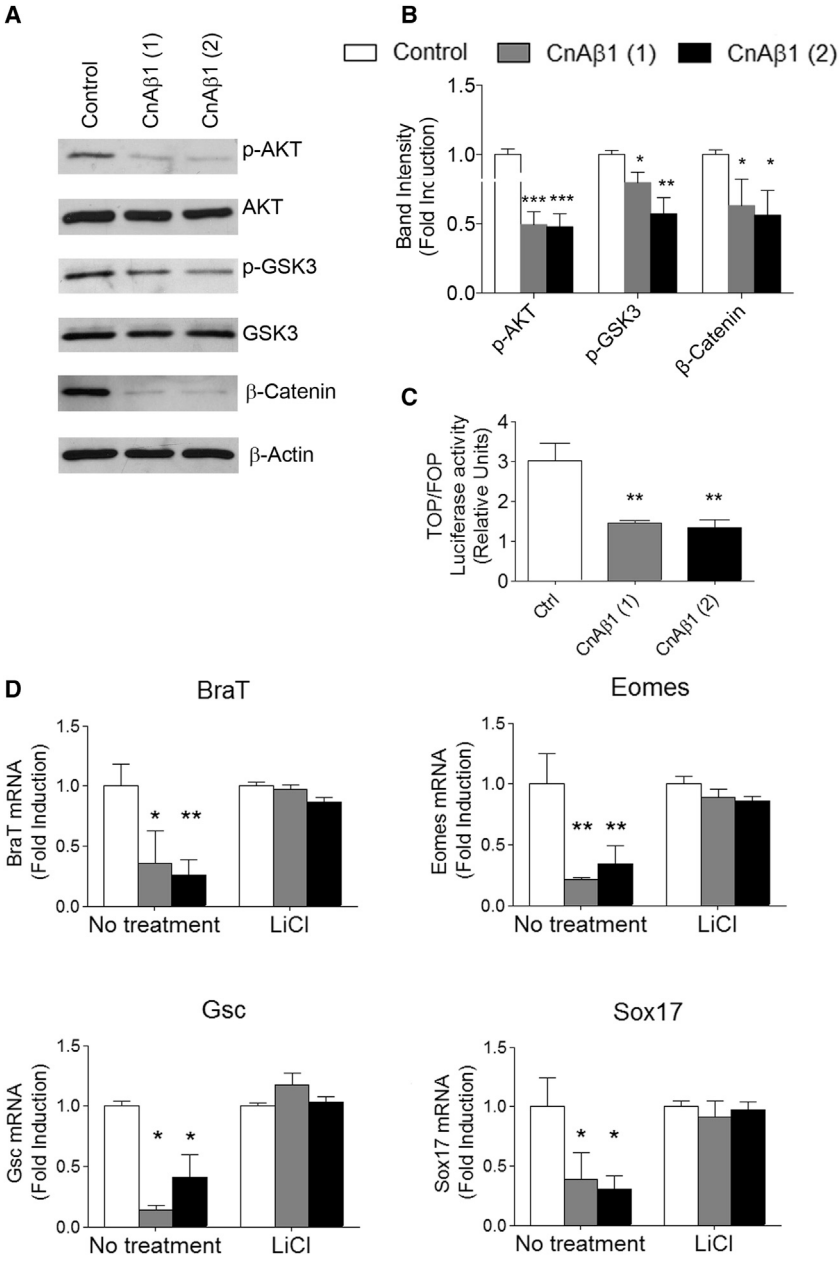

Figure 3. CnAβ1 Regulates the Differentiation of mESC to Mesoendoderm through β-Catenin

(A) mESCs were transfected with CnAβ1 siRNAs and p-AKT S473, total AKT, p-GSK3β S9, total GSK3β, β-catenin, and β-actin were analyzed by western blot at day 2 of differentiation. Molecular weights are indicated in kDa.

(B) The signal intensity of p-AKT/total AKT, p-GSK3β/total GSK3β, and β-catenin in the western blots was quantified and presented as fold induction ± SEM over the values of the control siRNA.

(C) mESCs were transfected as in (A) along with a reporter vector in which luciferase expression is under the control of a multimer of TCF binding sites in tandem (TOP) or the same multimer with the TCF binding sites mutated (FOP). Results are expressed as the ratio ± SEM of TOP/FOP for each condition after normalization for transfection efficiency with Renilla luciferase.

(D) mESC cells were transiently transfected with CnAβ1 siRNAs and differentiated through EBs toward mesoderm. Cells were treated for 8 hr with 20 mM LiCl at day 2 to inhibit GSK3. The expression of BraT, Eomes, Gsc, and Sox17 was analyzed at day 4. Results are presented as fold induction ± SEM over the values of the control siRNA from each condition.

*p < 0.05, **p < 0.01, ***p < 0.005, one-way ANOVA with Dunnett's post-test, n = 3 (B, C). *p < 0.05 **p < 0.01, two-way ANOVA with Bonferroni post-test, n = 3 (D).

in β-catenin-dependent transcription in cells transfected with CnAβ1 siRNAs and a luciferase reporter vector carrying a multimer of a TCF binding motif that is activated by β-catenin (TOP-Luc; Figure 3C).

To confirm the role of GSK3 in the reduction of mESC differentiation caused by CnAβ1 siRNAs, we inhibited GSK3 activity by treating cells with LiCl for 8 hr starting on the second day of differentiation. We allowed differentiation to proceed until day 4 and analyzed the expression of several mesoendoderm differentiation markers. As previously observed, CnAβ1 inhibition resulted in the downregulation of mesoendoderm genes at day 4 of differentiation (Figure 3D). Interestingly, this effect was prevented when GSK3 was inhibited with LiCl. Together, our results unveil an important role of CnAβ1 in early mesoendoderm specification by the control of the AKT/GSK3/β-catenin axis.

It has been previously described that the regulatory subunit of Cn (CnB) is required for the proper differentiation of mESCs through the activation of NFAT (Li et al., 2011b). To confirm that activation of the AKT pathway is specific to the CnAβ1 isoform, we investigated the role of CnAβ2 during differentiation. As expected, CnAβ2 knockdown resulted in decreased expression of mESC differentiation makers (Figures S4A–S4H). However, unlike with CnAβ1, this effect seemed independent of the AKT/GSK3/β-catenin pathway, which was not affected by CnAβ2 siRNA treatment (Figures S5A and S5B). Furthermore, chemical inhibition of the catalytic activity of all CnA isoforms using cyclosporin A (CsA) resulted in reduced mesodermal differentiation of mESCs with no effects on the AKT pathway (Figures S5C–S5E).

CnAβ1 and CnAβ2 Have a Distinct Intracellular Distribution

Previous reports have suggested that activation of Akt by mTOR occurs in the cell membranes (Zhao et al., 2015). However, it is not entirely clear how this signaling pathway is activated and, more specifically, how it is triggered by CnAβ1. To determine whether

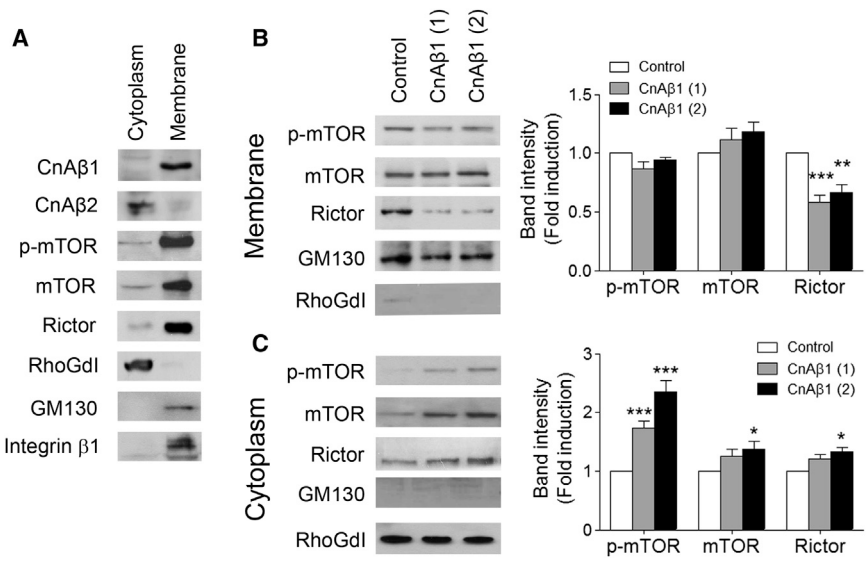

Figure 4. CnAβ1 Regulates mTORC2 Localization and Activation at Cellular Membranes

(A) mESCs were lysed using a homogenizer and separated into membrane and cytoplasm fractions. The localization of CnAβ1, CnAβ2, the mTORC2 components P-mTOR 2481, mTOR, and Rictor, the cytoplasmic marker RhoGdI, and membrane markers GM130 and integrin β1 were analyzed by western blot.

(B and C) mESCs were transiently transfected with CnAβ1 siRNAs and differentiated to mesoderm. Forty-eight hours after siRNA transfection, cells were lysed and homogenized to purify membrane (B) and cytoplasmic (C) fractions. The presence of CnAβ1, p-mTOR 2481, and Rictor was determined by western blot and normalized to the levels of the membrane and cytoplasmic markers GM130 and RhoGdI, respectively. Blots from three independent experiments were quantified, and the average signal was expressed as fold induction ± SEM. *p < 0.05, **p < 0.01, ***p < 0.001 two-way ANOVA with Bonferroni's post-test.

the intracellular distribution of CnAβ1 coincided with that of mTOR, we purified enriched fractions of cytoplasm and membrane extracts from mESCs and analyzed the distribution of CnAβ1 and CnAβ2. Surprisingly, we found CnAβ1 enriched in the membrane fraction together with membrane-bound proteins such as integrin β1 and GM130 (Figure 4A), whereas CnAβ2 was mainly present in the cytoplasm. The mTORC2 components Rictor and mTOR were also enriched in the membrane fraction, as was the auto-phosphorylated form of mTOR at S2481, associated with activation of the mTORC2 complex (Copp et al., 2009).

To investigate whether CnAβ1 was necessary for activation of the mTORC2 complex, we analyzed the distribution of mTOR and Rictor after knocking down CnAβ1. Interestingly, we found that CnAβ1 downregulation resulted in partial delocalization of phospho-mTOR and Rictor from the membranes to the cytoplasm fraction (Figures 4B and 4C). These results suggest that CnAβ1 is necessary for mTORC2 localization and activation at the membranes.

The C-Terminal Region in CnAβ1 Drives Its Localization to Intracellular Membranes

The role and structural characteristics of CnAβ1's C-terminal unique domain are not completely understood. We used Psipred to predict its secondary structure and found that CnAβ1's C-terminal domain contains two different α helixes corresponding to two highly conserved motifs that may confer CnAβ1 distinct biological properties (Figures S6A and S6B).

To determine the role of the C-terminal domain and its two α helices, we produced chimeras of different regions of CnAβ1 or CnAβ2 fused to EGFP. We transfected the different constructs into P19 cells and found a completely different localization of CnAβ1 and CnAβ2 within the cell. Whereas CnAβ2 was homogeneously distributed throughout the cytoplasm, CnAβ1 was mainly localized in the Golgi apparatus, as shown by colocalization with the *cis*-Golgi marker GM130 (Figure 5A). This localization was reproduced by a chimera carrying just the C-terminal domain of CnAβ1 linked to GFP, but not by one bearing the autoinhibitory domain of CnAβ2. To determine whether this specific localization is driven by any of the two α helices in the C-terminal domain of CnAβ1, we linked each α helix to GFP separately. We observed that the localization in the Golgi apparatus was only maintained in the chimera bearing the second α helix. Changes in the subcellular localization of each construct were quantified and shown as a percentage of cells with localization in the Golgi apparatus (Figure 5D). These results support the existence of two different evolutionarily conserved α helices with distinct properties in the C-terminal domain of CnAβ1.

Interestingly, we found a short amino acid sequence (ACREFLL) in the second α helix that is similar to a motif (AIREFLF) present in an mTOR domain that directs its localization to the Golgi apparatus (Liu and Zheng, 2007). To determine the role of this motif in CnAβ1, we substituted these amino acids with others of a similar group and size (VSKDLFF) in the GFP-CnAβ1 construct (CnAβ1-mut). Transfection of p19 cells with this construct showed a disperse CnAβ1-mut localization and low colocalization with GM130, compared with the wild-type CnAβ1 construct (Figures 5B and 5C). Importantly, mTOR co-precipitated with GFP-CnAβ1, whereas it failed to interact with GFP-CnAβ1-mut (Figure 5E), suggesting that CnAβ1's C-terminal domain defines both its localization and its interaction partners.

Cog8 Drives the Localization of CnAβ1 to the Golgi apparatus

To gain further insight into the mechanisms driving this localization, we carried out a yeast two-hybrid screening. In addition to known CnA-interacting proteins such as CnB (Felkin et al., 2011), we identified the interaction between CnAβ1 and Cog8, a protein enriched mainly in the external Golgi as well as other intracellular membranes that is involved in the interaction with the Cog and SNARE complexes (Laufman et al., 2013; Willett et al., 2013, 2014) (Table S4). To validate this interaction, we transfected cells with GFP-CnAβ1 chimeras and carried out immunoprecipitation and colocalization experiments. As shown in Figure 6A, Cog8 co-precipitated with GFP-CnAβ1 but not with GFP-CnAβ1-mut. In addition, GFP-CnAβ1 showed a strong colocalization with Cog8 in P19 cells (Figure 6B). To determine

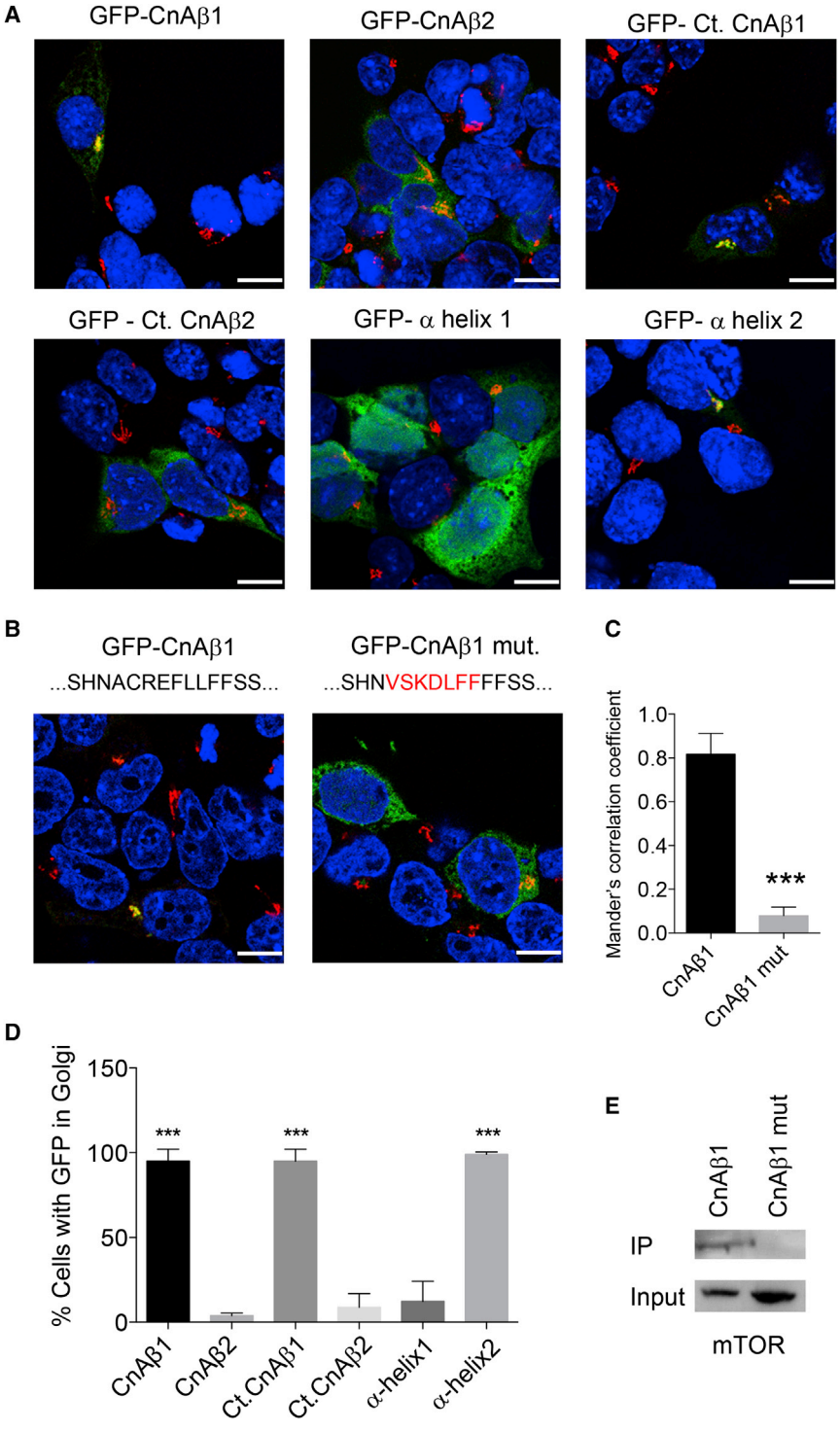

Figure 5. CnAβ1 Colocalizes with the Golgi Apparatus Using an Evolutionarily Conserved α Helix in Its C-Terminal Domain

(A) P19 cells were transfected with an expression vector carrying an EGFP chimera linked to full-length CnAβ1 or CnAβ2 proteins, the C-terminal regions of CnAβ1 or CnAβ2, or each of the two α helices in the CnAβ1 C-terminal region. Colocalization of all the constructs with the Golgi marker GM130 (red) was analyzed by immunofluorescence. Bar, 10 μm.

(B) P19 cells were transfected with a GFP chimera linked to full-length CnAβ1 or CnAβ1-mut protein and colocalization with the Golgi marker GM130 (red) was analyzed by immunofluorescence. The mutated amino acids in the CnAβ1-mut construct are indicated in red. Bar, 10 μm.

(C) Manders' colocalization coefficient analysis of the green channel over the red channel for both constructs in (B) was carried out using Jacob's plugin from ImageJ. ***$p < 0.005$, unpaired t test, $n = 3$.

(D) The percentage of cells with GFP localization in the Golgi apparatus was quantified. At least 100 cells were counted for each condition. ***$p < 0.005$, one-way ANOVA plus Bonferroni post-test, $n = 3$.

(E) 293T cells were transfected with expression vectors for GFP-CnAβ1 or GFP-CnAβ1-mut. Cells were lysed and GFP chimeras were immunoprecipitated (IP) with anti-GFP. Co-immunoprecipitation of mTOR was determined by western blot using anti-mTOR. Similar expression of mTOR in both conditions is shown in total lysates for reference.

whether this interaction is necessary for the localization of CnAβ1 in the Golgi, Cog8 was downregulated by transfecting two independent siRNAs into P19 cells together with the GFP-CnAβ1 chimera (Figures 6C–6E). We observed that GFP-CnAβ1 was delocalized from the Golgi after Cog8 knockdown, confirming that the interaction with Cog8 is necessary for the subcellular localization of CnAβ1.

To characterize the function of Cog8 in mESC differentiation, we downregulated its expression and analyzed different mesodermal expression markers after early differentiation. Although Cog8 siRNAs were only functional during the first 48 hr (Figure 7A), we found a significant downregulation of the mesodermal differentiation markers BraT, Gsc, and Eomes at day 4 (Figures 7B–7D), in agreement with the results obtained after CnAβ1 knockdown.

DISCUSSION

Here we provide insight into the mechanism of action of the calcineurin A beta splicing variant CnAβ1 and its role in mESC differentiation. Our results show that a novel motif in the alternative C-terminal domain of CnAβ1 drives its localization to the Golgi apparatus, where it serves as a scaffold for activation of the mTOR/AKT signaling pathway. Activation of this pathway is unique to this CnA isoform, since cyclosporin treatment or CnAβ2 downregulation did not have any effect on it.

Activation of the AKT pathway is thought to involve prior autophosphorylation of mTOR at S2481 within the mTORC2 complex

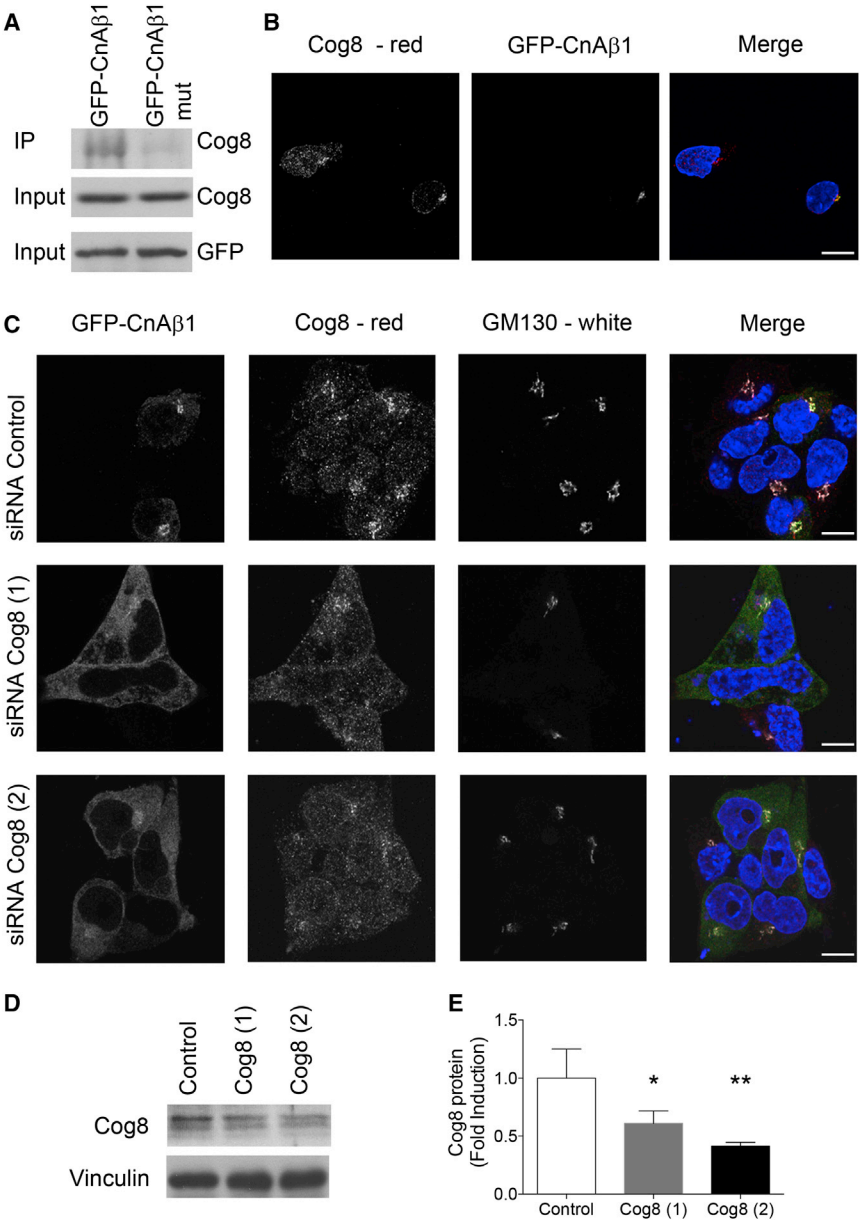

Figure 6. Cog8 Interacts with CnAβ1 and Mediates Its Localization in the Golgi Apparatus

(A) P19 cells were transfected with expression vectors for GFP-CnAβ1 or GFP-CnAβ1-mut. Cells were lysed and GFP chimeras were immunoprecipitated (IP) with anti-GFP. Co-immunoprecipitation of Cog8 was determined by western blot using anti-Cog8. Equal expression of Cog8 in both conditions is shown in total lysates for reference.

(B) P19 cells were transfected with an expression vector for GFP-CnAβ1. Colocalization with Cog8 (red) was analyzed by immunofluorescence. Nuclei were counterstained with DAPI (blue). Bar, 10 μm.

(C) P19 cells were transfected with control or Cog8 siRNAs together with a GFP-CnAβ1 expression vector. Localization of GFP-CnAβ1 (green), Cog8 (red), GM130 (white) was determined by immunofluorescence. Bar 10 μm.

(D and E) The downregulation of COG8 protein after siRNA transfection was confirmed by western blot (D) and quantified (E). *$p < 0.05$, **$p < 0.01$, one-way ANOVA, $n = 3$.

of CnAβ1 at the Golgi apparatus is similar to a motif found in the domain responsible for mTOR's localization at the Golgi (Liu and Zheng, 2007), suggesting a common regulatory mechanism. Loss of this motif in CnAβ1 results in delocalization of the protein and loss of its interaction with mTOR. These results suggest that CnAβ1 may be acting as an adaptor protein that recruits mTORC2 to specific intracellular membranes to facilitate its activation and the subsequent activation of the AKT pathway.

The role of Akt in mESC is controversial, with some reports implicating it in pluripotency and others suggesting its involvement in differentiation (Naito et al., 2005; Niwa et al., 2009). This differential role might be associated with the regulation of AKT by different complexes (Guertin et al., 2006). Similar results have been described for β-catenin in mESCs, where it has opposite effects depending on the complex it binds to (Miyabayashi et al., 2007). In this regard, we have not observed any contribution to pluripotency maintenance by CnAβ1, whereas we found a significant downregulation of ESC differentiation toward the mesoderm lineage after CnAβ1 depletion. Considering that CnAβ1 is necessary for activation of the AKT/GSK3/β-catenin pathway and that AKT has been reported to be involved in ESC differentiation (Naito et al., 2005), our results suggests that inactivation of AKT is the main reason behind the defective mesodermal differentiation observed after CnAβ1 knockdown. Interestingly, Cog8 knockdown, which delocalizes CnAβ1, also results in defective mesodermal differentiation. These results reinforce the notion that activation of AKT and its targets in different subcellular domains may contribute to their role in ESC pluripotency and differentiation.

(Copp et al., 2009), although the precise mechanism behind this auto-activation is still unclear. mTORC2 activation leads to subsequent phosphorylation and activation of AKT at S473 (Copp et al., 2009). Different components of mTORC2 have been described to localize at intracellular membranes (Betz and Hall, 2013; Liu and Zheng, 2007; Yuan et al., 2015), although the role and mechanisms regulating this localization are also not fully understood. Our work suggests that the localization and activation of mTORC2 at the cell membranes depends, at least in part, on CnAβ1. Loss of CnAβ1 results in delocalization of mTOR, Rictor, and the auto-phosphorylated form of mTOR to the cytoplasm as well as decreased AKT activation. AKT activation has been previously linked to its recruitment to the cellular membranes (Zhao et al., 2015). Therefore, our data suggest that AKT activation might be regulated by mTORC2's subcellular localization. Interestingly, the motif necessary for the localization

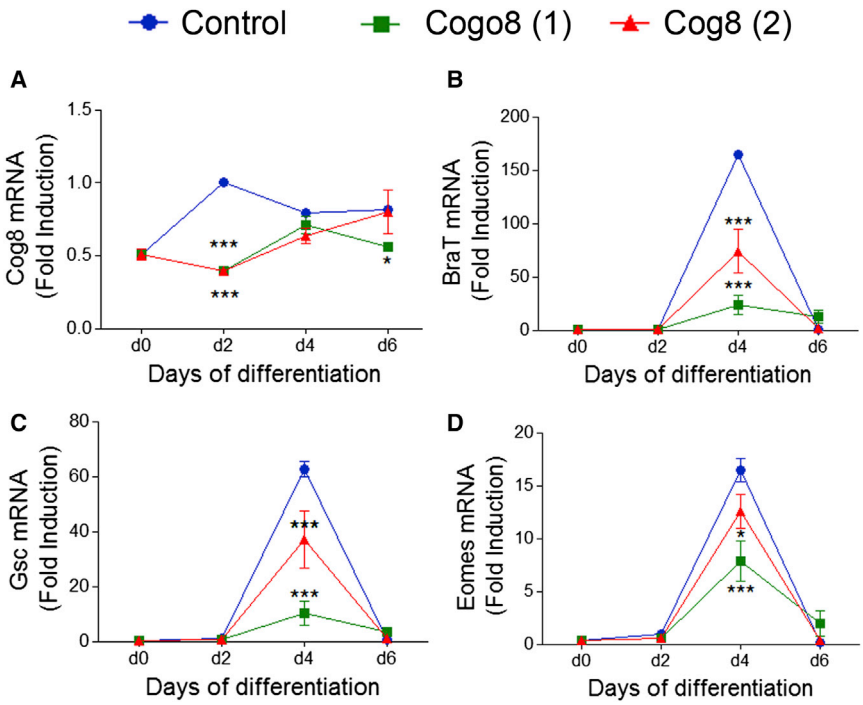

Figure 7. Cog8 Knockdown Inhibits Meso-endoderm Differentiation

mESCs were transiently transfected with two different siRNAs for Cog8 or a control siRNA and differentiated toward mesoderm by using EBs. (A–D) RNA was extracted at different days of differentiation, and Cog8, BraT, Gsc, and Eomes were analyzed by qRT-PCR. Results are presented as fold induction ± SEM over the values for undifferentiated stem cells. *$p < 0.05$, ***$p < 0.001$, two-way ANOVA with Bonferroni post-test, n = 3.

We also provide insight into the regulation of CnAβ post-transcriptional processing that leads to expression of CnAβ1. We show for the first time that CnAβ splicing is controlled, at least in part, by MBNL1, which has a similar role to that of CnAβ1 in the differentiation of ESCs (Han et al., 2013). MBNL1 was previously shown to favor ESC differentiation by controlling alternative slpicing of different genes. Interestingly, the inhibition of MBNL1/2 in somatic cells improves the efficiency of induced pluripotent stem cell reprogramming (Han et al., 2013), further confirming their role in the maintenance of a differentiation phenotype. MBNL1 expression is increased upon differentiation of ESCs and myoblast C2C12 cells, and it shows similar mRNA targets in both cell types (Han et al., 2013; Wang et al., 2012). CnAβ1 follows a similar expression pattern, and its regulation by MBNL1 suggests it could be part of a larger pathway involved in the control of early cell differentiation. Interestingly, reduced activation of Akt and mTOR targets has been described after MBNL loss of function in human ESC-derived neural stem cells (Denis et al., 2013), further suggesting that MBNL1 and CnAβ1 are involved in common pathways.

Alternative splicing of CnAβ results in the retention and translation of intron 12–13 into a unique C-terminal domain that confers CnAβ1 specific localization and function. We describe here the presence of two evolutionarily conserved α helixes in the C-terminal domain of CnAβ1 that have different functions. We show that the second α helix is necessary and sufficient to drive its localization to the intracellular membranes of the cell, mainly to the Golgi apparatus. This localization depends on the interaction of CnAβ1 with Cog8. Cog8 is an important player in stabilization of the Cog and SNARE complexes required for the tethering and transport of vesicles to the Golgi, and in the regulation of the proper compartmentalization of Golgi proteins (Laufman et al., 2013; Willett et al., 2013). Localization at the Golgi apparatus is specific for CnAβ1 and suggests that this Cn isoform plays a different role from that of CnAβ2, which is distributed throughout the cytoplasm of the cell.

The role of Cn itself in ESC differentiation is also unclear. It has been reported that the Cn regulatory subunit CnB, which binds to all CnA isoforms, is necessary for mESC differentiation to all lineages through a mechanism involving the transcription factor NFAT (Li et al., 2011b). In contrast, a recent work suggests that CnB activity may be specifically needed for ectoderm differentiation, but dispensable for mesoderm and endoderm differentiation, and that CnA controls BMP signaling by directly targeting Smad1/5 during this process (Cho et al., 2014). Knockout mice lacking the catalytic domain in CnAβ are born at normal Mendelian ratios (Bueno et al., 2002), suggesting that the phosphatase activity of CnAβ is not essential for mESC differentiation. It has also been described that the CnA inhibitor CsA enhances cardiomyocyte differentiation (Jansen Of Lorkeers et al., 2014). However, this effect might be related to other actions of CsA, which inhibits calcium release through the mitochondrial pore. In this context, we show here that CnAβ1 is necessary for mesodermal differentiation likely by activating β-catenin-mediated transcription through the activation of AKT and subsequent inhibition of GSK3. CnAβ2 knockdown and inhibition of CnA catalytic activity with CsA result in a similar defect in mesodermal differentiation to that observed for CnAβ1, although, unlike the latter, they have no effect on the AKT/GSK3/β-catenin axis. Together, these results suggest that different CnA isoforms contribute to ESC differentiation through different pathways (Figure S7).

In summary, we reveal a novel mechanism regulating ESC differentiation that involves the alternatively spliced CnAβ1 isoform. By binding to Cog8, CnAβ1 acts as a scaffold in the Golgi apparatus, where it regulates mTORC2 complex localization and is necessary for activation of the AKT/GSK3β/β-catenin pathway. These results may have implications for the control of ESC differentiation in regenerative medicine and for the treatment of diseases in which this pathway is strongly activated, such as cancer.

SIGNIFICANCE

Alternative splicing generates different proteins from a single transcript through the inclusion or exclusion of certain exons and introns, which often results in changes in protein

interactions, structure, localization, and/or function. Importantly, alternative splicing has been associated with the regulation of different cellular processes, including cell differentiation. However, the precise molecular mechanisms underlying this regulation remain poorly understood. We have observed that the calcineurin Aβ gene produces two variants that differ in their C-terminal domain (CnAβ1 and CnAβ2). Both of them control mouse embryonic stem cell differentiation through complementary mechanisms. The atypical CnAβ1 variant is localized at the Golgi apparatus, in contrast to other calcineurin isoforms, which are localized in the cytoplasm. This localization is mediated by an α helix in its alternative C-terminal domain, which is necessary for the interaction with mTORC2 and for the localization and activation of this complex at the membranes of the cell. CnAβ1 activates the AKT/GSK3β/β-catenin signaling pathway downstream of mTORC2 to promote mouse embryonic stem cell differentiation. The localization of CnAβ1 at the Golgi is regulated by the interaction between its C-terminal domain and the Golgi protein Cog8. Interestingly, both CnAβ1 and Cog8 are required for the differentiation of mouse embryonic stem cells, further confirming the importance of the localized regulation of this pathway for this cellular process. In summary, we unveil here the structural basis for the mechanism of action of CnAβ1 and its role in the differentiation of mESCs to the mesodermal lineage.

EXPERIMENTAL PROCEDURES

Complete experimental procedures can be found in the Supplement Information.

Cell Culture and Transfection

R1 mESCs in pluripotent conditions were grown on irradiated mouse embryonic fibroblast (MEFs) in Dulbecco's modified Eagle's medium (DMEM) supplemented with L-glutamine (2 mM), non-essential amino acids (NEAA) (1×), β-mercaptoethanol (50 μM), 15% high-quality fetal bovine serum (FBS) and leukemia inhibitory factor at 37°C in a 5% CO_2 atmosphere. mESCs were passaged every 2 days in pluripotent conditions using Trypsin (Sigma). For differentiation assays, mESCs were trypsinized and cultured first for 1 hr under pluripotent conditions in 0.1% gelatin-coated dishes to discard MEFs. We used the hanging drop method for mesoendoderm differentiation with a cell suspension of 5×10^4 cell/mL (1,000 cells per drop in 20 μL) in DMEM supplemented with L-glutamine (2 mM), NEAA (1×), β-mercaptoethanol (50 μM), and 20% FBS as previously described (Bondue et al., 2008). On day 2 of differentiation, the EBs where collected, cultured in an untreated dish for 5 days, and further cultured on a 0.1% gelatin-coated dish. Neural progenitor cell differentiation was induced using DMEM supplemented with L-glutamine (2 mM), NEAA (1×), β-mercaptoethanol (50 μM), and 10% knockout serum replacement (Kamiya et al., 2011).

mESCs were transfected in suspension with Lipofectamine 2000 (Invitrogen) and 10 μM siRNAs (Table S5) or 1 μg of modified RNA (Bernal, 2013; Mandal and Rossi, 2013) following the manufacturer's instructions. A luciferase siRNA and a GFP-modified RNA were used as negative controls, respectively. After transfection, cells were collected and differentiated to mesoendoderm or maintained under pluripotent conditions. The inhibition of GSK3β was performed as previously described (Lindsley et al., 2006). Briefly mESCs were transfected with CnAβ1 or control siRNAs and differentiated in EBs. At day 2 of differentiation, 20 μM LiCl was added for 8 hr in differentiation medium to inhibit GSK3β. Cells were then changed to normal differentiation medium. The expression of the differentiation markers was analyzed at day 4 and compared with expression in the control cells. The inhibition of Cn was performed using CsA at 200 ng/mL. Cells were differentiated in the presence or absence of CsA on the second day of differentiation for 8 hr and analyzed by western blot or differentiated until day 4 on the presence or absence of CsA, and the expression of the differentiation markers was analyzed.

P19 cells were maintained in DMEM supplemented with L-glutamine (2 mM), β-mercaptoethanol (50 μM), and 10% FBS. P19 cells were transfected in suspension with Lipofectamine 2000 on 1% gelatin-coated coverslips following the manufacturer's instructions. Cells were fixed in 4% paraformaldehyde (PFA) 24 hr after transfection. To study the localization of CnAβ1 after Cog8 knockdown, we transfected the cells for 2 days with Cog8 siRNAs (Table S6) to downregulate its expression, and then transfected the GFP-CnAβ1 construct. Cells were fixed 6 hr post transfection and immunostained for GFP, Cog8, and GM130 using specific antibodies.

RNA Isolation and qRT-PCR

Total RNA was isolated from mESCs with an RNeasy Mini Kit (QIAGEN). First-strand cDNA was synthesized using 100 ng of total RNA and a High Capacity cDNA Reverse Transcription Kit (Applied Biosystems). The cDNA was amplified using the primers described in Table S7. qRT-PCR was carried out in an Applied Biosystems 7900 Fast real-time PCR system (Applied Biosystems) using SYBR green for double-stranded DNA detection and quantification or TaqMan probes as indicated in Tables S7 and S8. Results were analyzed with LinReg PCR software (Ruijter et al., 2013). Values were normalized to GAPDH or 18S TaqMan probes.

CLIP-Seq Analysis and RNA-Seq Alignment

Bed file alignments from the Gene Expression Omnibus (GEO: GSE39911) were downloaded and aligned to the mm9 genome using IGV software. Localization of the MBNL1 binding sites in CnAβ (Ppp3cb) was identified in C2C12 myoblasts, C57/Bl6 heart, muscle, and brain samples. Raw sequencing data for brain, heart, and muscle samples from wild-type mice (five replicates per tissue) and C2C12 mouse myoblasts (single control sample) were retrieved from the NCBI Short Read Archive (SRA: SRP014709) and converted to FASTQ using fastq-dump in SRA Toolkit version 2.3.3–2. Reads were aligned with TopHat2 version 2.0.12 to the GRCm38 mouse genome using available transcript annotations from Ensembl release 76 (Gatto et al., 2014). For paired-end data (C2C12 control sample) the mean insert size and SD were computed empirically from uniquely mapping perfect matching mate pairs via a preliminary alignment with Bowtie2 version 2.2.3 and supplied as input parameters to TopHat2. Default options were used otherwise. Reads mapping to the genomic location spanning the last four exons of the Cn gene (chromosome 14: 20,499,364–20,509,500 reverse strand) were retrieved after sorting and indexing the corresponding BAM files with samtools version 1.0 (Li et al., 2009). Custom Python scripts were used to compute per base coverage, normalize raw counts to the maximum over the specified region, and plot the relative read distribution (median over five replicates in tissue samples) against Cn terminal exons.

Microarray Analysis

mESCs were transfected with siRNAs against CnAβ1 or a control siRNA targeting luciferase and analyzed 48 hr later in pluripotent or differentiation conditions. Microarray analysis was performed on eight samples: three control siRNA, three CnAβ1 siRNA #1, and two CnAβ1 siRNA #2. Labeling and hybridization to Affymetrix Mouse Gene 1.0 ST Arrays (Mouse) for mESCs in pluripotent conditions, or Agilent Whole Mouse Genome Microarray 4 × 44K v2 for mESCs in differentiation conditions were carried out at the CNIC Genomics Unit. Normalization and analysis of the data were performed using GeneSpring software. Gene Ontology (GO) analysis was performed using David Bioinformatics. GO results were considered significant at $p < 0.05$. The entirety of the Microarray dataset has been supplied to the Gene Expression Omnibus public database (GEO: GSE72103).

Western Blot

EBs were homogenized in lysis buffer (150 mM NaCl, 1% IGEPAL, 0.5% sodium deoxycholate, 0.1% SDS, and 50 mM Tris [pH 8.0]) in the presence of protease and phosphatase inhibitors (04693159001 and 04906845001; Roche Diagnostics). EB lysates were separated in SDS-PAGE gels, transferred to polyvinylidene fluoride (PVDF) membranes, and blocked with 3% non-fat dry milk in PBS for 30 min. The membranes were incubated with primary antibodies overnight, followed by appropriate horseradish peroxidase

(HRP)-labeled secondary antibodies (anti-mouse P0447 and anti-rabbit P0448; Dako). HRP activity was detected using a luminol-based reagent (RPN 2106; GE Healthcare). Primary antibodies were as follows: AKT (4691; Cell Signaling), p-AKT S473 (4058; Cell Signaling), GSK3β (9315; Cell Signaling), p-GSK3β (9323; Cell Signaling), β-actin (A5316; Sigma), β-catenin (9562; Cell Signaling), CnAβ1 (from our laboratory), Cog8 (PA5-29126; Thermo Scientific), vinculin (V4505; Sigma), integrin β1 (MA1997; Millipore), RhoGdI (sc360; Santa Cruz), p-mTOR S2481 (2971; Cell Signaling), MTOR (2983; Cell Signaling), GM130 (bd610823; BD Biosciences), Rictor (ab56578; Abcam). Western blot quantification was performed on ImageJ software. Brightness and contrast were linearly adjusted in Adobe Photoshop CS5.

Luciferase Assay

mESCs were lysed in 1× passive lysis buffer (Promega) and homogenized for 15 min at room temperature. Luciferase was measured following the manufacturer's instructions (Promega) and normalized for transfection efficiency with Renilla luciferase. As a negative control, we used the same reporter plasmid with the TCF sites mutated (FOP-Luc) and expressed the results as the ratio of luciferase activity obtained with the TOP-Luc divided by the activity of the FOP-Luc.

Cytoplasm and Membrane Fractionation

Cells were cultured under differentiation conditions and analyzed on the second day of differentiation. For purification of enriched cytoplasmic or membrane fractions, the EBs were collected in PBS in the presence of protease and phosphatase inhibitors (04693159001 and 04906845001; Roche Diagnostics). Cells were then lysed in a homogenizer and centrifuged for 5 min at 3,000 × *g* to remove the nuclei. The supernatant was centrifuged at 200,000 × *g* to separate the membranes (pellet) from the cytoplasm (supernatant). Both fractions were analyzed by a western blot to verify their purity using antibodies against RhoGdI for the cytoplasm and against GM130 and integrin β1 for the membranes.

DNA Constructs

pEGFP-CnAβ1, CnAβ2, the C-ter region of CnAβ1 and CnAβ2, and α helixes 1 and 2 of CnAβ1 were amplified by PCR using a KAPA HiFi HotStart Ready Mix PCR Kit (Kapa Biosystems) from pCDNA3.1-based CnAβ1 and CnAβ2 constructs (Lara-Pezzi et al., 2007) and inserted into pGEM-T vector. After the integrity of the constructs was confirmed by DNA sequencing, they were cloned into the pEGFP.C3 vector in frame with GFP. The localization mutant CnAβ1-mut carries the following amino acid mutations: ACREFLL > VSKDLFF. Modified mRNAs (modRNAs) were cloned and produced as previously described (Mandal and Rossi, 2013). Briefly the coding sequence of GFP (negative control), CnAβ1, or CnAβ1-mut were fused to a 3′ and a 5′ UTR that highly promote their expression, synthesized in vitro and purified.

Immunofluorescence

P19 cells were transfected with the different GFP constructs and grown overnight on 1% gelatin-coated glass. Cells were fixed with 4% PFA/PBS for 10 min at 4°C, washed with PBS, permeabilized for 10 min with 0.1% Triton X-100/PBS, and incubated in 10% goat serum/PBS for 30 min at room temperature. Cells were incubated overnight in 10% goat serum/PBS with anti-GFP (632592; Clontech [rabbit]; or 1010/0511FP12; Aves lab [chicken]), anti-GM130 (610823; BD Biosciences) or anti-Cog8 (PA5-29126; Thermo Scientific). After primary antibody incubation, cells were washed with PBS, incubated with Alexa Fluor 488 goat anti-rabbit IgG (A-11034; Thermo Scientific), Alexa Fluor 568 goat anti-mouse IgG (A-11004; Thermo Scientific), Alexa Fluor 488 goat anti-chicken IgG (A-11039; Thermo Scientific), Alexa Fluor 568 goat anti-rabbit IgG (A-11036; Thermo Scientific) or Alexa Fluor 633 goat anti-mouse IgG (A-21126; Scientific) in 10% goat serum/PBS for 1 hr at room temperature, and mounted in Vectashield mounting medium with DAPI. Images were acquired in a Leica SPE3 confocal coupled to a DM 2500 microscope with an objective ACS APO 63.0X 1.13 OIL at 20°C. The software used to acquire the images was LAS AF V 4.0.0 11706. The Manders' correlation coefficient was calculated in ImageJ software performing the total green channel (GFP) over the red channel (GM130). Images were amplified, and brightness and contrast were linearly adjusted using Adobe Photoshop CS5.

Statistical Analysis

All data are presented as means ± SEM. All datasets were analyzed for statistical significance using one-way ANOVA followed by Dunnett's post-test for multiple comparisons or two-way ANOVA followed by Bonferroni's post-test (GraphPad Prism), as indicated in the figure legends. Changes were represented as statistically significant at $p < 0.05$.

ACCESSION NUMBERS

The accession number for the microarray data reported in this paper is GEO: GSE72103.

SUPPLEMENTAL INFORMATION

Supplemental Information includes Supplemental Experimental Procedures, six figures, and eight tables and can be found with this article online at http://dx.doi.org/10.1016/j.chembiol.2016.09.010.

AUTHOR CONTRIBUTIONS

Conceptualization, E.L-P., P.G.P., and J.M.G-S.; Methodology, J.M.G.-S., L.E.F., P.J.R.B., B.S., G.G., G.W.Y., I.N.-L., M.A.P.; Performed the Experiments, J.M.G.-S., M.M.L.-O., P.O.-S., J.L.-A., A.G., L.E.F., P.J.R.B.; Formal Analysis, J.M.G.S., M.M.L.O., P.O.-S., J.L.-A., A.G., L.E.F., P.J.R.B., I.N.-L., E.L.-P.; Writing the Manuscript, J.M.G.-S., P.G.P., L.E.F., P.J.R.B., I.N.-L., M.A.P., and E.L-P.; Funding Acquisition, E.L.-P., P.G.P., P.J.R.B.; Supervision, E.L.-P.; Project Administration, E.L.-P.

ACKNOWLEDGMENTS

We would like to thank Dr. Miguel Manzanares (CNIC, Madrid) and his laboratory for their advice and discussions and Fernando Martínez de Benito for his advice related to the structure models. This work was supported by grants from the European Union's FP7 (CardioNext-ITN-608027 and CardioNeT-ITN-289600), from the Spanish Ministry of Science and Innovation (SAF2012-31451, CP08/00144), and from the Regional Government of Madrid (2010-BMD-2321 "Fibroteam") to E.L.-P. The CNIC is supported by the Spanish Ministry of Economy and Competitiveness and by the Pro-CNIC Foundation, and is a Severo Ochoa Center of Excellence (MINECO award SEV-2015-0505).

Received: March 17, 2016
Revised: August 28, 2016
Accepted: September 2, 2016
Published: October 13, 2016

REFERENCES

Bernal, J. (2013). RNA-based tools for nuclear reprogramming and lineage-conversion: towards clinical applications. J. Cardiovasc. Transl. Res. *6*, 956–968.

Betz, C., and Hall, M. (2013). Where is mTOR and what is it doing there? J. Cell Biol. *203*, 563–574.

Bondue, A., Lapouge, G., Paulissen, C., Semeraro, C., Iacovino, M., Kyb, A.M., and Blanpain, C. (2008). Mesp1 acts as a master regulator of multipotent cardiovascular progenitor specification. Cell Stem Cell *3*, 69–84.

Bueno, O., Wilkins, B., Tymitz, K., Glascock, B., Kimball, T., Lorenz, J., and Molkentin, J. (2002). Impaired cardiac hypertrophic response in Calcineurin Abeta -deficient mice. Proc. Natl. Acad. Sci. USA *99*, 4586–4591.

Cho, A., Tang, Y., Davila, J., Deng, S., Chen, L., Miller, E., Wernig, M., and Graef, I. (2014). Calcineurin signaling regulates neural induction through antagonizing the BMP pathway. Neuron *82*, 109–124.

Copp, J., Manning, G., and Hunter, T. (2009). TORC-specific phosphorylation of mammalian target of rapamycin (mTOR): phospho-Ser2481 is a marker for intact mTOR signaling complex 2. Cancer Res. *69*, 1821–1827.

Denis, J.A., Gauthier, M., Rachdi, L., Aubert, S., Giraud-Triboult, K., Poydenot, P., Benchoua, A., Champon, B., Maury, Y., Baldeschi, C., et al. (2013). mTOR-dependent proliferation defect in human ES-derived neural stem cells affected by myotonic dystrophy type 1. J. Cell Sci. *126*, 1763–1772.

Felkin, L., Narita, T., Germack, R., Shintani, Y., Takahashi, K., Sarathchandra, P., López-Olañeta, M., Gómez-Salinero, J., Suzuki, K., Barton, P., et al. (2011). Calcineurin splicing variant calcineurin Aβ1 improves cardiac function after myocardial infarction without inducing hypertrophy. Circulation *123*, 2838–2847.

Gatto, A., Torroja-Fungairiño, C., Mazzarotto, F., Cook, S.A., Barton, P.J.R., Sánchez-Cabo, F., and Lara-Pezzi, E. (2014). FineSplice, enhanced splice junction detection and quantification: a novel pipeline based on the assessment of diverse RNA-Seq alignment solutions. Nucl. Acids Res. *42*, e71.

Guerini, D., and Klee, C.B. (1989). Cloning of human calcineurin A: evidence for two isozymes and identification of a polyproline structural domain. Proc. Natl. Acad. Sci. USA *86*, 9183–9187.

Guertin, D., Stevens, D., Thoreen, C., Burds, A., Kalaany, N., Moffat, J., Brown, M., Fitzgerald, K., and Sabatini, D. (2006). Ablation in mice of the mTORC components raptor, rictor, or mLST8 reveals that mTORC2 is required for signaling to Akt-FOXO and PKCalpha, but not S6K1. Dev. Cell *11*, 859–871.

Hackett, J., and Surani, M. (2014). Regulatory principles of pluripotency: from the ground state up. Cell Stem Cell *15*, 416–430.

Han, H., Irimia, M., Ross, P., Sung, H., Alipanahi, B., David, L., Golipour, A., Gabut, M., Michael, I., Nachman, E., et al. (2013). MBNL proteins repress ES-cell-specific alternative splicing and reprogramming. Nature *498*, 241–245.

Jansen Of Lorkeers, S., Hart, E., Tang, X., Chamuleau, M., Doevendans, P., Bolli, R., and Chamuleau, S. (2014). Cyclosporin in cell therapy for cardiac regeneration. J. Cardiovasc. Transl. Res. *7*, 475–482.

Kamiya, D., Banno, S., Sasai, N., Ohgushi, M., Inomata, H., Watanabe, K., Kawada, M., Yakura, R., Kiyonari, H., Nakao, K., et al. (2011). Intrinsic transition of embryonic stem-cell differentiation into neural progenitors. Nature *470*, 503–509.

Kumar, R., Cahan, P., Shalek, A., Satija, R., DaleyKeyser, A., Li, H., Zhang, J., Pardee, K., Gennert, D., Trombetta, J., et al. (2014). Deconstructing transcriptional heterogeneity in pluripotent stem cells. Nature *516*, 56–61.

Lara-Pezzi, E., Winn, N., Paul, A., McCullagh, K., Slominsky, E., Santini, M., Mourkioti, F., Sarathchandra, P., Fukushima, S., Suzuki, K., et al. (2007). A naturally occurring calcineurin variant inhibits FoxO activity and enhances skeletal muscle regeneration. J. Cell Biol. *179*, 1205–1218.

Laufman, O., Freeze, H., Hong, W., and Lev, S. (2013). Deficiency of the Cog8 subunit in normal and CDG-derived cells impairs the assembly of the COG and Golgi SNARE complexes. Traffic *10*, 1065–1077.

Li, H., Handsaker, B., Wysoker, A., Fennell, T., Ruan, J., Homer, N., Marth, G., Abecasis, G., Durbin, R., and 1000 Genome Project Data Processing Subgroup. (2009). The Sequence Alignment/Map format and SAMtools. Bioinformatics *25*, 2078–2079.

Li, H., Rao, A., and Hogan, P.G. (2011a). Interaction of calcineurin with substrates and targeting proteins. Trends Cell Biol. *21*, 91–103.

Li, X., Zhu, L., Yang, A., Lin, J., Tang, F., Jin, S., Wei, Z., Li, J., and Jin, Y. (2011b). Calcineurin-NFAT signaling critically regulates early lineage specification in mouse embryonic stem cells and embryos. Cell Stem Cell *8*, 46–58.

Lindsley, R., Gill, J., Kyba, M., Murphy, T., and Murphy, K. (2006). Canonical Wnt signaling is required for development of embryonic stem cell-derived mesoderm. Development *133*, 3787–3796.

Liu, X., and Zheng, X. (2007). Endoplasmic reticulum and Golgi localization sequences for mammalian target of rapamycin. Mol. Biol. Cell *18*, 1073–1082.

López-Olañeta, M., Villalba, M., Gómez-Salinero, J., Jiménez-Borreguero, L., Breckenridge, R., Ortiz-Sánchez, P., García-Pavía, P., Ibáñez, B., and Lara-Pezzi, E. (2014). Induction of the calcineurin variant CnAβ1 after myocardial infarction reduces post-infarction ventricular remodelling by promoting infarct vascularization. Cardiovasc. Res. *102*, 396–406.

Mandal, P.K., and Rossi, D.J. (2013). Reprogramming human fibroblast to pluripotency using modified mRNA. Nat. Protoc. *8*, 568–582.

Miyabayashi, T., Teo, J., Yamamoto, M., McMillan, M., Nguyen, C., and Kahn, M. (2007). Wnt/beta-catenin/CBP signaling maintains long-term murine embryonic stem cell pluripotency. Proc. Natl. Acad. Sci. USA *104*, 5668–5673.

Naito, A., Akazawa, H., Takano, H., Minamino, T., Nagai, T., Aburatani, H., and Komuro, I. (2005). Phosphatidylinositol 3-kinase-Akt pathway plays a critical role in early cardiomyogenesis by regulating canonical Wnt signaling. Circ. Res. *97*, 144–151.

Niwa, H., Ogawa, K., Shimosato, D., and Adachi, K. (2009). A parallel circuit of LIF signalling pathways maintains pluripotency of mouse ES cells. Nature *460*, 118–122.

Ruijter, J., Pfaffl, M., Zhao, S., Spiess, A., Boggy, G., Blom, J., Rutledge, R., Sisti, D., Lievens, A., De Preter, K., et al. (2013). Evaluation of qPCR curve analysis methods for reliable biomarker discovery: bias, resolution, precision, and implications. Methods *59*, 32–46.

Wang, E., Cody, N., Jog, S., Biancolella, M., Wang, T., Treacy, D., Luo, S., Schroth, G., Housman, D., Reddy, S., et al. (2012). Transcriptome-wide regulation of pre-mRNA splicing and mRNA localization by muscleblind proteins. Cell *150*, 710–724.

Watanabe, S., Umehara, H., Murayama, K., Okabe, M., Kimura, T., and Nakano, T. (2006). Activation of Akt signaling is sufficient to maintain pluripotency in mouse and primate embryonic stem cells. Oncogene *25*, 2697–2707.

Willett, R., Kudlyk, T., Pokrovskaya, I., Schönherr, R., Ungar, D., Duden, R., and Lupashin, V. (2013). COG complexes form spatial landmarks for distinct SNARE complexes. Nat. Commun. *4*, 1553.

Willett, R., Pokrovskaya, I., Kudlyk, T., and Lupashin, V. (2014). Multipronged interaction of the COG complex with intracellular membranes. Cell Logist. *4*, e27888.

Yuan, Y., Pan, B., Sun, H., Chen, G., Su, B., and Huang, Y. (2015). Characterization of Sin1 isoforms reveals an mTOR-dependent and independent function of Sin1γ. PLoS One *10*, e0135017.

Zhao, Y., Lin, Y., Zhang, H., Mañas, A., Tang, W., Zhang, Y., Wu, D., Lin, A., and Xiang, J. (2015). Ubl4A is required for insulin-induced Akt plasma membrane translocation through promotion of Arp2/3-dependent actin branching. Proc. Natl. Acad. Sci. USA *112*, 9644–9649.


UAM
UNIVERSIDAD AUTONOMA
DE MADRID


cnic